

AN ANALYSIS OF MARINE ECOSYSTEM DYNAMICS
THROUGH DEVELOPMENT OF A COUPLED
PHYSICAL-BIOGEOCHEMICAL-FISHERIES FOOD WEB
MODEL

KELLY ANNE KEARNEY

A DISSERTATION
PRESENTED TO THE FACULTY
OF PRINCETON UNIVERSITY
IN CANDIDACY FOR THE DEGREE
OF DOCTOR OF PHILOSOPHY

RECOMMENDED FOR ACCEPTANCE
BY THE DEPARTMENT OF
GEOSCIENCES
ADVISER: JORGE L. SARMIENTO

NOVEMBER 2012

© Copyright by Kelly Anne Kearney, 2012.

All rights reserved.

Abstract

Over the past decade, fisheries management efforts have placed increased emphasis on ecosystem-based management, where the interactions between a target stock species and its physical and biological environment are considered in addition to sustainability of the stock itself. At the same time, global-scale climate models that historically focused only on physical and biogeochemical variables are increasingly incorporating biological variables. With these shifts, the historical separation between climate modeling and fisheries modeling is closing, with increased interest in the concept of end-to-end models, i.e. models that incorporate dynamics from physics to top predators.

In this dissertation, I develop a modeling framework that fully couples a one-dimensional physical mixed layer model, a biogeochemical model, and an upper trophic level fisheries food web model. I present a thorough description of the model itself, as well as an ensemble-based parameterization process that allows the model to incorporate the high level of uncertainty associated with many upper trophic level predator-prey processes. Through a series of model architecture experiments, I demonstrate that the use of a consistent functional response for all predator-prey interactions, as well as the use of density-dependent mortality rates for planktonic functional groups, are important factors in reproducing annual and seasonal observations.

Following the development and validation of the end-to-end ecosystem model, I use the model to simulate the response of an ecosystem to a bottom-up perturbation, namely an increase in net primary production due to alleviation of micronutrient limitation. I also look at the impact of non-predatory mortality, one of the least-constrained model processes, on the energy flow through the system. We find that the relative changes in production at higher trophic levels are amplified under density-independent non-predatory mortality assumptions but damped under density-dependent assumptions. However, the high parameter uncertainty masks this effect in predicted values for most functional groups.

Overall, the model developed in this dissertation addresses a growing need to thoroughly diagnose the behavior of, and quantify the uncertainty associated with, complex ecosystem models that bridge physical, biological, and socio-economic boundaries. Such detailed dynamical characterization of model behavior is essential before ecosystem models can be applied to management applications.

Acknowledgements

I would like to thank my advisor, Jorge Sarmiento, for his support and advice during my time as a graduate student, for encouraging travel, for surrounding me with a research group full of interesting and intelligent people, and for tolerating my absurd schedule of extracurriculars.

To Charlie Stock, I cannot thank you enough for the encouragement and guidance you have provided over the years. You were endlessly available to discuss the trials and tribulations of model development, to suggest new directions for my work, to introduce me to colleagues at conferences, to edit all my writing, to reassure me that my work was moving in the right direction, and of course to discuss the latest baseball season. I truly could not have completed this without you.

I thank those who have been on my academic committee. Thanks to Bess Ward, for going out of her way to reassure a panicked undergrad years before I came to Princeton, and for her helpful advice throughout my six years of graduate work. To Anand Gnanadesikan, who helped me focus the direction of my work, and to David Medvigy, for being such a cooperative reader despite the last-minute nature of my request.

I'd like to thank the Nancy Foster scholarship program, who provided financial support through much of my degree. I'd also like to thank Jeff Polovina, Kerim Aydin, and Sarah Gaichas for hosting me in Hawaii and Seattle under support from this program; the opportunity to spend time at NOAA Fisheries provided much insight into the world of fisheries science, and helped me fill in the final pieces of the modeling puzzle.

Thanks to all those who made Sayre Hall a great place to work... To my fellow grad students and officemates over the years, Patrick, Yves, Daniele, Joe, and Hannah, for providing conversation and commiseration that was always a welcome break from staring at the computer. To the many postdocs and researchers who have occupied the third and fourth floors over the years: Keith, Mike, Sarah, Stephanie, Eric, Stephanie, Jamie, Eun Young, Claudie, Allison, Brendan, James, Ryan, Greg, and anyone I may be forgetting, thank you for making this one of the most friendly working environments I've had the chance to experience. To Bob, Laura, and the rest of the Forrestal Village lunch crowd, the midday walks were a great break to the workday. And finally to Rick Slater, who helped with technical issues, allowed me to leech off his computer's processors, and got me addicted to the afternoon crossword; thanks for everything.

To all the friends I have met here in Princeton; in particular, Jeff, Silvia, Brookes, Kevin, Christina, and Aurelien deserve special mention for offering me more good food than I ever would

have encountered on my own (certainly in my own kitchen!). I really valued our weekly dinners and the friendships that evolved from them.

Finally, thank you to my wonderful family for all their love and support throughout my "science project". To my parents, who encouraged my love of science my whole life, as well as all my other eclectic hobbies: music, dance, sports... and supported me whole-heartedly throughout this journey. To my brothers, Frank, Patrick, and Bobby, for just being great guys. And to my incredible sister, Eileen, for being my person through all the highs and lows of grad school (and life), and of course for the wonderful critter artwork that decorates every dissertation-related paper, poster, and presentation I've created.

This work was supported by several funding sources: NASA (NNG06GE77G) from 7/1/07-8/31/07 and 9/1/08-8/31/09, NOAA Cooperative Institute for Climate Science (NA17RJ2612 and NA08OAR320752) from 9/1/07-8/31/08 and 9/1/09-1/31/11, Carbon Mitigation Initiative BP and Ford Motor Company from 2/1/11-6/30/11, NEREUS - Nippon Foundation from 7/1/11-present, and the NOAA Nancy Foster Scholarship (NA08NOS4290444) from 8/1/2008-8/1/2012.

Contents

Abstract	iii
Acknowledgements	iv
List of Tables	xi
List of Figures	xiv
1 Introduction	1
1.1 An overview of end-to-end ecosystem models	1
1.2 The Pacific Eastern Subarctic Gyre region	2
1.3 Dissertation outline	5
1.3.1 Publication and coauthor contributions	6
2 Ecopath food web models for the Eastern Subarctic Pacific	8
2.1 Capturing uncertainty through an intramodel ensemble	10
2.2 Determining primary energy pathways in a food web	11
2.3 Characteristics of the Eastern Subarctic Gyre food web	19
3 Coupling planktonic ecosystem and fisheries food web models for a pelagic ecosystem	28
3.1 Introduction	28
3.2 Methods	30
3.2.1 The water column ecosystem model framework	30
3.2.1.1 The physical model	30
3.2.1.2 The lower trophic level biogeochemical model	31
3.2.1.3 The upper trophic level model	32
3.2.2 Coupling the model components	33
3.2.2.1 The baseline case	36
3.2.2.2 Consistent feeding formulations across planktonic groups	37

3.2.2.3	Density dependent mortality	39
3.2.3	Simulations and model evaluation	40
3.3	Results	41
3.3.1	Choice of model architecture	41
3.3.2	Validation of final model	44
3.3.2.1	Surface nutrients	44
3.3.2.2	Productivity	45
3.3.2.3	Biomass of living groups	46
3.4	Discussion	46
4	Ecosystem response to a bottom-up perturbation	50
4.1	Introduction	50
4.2	Methods	52
4.3	Results	54
4.3.1	Primary productivity under enhanced iron deposition	54
4.3.2	Propagation of productivity to higher trophic levels	59
4.4	Discussion	61
5	Summary	66
A	Model description	69
A.1	The one-dimensional physical model	69
A.1.1	Description of equations	69
A.1.2	Input variables and datasets for the Eastern Subarctic Gyre	71
A.2	Process equations for the water column ecosystem model	71
A.2.1	Nitrogen flux equations for living state variables	74
A.2.1.1	Gross primary production (Gpp)	74
A.2.1.2	Respiration (Res)	74
A.2.1.3	Extracellular excretion (Ex)	74
A.2.1.4	Consumption (Con)	75
A.2.1.5	Excretion (Exc) and egestion (Ege)	76
A.2.1.6	Non-predatory mortality (Mor)	76
A.2.2	Additional fluxes	77
A.2.2.1	Proportional-to-nitrogen fluxes of silica and iron	77

A.2.2.2	Luxury iron uptake (Ufe)	77
A.2.2.3	Decomposition (Dec)	78
A.2.3	Iron dynamics in the quota model	78
A.2.4	Parameterization for the biological model	79
A.2.4.1	Ecopath input data	79
A.2.4.2	Tables of parameters	83
B	Software documentation for mixed_layer model with biological modules	103
B.1	Overview	103
B.2	The mixed_layer (with biology) toolbox	103
B.2.1	Code organization and installation	103
B.2.2	Usage guide	108
B.3	Function reference	112
B.3.1	aggregate	112
B.3.2	archivemldata	112
B.3.3	binary2netcdf	113
B.3.4	biomodule	114
B.3.5	calcclusteredparams	116
B.3.6	calcheat	116
B.3.7	cell2matfill	117
B.3.8	cellstr2	118
B.3.9	clearsky	118
B.3.10	climatology	118
B.3.11	cptcmap	119
B.3.12	createensemble2	121
B.3.13	ecopathinputcheck	122
B.3.14	ecopathinputinfo	122
B.3.15	ecopathlite	123
B.3.16	endonly	126
B.3.17	esabgcsetup	126
B.3.18	esafoodwebsetup	127
B.3.19	esaphysicssetup	129
B.3.20	eweunitconvert	129

B.3.21	fluxread	130
B.3.22	formatfornemurokak	131
B.3.23	formatforwce	132
B.3.24	initbiorelax	132
B.3.25	initialize	133
B.3.26	initinterpdata	136
B.3.27	integratebio	138
B.3.28	ivlev2forage	139
B.3.29	listfluxes	140
B.3.30	minmax	140
B.3.31	mixed_layer	141
B.3.32	mixtracer	146
B.3.33	mixturb_my	147
B.3.34	mycoef	147
B.3.35	nanmean	147
B.3.36	ncvarsget	147
B.3.37	nemuroecopathdata	148
B.3.38	nemuroflexinput	149
B.3.39	nemuroinputparser	151
B.3.40	nemurokak	153
B.3.41	nemurokakode	155
B.3.42	nemvarnames	155
B.3.43	np	156
B.3.44	npz	156
B.3.45	npzd	157
B.3.46	ode4splitsnonneg	158
B.3.47	odewrap	159
B.3.48	parseinput	160
B.3.49	parsepv	161
B.3.50	photosynthesis	161
B.3.51	plotmixed	162
B.3.52	readmixed	162
B.3.53	recovercrashed	163

B.3.54	regexpfound	164
B.3.55	runmixedlayer	164
B.3.56	sh2dewpoint	165
B.3.57	solve_velocities	165
B.3.58	sortewein	167
B.3.59	suplabel	167
B.3.60	tracer	168
B.3.61	tracerforced	168
B.3.62	trophiclevel	169
B.3.63	verticalflux	169
B.3.64	wce	170
B.3.65	wceode	172

Bibliography	172
---------------------	------------

List of Tables

2.1	Definitions and common sources for the variables in the Ecopath master equation (replicated from Table 2, Aydin <i>et al.</i> , 2003). For units, M = mass, A = area, and T = time. The production/biomass ratio is referred to interchangeably in Ecopath-related literature as P/B and PB, with the latter being the variable name used internally in code and occasionally in the documentation manual for the software. Likewise, consumption/biomass is referred to as both Q/B and QB.	9
2.2	The simplified food web model includes 24 functional groups, listed below along with the picture used to identify each in the food web diagram (Figure 2.5 on page 21). The type column indicates whether each group is classified as phytoplankton (P), zooplankton (Z), or nekton (K) in the fully-coupled model (see 3.2.2).	20
3.1	The process variables in this table describe the various types of fluxes connecting the physical and biological variables in the water column ecosystem model.	36
3.2	We ran the water column ecosystem model with a variety of different formulations for the grazing, predation, and mortality fluxes.	41
A.1	A description of the 47 functional groups included in the unsimplified version of the food web model. Species listed are not exhaustive, but represent the dominant members of each functional group.	81
A.2	A description of the 47 functional groups included in the unsimplified version of the food web model (continued).	82
A.3	Ecopath input variables for the 47-group food web, including biomass (B, tons wet weight m ⁻²), production/biomass (PB, yr ⁻¹), consumption/biomass (QB, yr ⁻¹), ecotrophic efficiency (EE), growth efficiency (GE), and fraction unassimilated (GS) .	84
A.4	Diet fraction input for the 47-group food web model.	85
A.5	Diet fraction input for the 47-group food web model (continued).	86

A.6 Diet fraction input for the 47-group food web model (continued)	87
A.7 Diet fraction input for the 47-group food web model (continued)	88
A.8 Diet fraction input for the 47-group food web model (continued)	89
A.9 Diet fraction input for the 47-group food web model (continued)	90
A.10 Ecopath input variables for the 24-group simplified food web, including biomass (B, tons wet weight m ⁻²), production/biomass (PB, yr ⁻¹), consumption/biomass (QB, yr ⁻¹), ecotrophic efficiency (EE), growth efficiency (GE), and fraction unassimilated (GS)	91
A.11 Diet fraction input for the 24-group food web model.	92
A.12 Diet fraction input for the 24-group food web model (continued).	93
A.13 Biogeochemical process-related parameters: Primary production	94
A.14 Biogeochemical process-related parameters: Iron quota model	94
A.15 Biogeochemical process-related parameters: Respiration	94
A.16 Biogeochemical process-related parameters: Extracellular excretion	95
A.17 Biogeochemical process-related parameters: Grazing	95
A.18 Biogeochemical process-related parameters: Egestion and excretion	95
A.19 Biogeochemical process-related parameters: Decomposition	96
A.20 Biogeochemical process-related parameters: Mortality	96
A.21 Derived parameters used in the equations in Appendix A.2. These parameters vary over time as a function of the state variables from both the physical and biological models.	97
A.22 Group-related, Ecopath-derived parameters for the water column ecosystem model, including mass-balanced biomass (B*), growth efficiency (GE), non-predatory mor- tality flux (M0), and unassimilated fraction (GS). Where values vary across ensem- ble members, mean, standard deviation, minimum, and maximum values, calculated across the 500 ensemble members, are given	98
A.23 Flux-related, Ecopath-derived parameters for the water column ecosystem model, including mass-balanced prey-to-predator flux (Q*), functional response top-down parameter (X), functional response bottom-up parameter (D), and functional response exponent (θ). Where values vary across ensemble members, mean, standard deviation, minimum, and maximum values, calculated across the 500 ensemble members, are given	99
A.24 Flux-related, Ecopath-derived parameters for the water column ecosystem model (continued).	100

A.25 Flux-related, Ecopath-derived parameters for the water column ecosystem model (continued).	101
A.26 Flux-related, Ecopath-derived parameters for the water column ecosystem model (continued).	102

List of Figures

1.1	The Eastern Subarctic gyre region is bordered by the Subarctic Current, Alaska Current, and Alaska Stream. The dotted line shows the corresponding region as designated by the North Pacific Marine Science Organization (PICES); much of the food web data presented later in this thesis was compiled using this definition for the region of interest. The location of Ocean Station Papa (OSP) is indicated by a gray dot.	3
2.1	Dendrogram showing similarity between the 47 groups in the Aydin-48 Ecopath model, based on shared predator-prey relationships, trophic level, and production level. The horizontal axis shows the Euclidean distance between groups connected by each vertical line. The pie plots at each junction illustrate the relative biomass of all subgroups combined at that point. Colors are provided to distinguish between the major organism types: detritus (brown), phytoplankton (green), zooplankton (grey), fish (purple), squid (orange), mammals (blue), and birds (red).	13
2.2	We analyzed all potential clustering levels to verify the relationships between biomass and trophic level. The top panels show biomass (on a log scale) versus trophic level for all 39 potential food webs, with each web labeled by the cutoff value used to create the clusters. The colored points indicate the values of individual ensemble members, color-coded by point density, while the black points show the sum of biomass binned as indicated by the vertical dotted lines; error bars indicate the upper and lower limits of these sums across the 100 ensemble members. The lower panel indicates the orders of magnitude spanned by the biomass values within each food web as well as the slope of linear fit for trophic level versus summed biomass.	15

2.3 Production/biomass ratios are an indicator of the growth rate of each functional group, and are expected to decrease when moving from lower to higher trophic levels. As in the previous figure, production/biomass is plotted versus trophic level for each potential food web. The lower panel indicates the slope of the line fitted directly to the individual ensemble points (unlike biomass, production rates are not additive across trophic levels and thus no binning was performed here).	17
2.4 Comparison of fluxes into and out of each cluster, both before and after clustering. All box-and-whisker plots indicate minimum, first quartile, median, third quartile, and maximum values across ensembles. The red boxes show the sum of fluxes into (production) or out of (mortality) the groups that make up a particular cluster, using the values from the 47-group unclustered model. The blue boxes show the respective flux for the clustered group where it appears throughout the 39 potential food webs. The pie plot labels along the bottom axis correspond to those from Figure 2.1 on page 13.	18
2.5 The food web used for this study incorporates 23 living functional groups. The axis to the left indicates the trophic level of each group, following the Ecopath definition where trophic level of a consumer is equal to 1 plus the diet-fraction-weighted average of its prey's trophic levels.	21
2.6 Cumulative distribution functions for the Ecopath input parameters that showed a significant difference in their distributions before and after the mass-balance criteria were applied (two-sample Kolmogorov-Smirnov test, $\alpha = 0.05$). Units on the x axis vary based on the parameter being plotted: Production (B) = tons wet weight m^{-2} , Production (PB) and consumption (QB) rates: yr^{-1} , Diet fraction (DC) = no unit.	22
2.7 Correlation analysis for all Ecopath input variables with pedigree values. The top plot shows the Spearman's rank correlation coefficients between each pair of input variables; this quantifies whether a monotonic trend exists between the two variables. The box-like features along the main diagonal are the locations of the within-predator diet fractions; because a predator's diet must sum to one, these will always be correlated. Beyond these, only 5 pairs of parameters were significantly correlated, as shown in the bottom five panels; x- and y-axes range from 0 to the marked values.	24

2.8 Both biomass and production rate span several orders of magnitude in this food web. The colored dots represent the specific parameter values found in the 1000-member ensemble; the convex hull outlines around each set of points are provided to clarify areas of high overlap.	25
2.9 Flux of biomass due to predation past each trophic level for individual ensembles (light blue) and the ensemble mean (dark blue). Flux is calculated by summing all fluxes that span a given trophic level throughout the food web. The dashed lines are provided for reference and show the trend expected if energy transfer was exactly 10% or 20% per trophic level.	26
2.10 This directed graph shows the fluxes of biomass between all functional groups in the 24-group food web. Colored lines indicate ensemble mean predator/prey fluxes between the 23 living groups, as well as primary production fluxes from the detritus group to primary producers, and non-predatory mortality fluxes from all living groups to the detritus pool; lines curve counterclockwise from source group to sink group. The bar graphs show, from left to right, the total prey consumption, total production, predatory loss, and non-predatory loss, in g wet weight $m^{-2} yr^{-1}$; the error bars indicate the 25th-75th percentiles across ensembles. Axes range from 0 to the value labeled to the right of each axis.	27
3.1 The WCE model includes 7 non-living state variables and 3 categories of living state variables; arrows indicate the flow of nitrogen, silica, and iron between these state variables. Zigzag arrows indicate sinking of material through the water column. Note that the phytoplankton, zooplankton, and nekton boxes in this schematic indicate variable classes that represent several different state variables. The phytoplankton groups included in the model include three different nutrient compartments, for nitrogen, silica, and iron content (non-diatom phytoplankton groups can be parameterized so that their growth is not dependent on silica). Zooplankton and nekton groups include only nitrogen compartments. Nitrogen and silica are conserved in the model; the iron cycle includes only partial remineralization, and is also relaxed toward a constant profile to approximate advective and airborne sources, and therefore is not conserved.	35

3.4 As an initial test of model architecture skill, we looked at whether each model was capable of maintaining the biomass of all living state variables within the uncertainty ranges used to choose initial conditions over a 20-yr simulation. The blue violin plots display the distribution of biomass across the 50-member ensemble at the end of each 20-yr simulation; width indicates the relative number of ensemble members at a given biomass value. The black bars indicate the interquartile range of the ensembles, with the black circle indicating the ensemble mean. Green horizontal lines show the upper and lower values of the target biomass ranges (micronektonic squid and pelagic forage fish are estimated by Ecopath rather than being assigned target ranges, and therefore are missing these lines). Vertical axes represent integrated biomass, ranging from 0 to the labeled value, in g C m ⁻² . The horizontal axis indicates the model architecture indices, which correspond to those found in Table 3.2 on page 41.	43
3.5 Modeled surface nutrient anomaly from yearly average over one simulation year versus observations at Ocean Station Papa. Observations for Ocean Station Papa (OSP) reflect measurement at this location over the period of 1969-1981(Whitney & Freeland, 1999). Also shown are the WOA05 climatological surface nitrate anomaly values averaged over the entire Eastern Subarctic Gyre (ESA) region (Garcia <i>et al.</i> , 2006). Inset figures show the histograms of yearly-averaged values at the end of the 50-year simulation period, along with the corresponding yearly-average for each observation dataset.	45
3.6 Modeled net primary production over one simulation year. For comparison, net primary production values estimated by the Eppley-VGPM model applied to SeaWiFS data near Ocean Station Papa (purple dashed) and over the entire Eastern Subarctic Gyre (red dash-dot) are also shown, as well as measured production values at Ocean Station Papa as compiled by Boyd & Harrison (1999) (squares, circles, and triangles indicate data from three different studies, as described in Boyd & Harrison (1999, Figure 7)).	46
3.7 Vertically-integrated biomass, in g C m ⁻² , for all living functional groups in the model over the final year of simulation. The green bars to the left of each axis correspond to the yearly-mean biomass ranges from Table A.10 on page 91 used to initialize biomass for each group. Axes are scaled such that pedigree values are consistent between groups, i.e. green bars of equal length indicate equal uncertainty as a fraction of biomass; the lower limit of all axes is 0.	47

4.1 Schematic of the water column ecosystem model processes and state variables. An explicit iron cycle, including cycling of iron between dissolved and particulate state variables as well as the phytoplankton groups, has been added to the processes described in the previous chapter (Figure 3.1 on page 35).	53
4.2 Interannual variability in dust deposition at Ocean Station Papa. The light grey line shows the sum of wet and dry deposition, as modeled by the Geophysical Fluid Dynamics Laboratory Global Chemical Transport model (Moxim <i>et al.</i> , 2011), while the dark line shows a 12-month running average. Dotted lines indicate $\pm 25\%$ of the mean value.	53
4.3 Net primary productivity under varying surface iron deposition. The top panels show net productivity versus time over a single year of each iron regime, with bold lines indicating the ensemble average and the shaded area the 25th-75th percentiles across ensemble members. The bottom panel shows the yearly-averaged total net production versus surface iron concentration for each ensemble member (points); the grey circle indicates the ensemble average for each iron regime.	56
4.4 Growth and limitation terms for both phytoplankton groups under climatological (Fe x 1) and high-iron (Fe x 5) surface deposition regimes. The panels show, from left to right and top to bottom: Maximum temperature-influenced growth rate; light limitation; nutrient limitation for small phytoplankton under climatological iron (Note: nitrogen limitation is an additive function of NO_3 and NH_4 limitation, and therefore can be greater than 1), nutrient limitation for small phytoplankton under high-iron conditions, nutrient limitation for large phytoplankton under climatological iron, nutrient limitation for small phytoplankton under high-iron conditions, realized growth rate (i.e. nutrient- and light-limited growth) for under climatological conditions, and realized growth rate under high-iron conditions. Shaded areas represent the 25-75% ensemble range, while the solid lines indicate the ensemble median.	57

4.5 The directed graphs above summarize the change in biomass and production fluxes between all groups in the ecosystem when one phytoplankton group is provided with enhanced primary production. Colors indicate the fraction change in biomass of each functional group (nodes) and fluxes between groups (edges); fluxes curve counter-clockwise from source to sink. When small phytoplankton production is increased, large phytoplankton production and biomass drop due to changing predation pressure. However, when large phytoplankton production is increased, the changing top-down controls lead to increased production by both phytoplankton groups.	58
4.6 Net consumer production, across all simulations. X-coordinates indicate the relative level of surface iron deposition, for linear (blue), 1.5 (green), and quadratic (red) mortality schemes, while the y-axis indicates the annually-averaged net consumer production.	60
4.7 Relative change in production, R_x , for consumers in the ecosystem. The upper panel boxplots show the spread of values for each consumer (points more than 1.5 times the interquartile distance outside the lower/upper quartiles, are considered outliers and marked as dots). The lower panel consolidates the same information grouped by trophic level; here, points indicate the values for each consumer vs. trophic level, while boxplots consolidate this information (outliers not included in these boxplots). The amplification effect under a linear mortality scheme can be seen clearly when the data is grouped by trophic level (lower panel); in this context, trophic level is defined a 1 plus the weighted average of prey's trophic levels, based on the mass-balance constraints for each ensemble member. Points show the trophic level and R_x values for each ensemble member and each raised-iron scenario; boxplots consolidate these points based on trophic level (outliers are not shown in the lower panel boxplots). . .	62
4.8 These histograms show the distributions of biomass (B , gC m 2) and net secondary production (NSP, gC m 2 yr $^{-1}$) for each consumer in the food web under the linear (blue), 1.5 (green), and quadratic (red) mortality structures, at the end of the 5-times surface iron flux perturbation. The shaded axes indicate variables where the median value is significantly higher or lower under the linear regime than the quadratic regime. 63	

A.1	Climatological datasets used to force the physical model, including wind speed, solar radiation, air temperature, dewpoint temperature, and salinity. Light lines in the upper three panels show the high-resolution data used to force the model; dark lines show a weekly running average, and are provided only for visual clarity.	72
B.1	Calling tree for all functions provided in the mixed_layer code package. Colors indicate which functions are found in each folder: mixed_layer (orange), private (pink), biomodules (blue), setup (green), utilities (yellow) or fex (turquoise).	109

CHAPTER 1

Introduction

1.1 An overview of end-to-end ecosystem models

End-to-end ecosystem models can be broadly defined as models that attempt to represent the entirety of a marine ecosystem, including both the abiotic and biotic components: physical dynamics of both atmosphere and ocean, ocean biogeochemistry, lower and upper trophic level biology, and human influences (fisheries, recreation, coastal development, etc.). These models have become more and more prevalent over the past few decades, as the questions posed by both the biogeochemical and fisheries communities have become more intertwined.

Physical and biogeochemical global climate models historically focused only on the biological components of an ecosystem necessary to capture global-scale patterns in chemical components, such as uptake and demineralization of nutrients by phytoplankton; often these effects were only modeled implicitly, rather than through explicit representations of the phytoplankton and their predators. However, as climate change studies have begun to elucidate a variety of potential long-term changes in biologically influential physical and chemical properties, such as temperature and pH, the models have moved towards quantifying the effect on biology.

At the other end of the food web, fisheries models have also been moving towards a more ecosystem-based perspective. Historically, the models used to manage fish stocks focused only on the growth rates and recruitment of a single target species, in isolation from both other target species in the region and the ecosystem as a whole (Beverton & Holt, 1957). However, with the decline of many global fisheries in recent decades, managers have begun to recognize that fish stocks are often vulnerable to changes in their physical environment as well as population shifts elsewhere in their food

web, and the current management recommendations have been shifting away from this single-species model, instead emphasizing ecosystem-based management (Pikitch *et al.*, 2004; Larkin, 1996). This term refers to management policies that recognize the many interactions between the components of an ecosystem.

The changes within both the biogeochemical and fisheries communities have led to a proliferation of end-to-end ecosystem model frameworks being introduced in the past decade (Fulton, 2010; Travers *et al.*, 2007). They vary widely in the portions of the ecosystem that they encompass, as well as the techniques used to resolve the many processes that can be important to ecosystem function. This dissertation presents another such model, which combines a physical water column model, a traditional biogeochemical/lower trophic level model, and a fisheries-style food web model, the latter of which encompasses species ranging from phytoplankton to top predators, such as birds and marine mammals. Its unique contribution to the growing collection of end-to-end models includes a detailed analysis of the various components and processes inherent within each of these individual model types, the assumptions associated with each of these processes, and the ways in which those assumptions may be altered when the model components are connected to each other in a fully-coupled (i.e. two-way) manner.

1.2 The Pacific Eastern Subarctic Gyre region

While the modeling framework developed within this dissertation is intended to be generic to any regional ecosystem, parameterization needs required that we choose a specific location for all development. We chose to parameterize it for the Eastern Subarctic Gyre of the North Pacific, for several reasons. This region is an important foraging ground for a variety of epipelagic species (Brodeur *et al.*, 1999) and a rearing and growth area for commercially-important Pacific salmon (Aydin *et al.*, 2005). The climate of this location is heavily influenced by variations in the Aleutian Low Pressure system, resulting in decadal scale variability in physical properties such as sea surface temperature, precipitation, downwelling, and stratification (Mantua *et al.*, 1997; Francis *et al.*, 1998a). Numerous studies have demonstrated corresponding population changes in the biology at multiple trophic levels, including that of phytoplankton (Polovina *et al.*, 1995), zooplankton (Brodeur & Ware, 1992), and salmon (Beamish & Bouillon, 1993). Finally, this area is home to a relatively high number of both biogeochemical and fisheries datasets, making it a convenient testbed for an end-to-end ecosystem model.

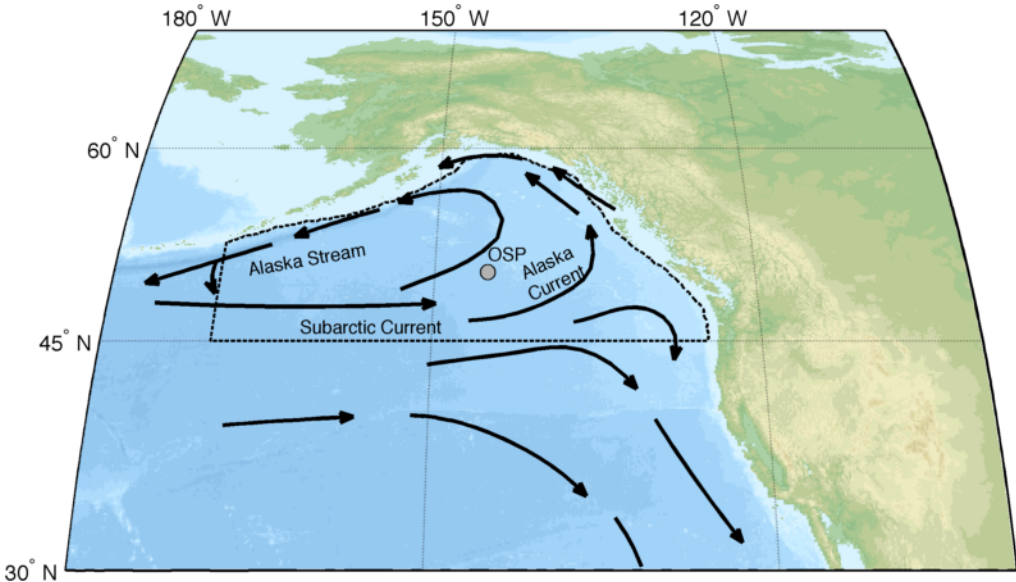


Figure 1.1: The Eastern Subarctic gyre region is bordered by the Subarctic Current, Alaska Current, and Alaska Stream. The dotted line shows the corresponding region as designated by the North Pacific Marine Science Organization (PICES); much of the food web data presented later in this thesis was compiled using this definition for the region of interest. The location of Ocean Station Papa (OSP) is indicated by a gray dot.

The Eastern Subarctic Gyre is one of two cyclonic gyres in the north Pacific Ocean. The east-flowing Subarctic Current separates subarctic water from the subtropical water to the south; due to the geometry of the Aleutian Islands chain, the subarctic surface currents are recirculated into two distinct gyre regions. The eastern gyre, which we focus on in this study, is bordered to the south by the Subarctic Current, to the north and east by the Alaska Current, and to the northwest by the Alaska Stream, which merges with the Subarctic current to the west of the gyre (Figure 1.1 on page 3). This region is also commonly referred to as the Gulf of Alaska, although the identically-named Gulf of Alaska Large Marine Ecosystem (www.lme.noaa.gov) refers to only the more coastal communities along the northeastern edge of the gyre. For our purposes, we will be considering only the pelagic, open ocean portion of the gyre community, and use the name Eastern Subarctic Gyre rather than Gulf of Alaska to avoid confusion.

The regional climate is highly influenced by the Aleutian Low Pressure system, a semi-coherent atmospheric pressure system that is situated over the gyre during the winter months. The high winter wind speeds of around 12 m/s created by this system lead to deep mixing of the surface layer, while in the summer months the wind speeds fall to 7 m/s and the water restratifies. Over this seasonal cycle, the mixed layer depth varies between 90-120 m in winter to only 40 m in the summer (Whitney & Freeland, 1999). Sea surface temperature varies between 5°C in the winter and 13°C

in late summer, while salinity cycles between 32.7 and 32.5 in the winter and summer, respectively (Whitney & Freeland, 1999).

Macronutrients, including both nitrate and silicate, are controlled primarily by seasonal stratification, replenished in the winter by deep mixing and then drawn down to lower levels in the spring and summer. However, this region is one of three high nutrient, low chlorophyll regions in the global ocean, and macronutrients remain relatively high ($8 \mu\text{M}$ NO_3 and $12 \mu\text{M}$ Si(OH)_4) even at their lowest point, with primary production typically limited by the micronutrient iron (and co-limited in winter by light). Iron is supplied to the central gyre through vertical mixing with the deep water, delivery by mesoscale eddies from the coastal regions to the north and east, and from dust deposition from the atmosphere, though the relative contributions of each source remain uncertain (Harrison *et al.*, 2004).

Advective processes are minimal in the gyre, with heating due to synoptic-scale weather patterns accounting for an order of magnitude more toward temperature changes than advective processes (Denman & Miyake, 1973). In addition, analysis of the major water masses in the region indicates similar salinity, temperature, and nutrient profiles throughout the Alaska Gyre region (north of the Subarctic Current and excluding the shelf region) (Wong *et al.*, 2002). The minimal influence of horizontal processes in this region allows us to simplify the physical model used in this study, which also contributed to our choice of this gyre over regions with more complicated physical dynamics.

Situated in the southeastern part of the gyre at 50°N , 145°W , Ocean Station Papa has been a site of regular physical and chemical data collection in this region for several decades. Weathership measurements of temperature profiles began at this location in 1949, with more regular, reliable physical measurements beginning on 1954 (prior to this, bathythermograph data was of poor precision and lacked accompanying salinity data) (Whitney & Freeland, 1999). Following the discontinuing of weather ships in 1981, measurements at this site were taken over by the Institute for Ocean Sciences in British Columbia, Canada. Measurements have continued at this site, and along the adjacent Line P stations, with data collected 2-6 times per year. The dataset now include measurements from a combination of CTD-based instruments, deep rosette water samples, and vertical mesh tows, and encompass a variety of hydrographic and biogeochemical variables.

The Eastern subarctic gyre region plays a key role in the life cycle of several commercially important fish species, most notably Pacific salmon. Salmon are anadromous species who spend their adult lives in saltwater but migrate upriver to freshwater sites to spawn. Pacific salmon from rivers ranging from the United States and Canada to Russia and Japan all migrate to the subarctic gyres, where they spend 1-5 years in the open ocean growing to maturity and putting on

the majority of their weight. A variety of studies have shown correlations between variability in salmon populations and variability in oceanographic and decadal-scale variability in environmental forcings (Mantua *et al.*, 1997; Beamish & Bouillon, 1993; Beamish *et al.*, 1999; Francis *et al.*, 1998b).

The model developed within this dissertation is intended to look closely at the processes that connect environmental variability and biogeochemistry of a region to the lower and upper trophic level species that rely on the region for food and habitat. The Pacific Eastern Subarctic Gyre presents an intersection of decadal-scale environmental variability with a commercially-important fisheries food web, and provides a relatively high number of both biogeochemical and fisheries datasets over a period of several decades, making it a convenient region to develop a model of this sort.

1.3 Dissertation outline

Including the introduction, this dissertation consists of five chapters, with two additional appendices.

In Chapter 2, we describe the development of the food web model used to represent the many species that inhabit, either continuously or as part of their migrations, our target region. We focus on distilling the necessary components to be considered in our ecosystem model such that it balances the need to incorporate the many complex interactions within the ecosystem while maintaining the simplicity needed for meaningful analysis. We also describe a method for quantifying the high observational uncertainty associated with the many ecosystem parameters included in a model of this complexity.

In Chapter 3, we move to the development of our full end-to-end ecosystem modeling framework, which couples a one-dimensional physical mixed layer model, a biogeochemical model, and an upper trophic level fisheries model. Through a series of model architecture experiments, we demonstrate that the use of a consistent functional response for all predator-prey interactions, as well as the use of density-dependent mortality rates for planktonic functional groups, are important factors in reproducing annual and seasonal observations. We present the results of a 50-year climatological simulation, which demonstrates that under contemporary physical forcing, the model is capable of reproducing long-term seasonal dynamics in primary production and biogeochemical cycling, while maintaining steady-state coexistence of upper trophic level functional groups at levels consistent with observations.

In Chapter 4, we attempt to quantify both the magnitude and the uncertainty of the response of the end-to-end ecosystem model to a bottom-up perturbation, namely an increase in net primary

production due to alleviation of micronutrient limitation. The impact of non-predatory mortality, a process whose magnitude and form remains largely unknown, on the energy flow through the system is quantified and drivers of the amplification of primary productivity perturbations are diagnosed. We find that the relative changes in production at higher trophic levels are amplified under density-independent non-predatory mortality assumptions but damped under density-dependent assumptions. However, the high parameter uncertainty masks this effect in predicted values for most functional groups.

Chapter 5 presents a brief summary of the work, and offers some thoughts on applying complex end-to-end models to management applications.

Appendix A gives a detailed overview of the process equations underlying the physical and biological components of the end-to-end ecosystem model. It also provides a list of the many input variables and datasets used to run the simulations in Chapters 3 and 4.

Finally, Appendix B provides a thorough documentation of the software developed as part of this dissertation. It provides instructions for installing the code, running simulations, and analyzing output. Technical documentation for all functions included in the package is also provided here for reference.

1.3.1 Publication and coauthor contributions

Chapter 3 is in large part a reproduction of Kearney *et al.* (2012), published in *Ecological Modelling* in 2012. A few changes have been made to the text of the introduction and methods sections to avoid redundancy with material presented more fully in this thesis in Chapters 1 and 2. In addition, Appendix A of this thesis includes much of the same text as the appendix in Kearney *et al.* (2012). I am the lead author of this publication; I developed the model, designed and implemented the simulations, wrote the text, and prepared all figures and tables for the manuscript. Coauthors Jorge Sarmiento (my graduate advisor at Princeton University) and Charlie Stock (NOAA's Geophysical Fluid Dynamics Laboratory, Princeton, NJ) provided invaluable advice and feedback throughout the model development and writing process. In addition, Charlie Stock was responsible for development of the original version of the one-dimensional physical model that underlies the final version of the ecosystem model described in this article. Kerim Aydin (NOAA's Alaska Fisheries Science Center, Seattle, WA) generously hosted me at AFSC for two weeks to study his version of the Ecosim code, and allowed me to incorporate the ensemble parameterization concept from his model into my own.

Material from Chapter 4 will be prepared for submission as an article following the completion of this dissertation. I will be lead author, with Charlie Stock and Jorge Sarmiento as coauthors for their advisory roles. The new iron dynamics introduced to the model in that chapter were developed primarily by Charlie Stock for his COBALT model (Stock *et al.*, n.d.), with some modification by myself so that they could be applied in a one-dimensional context. I was responsible for the remaining work, including further code development, running and analyzing simulations, and preparation of text, figures, and tables.

For consistency with the above sections, I use the first person plural throughout this thesis.

CHAPTER 2

Ecopath food web models for the Eastern Subarctic Pacific

The Ecopath with Ecosim model has become a widely-used tool in fisheries science for constructing food web models; the official website for the software (www.ecopath.org) lists over 400 publications based on the this modeling technique to date. The Ecopath idea, originally described by Polovina (1984) and later developed into a more comprehensive software package with additional components for time-dynamic (Ecosim) and spatially-explicit (Ecospace) simulations (Christensen & Walters, 2004), uses the concept of ecosystem mass balance in order to consolidate a wide range of fisheries-based data into a coherent picture of biomass or energy fluxes between various ecosystem components. The mass-balance model consists of a set of linear equations describing the flux of biomass into and out of each functional group in the food web. Depending on the focus of an individual study, functional groups can refer to specific species or more general groups of species that share certain growth and diet characteristics, as well as detrital pools and fishing fleets or gear types associated with the ecosystem. The primary equation for the Ecopath model states that fluxes into a functional group must balance fluxes out of the group or contribute to a known accumulation of biomass:

$$\underbrace{B_i \left(\frac{P}{B} \right)_i}_{\text{production}} = \underbrace{\sum_j \left(B_j \cdot \left(\frac{Q}{B} \right)_j \cdot DC_{ij} \right)}_{\text{predation mortality}} + \underbrace{Y_i}_{\text{fisheries mortality}} + \underbrace{E_i}_{\text{net emigration}} + \underbrace{P_i \cdot (1 - EE_i)}_{\text{other mortality}} + \underbrace{BA_i}_{\text{Biomass accumulation}} \quad (2.1)$$

where i refers to an individual functional group and j refers to the functional groups that prey on it. Table 2.1 on page 9 describes these variables and their typical data sources. Note that the

Table 2.1: Definitions and common sources for the variables in the Ecopath master equation (replicated from Table 2, Aydin *et al.*, 2003). For units, M = mass, A = area, and T = time. The production/biomass ratio is referred to interchangeably in Ecopath-related literature as P/B and PB, with the latter being the variable name used internally in code and occasionally in the documentation manual for the software. Likewise, consumption/biomass is referred to as both Q/B and QB.

Group	Includes	Details
B	Biomass	MA^{-1} Survey estimates, sampling programs, stock assessments
P/B (PB)	Production per unit biomass	T^{-1} Mortality rates, growth rates, bioenergetics models
Q/B (QB)	Consumption per unit biomass	T^{-1} Bioenergetics models, gut content analysis
DC	Diet composition, i.e. fraction of predator's diet composed of each prey	Gut content analysis
Y	Fisheries catch	$MA^{-1}T^{-1}$ Fisheries statistics
BA	Biomass accumulation	$MA^{-1}T^{-1}$ Biomass trend data
E	Net migration	$MA^{-1}T^{-1}$ Migration studies
EE	Ecotrophic efficiency, i.e. the fraction of a group's production that is passed up the food chain. A value of 1 implies that all loss is due to predation; a value of 0 implies that the group has no predators and all loss is due to non-predatory processes, such as old age or disease.	Estimated by Ecopath or set at a standard level to estimate biomass
GE	Gross growth efficiency. $GE = P/Q$	
GS	Fraction of ingested food that is not assimilated.	

inclusion of the biomass accumulation term (*BA*) means that the system does not necessarily need to be in steady state during the period from which data was collected, though often the assumption of stability is made to account for the use of datasets that are not completely contemporaneous (e.g. in this study, data was collected over a period of 10 years). By incorporating as much data as possible for the various groups, the Ecopath mass-balance algorithm is able to create a snapshot of the standing stock of biomass pools and the network of fluxes between these pools such that all mass within the ecosystem is accounted for in a manner consistent with the observations available for the system.

Because of its association with the Ecopath with Ecosim software package, the term “Ecopath model” in the literature is often used to refer not only to the mass-balance checks on input data but also to a suite of time-dynamic predictions of ecosystem changes resulting from different fisheries management strategies that can be run using the EwE software. However, in this thesis, we use the term “Ecopath model” in its original strict sense to refer to a specific set of population data (as listed in Tables A.3 through A.12) that can be run through the Ecopath algorithm to fill in

any missing values and verify that all numbers meet certain balance criteria. In the next chapter, these Ecopath models will be used to calculate parameter constraints for the fully coupled model. Therefore, the first step in developing an end-to-end ecosystem model was to construct an Ecopath model for the Eastern Subarctic gyre region. In this chapter, we will discuss the steps we took to create an ensemble of Ecopath models that isolate the most important trophic linkages in this particular ecosystem and incorporate the high level of uncertainty often associated with complex ecosystems models.

2.1 Capturing uncertainty through an intramodel ensemble

The construction of a typical Ecopath model involves the compilation of a large amount of population-related data, including biomass, production rates, consumption rates, diet fractions, growth efficiencies, and assimilation efficiencies for each functional group included in the model. These data can come from a wide variety of sources, ranging from high-quality scientific surveys to fisheries landing data, empirical relationships, and models. The uncertainty values on these numbers can be very high, up to or beyond an order of magnitude from the point estimates, and accurate measurement of these uncertainties is rare. To compensate for the lack of measured uncertainties, Ecopath input data can be assigned pedigree values based on origin. The pedigree values range from 0 to 1, and correspond to a confidence interval of the point estimate as a fraction of that point estimate. Higher accuracy data, such as that collected by a dedicated stock assessment survey in the region and at the time of interest, is assigned a low pedigree value (e.g. 10% uncertainty), while data collected via less accurate methods or estimated based on other ecosystems or models receive higher pedigree values.

Although the inclusion of pedigree values is relatively common when documenting Ecopath models, the uncertainty information is rarely incorporated into the predicted results deriving from these models (Christensen *et al.*, 2005). However, the wide range of uncertainty of some input values means that often a single simulation based on the mean inputs does not capture the true range of possible outcomes; in many cases even the direction of change in one functional group as a result of a perturbation to a different group cannot be fully ascertained when accounting for the entire input range. Particularly when coupling a predator/prey model to a seasonally-varying biogeochemical model, we found that the parameters derived from a single mean Ecopath model would not necessarily lead to output that represented the mean behavior, with small numerical differences occasionally leading to outlier-type results. Rather than constantly readjusting the hundreds of parameters to

find a single set of perfectly-tuned numbers representative of the entire ecosystem, we instead decided to use an ensemble of Ecopath models to derive our parameters and thereby encompass as much of the potential parameter space as possible.

Following the ideas of Aydin *et al.* (2007), rather than start with a single set of input data for our Ecopath model, we started with parameter ranges. For biomass, production/biomass, and consumption/biomass values, points were chosen from a uniform distribution ranging from the interval $x \pm p * x$, where x is the point estimate for the parameter and p is the respective pedigree value. Diet fraction values were also chosen from uniform distributions, with the same pedigree value applied to all prey components, but then renormalized such that each predator's diet still summed to 1, resulting in normal distributions across ensemble members for each predator-prey diet fraction value. Growth efficiencies, ecotrophic efficiencies, and assimilation efficiency data remained as point values, as these inputs are almost always rough estimates rather than measured values and are rarely published with pedigree data.

Once a single set of input data was chosen from these pedigree-derived ranges, we ran the Ecopath algorithm to test for balance. Balance within an Ecopath model is diagnosed via the ecotrophic efficiency (EE) values for each group, defined as the fraction of net group production that is passed up the food chain to predators. An ecotrophic efficiency value outside the range of 0-1 implies that the system requires an outside sink or source in order to account for all biomass fluxes, and results when input data contradict each other (for example, a predator has a consumption rate that cannot be sustained by the known biomass of its prey). By repeating the process of choosing parameters, testing for balance, and keeping only those models that satisfied the balance criteria, we were able to construct an ensemble of Ecopath food web models that incorporate the potential measurement uncertainty.

2.2 Determining primary energy pathways in a food web

When constructing the Ecopath models for the Eastern Subarctic Pacific ecosystem, we began with a previously published Ecopath model that was developed through series of workshops by the North Pacific Marine Science Organization (PICES) Basin Ecosystem (BASS) Task Team (Aydin *et al.*, 2003); this food web included 48 functional groups, so we refer to it hereafter as the Aydin-48 model. This model, like many Ecopath models developed for fisheries management applications, included a large number of functional groups representing specific managed stocks that from an ecological standpoint occupy very similar niches in the food web. While the resolution of these

stocks can be useful, and sometimes necessary, for fisheries management applications, our study is focused instead on the trophic interactions throughout the food web, and in distilling the processes that can affect the propagation of energy from primary producers to higher levels in the food web; for this purpose, a simpler web that emphasizes only the most important energy pathways is ideal. In addition, while the model framework introduced in the following chapter can in theory be adapted to include complex food webs with a very large number of functional groups and predator-prey interactions, practical limitations such as simulation time and output size favor models with fewer state variables. To this end, we decided to try to reduce the number of functional groups in the food web to as few as possible while still maintaining the major energy pathways through the food web.

The simplification process we developed centered on a hierarchical clustering routine. Each of the 47 functional groups (the bacteria group was eliminated from the Aydin-48 model prior to clustering; see Section A.2.4.1 for details) was assigned a “location” in parameter space quantified by 96 different factors. The first 47 factors described whether a group preyed upon each other group in the food web (1) or not (0), with the following 47 factors representing the reverse, i.e. whether they were eaten by each other group. In earlier versions of the algorithm, we considered using the specific diet input and predatory loss fractions associated with each feeding link, rather than the all-or-nothing logical distinction, but found that the behavior of the clustering algorithm was less desirable with these numbers; a group with small diet fractions spread over a large number of prey items was more numerically similar to another group with mutually exclusive but similarly spread out diet than to one that fed on a subset of its prey in higher quantity. While the logical categorization of prey and predator links was able to isolate most of the energy pathways we needed, a few unwanted links were produced between top predators with few prey items and no predators, and primary producers with few predators and no prey groups; adding trophic level as an additional clustering variable (factor 95) removed these unwanted links. Lastly, we added ecosystem role as a final 96th clustering variable, categorizing each functional group as either a primary producer (0), consumer (4), or detritus (8). The specific values for this final variable were chosen such that all consumers would be more similar to each other than to any producer or detrital group, maintaining the separation necessary such that the proper ecosystem processes (e.g. primary production versus consumption of prey) could be modeled with the resulting clustered groups. The final clustering was performed by calculating the Euclidean distance between each pair of the 47 functional groups over the 96-dimensional clustering parameter space, then building an agglomerative hierarchical cluster tree using single-linkage clustering. The resulting dendrogram is shown in Figure 2.1 on page 13.

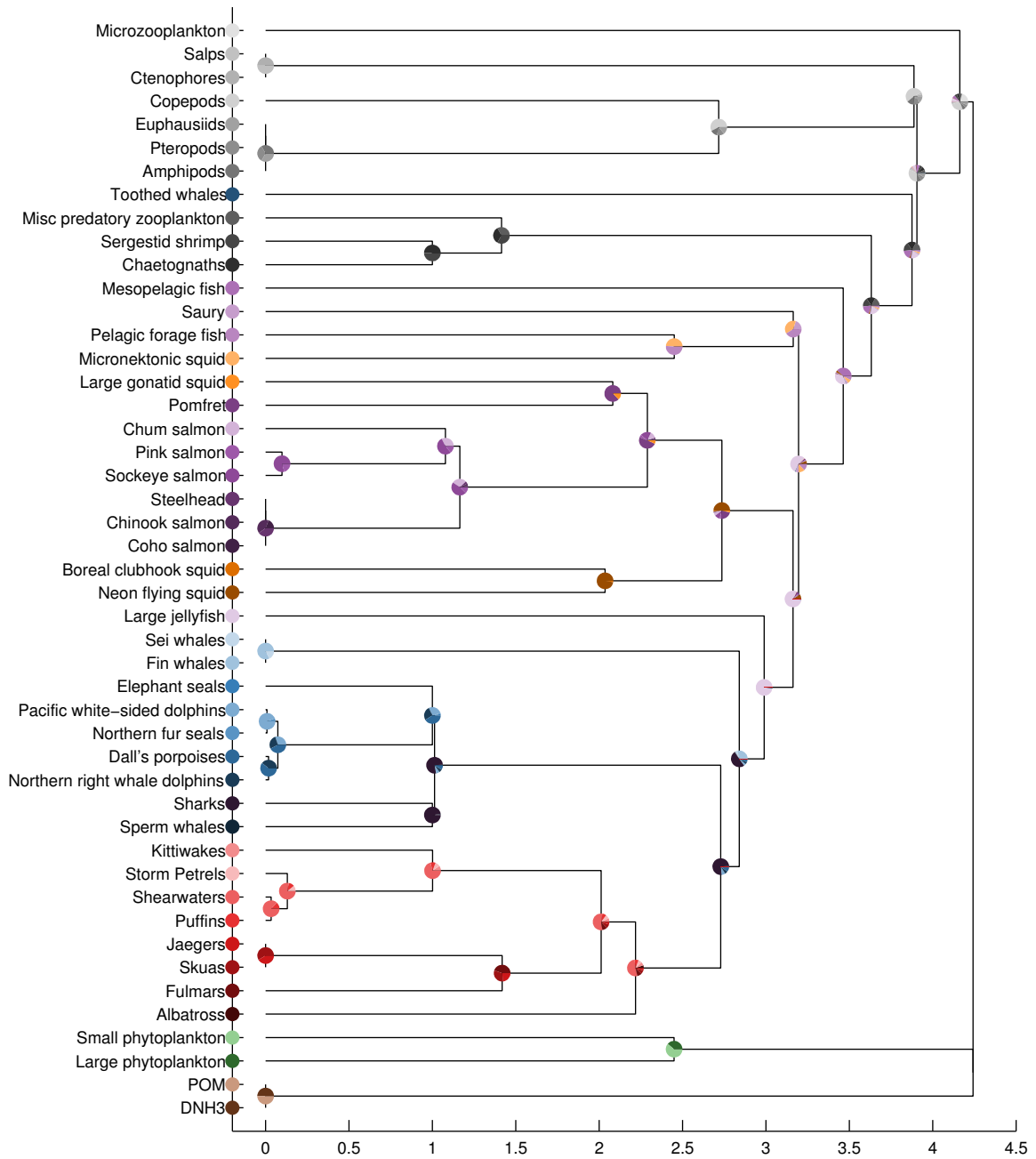


Figure 2.1: Dendrogram showing similarity between the 47 groups in the Aydin-48 Ecopath model, based on shared predator-prey relationships, trophic level, and production level. The horizontal axis shows the Euclidean distance between groups connected by each vertical line. The pie plots at each junction illustrate the relative biomass of all subgroups combined at that point. Colors are provided to distinguish between the major organism types: detritus (brown), phytoplankton (green), zooplankton (grey), fish (purple), mammals (blue), and birds (red).

To create clusters from this dendrogram, we choose a cutoff point; any pairs of groups whose between-group distance is less than this cutoff value are combined into one. In the dendrogram, this can be visualized by drawing a vertical line at a given cutoff value, and tracing each intersected horizontal line to the left; if the horizontal line hits one of the clusters (junctions with pie plots), then those groups will be combined in the resulting clustered food web. The clustering routine created a cluster tree with 39 potential cutoff points, each of which results in a different combination of clustered and unclustered groups. To determine the best cutoff point for our purposes, we began with several diagnostics of ecosystem properties, based on those described by Link (2010b) to ensure that ecosystem network models like Ecopath capture the expected characteristics of marine ecosystems. At each new cutoff point, we generated new Ecopath parameter ranges. The central biomass value for each new clustered group consisted of the sum of biomasses of the contributing subgroups. All other applicable Ecopath parameters, including production/biomass, consumption/biomass, growth efficiency, and ecotrophic efficiency were calculated using an average of the contributing groups' values, weighted by biomass; a value was considered missing (to be solved for by the Ecopath algorithm) only if all contributing groups were missing that value. Pedigree values were also calculated using the biomass-weighted averages of the contributing groups. Using these new Ecopath input parameter central values and pedigrees, we generated 39 sets of food webs, one for each potential cutoff value, with 100 ensemble members each. We then looked at the ecosystem properties of each of these food web sets.

The first property we looked at was the biomass distribution across trophic levels. Link (2010b) suggested that biomass values in a marine ecosystem should span 5-7 orders of magnitude from primary producer to top predator, and that total biomass of all groups at a particular trophic level should decrease 5-10% (on a log scale) with each full step in trophic level. For the following analyses, we define trophic level according to the Ecopath definition, where primary producers are placed at trophic level one, and consumers' trophic levels are calculated as one plus the sum of their prey's trophic levels, weighted by fraction of diet composed by each prey. Based on this definition, trophic level for each group will vary slightly across ensemble members due to variations in diet composition. We found that both the total range of biomass, as well as the change in biomass per trophic level, were robustly maintained by our clustering algorithm up to a very high level of consolidation, only breaking down when the number of functional groups had been reduced below seven (Figure 2.2 on page 15) (at that point in the clustering, almost all upper trophic level species have been combined into one “top predator” group).

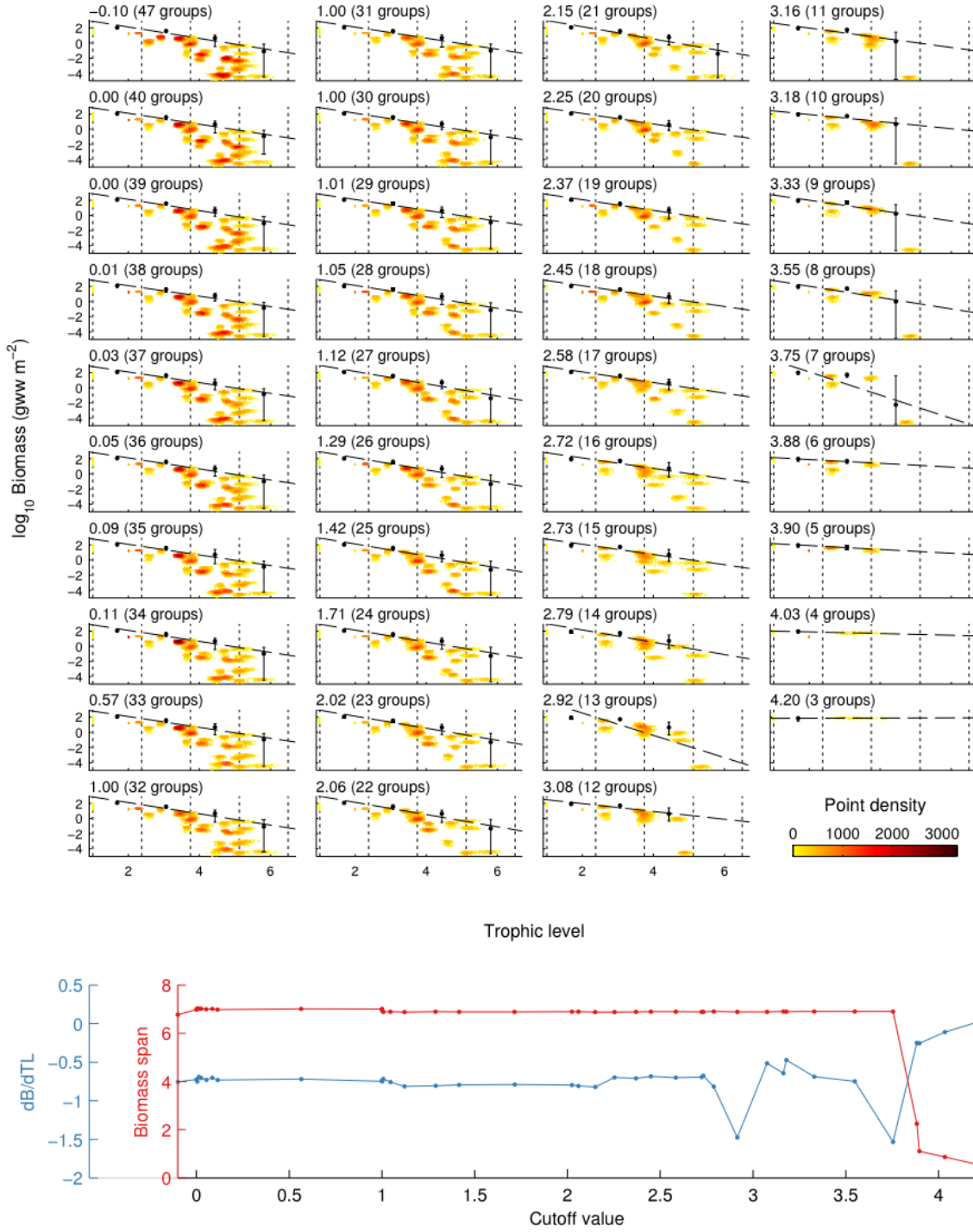


Figure 2.2: We analyzed all potential clustering levels to verify the relationships between biomass and trophic level. The top panels show biomass (on a log scale) versus trophic level for all 39 potential food webs, with each web labeled by the cutoff value used to create the clusters. The colored points indicate the values of individual ensemble members, color-coded by point density, while the black points show the sum of biomass binned as indicated by the vertical dotted lines; error bars indicate the upper and lower limits of these sums across the 100 ensemble members. The lower panel indicates the orders of magnitude spanned by the biomass values within each food web as well as the slope of linear fit for trophic level versus summed biomass.

We next examined the vital rates of functional groups across trophic levels. Like biomass, these rates are expected to decrease across trophic levels in a linear fashion (on a log scale), with lower trophic level functional groups exhibiting higher growth rates, higher consumption rates, and shorter lifespans than long-lived upper trophic level predators. With respect to production rates, we again found that the slope of the production rate versus trophic level line remained relatively constant up to a high level of consolidation, with no substantial changes until the web had been reduced to seven groups (Figure 2.3 on page 17). We also examined the consumption rates of groups in the same manner. However, this particular food web includes a large number of homeothermic species, which require much higher consumption rates to maintain their metabolism than poikilothermic groups occupying a similar trophic level. Therefore, the spectrum data for consumption rates across trophic levels showed two linear trends in the original 47-group model (one that included the poikilothermic fish, squid, and plankton groups, and one for the homeothermic birds and marine mammals), which became difficult to numerically quantify across different levels of clustering as the two lines merged together. Therefore, we chose not to use consumption rate as a metric for cluster choice.

As a final check of the ecosystem robustness across different levels of clustering, we checked to see if each newly-formed cluster group played the same role in passing biomass to different parts of the food web as the original unclustered groups from which they were derived. We looked at the production fluxes into each group, and both the predatory and non-predatory losses from each group, and determined whether the amount passing into and out of each clustered group was approximately the same as the sum of the corresponding fluxes through its subgroups in the unclustered model. We found that overall, the role of each clustered group in redistributing biomass remained very similar, even when the food web was reduced to only three functional groups (Figure 2.4 on page 18).

Having verified that our clustering algorithm maintained the general trophic characteristics of this particular ecosystem up to a very high level of consolidation, we decided to use a cutoff value of 1.5. We felt that this level provided the computational benefits of a smaller number of functional groups while still maintaining recognizable groupings that could be useful for the types of questions we hope to analyze with this model. For example, a group that combines all salmon is sensible for addressing fisheries-related inquiries, while a salmon-squid hybrid (the result of the next higher level of clustering) becomes less practical in this context. Using this cutoff value, we reduced the food web to 24 functional groups.

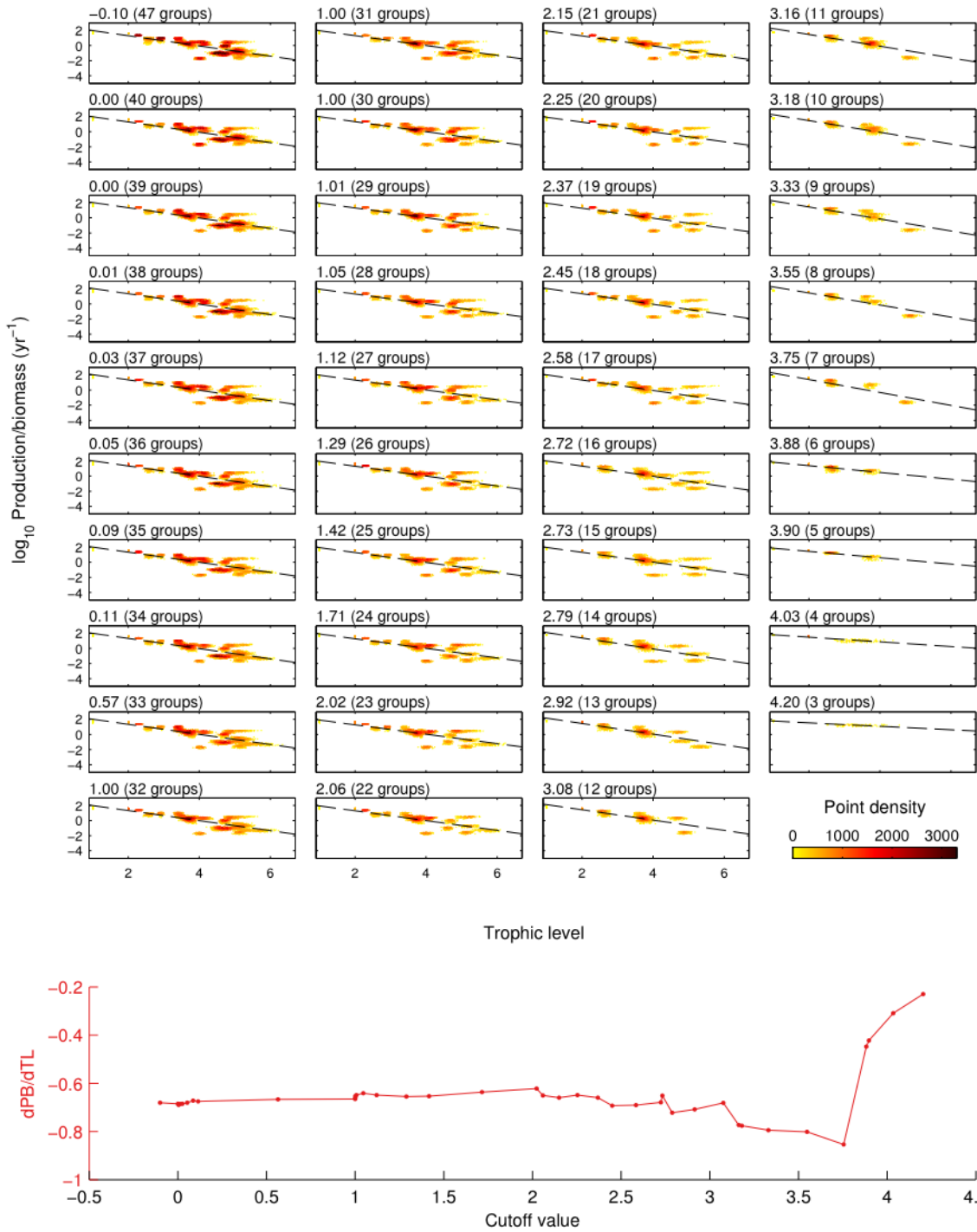


Figure 2.3: Production/biomass ratios are an indicator of the growth rate of each functional group, and are expected to decrease when moving from lower to higher trophic levels. As in the previous figure, production/biomass is plotted versus trophic level for each potential food web. The lower panel indicates the slope of the line fitted directly to the individual ensemble points (unlike biomass, production rates are not additive across trophic levels and thus no binning was performed here).

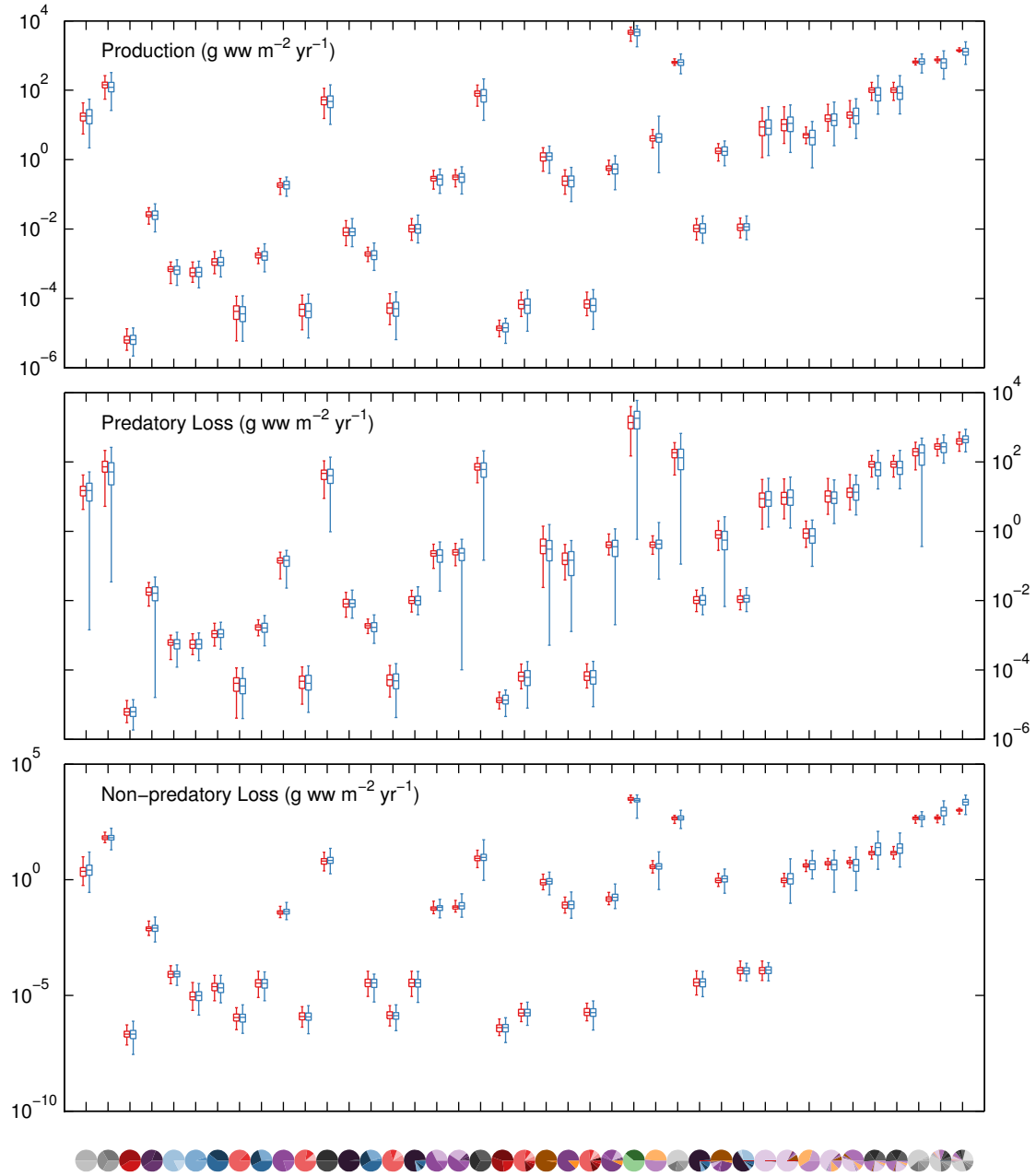


Figure 2.4: Comparison of fluxes into and out of each cluster, both before and after clustering. All box-and-whisker plots indicate minimum, first quartile, median, third quartile, and maximum values across ensembles. The red boxes show the sum of fluxes into (production) or out of (mortality) the groups that make up a particular cluster, using the values from the 47-group unclustered model. The blue boxes show the respective flux for the clustered group where it appears throughout the 39 potential food webs. The pie plot labels along the bottom axis correspond to those from Figure 2.1 on page 13.

2.3 Characteristics of the Eastern Subarctic Gyre food web

Following the simplification and ensemble-generating processes detailed in the previous two sections, we generated a 1000-member ensemble of food webs to represent the 24-group ecosystem of the Eastern Subarctic Gyre, which will provide parameter constraints for the end-to-end model developed in the following chapter (though due to practical limitations only 20-50 ensemble members will be used for those simulations). The 24 functional groups encompass a wide variety of organisms, including 1 detritus, 2 phytoplankton, 5 zooplankton, 5 fish, 1 jellyfish, 4 squid, 3 mammal, and 3 bird groups (Table 2.2 on page 20). Despite the simplification process, the food web remains relatively complex, including 102 different predator/prey interactions (Figure 2.5 on page 21). For an in-depth description of the functional groups and their Ecopath input parameters, see Section A.2.4.1.

A relatively small portion of the Ecopath parameter space as defined by the pedigree-based input ranges serves as a valid source of input parameters, with only approximately 2% of the parameter space leading to a balanced model. Due to the very high dimensionality of this parameter space, it was not computationally possible to compute the analytical bounds of the 171-dimensional manifold that encompasses the “balanced model” parameter space (between biomass, production rate, consumption rate, growth efficiency, ecotrophic efficiency, assimilation rate, and diet fraction inputs, there are 202 input parameters to the mass-balance calculation for this particular ecosystem, 171 of which include pedigree values). However, an analysis of the resulting parameters defining our 1000-member ensemble showed only a few parameters deviated from the uniform or normal distributions they started with after unbalanced models were eliminated (Figure 2.6 on page 22). The upper ends of both the small and large phytoplankton biomass ranges tended to be favored by the balance; the lower end was often too low to support the production required by the rest of the ecosystem. For the same reason, the upper ends of several of the zooplankton groups’ consumption rate ranges were less favored, since those higher rates could not be supported by the given phytoplankton population. The two cannibalistic groups, particularly the neon flying squid, were pushed to the lower end of their consumption rate and the upper end of their biomass ranges, as the positive feedback created by them feeding on themselves easily leads to imbalance. Even within those examples, though, there were no “empty spaces” in the range for any individual input variable.

Similarly, no strong correlations emerged between any two input parameters, with the exception of within-predator diet fraction, which by definition must sum to one and hence will always be

Table 2.2: The simplified food web model includes 24 functional groups, listed below along with the picture used to identify each in the food web diagram (Figure 2.5 on page 21). The type column indicates whether each group is classified as phytoplankton (P), zooplankton (Z), or nekton (K) in the fully-coupled model (see 3.2.2).

Index	Name	Type	Symbol	Consolidated groups
1	Albatross	K		Albatross
2	Mammals and sharks	K		Northern elephant seals, Northern fur seals, Sperm whales, Dall's porpoises, Pacific white sided dolphins, Northern right whale dolphins, Sharks
3	Neon flying squid	K		Neon flying squid
4	Orcas	K		Toothed whales
5	Boreal clubhook squid	K		Boreal clubhook squid
6	Seabirds	K		Skuas, Jaegers, Fulmars
7	Pomfret	K		Pomfret
8	Piscivorous seabirds	K		Shearwaters, Storm petrels, Kittiwakes, Puffins
8	Large gonatid squid	K		Large gonatid Squid
10	Salmon	K		Coho salmon, Pink salmon, Sockeye salmon, Chum salmon, Chinook salmon, Steelhead
11	Baleen whales	K		Fin whales, Sei whales
12	Micronektonic squid	K		Micronektonic squid
13	Mesopelagic fish	K		Mesopelagic fish
14	Pelagic forage fish	K		Pelagic forage fish
15	Saury	K		Saury
16	Large jellyfish	K		Jellyfish
17	Predatory zooplankton	Z		Sergestid shrimp, chaetognaths, Miscellaneous predatory zooplankton (mainly larvaceans and polychaetes)
18	Large zooplankton	Z		Euphausiids, Amphipods, Pteropods
19	Gelatinous zooplankton	Z		Salps, Ctenophores
20	Copepods	Z		Copepods
21	Microzooplankton	Z		Microzooplankton
22	Small phytoplankton	P		Small phytoplankton
23	Large phytoplankton	P		Large phytoplankton

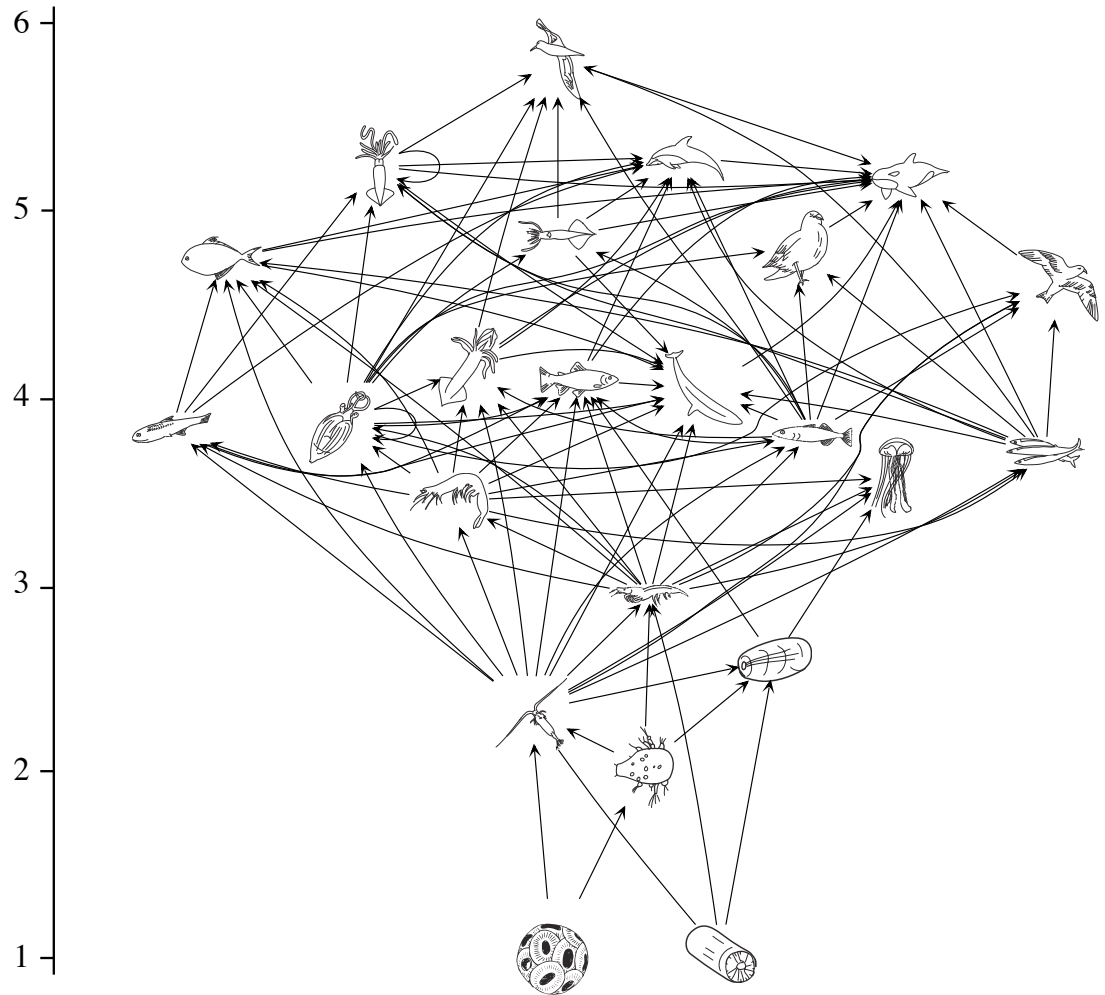


Figure 2.5: The food web used for this study incorporates 23 living functional groups. The axis to the left indicates the trophic level of each group, following the Ecopath definition where trophic level of a consumer is equal to 1 plus the diet-fraction-weighted average of its prey's trophic levels.

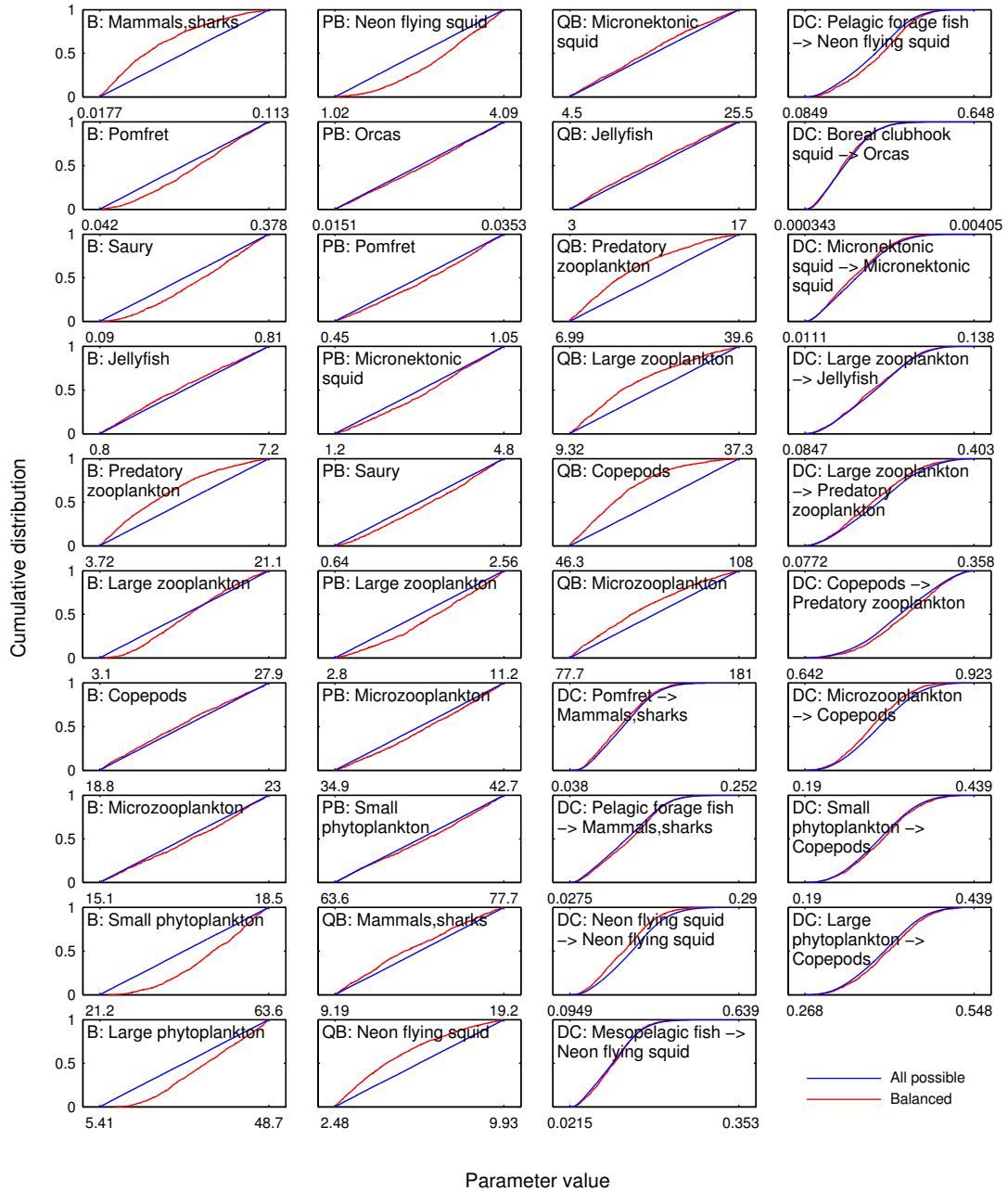


Figure 2.6: Cumulative distribution functions for the Ecopath input parameters that showed a significant difference in their distributions before and after the mass-balance criteria were applied (two-sample Kolmogorov-Smirnov test, $\alpha = 0.05$). Units on the x axis vary based on the parameter being plotted: Production (B) = tons wet weight m^{-2} , Production (PB) and consumption (QB) rates: yr^{-1} , Diet fraction (DC) = no unit.

correlated (Figure 2.7 on page 24). Those correlations that did emerge were weak, and reflected the same skewing towards one end of parameter space discussed in the previous paragraph. For example, the low neon flying squid production/high neon flying squid consumption corner of parameter space is empty, due to the cannibalism of this group, leading to a weak correlation between these parameters. Overall, although the total input parameter space contains far more imbalanced space than balanced, the imbalance is usually caused by the interplay of many different input variables, rather than any of the particular input parameter ranges being implausible in and of themselves. In other words, there are certain pairs (or small groups of three or four) of variables that will never combine to create a balanced model, but no single value of one parameter leads to imbalance any more often than any other.

The parameter ranges encompassed by this particular food web span several orders of magnitude. Functional group biomasses cross over six orders of magnitude, while production rates span almost four (Figure 2.8 on page 25), both of which reflect the typical span in a pelagic marine ecosystem (Link, 2010b). Similarly, the transfer of biomass follows the expected pattern, with an average of 17% transfer of biomass per trophic level (Figure 2.9 on page 26), from primary producers to top predators. This is on par with ecological theory, which suggests a transfer efficiency of approximately 10% per trophic level (May & McLean, 2007). The breakdown of fluxes into and out of each group, including predatory consumption, production (i.e. primary production for producers, and the product of consumption and growth efficiency for consumers), predatory mortality, and non-predatory mortality, can be seen in Figure 2.10 on page 27. These fluxes, along with biomass, will be used to constrain the process equations for the end-to-end model developed in the next chapter.

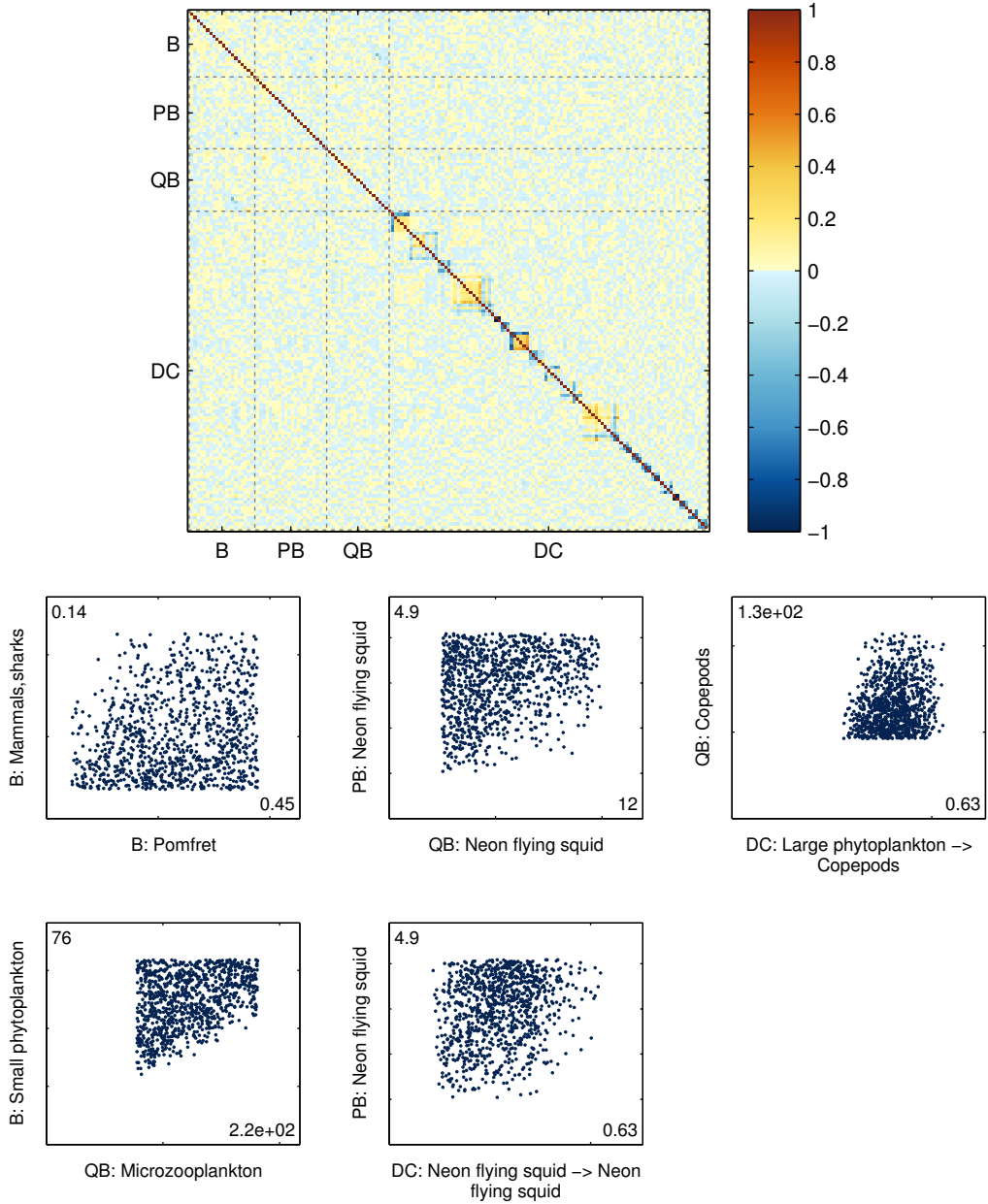


Figure 2.7: Correlation analysis for all Ecopath input variables with pedigree values. The top plot shows the Spearman's rank correlation coefficients between each pair of input variables; this quantifies whether a monotonic trend exists between the two variables. The box-like features along the main diagonal are the locations of the within-predator diet fractions; because a predator's diet must sum to one, these will always be correlated. Beyond these, only 5 pairs of parameters were significantly correlated, as shown in the bottom five panels; x- and y-axes range from 0 to the marked values.

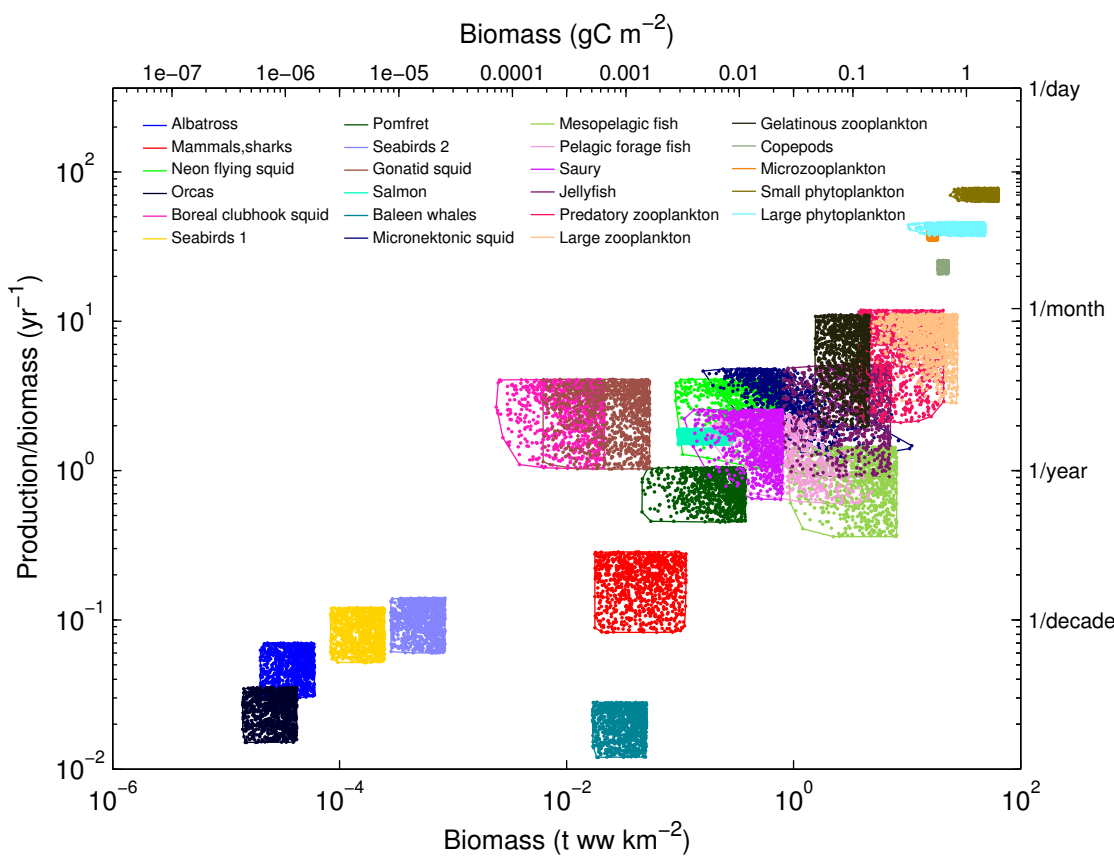


Figure 2.8: Both biomass and production rate span several orders of magnitude in this food web. The colored dots represent the specific parameter values found in the 1000-member ensemble; the convex hull outlines around each set of points are provided to clarify areas of high overlap.

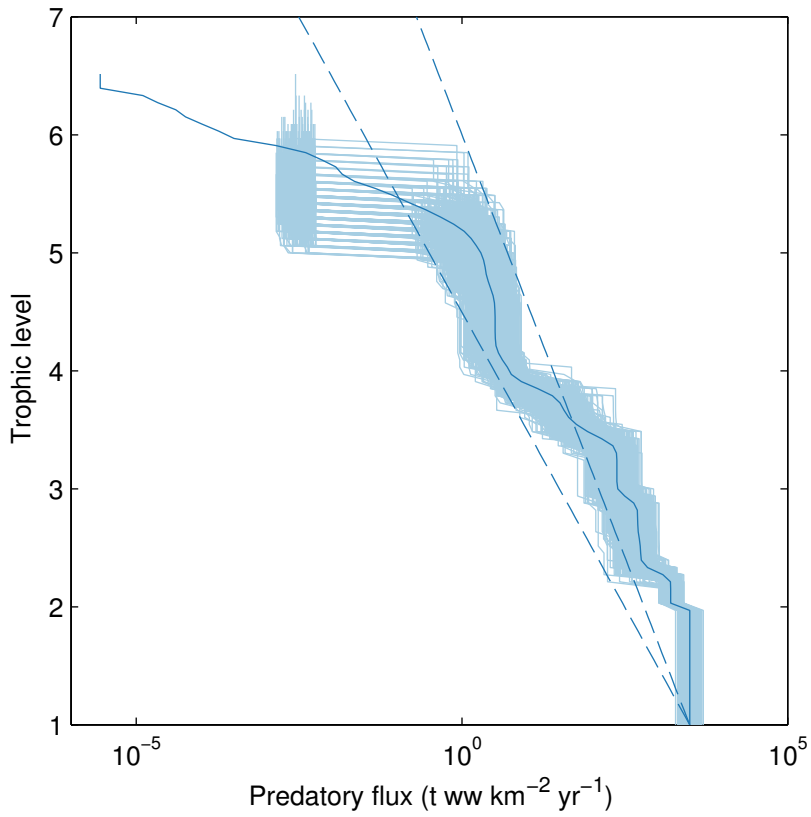


Figure 2.9: Flux of biomass due to predation past each trophic level for individual ensembles (light blue) and the ensemble mean (dark blue). Flux is calculated by summing all fluxes that span a given trophic level throughout the food web. The dashed lines are provided for reference and show the trend expected if energy transfer was exactly 10% or 20% per trophic level.

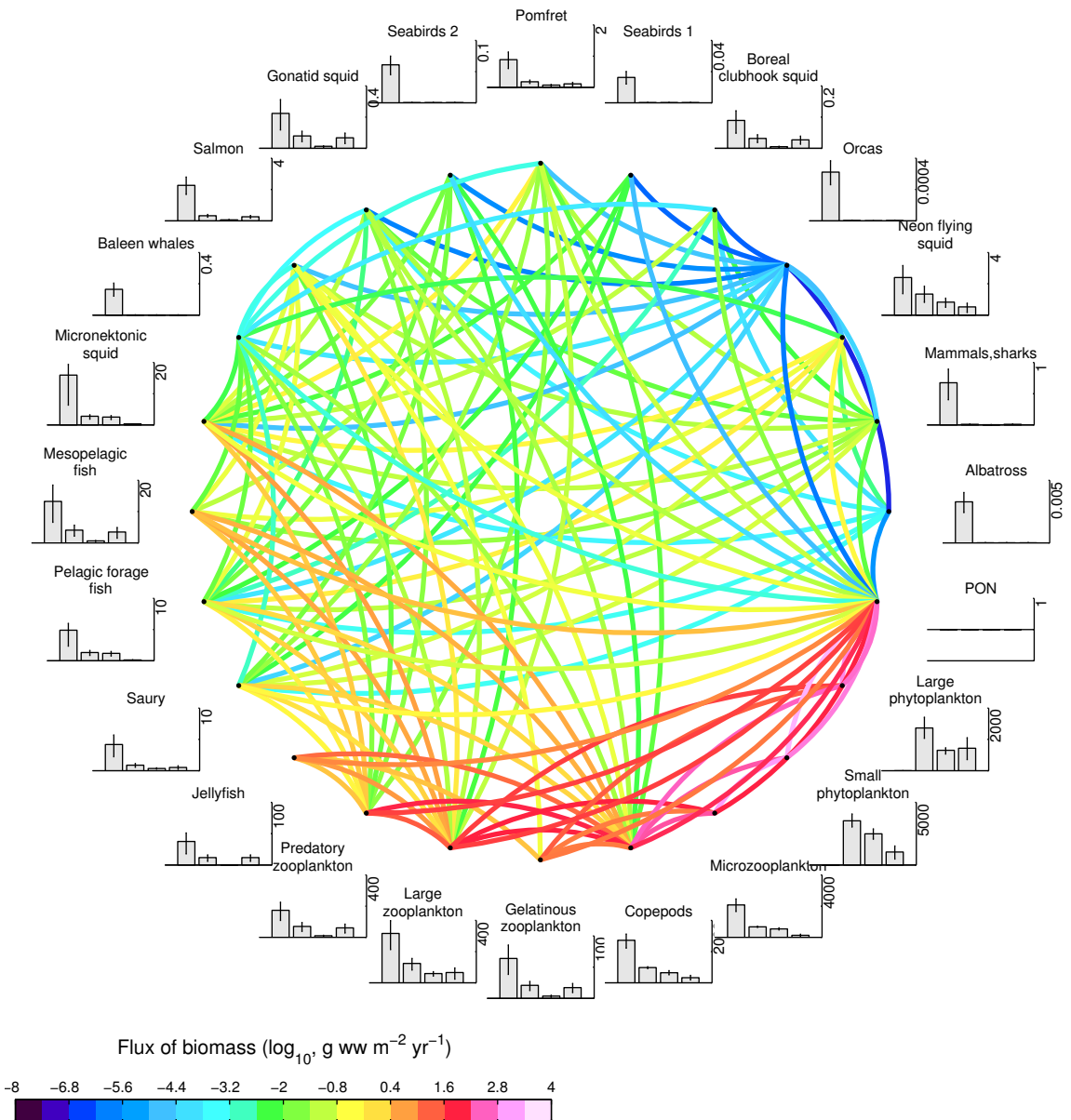


Figure 2.10: This directed graph shows the fluxes of biomass between all functional groups in the 24-group food web. Colored lines indicate ensemble mean predator/prey fluxes between the 23 living groups, as well as primary production fluxes from the detritus group to primary producers, and non-predatory mortality fluxes from all living groups to the detritus pool; lines curve counterclockwise from source group to sink group. The bar graphs show, from left to right, the total prey consumption, total production, predatory loss, and non-predatory loss, in g wet weight $m^{-2} \text{yr}^{-1}$; the error bars indicate the 25th-75th percentiles across ensembles. Axes range from 0 to the value labeled to the right of each axis.

CHAPTER 3

Coupling planktonic ecosystem and fisheries food web models for a pelagic ecosystem

3.1 Introduction

In the past decade, fisheries management efforts have placed increased emphasis on ecosystem-based management, where the interactions between a target stock species and its physical and biological environment are considered in addition to sustainability of the stock itself (e.g. Link, 2010a). At the same time, global-scale climate models that historically focused only on physical and biogeochemical variables are increasingly incorporating biological variables (Denman *et al.*, 2007). With these shifts, the historical separation between climate modeling and fisheries modeling is closing, with increased interest in the concept of end-to-end models, i.e. models that incorporate dynamics from physics to top predators (Travers *et al.*, 2007; Fulton, 2010).

In their review of over fifty different fisheries models, Keyl & Wolff (2008) demonstrated that the incorporation of environmental and climate variability in almost all cases increased the predictive power of the model. They also noted that in many cases, the use of a climate index, such as the Pacific Decadal Oscillation (PDO) or North Atlantic Oscillation (NAO), had more predictive power than any single local environmental variable, such as sea surface temperature, due to the collective nature of a climate index in incorporating many different physical changes. However, while climate indices can demonstrate correlation between climate variability and ecosystem dynamics, they fail to provide a mechanistic link between the physical and biogeochemical changes and higher trophic level dynamics. Such mechanistic linkages are particularly essential for reliable projections of climate

change impacts as the baseline upon which empirical relationships are based changes (Stock *et al.* , 2011).

A variety of modeling methodologies have been introduced in recent years to resolve the mechanistic connections between environmental variability and upper trophic level dynamics (Travers *et al.* , 2007; Plaganyi, 2007; Fulton, 2010). Some of these couple biogeochemical-physical models to species-focused individual-based or bioenergetics models, e.g. the SEAPODYM model for tuna (Lehodey *et al.* , 2008) and the NEMURO.FISH model for herring and saury(Megrey *et al.* , 2007). While this allows for detailed investigation of the effect of the environment on the target fish species, most models of this type do not explicitly resolve ecosystem dynamics between the modeled fish species and its predators and competitors, or take into account community reorganization that could result from changing climate. Other efforts have added lower trophic level forcing with modeled or observed primary production to established food web models, such as with Ecopath with Ecosim (Christensen & Walters, 2004) and ATLANTIS (Fulton *et al.* , 2004a,b); this allows resolution of feedbacks between various functional groups in an ecosystem in response to climate variations, but does not allow two-way feedback of these effects back down to the level of primary production or biogeochemistry. Size-based efforts, such as APECOSM (Maury, 2010) provide a simple framework to look at flows through the entire food chain, though they lack resolution of individual species or functional groups.

Here, we introduce a modeling structure that combines a fisheries food web model, a biogeochemical model, and a physical model into a fully-coupled end-to-end ecosystem model. The goal of this framework is to represent the primary trophic interactions of an ecosystem and their response to both bottom-up climate variability and top-down predation changes in a fully integrated manner. The challenge in constructing a model of this type derives from the high level of uncertainty associated with measurements and calculations of upper trophic level feeding and growth parameters, as well as the sensitivity of lower trophic level plankton dynamics to mortality rates that are altered by direct modeling of upper trophic level predation (Yoshie *et al.* , 2007). Furthermore, differences in modeling approaches that traditionally have been used for plankton ecosystems versus fisheries food webs can exacerbate these issues by introducing subtle dynamical differences that lead to significant changes over long time scales. We will describe an approach that addresses these challenges, producing an ensemble of simulations capable of reproducing long-term seasonal dynamics in primary production and biogeochemical cycling, while maintaining steady-state coexistence of upper trophic level functional groups at levels consistent with observations under contemporary physical forcing.

Critical aspects of the coupling between plankton ecosystem and fisheries food web models that are required to achieve such robust simulations are identified through a series of sensitivity tests.

3.2 Methods

3.2.1 The water column ecosystem model framework

The end-to-end ecosystem model framework developed here is based on three different components: a one-dimensional physical mixed layer model component, a lower trophic level biogeochemical component based on the NEMURO model (Kishi *et al.*, 2007b), and an upper trophic level food web component based on the Ecopath with Ecosim model (Christensen & Walters, 2004). The three components are fully coupled, allowing the simulation of feedbacks between the physical environment and all levels of the food chain.

3.2.1.1 The physical model

The physical model used in this study simulates the seasonal evolution of a one-dimensional water column, resolved vertically and forced at the surface by winds, shortwave radiation, and air and dew point temperatures. Simulations were run under climatological conditions at a single location (Ocean Station Papa, 50°N, 145°W). Because advective processes are minimal in the gyre, a one-dimensional model can capture the predominant processes at this location (Denman & Miyake, 1973), and analysis of the major water masses in the region indicates similar salinity, temperature, and nutrient profiles throughout the Alaska Gyre region (north of the Subarctic Current and excluding the shelf region) (Wong *et al.*, 2002). Therefore, for our purposes, we consider this one-dimensional water column to be representative of the entire gyre region.

Salinity is relaxed towards a depth- and time-resolved timeseries on a 7-day timescale, which allows salinity profiles to respond to storm events (2-3 days) but preserves the seasonal evolution of the salinity field. Observed winds are translated to surface wind stresses using the bulk formulae of Large & Pond (1981). Latent and sensible heat fluxes are calculated from the wind speed, air-sea temperature difference, and dew point temperature using the bulk formulae of Friehe & Schmitt (1976). Longwave radiation losses are calculated using the Efimova formula, per Simpson & Paulson (1979). We assume 45% of the incoming shortwave radiation is photosynthetically available, with a background attenuation of 0.15 m^{-1} ; self-shading by phytoplankton is applied within the primary production calculations but does not feed back to the physical state variables. Mixing is calculated

following the Mellor-Yamada 2.5 algorithm with a background diffusivity of $1.0 \times 10^{-4} \text{ m}^2\text{s}^{-1}$, over a water column of 500 m depth with a vertical grid spacing of 10 m. See A.1 for further details of the physical model formulation.

3.2.1.2 The lower trophic level biogeochemical model

The NEMURO (North Pacific Ecosystem Model for Understanding Regional Oceanography) model is a nutrient-phytoplankton-zooplankton model developed to study the interactions between the planktonic communities of the North Pacific and their environment. The model tracks 11 state variables: small and large phytoplankton; small, large, and predatory zooplankton; nitrogen in the forms of particulate and dissolved organic nitrogen (PON and DON, respectively), nitrate (NO_3^-), and ammonium (NH_4^+); and silica as particulate opal and silicic acid (Si(OH)_4) (Kishi *et al.*, 2007b). Since its origin, many variations on the NEMURO model have been developed (Werner *et al.*, 2007; Kishi *et al.*, 2010). These include spatial variations ranging from surface-layer only (Kishi *et al.*, 2007b) or one-dimensional water column physics (Fujii *et al.*, 2007) to three-dimensional regional models (Aita *et al.*, 2007); versions that incorporate the carbon cycle (Fujii *et al.*, 2007); and NEMURO.FISH, which adds a bioenergetic component for certain fish species (Megrey *et al.*, 2007).

In this study, we use a version of the NEMURO model based on Kishi *et al.* (2007b) with a few modifications. First, we replaced the Steele light curve (Steele, 1962) with a Platt curve (Platt & Jassby, 1976), reducing the effect of photoinhibition at higher light levels. We raised the maximum grazing rate of small zooplankton from 0.4 day^{-1} to 0.8 day^{-1} to be consistent with observed allometric relationships for zooplankton (Hansen *et al.*, 1997). In order to reflect the difference in sinking behavior between small phytoplankton, which usually have low export- and f-ratios, and larger phytoplankton whose blooms sink and contribute to export out of the surface layer, we rerouted half of the small phytoplankton non-predatory losses from the particulate sink (PON) to the dissolved nitrogen pools (DON and NH_4^+). We also rerouted the egestion of microzooplankton to the dissolved nitrogen pools to be consistent with the observed importance of microzooplankton egestion to dissolved organic matter (Nagata, 2000). Finally, we lowered the silica dissolution rate to $1/(23 \text{ day})$, in line with globally-averaged surface observations (Van Cappellen *et al.*, 2002).

In addition to these parameter adjustments, we introduced a simple iron cycle to the model. In previous versions of NEMURO, iron limitation has been approximated through parameterization by reducing the growth rates of iron-limited phytoplankton (Denman & Pena, 1999). The Eastern Subarctic Gyre is a high-nutrient, low-chlorophyll region where iron plays a key role in limiting growth,

and we found we were unable to create a simulation that produced realistic large phytoplankton (diatom) blooms while also maintaining surface nutrients at observed levels without explicitly including the effects of iron limitation. Therefore, we added additional iron dynamics following the model of Fiechter *et al.* (2009). This model adds an iron limitation term to the already-existing nitrogen, silica, and light limitation terms that moderate gross primary production; iron limitation is based on the iron to carbon ratio within phytoplankton cells, and allows for luxury iron uptake during iron-rich conditions.

In addition to its incorporation into the fully coupled model described below, this version of NEMURO was used for comparison and parameterization purposes. Tables A.13 through A.20 include the full list of parameters used when running our NEMURO in its standalone form. In this form, it is run within the physical model described above but not coupled to any upper trophic level dynamics. Loss to higher trophic levels is approximated through a quadratic mortality closure term.

3.2.1.3 The upper trophic level model

The upper trophic level model is based on the Ecopath model for the Eastern Subarctic Gyre ecosystem, as described in detail in Chapter 2.

The Ecopath models themselves do not provide time-dynamic simulations, but rather a single snapshot of the fluxes within an ecosystem at a given point in time. The Ecosim model, which is the second component in the Ecopath with Ecosim software package, uses these snapshots to calculate time-varying predictions in the populations of each functional group. It does this by assigning functional forms to each flux process (predation, non-predatory mortality, etc.), then constraining the parameters based on the Ecopath mass-balance values.

For example, predation of one group on another is generally assumed to be a function of both the predator group and prey group biomass: $Pre_{ij}(t) = f(B_i(t), B_j(t))$, where $Pre_{ij}(t)$ is the flux due to predation from group i to group j at time t , and $B(t)$ is the biomass of a group at time t . The simplest form of this function would assume a simple linear relationship, as in a classic Lotka-Volterra system, with the function f in the form $aB_i(t)B_j(t)$. Our Ecopath model provides values for Pre_{ij} , B_i , and B_j at time $t = 0$, allowing us to assign a value to the coefficient: $a = Pre_{ij}(0)/(B_i(0)B_j(0))$. We use this parameter-constraint process to calculate functions associated with grazing, predation, and non-predatory mortality processes in our model. In addition, the mass-balance biomass values serve as initial biomass values for all ensemble members. We shy away from naming this portion of the model “Ecosim”, since we have chosen different functional forms for our process equations than

can be found in the Ecosim software package; however, the concepts underlying our upper trophic level model and that one are the same.

For this study, we used a 50-member ensemble of Ecopath models; each ensemble member starts with a slightly different set of parameters constraining these three flux processes, as well as slightly different values of initial biomass. In the absence of any external forcing, these processes would remain in steady-state, i.e. no change in biomass would be seen for any functional group. This particular property of Ecosim-like models underlies our goal of maintaining steady-state values over decadal timescales with our fully coupled model.

3.2.2 Coupling the model components

The coupled biogeochemical-lower trophic level-upper trophic level model, referred to hereafter as the water column ecosystem (WCE) model, merges aspects of both the NEMURO model and an Ecopath-derived food web model to create an end-to-end ecosystem model. The nutrient state variables were drawn from the NEMURO model. The remaining living state variables are classified into three types: phytoplankton (P), zooplankton (Z), or nekton (K) (Figure 3.1 on page 35). The designation of living functional groups as either planktonic or nektonic reflects both their relationship to the physical model and their interactions with other functional groups. The planktonic label refers to any group whose movement is strongly influenced by the movement of the water in which they reside; these groups are resolved with depth, can feed only on functional groups occupying the same depth layer as themselves, and are subject to mixing via advection and diffusion in the same manner as all physical tracers. The nektonic label refers to all other living organisms, including those that do not live in the water but feed on marine organisms (such as birds); these groups are not subject to any mixing, and they feed on the integrated sum over depth of their prey groups.

The plankton/nekton distinction can be difficult to make since nearly all organisms are generally capable of some movement relative to advective and mixing processes. In this context, it is used to distinguish those functional groups whose foraging distance over a single model time step (3 hours) is comparable to or less than the physical model resolution (10 m) and therefore limited to a single grid cell, and whose distribution in the water column can be important to their feeding, versus those whose foraging covers multiple grid cells and is not strongly depth-dependent. Therefore, for the purposes of the WCE model, zooplankton are designated as planktonic even if they are capable of vertical migration; vertical movement can be parameterized through the sinking/rising

rate parameter in the physical model if necessary to capture the dynamics of a particular ecosystem. The impact of these assumptions will be discussed in Section 3.3.1.

For the fully-coupled model, 23 of the 24 functional groups from the Ecopath food webs described in the previous chapter were used as state variables, with the detrital group being discarded in favor of the more detailed nutrient cycling from the NEMURO model. These 23 groups encompass 2 phytoplankton groups, 5 zooplankton groups, and 16 nekton groups. Both phytoplankton groups and three of the zooplankton groups in the Ecopath model fill the same functional roles as the five plankton groups in the NEMURO model.

Figure 3.1 on page 35 displays a schematic of the processes linking the state variables to each other. A brief description of each process type can be found in Table 3.1 on page 36, with detailed process equations in A.2. Most of these processes were exclusive to a single parent model component; gross primary production, phytoplankton respiration, extracellular excretion, and decomposition are only explicitly modeled in NEMURO, while non-depth-resolved consumption is included only in Ecopath. Egestion and excretion by consumers are modeled identically in both models as a fraction of consumption. However, planktonic consumption and non-predatory mortality differ in several fundamental ways between the two parent models:

1. Resolution: NEMURO models all fluxes volumetrically (biomass per volume), while Ecopath models are typically built using depth-integrated units (biomass per area).
2. Grazing/predation functional response: NEMURO uses a thresholded Ivlev functional response for zooplankton grazing and predation, while Ecopath with Ecosim models use a foraging arena functional response (Walters *et al.*, 1997) for all predator-prey consumption, including that between planktonic groups.
3. Effect of temperature on rates: In NEMURO, almost all rate processes, including grazing, predation, and mortality, are affected by temperature, increasing exponentially with increasing temperature. The standard implementation of Ecopath with Ecosim does not include any direct effects of temperature (though time forcing and trophic mediation timeseries can be used to approximate this effect).
4. Mortality: In NEMURO, non-predatory mortality is proportional to the square of the biomass, while Ecopath with Ecosim uses a linear mortality function.

When building the WCE model, decisions regarding how to treat these differences proved very important in determining the stability and realism of the final model. A set of experiments using

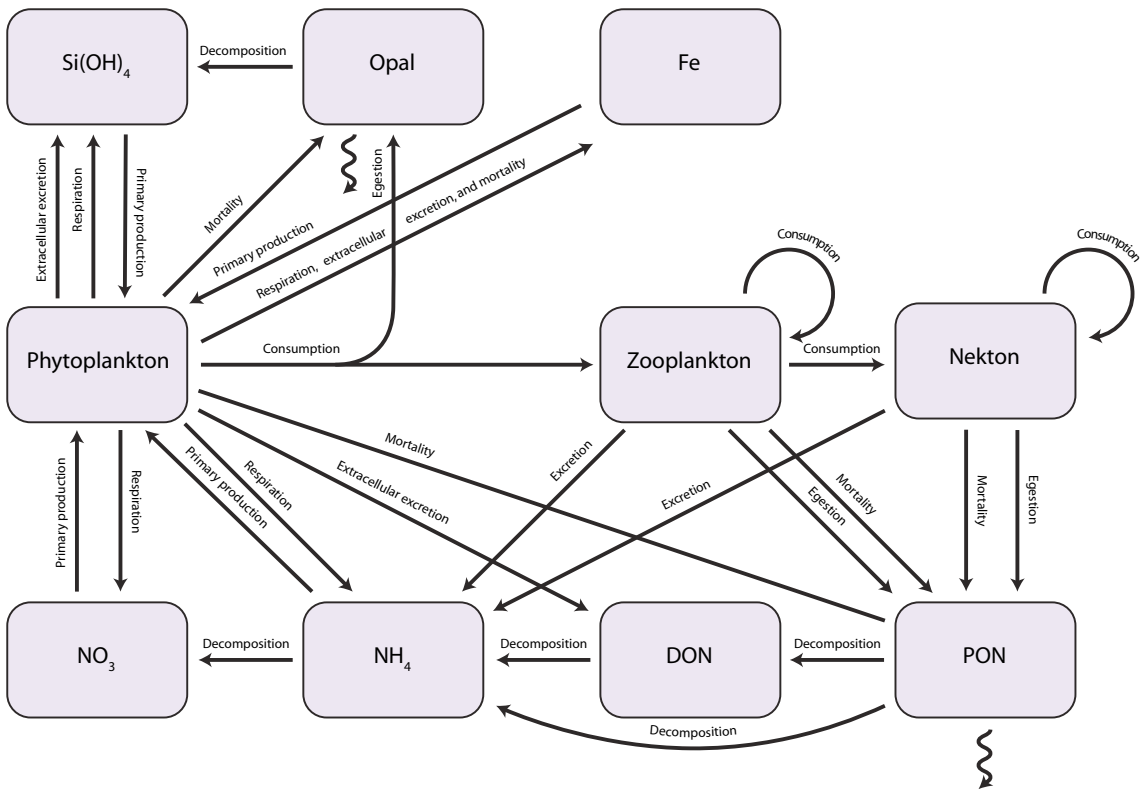


Figure 3.1: The WCE model includes 7 non-living state variables and 3 categories of living state variables; arrows indicate the flow of nitrogen, silica, and iron between these state variables. Zigzag arrows indicate sinking of material through the water column. Note that the phytoplankton, zooplankton, and nekton boxes in this schematic indicate variable classes that represent several different state variables. The phytoplankton groups included in the model include three different nutrient compartments, for nitrogen, silica, and iron content (non-diatom phytoplankton groups can be parameterized so that their growth is not dependent on silica). Zooplankton and nekton groups include only nitrogen compartments. Nitrogen and silica are conserved in the model; the iron cycle includes only partial remineralization, and is also relaxed toward a constant profile to approximate advective and airborne sources, and therefore is not conserved.

Table 3.1: The process variables in this table describe the various types of fluxes connecting the physical and biological variables in the water column ecosystem model.

Process	Variable	Parent component	Description
Gross primary production	Gpp	NEMURO	Function of light, temperature, and nutrient concentration, following Kishi <i>et al.</i> (2007b) and Fiechter <i>et al.</i> (2009)
Respiration	Res	NEMURO	First-order relationship to biomass, with Q10=2 temperature effect, following Kishi <i>et al.</i> (2007b)
Extracellular excretion	Ex	NEMURO	First-order relationship to gross primary production, following Kishi <i>et al.</i> (2007b)
Planktonic consumption	Con	NEMURO and Ecopath	Variation of foraging arena functional response, parameterized where applicable to mimic NEMURO Ivlev functional response, with Q10=2 temperature effect
Nektonic consumption	Con	Ecopath	Variation of foraging arena functional response
Non-predatory mortality	Mor	NEMURO and Ecopath	Second-order relationship to biomass.
Luxury iron uptake	Ufe	NEMURO	Follows Fiechter <i>et al.</i> (2009)
Egestion	Ege	Ecopath	First-order relationship to consumption
Excretion	Exc	Ecopath	First-order relationship to consumption
Decomposition	Dec	NEMURO	First-order relationship to concentration (i.e. biomass), with a Q10=2 temperature effect

different coupling strategies was conducted to identify the key features essential for robust simulations on climate time scales. A list of the different model architectures we tested can be found in Table 3.2 on page 41. We started with a “brute force” baseline coupling between the NEMURO and fisheries food web models (Section 3.2.2.1), resulting in a model that contains inconsistencies between formulations of closely interacting groups. We then took steps to increase the internal consistency of the planktonic and nektonic formulations, and to evaluate the necessity of additional mortality regimes for plankton and nekton groups (Section 3.2.2.2, Section 3.2.2.3).

3.2.2.1 The baseline case

We started with an Ecosim-style model and replaced all fluxes that overlapped with NEMURO, namely grazing and predation by microzooplankton (small zooplankton ZS in NEMURO), copepods (large zooplankton ZL), and large zooplankton (predatory zooplankton ZP), as well as net primary production, with the corresponding process functions from NEMURO. We opted to use the Ecosim-derived linear form for mortality for all groups, on the assumption that a linear form would be more applicable to a system where all predator-prey relationships are explicitly resolved rather than being modeled implicitly through quadratic loss terms.

3.2.2.2 Consistent feeding formulations across planktonic groups

For its grazing and predation processes, the NEMURO model uses a thresholded Ivlev curve of the form

$$I = m(1 - \exp(-\lambda(B - B_{thresh}))) \quad (3.1)$$

where m is a maximum grazing rate, λ is the Ivlev constant, B_{thresh} is the threshold prey concentration for grazing to occur, B is the biomass of prey, and I is the ingestion rate of prey per unit predator. The upper trophic level model, on the other hand, uses the foraging arena functional response (Walters *et al.*, 1997) as modified by Aydin:

$$ConI_{ij} = Q_{ij}^* \left(\frac{X_{ij} \cdot \frac{B_{intj}}{B_j^*}}{X_{ij} - 1 + \frac{B_{intj}}{B_j^*}} \right) \left(\frac{D_{ij} \cdot \left(\frac{B_{inti}}{B_i^*} \right)^{\theta_{ij}}}{D_{ij} - 1 + \left(\frac{B_{inti}}{B_i^*} \right)^{\theta_{ij}}} \right) \quad (3.2)$$

where the subscripts i and j represent the prey and predator groups, respectively. Note that Eq. (3.2) calculates the total consumption flux from prey to predator, such that the ingestion rate (similar to I in Eq. (3.1)) would be equal to $\frac{ConI_{ij}}{B_j}$. The parameters in this functional response are derived from the Ecopath model for the food web being modeled: Q^* is the mass-balanced depth-integrated consumption between two groups, and B^* is the mass-balanced depth-integrated biomass of a group. The remaining parameters in Eq. (3.2), i.e., X , D , and θ , are non-dimensional parameters that control the shape of the functional response curve.

Qualitatively, the Ivlev and foraging arena formulations differ in several ways (Figure 3.2 on page 39). In NEMURO, the maximum grazing rate parameter (m) is temperature-dependent, while the consumption parameter in Ecosim (Q_{ij}^*) is fixed over time. The Ivlev formulation calculates an ingestion rate that is independent of the predator biomass, while the foraging arena ingestion rate can be modulated by both the prey and predator biomasses, with the parameter X defining the strength of the predator-related term. As X approaches infinity, the predator-related portion of Eq. (3.2) disappears, creating a linear relationship between grazing rate and number of predators for a constant amount of prey. However, if X is set to a lower number, the grazing rate versus predator density relationship saturates. A lower value of X can be used to approximate predator avoidance behaviors of prey, which effectively make only a small portion of a prey population vulnerable to predation (Walters *et al.*, 1997). With X equal to infinity, the foraging arena functional response

simplifies to a classic Holling Type 2 ($\theta = 1$, Eq. (3.3)) or Holling Type 3 ($\theta = 2$, Eq. (3.4)) functional response:

$$\frac{Con_{ij}}{B_j} = \frac{mB_i}{k + B_i} : m = \frac{Q_{ij}^* D_{ij}}{B_j^*}, k = B_i^*(D_{ij} - 1) \quad (3.3)$$

$$\frac{Con_{ij}}{B_j} = \frac{mB_i^2}{k^2 + B_i^2} : m = \frac{Q_{ij}^* D_{ij}}{B_j^*}, k = B_i^* \sqrt{D_{ij} - 1} \quad (3.4)$$

Eq. (3.3) and Eq. (3.4) are similar in shape to the Ivlev functional response, but with different treatment of ingestion rates at low prey densities.

Because the food web used in this study includes five planktonic groups that overlap with the NEMURO model and two that do not, the baseline version of the coupled model included a mix of these two functional responses. In order to achieve internal consistency, we wanted to choose a single functional response that is consistent with the Ecopath mass-balance formulation used to parameterize the rest of the model while also remaining consistent with the NEMURO formulation, which we know produces reasonable seasonal dynamics. To accomplish this, we modified the foraging arena functional response so that it could be applied to either nektonic or planktonic functional groups links. We first converted the Ecopath-derived parameters to volumetric terms to correspond to the units of planktonic groups within the WCE model. It is necessary to make an assumption about the depth distribution of planktonic organisms in order to convert the outputs of Ecopath into these per-volume quantities. The WCE model uses an average mixed layer depth, MLD , to make this conversion, so $Q' = \frac{Q^*}{MLD}$ and $B' = \frac{B^*}{MLD}$. The MLD parameter is also used to set initial concentration profiles for all planktonic groups in the model.

To parameterize this response for planktonic groups, the NEMURO model zooplankton responses were used as the target functional response curves for all predator-prey interactions found in both the Eastern Subarctic Gyre ecosystem described above and the NEMURO model. The shape of the thresholded Ivlev curve can be best approximated by the grazing response used in the water column ecosystem model (Eq. (3.2)) when X is set to infinity and θ to 2, creating a sigmoidal type 3 functional response (Figure 3.2 on page 39). The remaining parameter, D , is then calibrated so that the maximum grazing rates and half-saturation concentrations are as close as possible between the sigmoidal curve and Ivlev curve (Figure 3.3 on page 40).

For the final formulation, we also reintroduced the Q10 temperature effect from NEMURO by assuming that the mass-balanced values correspond to the rates under average mixed layer temper-

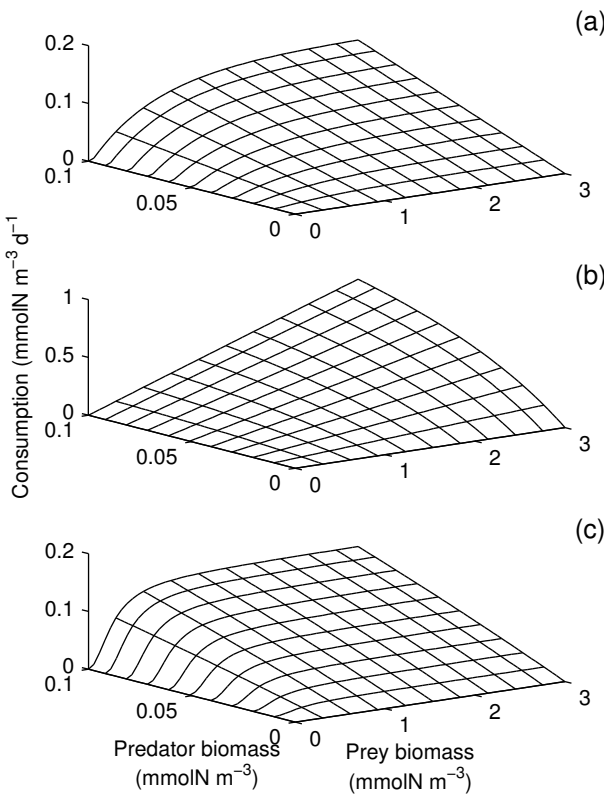


Figure 3.2: Under their default parameter choices, the functional responses used in the NEMURO model and the Ecopath with Ecosim model differ greatly from each other. The Ivlev response varies linearly (type 1) with increasing predator biomass and follows a type 2 relationship with increasing prey biomass. The foraging arena response can vary between linear (high X) and type 2 (low X) with increasing predator biomass, and linear (high D) and type 2 (low D , $\theta = 1$) or type 3 (low D , $\theta = 2$) with increasing prey biomass. With careful choice of parameters, the two functional responses become quantitatively very similar. Shown here are a) the thresholded Ivlev functional response for ZS grazing on PS in the NEMURO model, b) the foraging arena functional response for microzooplankton grazing on small phytoplankton, with Ecosim default values $D = 1000$ and $X = 2$, and c) the planktonic version of the foraging arena response used for WCE, where X and D have been calibrated so that the functional response has the same maximum grazing rate and half-saturation constant as the Ivlev response ($X = 10$, $D = 2.234$).

ature conditions. This assured that all planktonic groups shared one consistent grazing functional response while also replicating the lower trophic level dynamics of the NEMURO model.

3.2.2.3 Density dependent mortality

In many biogeochemical models, a density-dependent mortality rate is used to capture predation losses from predators not explicitly resolved by the modeled system (e.g. Steele & Henderson, 1981). In the baseline scenario, we adopted a linear mortality rate because we had resolved all upper trophic level predation losses. However, density-dependent mortality can also arise for zooplankton due to

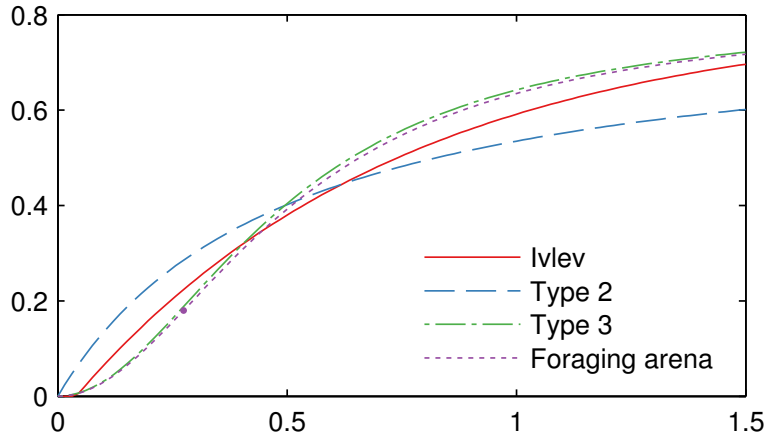


Figure 3.3: The functional response for copepods grazing on large phytoplankton is shown here as an example of the functional response fitting process. Shown for reference are the NEMURO-derived Ivlev curve for this feeding link, as well as Holling Type 2 and Type 3 curves with identical half-saturation constants (i.e. $k = \frac{\ln 2}{\gamma}$). The Ecopath mass balance constrains the foraging arena functional response to pass through the yearly-averaged biomass vs. consumption rate, indicated by the purple dot, so we fit the parameter D such that the resulting curve is as close as possible to the target Type 3 curve while respecting this constraint.

egg cannibalism (Ohman & Hirche, 2001), and for phytoplankton due to aggregation (Thornton, 2002) and viral loss (Brussaard, 2004). Classic stock-recruitment theory also suggests that net reproduction rates for many fishes peaks at an intermediate population, suggesting an increased mortality rate at higher population densities (Ricker, 1954). A nonlinear mortality rate may be needed to capture all of these processes, though the precise form is uncertain. Due to the lack of specific data to constrain our choice, we tested the model with both linear and quadratic mortality formulations.

3.2.3 Simulations and model evaluation

To evaluate the water column ecosystem model, we ran two series of simulation experiments. The first was a series of 20-yr simulations used to determine a robust coupling strategy. Once we had chosen a satisfactory architecture, we used a 50-yr simulation to further validate the model against observations.

The 20-yr simulations included six different sets of simulations, each using one of the model architectures outlined in Table 3.2 on page 41. Shortwave radiation, air temperature, and wind speeds were extracted from the Coordinated Ocean-ice Reference Experiments (CORE) normal-year datasets (Large & Yeager, 2009). Dew point temperature was derived from the same dataset. A climatological salinity cycle was derived from the GECCO model's 1950-2000 salinity product; initial

Table 3.2: We ran the water column ecosystem model with a variety of different formulations for the grazing, predation, and mortality fluxes.

Run	Predator-prey functional response	Mortality formulation
1 (baseline)	Ivlev curve for NEMURO-derived interactions, foraging arena for all others	linear
2	modified foraging arena	linear
3	Ivlev curve for NEMURO-derived interactions, foraging arena for all others	quadratic for plankton, linear for nekton
4	modified foraging arena	quadratic for plankton, linear for nekton
5	Ivlev curve for NEMURO-derived interactions, foraging arena for all others	quadratic
6	modified foraging arena	quadratic

profiles for both salinity and temperature were set to the climatological January profiles derived from the same product.

We quantified the success of each model architecture based on its ability to maintain yearly-averaged biomass values for all functional groups within the uncertainty ranges used for the initial conditions over the entire 20-yr simulation period. These initial biomass ranges reflect a compilation of the sparse observations of standing stock biomass available for the region, and therefore a model forced by average seasonal conditions should not deviate from these ranges.

Once we determined the best choice of model architecture, we further validated the model with a 50-year simulation, again using climatological forcings, and compared the results against a broader suite of observations from the Eastern Subarctic Gyre region. The majority of these observations come from Ocean Station Papa. This location has been a site of regular physical and chemical sampling since the 1950's, thus allowing us to validate the lower trophic level biogeochemical results of the WCE model. We looked at several characteristics of the region in order to measure the skill of our model, including annual and seasonal macronutrient concentrations and drawdown, annual and seasonal primary production, and annual standing stock biomass for all living groups.

3.3 Results

3.3.1 Choice of model architecture

When running the baseline model simulation, we immediately encountered problems with competitive exclusion. For the particular ecosystem discussed here, the gelatinous zooplankton group biomass dropped well below the initial level within five years, with approximately 25% of the ensemble runs showing complete extinction of this group (Figure 3.4 on page 43, architecture 1).

The exclusion resulted due to the overlapping prey preferences of the gelatinous zooplankton group (a non-NEMURO plankton group) and the large zooplankton group (a NEMURO-derived group). The difference between the numerical formulation for feeding behavior for the NEMURO- and non-NEMURO-based plankton groups granted a spurious competitive advantage to large zooplankton over gelatinous zooplankton. In this particular ecosystem, the consolidation of the food web via cluster analysis (Section 3.2.1.3) led to a minimal amount of overlap between diets of the modeled functional groups, and therefore the problem only manifested itself for one particular functional group. However, Ecopath models are often designed to resolve the dynamics of dozens of individually-managed stocks that occupy very similar trophic niches. When applied to such a complex ecosystem, we would expect these spurious exclusions to increase.

Applying the modified foraging arena functional response consistently to all groups allowed all plankton groups to coexist (Figure 3.4 on page 43, architecture 2). However, even with the internally-consistent functional responses, several plankton groups tended to wander outside their initial biomass ranges over the 20-yr simulation period. While the yearly-averaged biomass of the phytoplankton groups fell within the target ranges, the seasonal dynamics often departed from observations (not shown), with small phytoplankton showing an unrealistically large spring bloom along with a fall bloom not seen in observations in this location. The small phytoplankton blooms propagated up the food chain, with microzooplankton and large zooplankton increasing above their target ranges, while copepods and gelatinous zooplankton dropped below theirs.

Switching to a quadratic mortality function for all plankton groups produced much more realistic phytoplankton blooms and brought all zooplankton groups within their target ranges (Figure 3.4 on page 43, architecture 4). This may suggest that density-dependent mortality terms not linked to higher predators are indeed important factors to consider when modeling planktonic functional groups. The population dynamics of nektonic groups, on the other hand, were relatively unaffected by the switch between linear and quadratic mortality rates (Figure 3.4 on page 43, architectures 4 and 6).

We also found that the use of the quadratic mortality term could mask the inconsistencies in the mix of grazing functional responses used in the baseline scenario. Simply applying quadratic mortality to planktonic groups, and leaving the mix of functional responses (Figure 3.4 on page 43, architectures 3 and 5), could bring most ensemble members within the target ranges. However, the spread between ensemble members tended to be wider in this case, and a few simulations also created fall blooms under this architecture. Overall, the combination of a consistent predation functional response for all groups, as well as a quadratic mortality rate for all plankton groups,

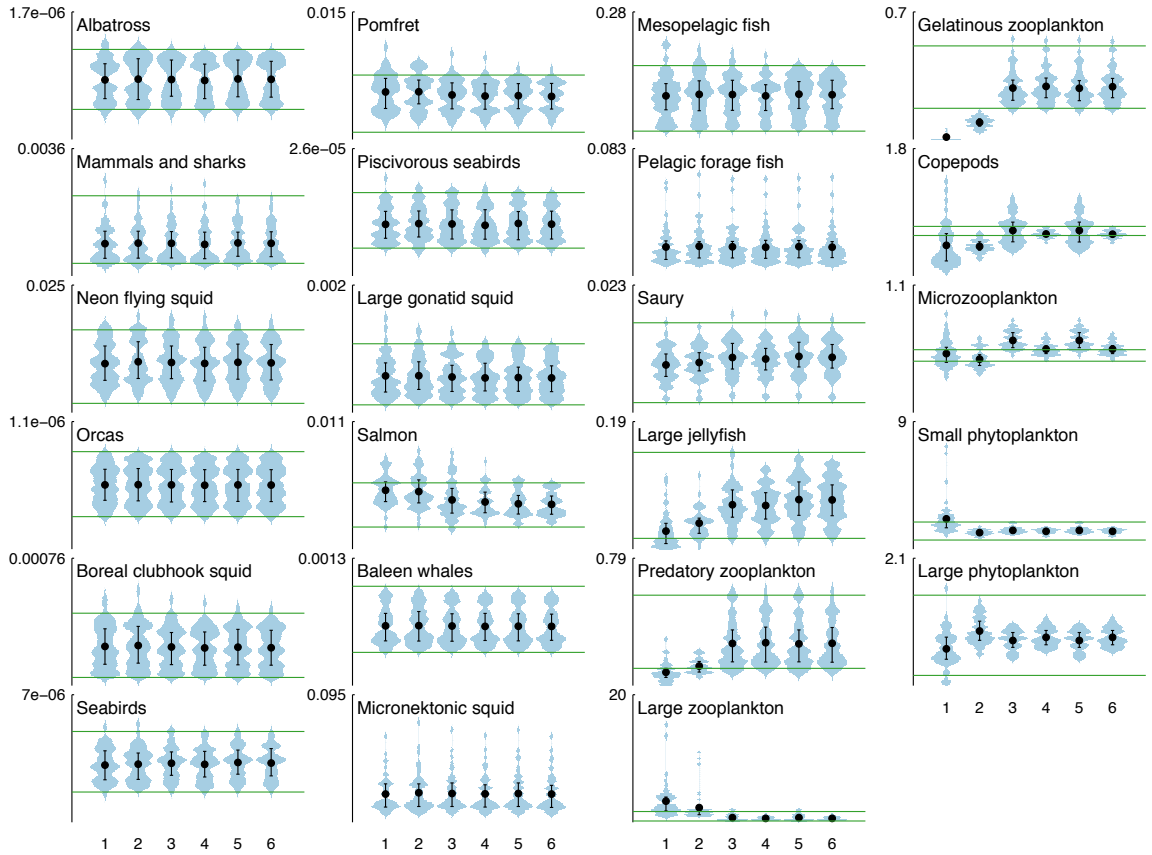


Figure 3.4: As an initial test of model architecture skill, we looked at whether each model was capable of maintaining the biomass of all living state variables within the uncertainty ranges used to choose initial conditions over a 20-yr simulation. The blue violin plots display the distribution of biomass across the 50-member ensemble at the end of each 20-yr simulation; width indicates the relative number of ensemble members at a given biomass value. The black bars indicate the interquartile range of the ensembles, with the black circle indicating the ensemble mean. Green horizontal lines show the upper and lower values of the target biomass ranges (micronektonic squid and pelagic forage fish are estimated by Ecopath rather than being assigned target ranges, and therefore are missing these lines). Vertical axes represent integrated biomass, ranging from 0 to the labeled value, in g C m⁻². The horizontal axis indicates the model architecture indices, which correspond to those found in Table 3.2 on page 41.

proved necessary to consistently reproduce both the target yearly-averaged biomass values as well as the proper seasonal dynamics for lower trophic level groups. For simplicity, in our final architecture, we chose to use a quadratic mortality rate for nektonic groups as well; results using a linear mortality for nekton are similar.

3.3.2 Validation of final model

An ensemble of 50-yr simulations was run to look more closely at the seasonal dynamics of the final model architecture over multi-decadal timescales. In this section we compare surface nutrient concentration, primary productivity, and functional group biomass of the simulations to a variety of measurements collected from the Eastern Subarctic Gyre region.

3.3.2.1 Surface nutrients

Ocean Station Papa is characterized by seasonal stratification, which plays a large role in controlling macronutrient concentrations in the surface ocean at this location. Increased winds and decreased surface temperatures lead to deep mixing in the winter months (Nov. - Feb.), with the mixed layer depth reaching 90-120 m and allowing replenishment of nitrate and silicate to the mixed layer. In the summer, stratification increases and the mixed layer shoals to approximately 40 m. The increased light levels along with plentiful macronutrients allow phytoplankton to bloom, leading to nutrient drawdown as the summer months progress. Typical nitrate drawdown, from peak winter level to lowest summer level, is 7 mmol m⁻³ nitrate and 10-11 mmol m⁻³ silicate . This region is a high nutrient, low chlorophyll region, with phytoplankton production primarily being limited by iron and light, so surface levels of nitrate and silicate remain high even during the summer (Whitney & Freeland, 1999; Harrison *et al.* , 2004).

Maintaining surface nutrient concentrations consistent with observations requires both that the model properly replicates the seasonal deepening and shoaling of the mixed layer, and that it maintains the proper assemblages of phytoplankton. In particular, the seasonal changes in ratios between small phytoplankton that do not use silica, and diatoms (large phytoplankton) that do, will affect the relative drawdown of nitrate and silicic acid. Modeled nitrate drawdown in the WCE model ranges from 6.90 - 9.22 mmol m⁻³ over the ensemble members, with an average drawdown of 8.27 mmol m⁻³, and annually-averaged surface nitrate levels stabilize at 14.90 - 21.84 mmol m⁻³, consistent with observations. Silicate drawdown varies more widely between ensemble members, from 8.78 - 13.83 mmol m⁻³, but the ensemble average of 12.17 mmol m⁻³ is very near the drawdown seen at Ocean Station Papa (Figure 3.5 on page 45). Surface concentrations of silica tended to drift a bit over the 50-year span of the simulations, reaching levels between 8.69 - 36.84 mmol m⁻³. However, because neither nitrate nor silicate serve as the limiting growth factor for phytoplankton, drifts in surface concentrations of either nutrient over the 50-year simulations did not affect the production

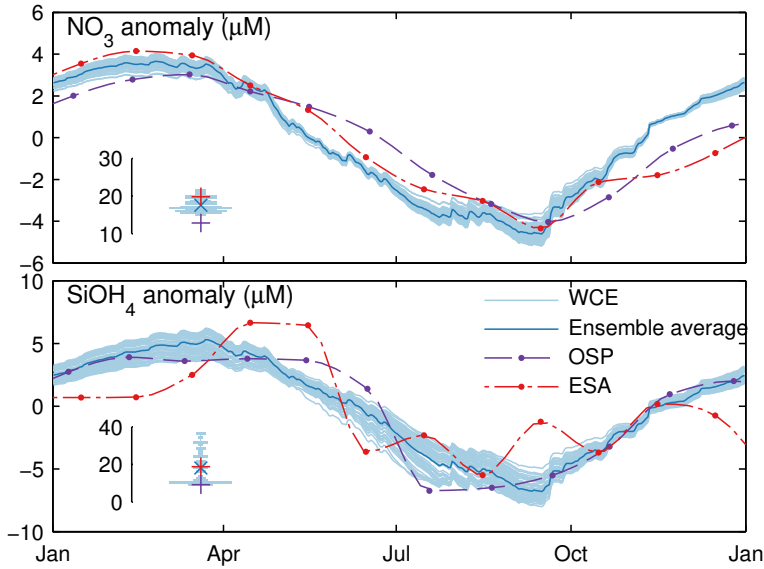


Figure 3.5: Modeled surface nutrient anomaly from yearly average over one simulation year versus observations at Ocean Station Papa. Observations for Ocean Station Papa (OSP) reflect measurement at this location over the period of 1969-1981(Whitney & Freeland, 1999). Also shown are the WOA05 climatological surface nitrate anomaly values averaged over the entire Eastern Subarctic Gyre (ESA) region (Garcia *et al.*, 2006). Inset figures show the histograms of yearly-averaged values at the end of the 50-year simulation period, along with the corresponding yearly-average for each observation dataset.

level or standing stock of phytoplankton, and therefore did not lead to drift in any of the other state variables.

3.3.2.2 Productivity

Measurements of productivity at Ocean Station Papa have varied over time, from $60 \text{ g C m}^{-2} \text{ yr}^{-1}$ during the earlier sampling period from 1960-1976, $140\text{-}170 \text{ g C m}^{-2} \text{ yr}^{-1}$ in studies conducted during the mid-1980's to early 1990's, to a higher summer value of $215 \text{ g C m}^{-2} \text{ yr}^{-1}$ during the JGOFS surveys of 1992-1997 (Harrison *et al.*, 2004). There is debate regarding whether the range in values results from the development of more accurate clean sampling techniques for the later measurements (Fitzwater *et al.*, 1982), or whether it (or some of it) reflects an actual change in productivity over this time period. Seasonally, observations show between a doubling and tripling of productivity between winter and summer (Boyd & Harrison, 1999). The modeled WCE productivity, with an annual average ranging between 122.04 - 145.8 and averaging $136.1 \text{ g C m}^{-2} \text{ yr}^{-1}$ over all ensemble members, falls within the range seen in observations. (Figure 3.6 on page 46).

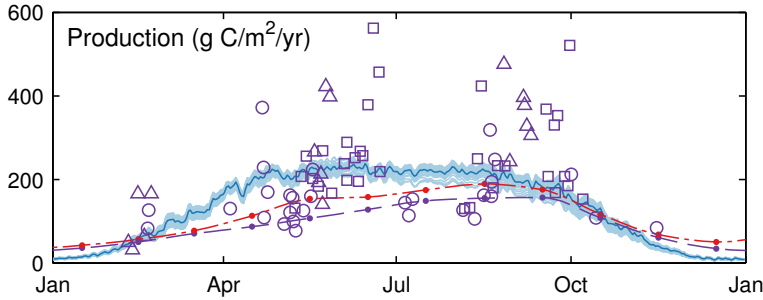


Figure 3.6: Modeled net primary production over one simulation year. For comparison, net primary production values estimated by the Eppley-VGPM model applied to SeaWiFS data near Ocean Station Papa (purple dashed) and over the entire Eastern Subarctic Gyre (red dash-dot) are also shown, as well as measured production values at Ocean Station Papa as compiled by Boyd & Harrison (1999) (squares, circles, and triangles indicate data from three different studies, as described in Boyd & Harrison (1999, Figure 7)).

3.3.2.3 Biomass of living groups

As with the initial 20-year simulations, we considered the model successful at capturing upper trophic level dynamics if it was capable of maintaining yearly-mean biomass levels within the initial uncertainty ranges over the entire simulation. Over all 50 ensemble members, only very small drifts out of this range were observed over the 50-year climatological simulation, indicating that this parameterization scheme is stable over decadal timescales (Figure 3.7 on page 47).

3.4 Discussion

In recent years, a large number of different modeling approaches have been applied to the end-to-end problem, and have been compared and contrasted in several reviews (Fulton, 2010; Travers *et al.*, 2007). The complexity of these model frameworks and the processes they resolve cover a wide spectrum. In creating the water column ecosystem model, we intended to create a tool capable of analyzing ecosystem response to environmental perturbations at both the bottom and top of the food chain. The model presented here has a combination of strengths that make it valuable for diverse climate-ecosystem applications.

It provides a true two-way coupling between upper and lower trophic level species, nutrient cycling, and physics, allowing full analysis of the interacting effects of bottom-up climate effects and top-down predation and fisheries effects. The coupling includes both propagation of effects through

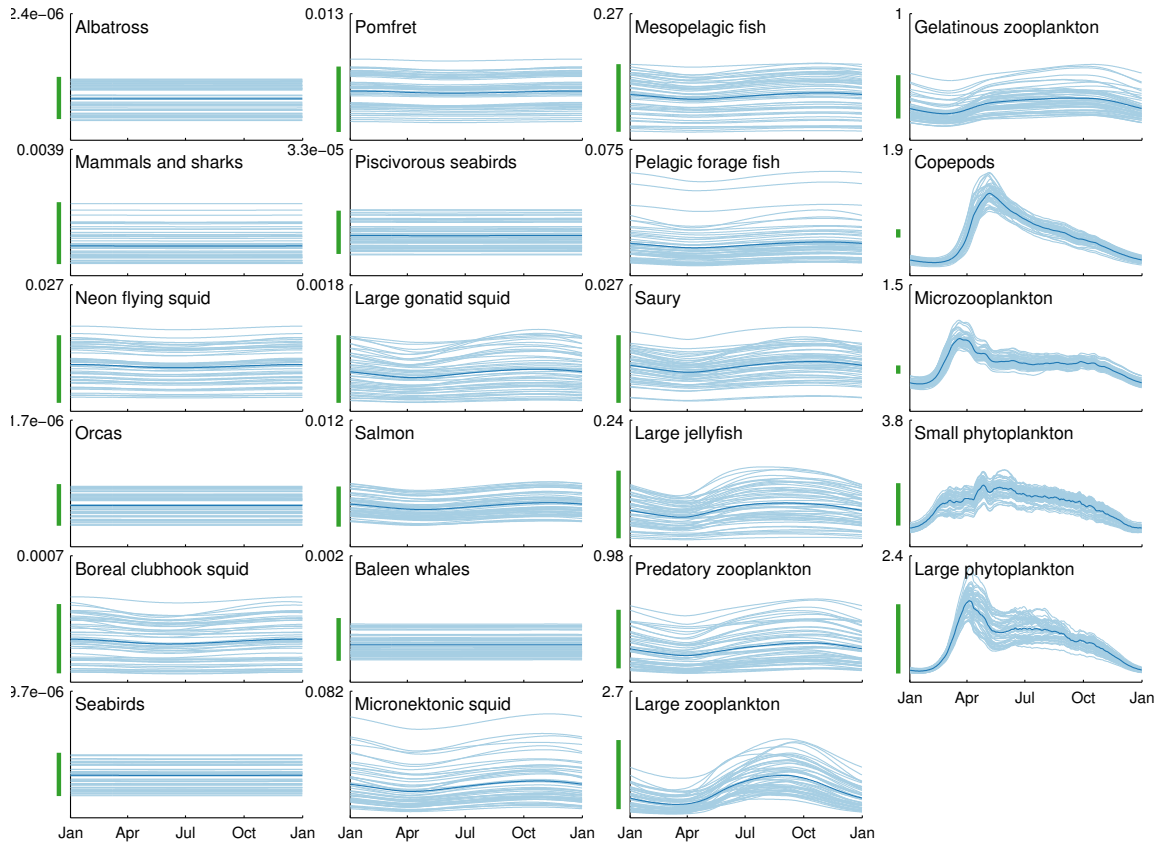


Figure 3.7: Vertically-integrated biomass, in g C m^{-2} , for all living functional groups in the model over the final year of simulation. The green bars to the left of each axis correspond to the yearly-mean biomass ranges from Table A.10 on page 91 used to initialize biomass for each group. Axes are scaled such that pedigree values are consistent between groups, i.e. green bars of equal length indicate equal uncertainty as a fraction of biomass; the lower limit of all axes is 0.

the food web via predator-prey interactions, as well as direct feedback between all levels of the food chain and the physical and chemical environment.

The model maintains robust and stable population dynamics when run over decadal to centennial timescales. Natural climate variability often manifests itself with periods on the order of a decade, as quantified by indices such as ENSO or the PDO, while anthropogenic climate change studies often look 50-100 years into the future. Therefore this model is suited for the study of such climate effects on population dynamics.

Finally, the intra-model ensemble approach used in this study allows us to simulate many potential manifestations of a single ecosystem that all fall within the uncertainty ranges of the observed data. When modeling complex food web interactions, a single representation of a food web is often not capable of capturing the full range of potential effects resulting from a change in the environment

or a change in fishing pressure. Therefore, this ensemble method allows us to better quantify the uncertainty of the simulation results.

This model also provides an example for coupling multiple vertical spatial scales into a single model. In this particular case, using only one dimension, we were able to link lower trophic level functional groups that required a high spatial resolution with upper trophic level groups whose population dynamics could be resolved in a zero-dimensional physical space. The varying spatial scales allowed us to capture the necessary high-resolution variations in physical properties (such as light level, temperature, and stratification) that directly affect the locations and concentrations of smaller organisms without slowing down the upper trophic level calculations with an unnecessarily fine spatial grid.

The model architecture experiments discussed in Section 3.3.1 elucidated a number of important points regarding the coupling of plankton ecosystem models with fisheries food web models. The first point is that density-dependent mortality remains important for capturing the seasonal dynamics of planktonic organisms, even when the model fully resolves all predators of these planktonic groups. This is particularly true at the phytoplankton level, where a linear mortality rate allows blooms to grow well beyond the levels seen in observations in this region. The quadratic mortality term is likely encompassing a variety of processes not explicitly resolved by the process equations of this model. Phytoplankton aggregation, particularly of diatoms, is known to be a major contributor to sinking marine snow and occurs primarily when diatom concentrations are high (Thornton, 2002). In addition, recent research has shown that viruses can be important agents of mortality for phytoplankton, on the same order as loss due to predation, and that density-dependent viral infection rates play a key role in limiting phytoplankton blooms (Brussaard, 2004, and references therein). At the zooplankton level, Ohman & Hirche (2001) observed density-dependent rates of copepod egg mortality uncorrelated with resource availability, which they attributed to egg cannibalism by conspecific and similarly-sized zooplankton. The results of the architecture experiments provide further support that density-dependent mortality is not simply a closure term to represent higher-level predators, but rather incorporates a variety of important loss processes that control the seasonal dynamics of planktonic organisms.

The experiments also clarified the importance of using a consistent functional form for grazing/predation that incorporates the strengths of both lower- and upper-trophic level models, so as to capture both seasonal variations and long-term coexistence among functional groups. The functional groups included in this model operate across a wide range of time scales, with doubling times ranging from a few days to over a decade. The population dynamics of groups with high turnover

rates, whose growth and mortality processes operate on a scale of less than a month, can be very sensitive to assumptions regarding prey functional responses (Gentleman *et al.*, 2003; Fulton *et al.*, 2003). Analysis of piscivorous feeding among pelagic and demersal Atlantic fishes (Moustahfid *et al.*, 2010), and a sensitivity study of a full ecosystem model to changes in functional responses (Fulton *et al.*, 2003) both indicated that marine ecosystem dynamics are better captured by classic Holling Type 2 and Type 3 responses than by a linear assumption, though Fulton *et al.* (2003) also suggested that further complexity in functional response formulation may add unnecessary data requirements to the parameterization process with little additional payoff. The foraging arena functional response used in this model incorporates key elements elucidated in these studies, allowing it to resolve predator/prey dynamics at both the bottom and top of the food web.

Although the model discussed here is tailored to the North Pacific Subarctic region, the basic framework used can be extended to almost any oceanic ecosystem. The NEMURO biogeochemical model uses a structure common to many lower trophic level models in use today, where a minimal number of phytoplankton and zooplankton groups interact with nutrient pools, sinking and non-sinking detrital pools, and bacteria through processes of uptake, grazing, death, sinking, decomposition and mineralization (Fasham *et al.*, 1990). The widespread use of Ecopath with Ecosim has also led to an abundance of food web models spanning the globe; over 100 published food web models can be found on the EwE website (<http://www.ecopath.org>). The Ecopath algorithm is also very flexible in the level of ecosystem complexity modeled, such that a user can aggregate or disaggregate species as necessary to suit the purposes of a given study. While the parameterization process, including parameterization of the biogeochemical model and the construction of an Ecopath food web specific to a particular region, is not a simple task, we do believe that the water column ecosystem framework can be applied to many pelagic ecosystems throughout the global ocean.

Implementing the model globally for climate change applications would require additional consideration of fundamental ecological and physiological considerations which would allow the model to extrapolate into data poor regions and into the novel environments expected under changing climate conditions. The methodologies for coupling fisheries food web and planktonic food web models developed herein, however, are readily adaptable to end-to-end model applications spanning a range of spatiotemporal scales.

CHAPTER 4

Ecosystem response to a bottom-up perturbation

4.1 Introduction

How closely linked to net primary production is the production of upper trophic level consumers? Classical food chain theory suggests that a constant fraction of production (approximately 10%) is transferred from each trophic level to the next May & McLean (2007), and a variety of regional studies have shown positive linear trends between common indicators of primary production (such as chlorophyll *a*) and fisheries yields (Ware *et al.*, 2005; Frank *et al.*, 2006; Chassot *et al.*, 2007) However, in their analysis of bottom-up predictor variables versus fisheries production, Friedland *et al.* (2012) found that phytoplankton production itself was a very poor predictor of fisheries production over globally-distributed systems. Across ecosystems, they found that metrics that accounted for variations in trophic transfer efficiency and the size-structure of the planktonic food web, such as particle export ratio or mesozooplankton to primary production ratio, were more highly correlated with fisheries production than primary production. That the relationship between primary production and fisheries production varies across different ocean environments is in keeping with classical studies, which found very different transfer efficiencies in marine food webs under varying environmental conditions (coastal vs. open ocean vs. upwelling areas) (Ryther, 1969). Improved understanding of fisheries yields and fisheries capacity requires refinements beyond an assumed 10% transfer efficiency between trophic levels (e.g., Pauly & Christensen, 1995).

A nearly universal characteristic of marine ecosystem models is the inclusion of "non-predatory loss terms." These terms are used to represent the net effect of a diversity of loss processes, including natural mortality (i.e. death due to old age), loss to disease and viruses, unresolved intra-group mor-

tality (such as egg cannibalism and predation on juveniles of similar species), aggregation and sinking out of the modeled system (primarily of large phytoplankton), and basal metabolic rate. Since these terms channel energy away from higher predators, choices concerning the size and functional form of these terms also have the potential to influence the flow of energy to higher trophic levels. Historically, fisheries ecosystem models such as Ecopath with Ecosim tend to assume a linear relationship between biomass of a functional group and loss due to non-predatory processes. However, plankton models tend to use quadratic mortality closures in order to achieve stability and match observed seasonal cycles (Steele & Henderson, 1992). Both functional forms can be appropriate for different contributing processes of the non-predatory loss; viral loss, intra-group mortality, and aggregation are often observed to be density-dependent processes, and may be better modeled by a quadratic form, while basal metabolic rate is generally assumed to be constant per unit biomass and thus would be better modeled with a linear formula.

The structural uncertainties presented by uncertain process formulations, such as that of non-predatory mortality, are further complicated by the already high parameter uncertainty that exists in complex models such as this one. Population-scale variables such as standing stock biomass are challenging to compile for an entire ecosystem. The large range in spatial scales covered by these ecosystems makes it very difficult to thoroughly survey the population of even a single target fish species, for which there may be regular scientific sampling programs as well as plentiful fisheries-based observations. Non-target species, such as myctophids or other forage fish, play equally key roles in ecosystem dynamics as fisheries-targeted species, but there is far less data available regarding the populations of these species. Seabirds are often counted only at their roosting spots, but forage over a much larger swath of ocean, while whales may migrate thousands of miles to forage. Gelatinous zooplankton may play important roles in mesozooplankton communities, but are unable to be sampled by traditional net tows and therefore there is far less data on them than their crustacean counterparts. The lack of plentiful observations at all levels of the food web can lead to wide error bars on the input parameters used in ecosystem models, and this uncertainty is propagated to the output of any simulations.

In this study, we attempt to quantify both the magnitude and the uncertainty of the response of the end-to-end ecosystem model to a bottom-up perturbation, namely an increase in net primary production due to alleviation of micronutrient limitation. The impact of non-predatory mortality on the energy flow through the system is quantified and drivers of the amplification of primary productivity perturbations are diagnosed. We also assess the contribution of uncertainties in non-predatory loss structure to the overall spread of predicted changes in upper trophic level productivity.

4.2 Methods

In the previous chapter, we found that our modeled Eastern Subarctic Gyre region is limited by iron (at times co-limited by light) throughout the entire year under climatological conditions. Therefore, the easiest way to systematically augment primary production in this region in the model is to alleviate the iron limitation through increased surface deposition of iron. Note that in designing this experiment, we were not attempting to replicate a short-term iron fertilization experiment, but rather to look at the response of the entire ecosystem to a long-term change in productivity.

Because we are doing a series of iron fertilization experiments, we implemented an improved representation of iron dynamics following Stock *et al.* (n.d.). Rather than the relaxation scheme used in Kearney *et al.* (2012), we now explicitly resolve two forms of iron: bioavailable dissolved iron (Fe), and particulate iron (POFe) (Figure 4.1 on page 53). Like the simpler scheme used in the previous chapter, this model adds an additional limitation term to macronutrient uptake, based on the available dissolved iron, and allows phytoplankton to take up and store luxury iron during periods of high availability. But in this case, rather than simply relaxing to an observed profile, we explicitly model interaction with ligands, adsorption of dissolved iron onto particles, and remineralization of particulate iron. See Section A.2.3 for further details of this formulation.

In this set of experiments, we ran 5 sets of simulations, with 30 ensemble members each, in which we systematically raised the surface deposition flux of iron from its climatological value of 2.83 pmol Fe/m²/s to values 1.25, 1.5, 2, 3, and 5 times higher than that. The 1.25-times perturbation captures the approximate magnitude of interannual variability in dust deposition in the subarctic gyre (Figure 4.2 on page 53), while the higher values represent levels that might be expected more rarely, such as in response to volcanic activity in the nearby Aleutian Islands. Each simulation was run for 10 years under climatological conditions, followed by 10 years of the raised-iron conditions, and we used the final year of each simulation for our data analysis. While not every functional group had reached a completely new steady state by the 10-year mark, all groups showed less than 1.5% change in biomass per year at the end of the climatological period and even the slowest-growing groups showed less than a 5% change 10 years after the strongest perturbations; therefore we felt this spinup time was sufficient for our analyses.

In initial trial runs, as described briefly in the previous chapter, we found that a quadratic mortality function needs to be applied to phytoplankton groups in order to replicate the proper seasonal cycles seen in observations. To assess the impact of the assumed form of non-predatory

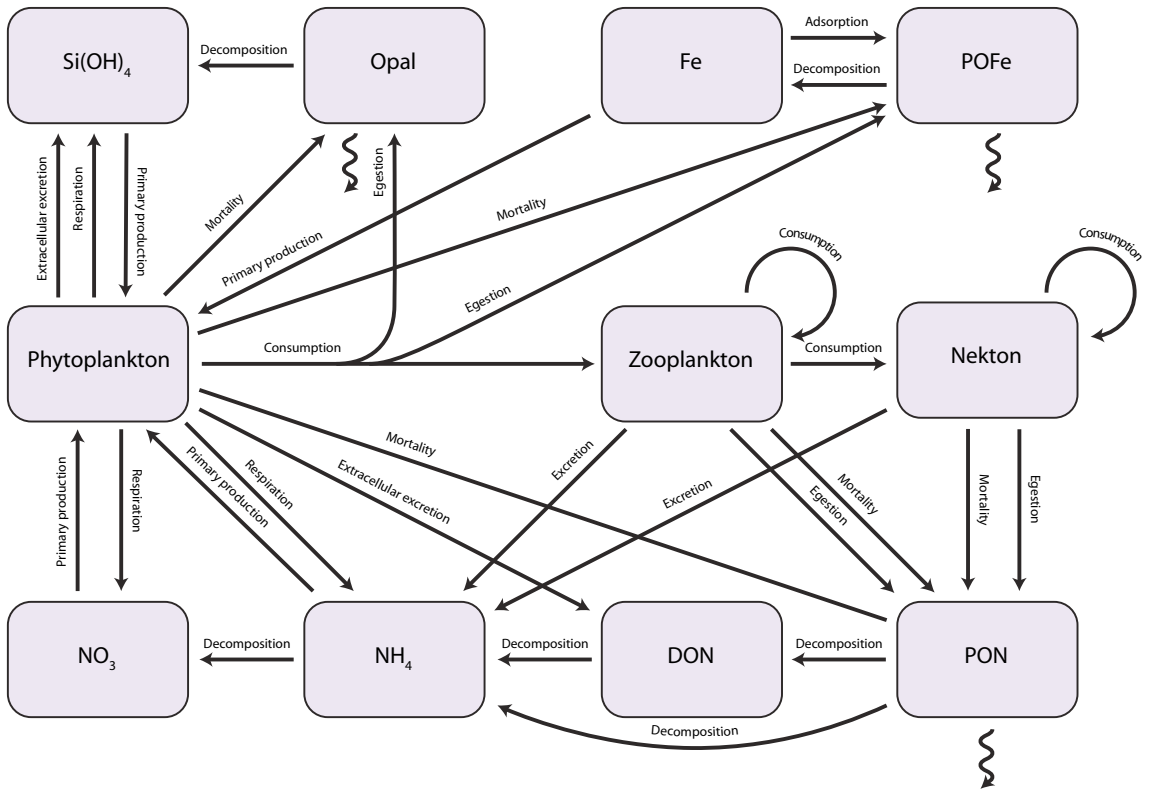


Figure 4.1: Schematic of the water column ecosystem model processes and state variables. An explicit iron cycle, including cycling of iron between dissolved and particulate state variables as well as the phytoplankton groups, has been added to the processes described in the previous chapter (Figure 3.1 on page 35).

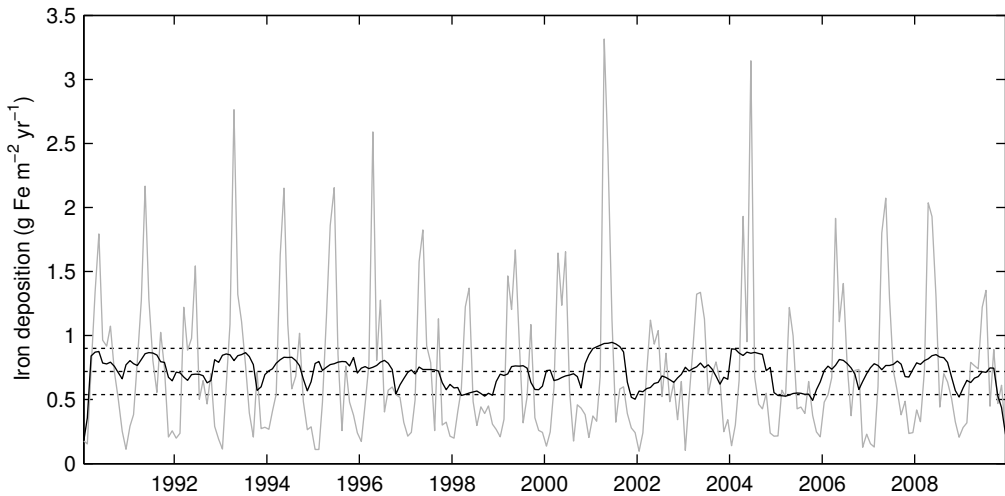


Figure 4.2: Interannual variability in dust deposition at Ocean Station Papa. The light grey line shows the sum of wet and dry deposition, as modeled by the Geophysical Fluid Dynamics Laboratory Global Chemical Transport model (Moxim *et al.*, 2011), while the dark line shows a 12-month running average. Dotted lines indicate $\pm 25\%$ of the mean value.

mortality, the remainder of the living functional groups (consumers) were run with non-predatory mortality functions of the form

$$M_0 = aB^c \quad (4.1)$$

where M_0 is the total loss due to non-predatory mortality ($\text{molN}/\text{m}^3/\text{s}$ for plankton, $\text{molN}/\text{m}^2/\text{s}$ for nekton), B is the biomass of the group (molN/m^2 ^[3]), and c was set to either 1, 1.5, or 2, representing linear, mixed, and quadratic mortality, respectively. The coefficient a was constrained through the Ecopath-derived values for biomass (B^* , the mass-balanced biomass of a functional group) and M_0^* (the mass-balance value for all group production not passed to higher trophic levels) such that $a = M_0^*/(B^{*c})$. The quadratic structure captures the end case where density-dependent processes are the primary contributors to non-predatory loss, while the linear structure represents the other end case where density-independent processes predominate.

We encountered some issues when attempting to analyze the results of the purely linear mortality case. While we wanted to include this formulation as a critical end case representing non-density dependent processes, the linear case is mathematically less stable than higher order functions. Coupled with the high-temporal-resolution physical forcing included in this model, the instability manifests itself by causing some ensemble members to deviate from their target ranges, even under climatological conditions. We were unable to eliminate this undesirable behavior, even through meticulous balancing of our initial parameters. In order to make consistent comparisons between results under the different mortality regimes, we chose to eliminate certain ensemble members from our calculations of consumer productivity; for each consumer, those ensemble members that produced climatological results outside of the mass-balance target ranges at the end of the first 10-year period were eliminated from all from the values considered across all three mortality structures.

4.3 Results

4.3.1 Primary productivity under enhanced iron deposition

Increased iron deposition leads to an increase in total net primary productivity, although there is considerable variability in the magnitude of this increase across ensemble members, particularly at very high iron levels (Figure 4.3 on page 56). Surface iron concentrations increase approximately linearly as surface deposition increases. In response, net productivity increases until surface dissolved

iron levels reach approximately 0.2 nM Fe, which occurs in the 3x deposition regime; beyond this level, macronutrients become limiting once more and primary production levels off.

The increased primary productivity manifests itself almost entirely through increases in the small phytoplankton group, while the large phytoplankton group shows very little change in either biomass or production over the different surface iron regimes. This is due to a combination of both bottom-up and top-down controls on the population growth of the larger size class. Immediately following the increase in surface iron that occurs at the 10-year mark in all simulations, the alleviation of micronutrient limitation increases the realized growth rates of both phytoplankton groups (Figure 4.4 on page 57). As a result, both phytoplankton groups see enhanced production levels during the spring and early summer of the first year. However, this early bloom leads to the onset of macronutrient limitation and also supports an enhanced mesozooplankton community, both of which strongly limit the growth of the large phytoplankton population. The newly-strengthened mesozooplankton community maintains a strong top-down control on the microzooplankton group, which is the primary predator of small phytoplankton, allowing small phytoplankton biomass and production to expand. To further isolate the top-down controls resulting from increased net primary production, we ran a simplified version of the food web model, where food web dynamics are uncoupled from the physical and biogeochemical portions of the model, without spatial resolution or seasonal variations. Here we simply imposed a 20% increase in the net primary production of a single phytoplankton group and ran the ecosystem to a new steady state (Figure 4.5 on page 58). When only the small phytoplankton group was given increased production, the mesozooplankton groups all increased, leading to higher grazing rates on large phytoplankton and hence decreased large phytoplankton biomass. On the other hand, when large phytoplankton were given the increased production, the increased mesozooplankton grazers cropped the microzooplankton group, leading to an overall increase in small phytoplankton biomass and production. This demonstrates clearly that in this particular food web structure, the small phytoplankton are able to benefit from food web restructuring resulting from increased production by large phytoplankton, while large phytoplankton are negatively impacted by the restructuring under high production by small phytoplankton.

While observations of phytoplankton community response to a long-term change like the one we simulated are not available to either confirm or refute our results, the increased net primary production levels under the higher surface flux conditions allow us to closely analyze the propagation of production to higher trophic levels.

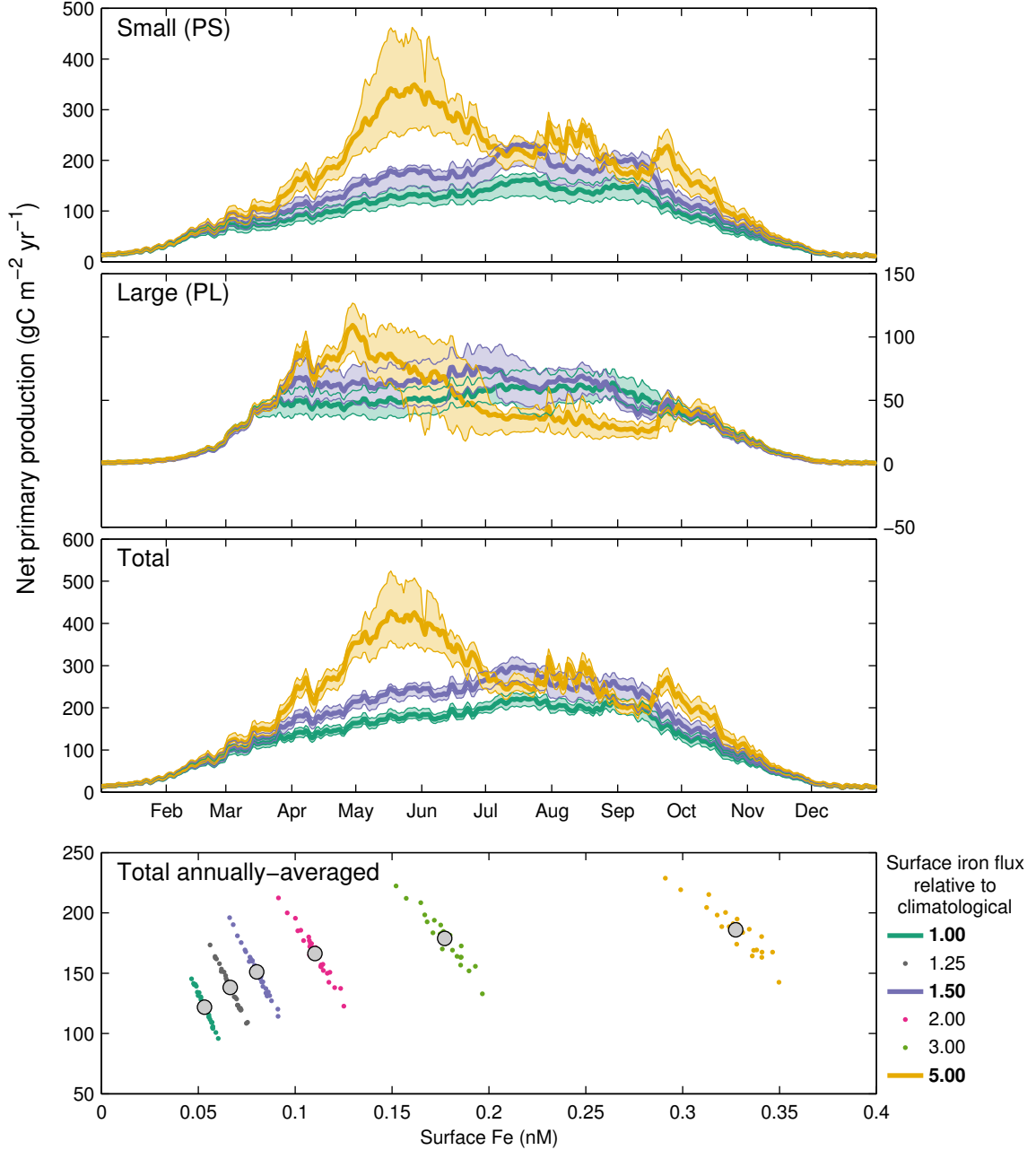


Figure 4.3: Net primary productivity under varying surface iron deposition. The top panels show net productivity versus time over a single year of each iron regime, with bold lines indicating the ensemble average and the shaded area the 25th-75th percentiles across ensemble members. The bottom panel shows the yearly-averaged total net production versus surface iron concentration for each ensemble member (points); the grey circle indicates the ensemble average for each iron regime.

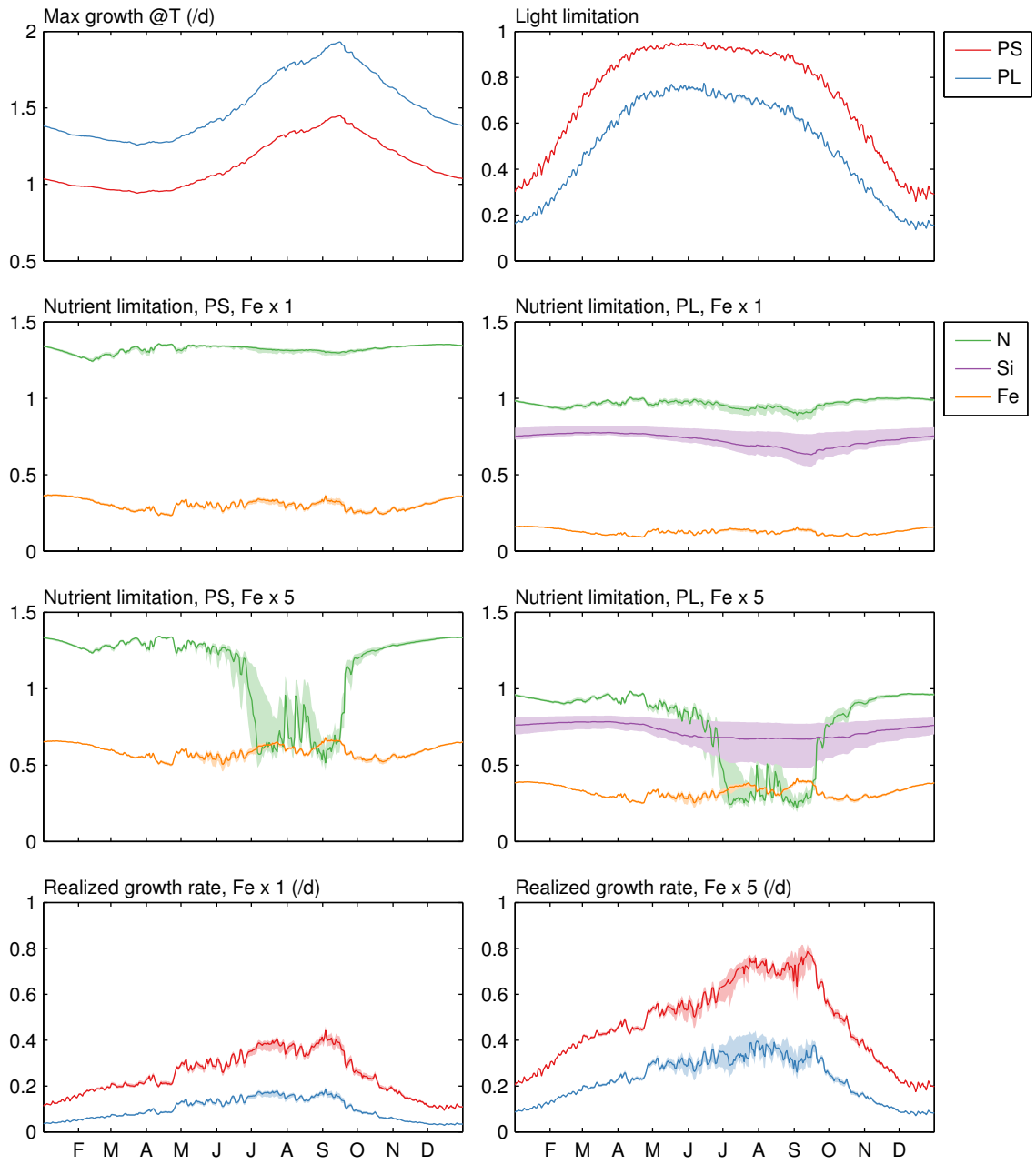


Figure 4.4: Growth and limitation terms for both phytoplankton groups under climatological (Fe x 1) and high-iron (Fe x 5) surface deposition regimes. The panels show, from left to right and top to bottom: Maximum temperature-influenced growth rate; light limitation; nutrient limitation for small phytoplankton under climatological iron (Note: nitrogen limitation is an additive function of NO_3 and NH_4 limitation, and therefore can be greater than 1), nutrient limitation for small phytoplankton under high-iron conditions, nutrient limitation for large phytoplankton under climatological iron, nutrient limitation for small phytoplankton under high-iron conditions, realized growth rate (i.e. nutrient- and light-limited growth) for under climatological conditions, and realized growth rate under high-iron conditions. Shaded areas represent the 25-75% ensemble range, while the solid lines indicate the ensemble median.

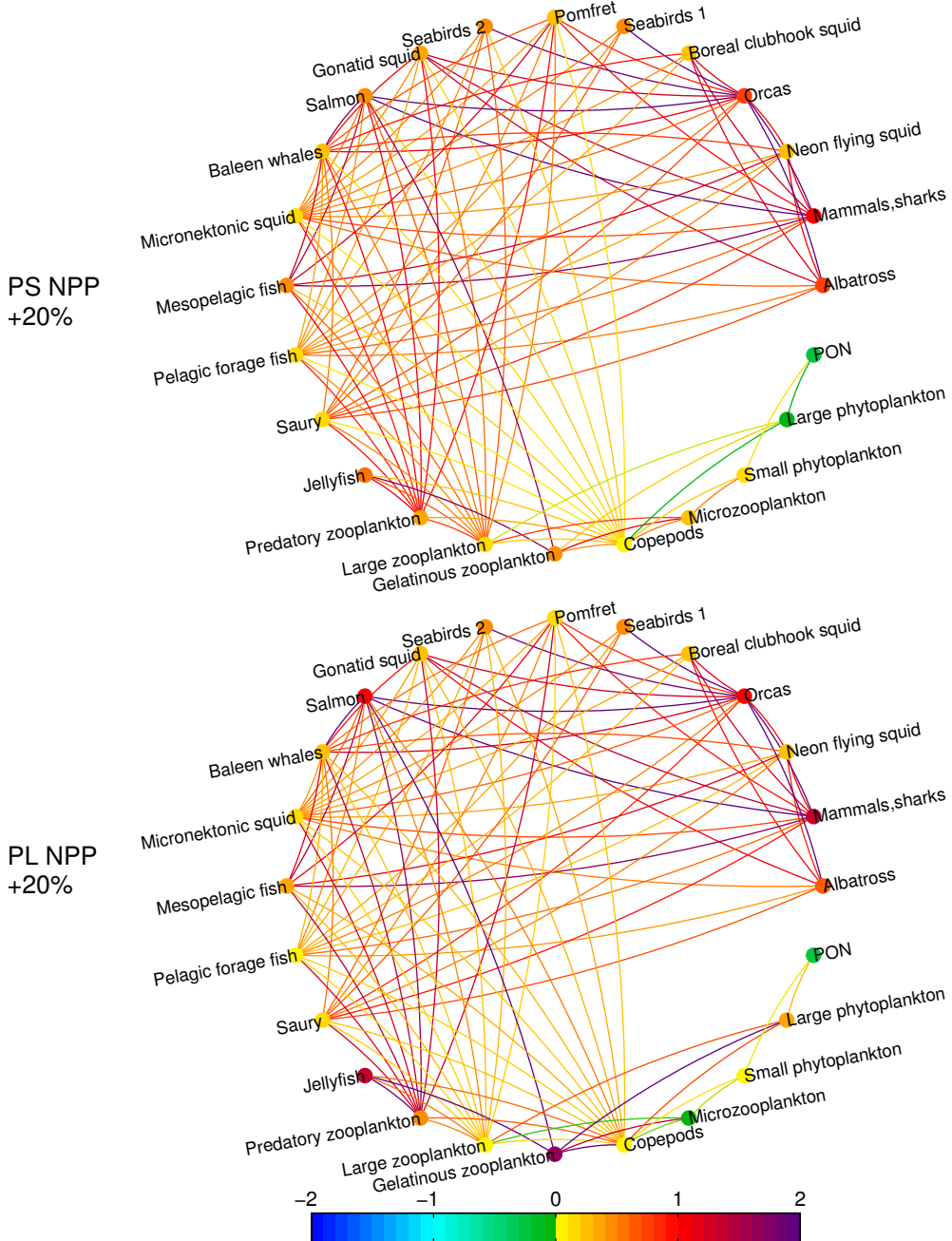


Figure 4.5: The directed graphs above summarize the change in biomass and production fluxes between all groups in the ecosystem when one phytoplankton group is provided with enhanced primary production. Colors indicate the fraction change in biomass of each functional group (nodes) and fluxes between groups (edges); fluxes curve counterclockwise from source to sink. When small phytoplankton production is increased, large phytoplankton production and biomass drop due to changing predation pressure. However, when large phytoplankton production is increased, the changing top-down controls lead to increased production by both phytoplankton groups.

4.3.2 Propagation of productivity to higher trophic levels

In the broadest sense, our simulations demonstrated that increased primary production leads to an increase in consumer net production at almost all levels of the food web. However, the sensitivity of consumer production to changes in net primary production varied widely across both ensemble members and mortality structures. The analysis below looks closely at the relationship between net primary production in this ecosystem and the net production of each consumer group in the food web.

The relationship between net primary production and consumer net production generally followed a linear trend, when analyzed per simulation (i.e one ensemble member and mortality structure, across all iron levels). We see smaller absolute changes in consumer production per change in primary production at higher trophic levels, but this is primarily a reflection of the overall decline in energy flows as one moves to higher trophic levels (Figure 4.6 on page 60). By looking at the relative, rather than absolute, changes in productivity values, we can uncover a few key patterns that emerge across trophic levels under the different model structures.

While both the linear and quadratic mortality structures in the model result in a positive linear trends of consumer production vs. net primary production, the slope of this linear trend can differ significantly between structures at higher trophic levels. To quantify the different patterns of propagation throughout the food web (and across the many orders of magnitude spanned by production rates from producers to top consumers), we defined a metric to relate relative change in net primary productivity to relative change in consumer productivity:

$$R_{x,i} = \frac{\left(\frac{NSP_{x,i}}{NSP_{0,i}} \right)}{\left(\frac{NPP_{x,i}}{NPP_{0,i}} \right)} \quad (4.2)$$

where NPP is net primary production, NSP is the net secondary production associated with each consumer group, the subscript 0 indicates the climatological surface iron flux period, the subscript x indicates any of the raised-surface-iron-flux periods, and the subscript i indicates the ensemble member index. A value of $R_{x,i}$ equal to one would indicate no rearrangement of the food web in response to increased production, i.e. all increases are distributed in the same proportion as the original production levels, while values greater than 1 would indicate an amplification of the relative production at the consumer level.

This metric reveals a difference in the response of the food web under the three different mortality structures (Figure 4.7 on page 62). Under the quadratic scheme, the food web sees little

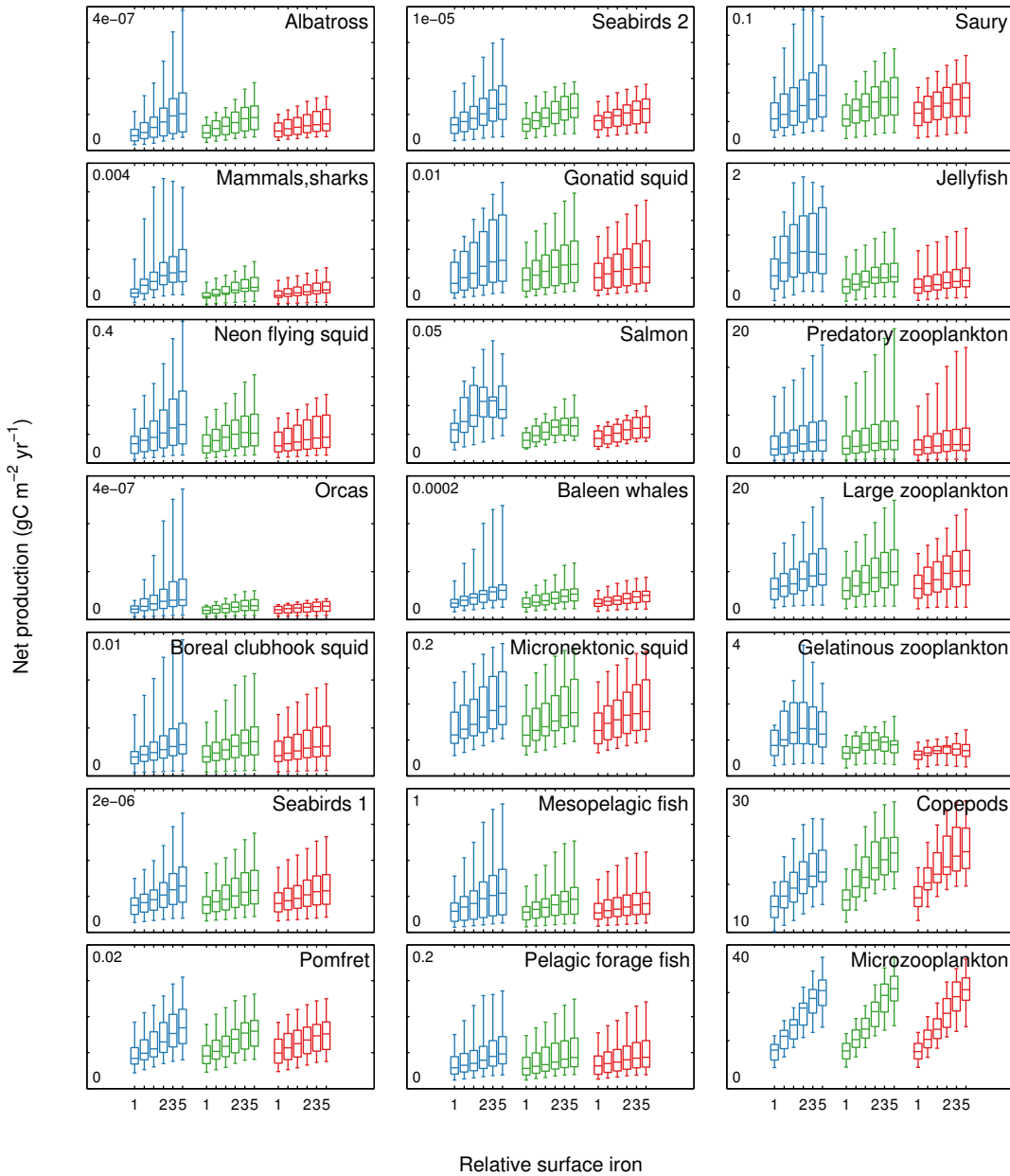


Figure 4.6: Net consumer production, across all simulations. X-coordinates indicate the relative level of surface iron deposition, for linear (blue), 1.5 (green), and quadratic (red) mortality schemes, while the y-axis indicates the annually-averaged net consumer production.

rearrangement, with all values of R_x falling close to 1. However, under the linear mortality scheme, the increased production outpaces static non-predatory loss rates throughout the food web, leading to an amplification of the relative production reaching consumers.

The amplification of changes in consumer production relative to primary production was large for several groups with high non-predatory losses under climatological conditions (including gelatinous zooplankton, salmon, marine mammals, and birds, see Figure 2.10 on page 27). However, a regression of the amplification metric against fraction mortality due to non-predatory loss explains only 7% of the variation. This suggests that amplification patterns may not arise from just the local balance of predatory versus non-predatory mortality, but effects that accumulate throughout the food web. Regressing against both local non-predatory to predatory ratio and trophic level explains 15% of variance in the amplification metric.

While the differences in amplification between the three mortality structures is clear when considering each ensemble member relative to itself, the structural differences become far less apparent when properties are analyzed across all ensemble members. We tested both the distributions of biomass and net production of each consumer to see if they were significantly higher under the linear mortality structure than with the quadratic structure. Even following the strongest perturbation, the majority of variables did not display any statistically significant differences (Mann-Whitney U-test, $\alpha=0.05$) in their distributions. The exceptions to this fell into two groups. First, as with the relative metric discussed in the previous paragraph, functional groups with a high non-predatory mortality rate, including jellyfish, salmon, mammals, and orcas, showed significantly higher biomass and production values under the linear mortality structure than the quadratic one. At the other end of the trophic spectrum, microzooplankton biomass, copepod biomass and production, and gelatinous zooplankton biomass and production were all lower under the linear scheme than the quadratic one (Figure 4.8 on page 63). This difference at the bottom of the food chain seems to stem from changing predation pressure as a result of the larger jellyfish population; jellyfish feed on several of the zooplanktonic groups, and therefore the increase in this group leads to a decrease in many of its prey groups.

4.4 Discussion

The results of this analysis elucidate some interesting points regarding the response of a complex ecosystem model to a seemingly straightforward perturbation, as well as the interplay of structural and parameter uncertainty in that response.

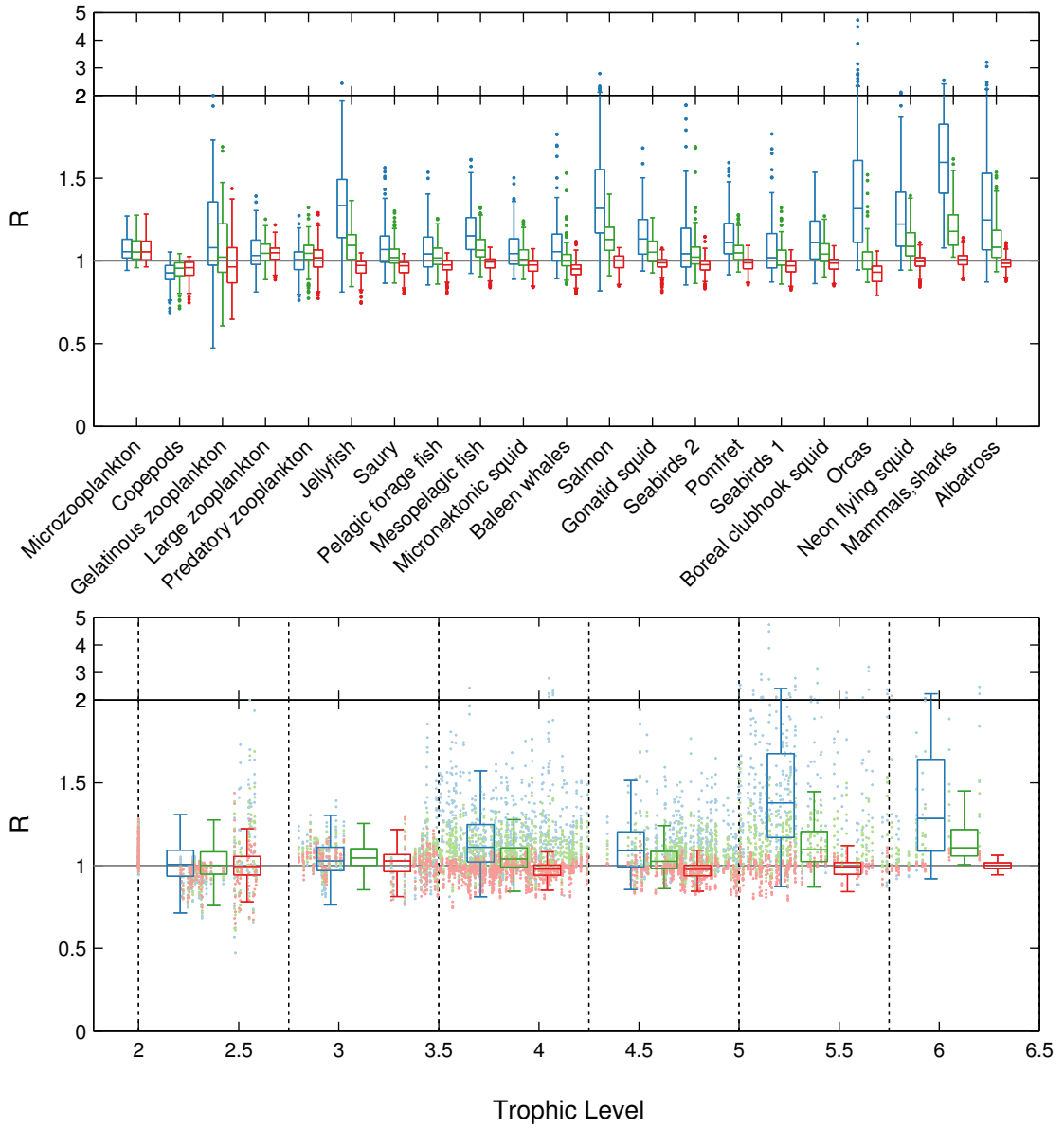


Figure 4.7: Relative change in production, R_{x_i} , for consumers in the ecosystem. The upper panel boxplots show the spread of values for each consumer (points more than 1.5 times the interquartile distance outside the lower/upper quartiles, are considered outliers and marked as dots). The lower panel consolidates the same information grouped by trophic level; here, points indicate the values for each consumer vs. trophic level, while boxplots consolidate this information (outliers not included in these boxplots). The amplification effect under a linear mortality scheme can be seen clearly when the data is grouped by trophic level (lower panel); in this context, trophic level is defined a 1 plus the weighted average of prey's trophic levels, based on the mass-balance constraints for each ensemble member. Points show the trophic level and R_x values for each ensemble member and each raised-iron scenario; boxplots consolidate these points based on trophic level (outliers are not shown in the lower panel boxplots).

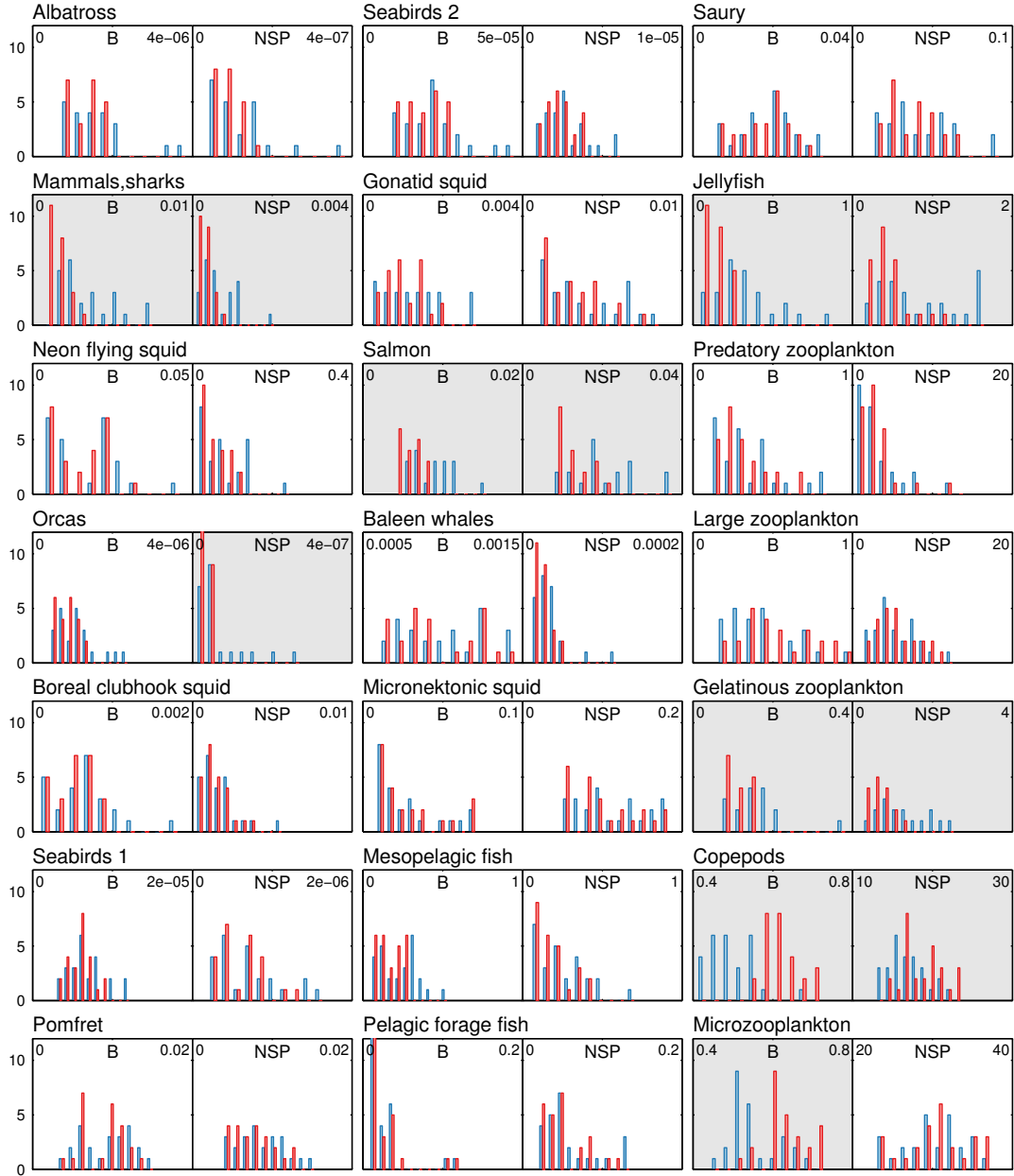


Figure 4.8: These histograms show the distributions of biomass (B , gC m^2) and net secondary production (NSP , $\text{gC m}^2 \text{ yr}^{-1}$) for each consumer in the food web under the linear (blue), 1.5 (green), and quadratic (red) mortality structures, at the end of the 5-times surface iron flux perturbation. The shaded axes indicate variables where the median value is significantly higher or lower under the linear regime than the quadratic regime.

First, this experiment demonstrated that the interacting effects of light limitation, temperature dependence, and nutrient limitation on each individual phytoplankton group, as well as their indirect effects on each other through top-down effects of changing grazing pressure, can lead to unexpected changes in primary production even with a relatively simple forcing factor. While both phytoplankton groups benefit directly, through an increased growth rate, from the increased iron deposition levels, the long-term population-scale benefit was isolated to only one of these functional groups. Prior to running the simulations, we had hypothesized that the large phytoplankton would be more likely to benefit from the increased iron levels, since traditional wisdom suggests that small phytoplankton are more tightly regulated by the quick-responding microzooplankton. While that traditional wisdom held briefly, over longer periods of time the microzooplankton were kept in check by their predators, who also happened to feed on large phytoplankton, allowing small phytoplankton to escape predation more so than the large.

While our simulations, with their long-term changes in surface iron flux, cannot be directly compared to short-term iron fertilization experiments, it is interesting to note that iron addition experiments in the subarctic Pacific region have demonstrated mixed responses by the phytoplankton community. Three mesoscale iron fertilization experiments have been carried out in the Eastern Subarctic gyre since the iron hypothesis was first proposed as a mechanism for incomplete nutrient use in this region (Martin & Fitzwater, 1988; Martin *et al.*, 1989): the Subarctic iron Enrichment for Ecosystem Dynamics Study (SEEDS) in 2001, Subarctic Ecosystem Response to Iron Enrichment Study (SERIES) in 2002, and SEEDS II in 2006. The phytoplankton communities were very similar prior to fertilization for all three experiments, with the small phytoplankton (primarily prymnesiophytes and chlorophytes) dominating, and similar chlorophyll levels were measured each time (Suzuki *et al.*, 2009). Over the 13-day post-fertilization observation period, SEEDS saw an increase of 2-5 times in the nanoplankton, but the response was dominated by a 45-fold increase in the diatom community, with a shift towards centric diatoms (Takeda & Tsuda, 2005). The SERIES experiment observed increases in all size classes over the first 10 days of observations, followed by a bloom of diatoms, this time primarily the smaller pennate diatoms, over the final 8 days of observation (Marchetti *et al.*, 2006). Contrary to these two studies, the SEEDS II fertilization observed no bloom of diatoms, with the picophytoplankton instead dominating the increase in biomass and productivity seen over the 26-day study (Uematsu *et al.*, 2009). The diversity of responses may indicate that higher predation closures are more dynamic than we consider them, and that they may structure changes in planktonic food web.

In our study, the upper trophic level consumers showed fairly regular increases in production as a result of the increased primary production. Despite the complex network of pathways connecting the various functional groups to each other, there were no clear “winners” or “losers” resulting from this particular ecosystem perturbation. Instead, all consumer groups tended to experience an increase in both net production and biomass following ten years of increased primary production.

We found that when quantified in terms of relative change, the structural form of non-predatory mortality could affect whether the increased production was amplified as it moved up the food chain. Linear mortality functions tend to pass the production to the top of the food web, benefiting top predators more so than lower trophic level consumers. In contrast, quadratic mortality functions lead to damping of this response, as much of the increased production is recycled through the non-predatory loss terms rather than being passed to higher trophic level predators. The difference between these two structural regimes can be important to note when constructing complex ecosystem models, particularly when not explicitly accounting for the uncertainty in input parameters. Often, ecosystem studies look only at the relative change in population variables, rather than the absolute change, recognizing that input uncertainty may render the latter less useful than the former. However, this study demonstrates that the relative change in ecosystem variables can be strongly influenced by structural uncertainties, more so than the absolute values of these variables.

However, whether choices regarding the functional form of non-predatory mortality significantly altered predicted productivity of a single group was less clear. When considering the full range of parameter uncertainty, we found that the differences in the responses predicted by the three non-predatory mortality structures could only be seen for a few variables, related to top predators with low predatory mortality. However, it is important to note that the salmon group, representing the most commercially-important species in this food web, was one of the functional groups that did show different responses under different mortality structures. Because we did not explicitly model fishing mortality, loss to fishing pressure was considered part of this functional group’s non-predatory mortality. This perturbation experiment suggests that capturing the correct structural form of fishing loss and other non-predatory losses is crucial when modeling fisheries target groups.

In this context, our coupling of biogeochemistry to a food web has not completely eliminated closure terms, but rather pushed them higher in the food chain, toward the level of commercially-targeted species and the fisheries that “prey” on them. The likely role of fishing in these closure terms makes it essential to further push the end-to-end concept toward the linkages connecting the diverse social and economic factors that control dynamic fishing responses.

CHAPTER 5

Summary

In this dissertation, an end-to-end ecosystem model that explicitly links physics, biogeochemistry, and food web dynamics was developed, validated against observations, and applied to analyze ecosystem response to a bottom-up perturbation.

In Chapter 2, we developed several techniques to expand upon traditional Ecopath models such that they isolate the primary pathways of energy through a food web and encompass parameter uncertainty. We found that our group reduction technique, based on hierarchical clustering quantified by shared predator and prey linkages, was able to maintain a wide variety of ecosystem properties, even when the number of functional groups resolved was varied between 47 and 7. We also presented an ensemble-generation technique that allowed us to create many different Ecopath models based on the same set of data, all of which represented a possible representation within the bounds of the observation uncertainty. By running simulations with a suite of upper trophic level models, rather than a single one, we are able to quantify not just the mean predicted outcome, but a full range of possible outcomes critical for evaluating scientific robustness and for potential applications to management.

Coupling these upper trophic level models to lower trophic level biogeochemical models proved much more tricky than originally anticipated. Simply connecting the models together in a brute force manner revealed certain clashes in the formulations of each model. Through our series of model architecture experiments, discussed in Chapter 3, we determined that consistent treatment of predator/prey functional response for both planktonic and nektonic groups was necessary in order to maintain coexistence throughout the food web. We also found that phytoplankton groups required the stability provided by density-dependent non-predatory mortality terms in order to

properly replicate their seasonal dynamics. The final model framework, run for 50 years under climatological forcings in the Eastern Subarctic Pacific ecosystem, was able to reproduce observed seasonal dynamics in primary production and nutrient drawdown. It was also able to maintain stable populations of upper trophic level functional groups over the entirety of the simulation, as would be expected given the lack of perturbations imposed on the system in this set of experiments.

Finally, in Chapter 4, we used our model to investigate the propagation of increased primary production through the full food web. We also looked at how assumptions regarding the formulation of non-predatory mortality affected the amplification of changes as they moved to higher trophic levels. This experiment revealed that density-independent formulations of non-predatory mortality led to an amplification of relative changes in production at higher trophic levels, particularly in groups that started with low predatory to non-predatory loss ratios in the initial parameterization process. This included top predators with few marine predators, such as whales, birds, and jellyfish, as well as commercially-targeted species like salmon. Density-dependent formulations tended to damp the propagation of production increases, leading to relatively uniform relative changes in biomass and production throughout the food web. However, while these differences in amplification between density-dependent and non-density-dependent mortality terms were consistently seen across ensemble members, the effect of non-predatory mortality on the ensemble of solutions for any given functional group was often masked by uncertainties in the food web parameterization. The differences that did emerge were seen in the populations of top predators, indicating that the closure terms of these groups may need to be more carefully linked to specific mechanisms, including dynamic representations of fisheries.

As (Link *et al.* , 2012) notes, the use of ecosystem models in the context of natural resource management is often accompanied by a high burden of proof, due to the many biological and socio-economic consequences that can result from management decisions. While uncertainty cannot be eliminated from models that incorporate so many complex processes, we can take steps toward quantifying the uncertainty associated with them. We feel the model presented in this dissertation addresses this need. By running an ensemble of simulations, we were able to place error bounds on all of our simulated predictions. In addition, we believe we have presented the process equations we used in a very transparent manner, differentiating between those that are well-verified by field and laboratory studies (such as primary production), those that can only be roughly estimated based on ecological theory (such as predator-prey functional responses), and those that remain very uncertain in both magnitude and form (such as non-predatory mortality). Our study of the contribution of non-predatory mortality structural uncertainty to the overall spread in simulated

results demonstrated how even very poorly constrained processes can be included in models with some degree of confidence. Such detailed dynamical characterization of model behavior is essential before complex models can be applied to management applications.

While we feel this model presents an important step forward in modeling complex marine ecosystems, there are still many places where improvements can be made. The model presented in this thesis encompasses a variety of ecosystem processes, including nutrient cycling, primary production, planktonic grazing, upper trophic level predator-prey interactions, and non-predatory mortality. To parameterize these processes, this model is heavily reliant on contemporary observations of population-scale properties, including biomass, vital rates, and diet composition. While effective incorporation of observational constraints is a strength for many contemporary applications, these observations may fail to capture the true range of variability possible when the ecosystem is presented with novel environmental conditions, such as those that are predicted as a result of anthropogenic climate change. For example, the migration of entirely new species into a region may drastically shift the diet composition of former residents, in ways not predicted by contemporary observations. Changes in temperature or pH may directly affect the growth, reproduction, and recruitment of species throughout the food web. To truly capture this range of potential changes, observation-based models such as this should move toward more physiological representations of all processes included within them.

APPENDIX A

Model description

A.1 The one-dimensional physical model

A.1.1 Description of equations

The physical model used in this study is a Matlab-based code designed to simulate a one-dimensional water column. The code is designed so that a variety of different biological models can be run within the same physical context, as was done in this study with the standalone NEMURO simulations and the fully-coupled water column ecosystem simulations.

The mixed-layer model simulates the evolution of water column properties under specified forcing by wind, heat, and salinity forcing. Allowance is also made for currents via a depth-independent pressure acceleration. There are six physical state variables in the physical model formulation: U and V are the east to west and south to north current velocities, and T and S are the temperature and salinity. The turbulence closure scheme introduces the remaining two state variables: q^2 is a turbulent quantity equal to twice the turbulent kinetic energy, and ℓ is a turbulent length scale. These two state variables are used to calculate mixing-related parameters (K_M and K_V) in Eq. (A.1), Eq. (A.2), Eq. (A.3), and Eq. (A.4).

The momentum equations are standard one-dimensional formulations:

$$\frac{\partial U}{\partial t} - fV = -\frac{1}{\rho_0} \frac{\partial p}{\partial x} + \frac{\partial}{\partial z} K_M \frac{\partial U}{\partial z} - \epsilon U \quad (\text{A.1})$$

$$\frac{\partial V}{\partial t} + fU = -\frac{1}{\rho_0} \frac{\partial p}{\partial y} + \frac{\partial}{\partial z} K_M \frac{\partial V}{\partial z} - \epsilon V \quad (\text{A.2})$$

where f is the Coriolis parameter, ρ is the density, K_M is the viscosity, $\frac{\partial p}{\partial x}$ is a specified pressure gradient (to impose a mean current) and ϵ is a momentum dissipation term. The dissipation term serves as a surrogate for horizontal momentum divergence. It removes energy from past storm events over a specified time-scale as though energy was being transferred to more quiescent surrounding waters. Energy tends to accumulate unrealistically in one-dimensional water columns without this effect (Mellor, 2001). The value of ϵ was tuned such that the energy in the modeled currents is consistent with that observed. Values comparable to the time scales of storm events ($1/3$ day $^{-1}$) yielded reasonable results. The equations are solved using a semi-implicit Crank-Nicolson scheme.

The Mellor-Yamada turbulence closure scheme (Mellor & Yamada, 1982) is used to calculate mixing coefficients. The reader is referred to this reference and Mellor (2004) for the governing equations and other details of this formulation. A k-epsilon formulation (see review by Umlauf & Burchard (2005)) was also tested and yielded similar results to those presented herein. The top and bottom boundary conditions for Eq. (A.1) and Eq. (A.2) are provided by the wind stress formulation of Large & Pond (1981) and a quadratic bottom drag law, respectively. Mixing at the surface was augmented by the wave breaking scheme of Mellor & Blumberg (2004).

The temperature and salinity equations are given by:

$$\frac{\partial T}{\partial t} = \frac{\partial}{\partial z} K_V \frac{\partial T}{\partial z} + ss \quad (\text{A.3})$$

$$\frac{\partial S}{\partial t} = \frac{\partial}{\partial z} K_V \frac{\partial S}{\partial z} + ss \quad (\text{A.4})$$

where K_V is the vertical turbulent diffusion coefficient, and ss is used to indicate sources minus sinks. The temperature source minus sink term (shortwave heat flux) and boundary conditions (longwave heat flux, sensible and latent heating and cooling) are described in Section 3.2.1.1 in this paper. The salinity source minus sink term derives from the relaxation to observations as described in Section 3.2.1.1.

Biological state variables are mixed, where applicable, following the same formulation as Eq. (A.3), with the source minus sink term representing any additional vertical movement; in the simulations described in this paper, this term was used to apply sinking velocities to the particulate

state variables (*PON* and *Opal*). The set of equations describing the remaining biological sources and sinks (Appendix A.2) is solved following the mixing calculations at each time step.

A.1.2 Input variables and datasets for the Eastern Subarctic Gyre

Shortwave radiation, air temperature, and wind speeds were extracted from the Coordinated Ocean-ice Reference Experiments (CORE) normal-year datasets (Large & Yeager, 2009). The CORE datasets provide 6-hourly timeseries of various air-sea fluxes (Figure A.1 on page 72). Dew point temperature was derived from the same dataset. A climatological salinity cycle was derived from the GECCO model's 1950-2000 salinity product. The resulting timeseries was resolved monthly; the modeled salinity relaxation used bilinear interpolation to translate this timeseries to the higher-resolution model grid. Initial profiles for both salinity and temperature were set to the climatological January profiles, also derived from the GECCO product.

A.2 Process equations for the water column ecosystem model

The water column ecosystem model consists of 7 non-living state variables, and 3 classes of living state variables, coupled together by three sets of ordinary differential equations, one for each of the three nutrients included in the model. For simplicity, the following equations omit indicators of depth resolution, but unless otherwise indicated, all equations apply to a single model grid cell.

A note on subscripts, which are plentiful in this documentation: subscripts indicate the index of a functional group to which a given process variable or parameter pertains. I typically use i as this index, and expand to j and k when I need to represent more than one functional group in a single equation. Where variables are related to fluxes between groups, they are denoted by two subscripts (e.g. x_{ij}), with the source group index followed by the sink group index. For clarity I often separate multiple subscripts from each other with commas (e.g. x_{NH_4,NO_3} represents a parameter relating to a flux from the NH_4 state variable to the NO_3 variable); commas also separate parameter-name subscripts from functional group subscripts (e.g. $V_{max,PS}$ is the V_{max} growth rate parameter associated with the PS state variable).

The values of the various biological state variables are referred to as B_i in all the equations below; depending on the particular state variable, these can be thought of as either biomass values or nutrient concentrations. All phytoplankton groups are represented by three state variables: phytoplankton nitrogen (B_i), phytoplankton silica ($B_{Si,i}$), and phytoplankton iron ($B_{Fe,i}$), while zooplankton and nekton groups consist of only nitrogen state variables. Equations A.5, A.6, and

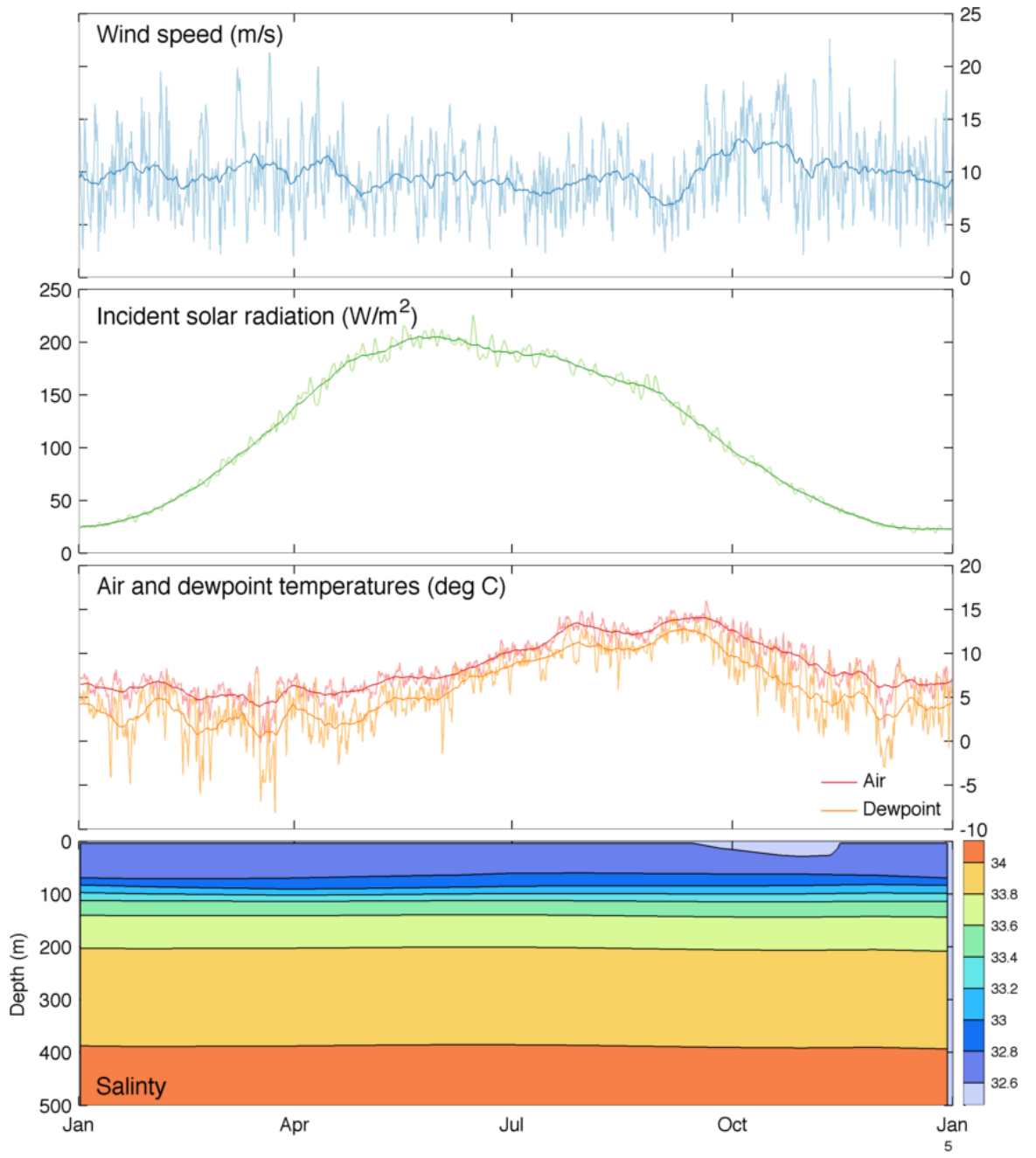


Figure A.1: Climatological datasets used to force the physical model, including wind speed, solar radiation, air temperature, dewpoint temperature, and salinity. Light lines in the upper three panels show the high-resolution data used to force the model; dark lines show a weekly running average, and are provided only for visual clarity.

A.7 encompass the equations used in the version of the model used in Chapter 3; further elaboration of the process variables within these equations are found in Section A.2.1 and Section A.2.2. In Chapter 4, modifications were made to the iron cycle; Eq. (A.8) describes the new dynamics, and the process variables are described in Section A.2.3.

$$\frac{d(B_i)}{dt} = \begin{cases} Gpp_i - Res_i - Ex_i - \sum_j Con_{ij} - Mor_i & i = \text{phytoplankton} \\ \sum_k Con_{ki} - Ege_i - Exc_i - \sum_j Con_{ij} - Mor_i & i = \text{zooplankton} \\ \sum_k ConI_{ki} - \int_0^{z_{max}} Ege_i - \int_0^{z_{max}} Exc_i - \sum_j ConI_{ij} - MorI_i & i = \text{nekton} \\ Dec_{NH_4, NO_3} + f \left(\sum_j Res_j - \sum_j Gpp_j \right) & i = NO_3 \\ Dec_{DON, NH_4} + Dec_{PON, NH_4} + \sum_i Exc_i - Dec_{NH_4, NO_3} + \\ (1-f) \left(\sum_j Res_j - \sum_j Gpp_j \right) & i = NH_4 \\ Dec_{PON, DON} + \sum_j Ex_j - Dec_{DON, NH_4} & i = DON \\ \sum_j Mor_j + \sum_j Ege_j - Dec_{PON, DON} - Dec_{PON, NH_4} & i = PON \end{cases} \quad (\text{A.5})$$

$$\frac{d(B_{Si,i})}{dt} = \begin{cases} R_{Si:N} \cdot \left(Gpp_i - Res_i - Ex_i - \sum_j Con_{ij} - Mor_i \right) & i = \text{phytoplankton} \\ R_{Si:N} \cdot \left(\sum_{j=\text{diatom}} Res_j + \sum_{j=\text{diatom}} Ex_j - \sum_{j=\text{diatom}} Gpp_j \right) + \\ Dec_{Opal, SiOH_4} & i = Si(OH)_4 \\ R_{Si:N} \left(\sum_{j=\text{diatom}} Mor_j + \sum_{j=\text{diatom}} \sum_k Con_{jk} \right) - \\ Dec_{Opal, SiOH_4} & i = Opal \end{cases} \quad (\text{A.6})$$

$$\frac{d(B_{Fe,i})}{dt} = \begin{cases} \frac{B_{Fe,i}}{B_i} \cdot \left(Gpp_i - Res_i - Ex_i - \sum_j Con_{ij} - Mor_i \right) + Ufe_i & i = \text{phytoplankton} \\ \sum_j \left(f_{rem} \cdot \frac{B_{Fe,j}}{B_j} \cdot (Res_j + Ex_j + \sum_k Con_{jk} + Mor_j) - \right. \\ \left. \frac{B_{Fe,j}}{B_j} \cdot Gpp_j - Ufe_j \right) & i = Fe \end{cases} \quad (\text{A.7})$$

$$\frac{d(B_{Fe,i})}{dt} = \begin{cases} \frac{B_{Fe,i}}{B_i} \cdot \left(- \sum_j Con_{ij} - Mor_i \right) + Qup_i & i = \text{phytoplankton} \\ Dec_{POFe, Fe} + \sum_j \frac{B_{Fe,j}}{B_j} \sum_k Con_{jk} \cdot GE_k - \sum_j Qup_j - Ads & i = Fe \\ Ads + \frac{B_{Fe,j}}{B_j} \sum_j \left(\sum_k (Con_{jk} \cdot GS_k) + Mor_j \right) - Dec_{POFe, Fe} & i = POFe \end{cases} \quad (\text{A.8})$$

The tables in Section A.2.4.2 provide definitions and values for all parameters in the above set of equations, as well as the process variable equations in the following sections. Table A.13 on page 94 through Table A.20 on page 96 include all parameters related to the biogeochemistry, most of which came from the NEMURO model. The following table, Table A.21 on page 97, defines variables that vary over time in the simulations; these variables are functions of the various state variables in the model. Finally, Table A.22 on page 98 through Table A.26 on page 102 provide parameters that are derived from the Ecopath algorithm.

A.2.1 Nitrogen flux equations for living state variables

A.2.1.1 Gross primary production (Gpp)

Gross primary production fluxes flow from the NO_3 and NH_4 variables to each phytoplankton group, following (Kishi *et al.*, 2007b), with the addition of iron limitation following Fiechter *et al.* (2009). The uptake of nitrogen is described by:

$$Gpp_i = V_{max,i} \exp(K_{gpp,i}T) \cdot L_{nut,i} \cdot L_{light,i} \cdot B_i \quad (\text{A.9})$$

where B_i is the nitrogen-based biomass of group i , resolved with depth.

A.2.1.2 Respiration (Res)

Respiration applies to all phytoplankton groups, and flows from the phytoplankton to the NO_3 and NH_4 groups following the same f-ratio as uptake via primary production:

$$Res_i = Res_{0i} \exp(K_{res,i}T) B_i \quad (\text{A.10})$$

A.2.1.3 Extracellular excretion (Ex)

Extracellular excretion applies to all phytoplankton groups, and flows from the phytoplankton to the DON group. Following Kishi *et al.* (2007b), extracellular excretion is proportional to the flux due to gross primary production:

$$Ex_i = \gamma_i \cdot Gpp_i \quad (\text{A.11})$$

A.2.1.4 Consumption (Con)

Predator/prey interactions between functional groups follow the Aydin version of the foraging arena functional response. The exact form of the functional response varies based on whether the predator and prey groups are planktonic or nektonic. For interactions between two planktonic groups, the flux is resolved with depth for both the predator and prey group, and the uptake rates are temperature-dependent:

$$Con_{ij} = \frac{Q'_{ij}}{\exp(K_{Gra,i} \cdot T_{avg})} \exp(K_{Gra,i} \cdot T) \left(\frac{X_{ij} \cdot \frac{B_j}{B'_j}}{X_{ij} - 1 + \frac{B_j}{B'_j}} \right) \left(\frac{D_{ij} \cdot \left(\frac{B_i}{B'_i} \right)^{\theta_{ij}}}{D_{ij} - 1 + \left(\frac{B_i}{B'_i} \right)^{\theta_{ij}}} \right) \quad (\text{A.12})$$

where here, the subscripts i and j represent the prey and predator groups, respectively. As described in Section 3.2.2.2, the biomass and consumption rate parameters are derived from the Ecopath mass balance: $Q' = \frac{Q^*}{MLD}$ and $B' = \frac{B^*}{MLD}$, where Q^* and B^* are the per-area mass-balanced quantities returned directly from Ecopath. The parameters MLD and T_{avg} describe the yearly averaged mixed layer depth and mixed layer temperature, respectively, as simulated by the one-dimensional physical model.

For interactions between two nektonic groups, the functional response follows the same form, but in units of biomass integrated over depth. Nektonic consumption does not vary with temperature.

$$ConI_{ij} = Q^*_{ij} \left(\frac{X_{ij} \cdot \frac{Bint_j}{B^*_j}}{X_{ij} - 1 + \frac{Bint_j}{B^*_j}} \right) \left(\frac{D_{ij} \cdot \left(\frac{Bint_i}{B^*_i} \right)^{\theta_{ij}}}{D_{ij} - 1 + \left(\frac{Bint_i}{B^*_i} \right)^{\theta_{ij}}} \right) \quad (\text{A.13})$$

When a nektonic group preys upon a planktonic group, the total flux is calculated in depth-integrated units. However, the loss on the plankton side is resolved with depth and distributed proportionally to the prey biomass at each depth, while the flow to the predator remains in depth-integrated units:

$$Con_{ij} = Q^*_{ij} \left(\frac{X_{ij} \cdot \frac{Bint_j}{B^*_j}}{X_{ij} - 1 + \frac{Bint_j}{B^*_j}} \right) \left(\frac{D_{ij} \cdot \left(\frac{\int_0^{z_{max}} B_i dz}{B^*_i} \right)^{\theta_{ij}}}{D_{ij} - 1 + \left(\frac{\int_0^{z_{max}} B_i dz}{B^*_i} \right)^{\theta_{ij}}} \right) \cdot \frac{1}{\Delta z} \cdot \frac{B_i \Delta z}{\int_0^{z_{max}} B_i dz} \quad (\text{A.14})$$

$$ConI_{ij} = Q^*_{ij} \left(\frac{X_{ij} \cdot \frac{Bint_j}{B^*_j}}{X_{ij} - 1 + \frac{Bint_j}{B^*_j}} \right) \left(\frac{D_{ij} \cdot \left(\frac{Bint_i}{B^*_i} \right)^{\theta_{ij}}}{D_{ij} - 1 + \left(\frac{Bint_i}{B^*_i} \right)^{\theta_{ij}}} \right) \quad (\text{A.15})$$

where $ConI = \int_0^{z_{max}} Con dz$.

A.2.1.5 Excretion (Exc) and egestion (Ege)

Egestion and excretion are proportional to the total consumption of prey by a predator. Egestion flows from the predator to the *PON* group, with the exception of egestion by microzooplankton, where egestion is split between the *PON*, *DON*, and *NH₄* groups. Excretion flows from the predator group to the *NH₄* group. All excretion and egestion by nektonic groups is assumed to take place in the surface layer:

$$Ege_i = GS_i \cdot \left(\sum_{k=plank} Con_{ki} + \frac{\sum_{\ell=nek} ConI_{\ell i}}{\Delta z_1} \right) \quad z = 1 \quad (\text{A.16})$$

$$Ege_i = GS_i \cdot \sum_k Con_{ki} \quad z \neq 1 \quad (\text{A.17})$$

$$Exc_i = (1 - GE_i - GS_i) \cdot \left(\sum_{k=plank} Con_{ki} + \frac{\sum_{\ell=nek} ConI_{\ell i}}{\Delta z_1} \right) \quad z = 1 \quad (\text{A.18})$$

$$Exc_i = (1 - GE_i - GS_i) \cdot \sum_k Con_{ki} \quad z \neq 1 \quad (\text{A.19})$$

A.2.1.6 Non-predatory mortality (Mor)

Non-predatory mortality, e.g. loss to old age or disease, is modeled as a quadratic function of biomass. For planktonic groups, this flux is in units of mass per volume:

$$Mor_i = \left(\frac{M_{0i}}{B'_i} \right) \cdot B_i^2 \quad (\text{A.20})$$

while for nektonic groups it is in units of mass per area:

$$MorI_i = \left(\frac{M_{0i}}{B''_i} \right) \cdot Bint_i^2 \quad (\text{A.21})$$

As with egestion and excretion by nektonic groups, non-predatory mortality of nektonic groups is assumed to occur in the surface layer, such that in the surface layer,

$$Mor_i = \frac{MorI_i}{\Delta z_1} \quad (\text{A.22})$$

when $i = \text{nekton}$.

A.2.2 Additional fluxes

A.2.2.1 Proportional-to-nitrogen fluxes of silica and iron

The majority of fluxes between iron- and silica-based state variables occur in proportion to nitrogenous fluxes. Silica fluxes due to gross primary production (Gpp), extracellular excretion (Ex), and respiration (Res) between phytoplankton groups and $SiOH_4$ occur in a constant proportion to the respective fluxes in nitrogen between phytoplankton groups and all dissolved nitrogen pools (NO_3 , NH_4 , and DON). Similarly, fluxes due to non-predatory mortality (Mor) from phytoplankton groups to the PON group are accompanied by proportional fluxes of silica from the large phytoplankton to particulate opal group. Silica is assumed to be completely egested by phytoplankton grazers, so the proportional flux due to predator consumption (Con) of phytoplankton silica is routed entirely to the particulate opal group, rather than being split between predator, egestion, and excretion as is the case for nitrogenous consumption.

Iron fluxes between the two phytoplankton groups and the dissolved iron group also occur proportionally to nitrogen fluxes, though the ratio between the two elements varies over time (see Section A.2.2.2). However, only a fraction of the iron fluxes out of the phytoplankton groups ends up in the dissolved iron pool, with the remainder leaving the system.

A.2.2.2 Luxury iron uptake (Ufe)

In addition to the proportional-to-nitrogen uptake and loss of iron due to gross primary production, respiration, extracellular excretion, grazing loss, and natural mortality, phytoplankton can also gain and lose iron through a relaxation process following the model of Fiechter *et al.* (2009). This model allows phytoplankton to take up dissolved iron in order to adjust their internal Fe:C ratios toward a value predicted by the ambient dissolved iron in the surrounding water. This additional uptake term accounts for the fact that iron uptake, unlike macronutrient uptake, is not necessarily a function of dissolved iron concentration, and that iron to carbon ratios within phytoplankton cells can vary widely over time depending on conditions. The luxury uptake in the WCE module is described by:

$$Ufe_i = \frac{R_{0i} - R_i}{t_{Fe,i}} \cdot B_i \cdot R_{C:N} \quad (\text{A.23})$$

A.2.2.3 Decomposition (Dec)

Decomposition fluxes follow the model of Kishi *et al.* (2007b), with a decay rate related to temperature:

$$Dec_{ij} = V_{Dec,ij} \exp(K_{Dec,ij} T) \cdot B_i \quad (\text{A.24})$$

where the subscripts i and j represent the source and sink groups, respectively, and B_i the concentration of the source group.

A.2.3 Iron dynamics in the quota model

The iron model used in Chapter 4 is based closely on one developed for the Carbon, Ocean Biogeochemistry and Lower Trophics (COBALT) marine ecosystem model (Stock *et al.*, n.d.), with only a few adjustments to parameter values in order to tune the dynamics to a one-dimensional water column.

Iron uptake for phytoplankton is based on an internal cell quota, accounting for both requirements and additional luxury uptake. Iron's contribution to overall nutrient limitation, which regulates the uptake of macronutrients, is termed iron deficiency ($D_{Fe,i}$) and is calculated based on the internal ratio of iron to nitrogen. However, uptake of iron is not proportional to uptake of nitrogen, but instead based on a separate limitation term ($L_{Fe,i}$), allowing phytoplankton to increase their internal Fe:N ratios to a preset limit:

$$Qup_i = \begin{cases} V_{max,i} \exp(K_{gpp,i} T) \cdot B_{Fe,i} \cdot L_{Fe,i} \cdot \mu_{Fe:N,i}, & \text{if } R_{Fe:N,i} < R_{Fe:Nmax,i} \\ 0, & \text{otherwise} \end{cases} \quad (\text{A.25})$$

Iron is not tracked beyond the level of phytoplankton, but upon loss to predation is recycled to the dissolved and particulate iron state variables proportionate to the nitrogenous excretion and egestion fluxes of their predators.

Scavenging of dissolved iron onto particles follows a single ligand model, where only non-ligand-bound iron is available for adsorption onto particles. Light is assumed to greatly reduce the effectiveness of ligand binding through the production of oxygen free radicals (Fan, 2008). This impact is assumed to decay at light levels below 10 W m^{-2} in a manner consistent with the observed decline

of hydrogen peroxide in the water column (Yuan & Shiller, 2001). The free unbound iron, Fe_{free} , is calculated via:

$$K_{Lig} \cdot Fe_{free}^2 + (1 + K_{Lig} \cdot (Lig_{bkg} - Fe)) \cdot Fe_{free} - B_{Fe} = 0 \quad (\text{A.26})$$

with adsorption onto particles directly proportional to this free iron:

$$Ads = \alpha_{scav} \cdot Fe_{free} \quad (\text{A.27})$$

Finally, a fraction of particulate iron is remineralized to the dissolved iron pool, proportional to remineralization of particulate nitrogen to ammonium.

$$Dec_{POFe,Fe} = Dec_{PON,NH_4} \cdot \frac{B_{PON}}{B_{POFe}} \cdot r_{eff} \quad (\text{A.28})$$

A.2.4 Parameterization for the biological model

A.2.4.1 Ecopath input data

The majority of the Ecopath data used to construct our food web model came the previously-published Aydin-48 model (Aydin *et al.*, 2003). However, a few modifications were made to this data prior to running the simplification process described in the previous section.

The first modification made was to eliminate the bacteria functional group from the Aydin-48 model. In the original model, this functional group was included as a prey item for microzooplankton, “preying” itself on the two detrital functional groups. However, in their time-dynamic simulations, Aydin *et al.* (2003) found that their results were highly sensitive to this representation of the microbial loop, and it led to some lower trophic level dynamics that disagreed with accepted biogeochemical models from the region; they concluded that it was sufficient to assume that bacterial processes occurred within the detrital pools and removed the bacteria group from some of their later simulations. Because we intended to link the Ecopath-derived food web model directly to a biogeochemical model that already included parameterizations for the microbial loop, we decided to eliminate the bacteria group from the food web dynamics entirely, and we replaced the microzooplankton diet with one of 100% small phytoplankton.

Table A.1 on page 81 and A.2 provide descriptions of the 47 functional groups that remained in the model, including the most common species classified under each functional group and a very basic description is listed for each. Pertinent information regarding each group's lifecycle are also provided.

After examining the sources of zooplankton data for the Aydin-48 model, we made several adjustments to the data for those groups. (Aydin *et al.*, 2003) resolved the zooplankton community into eleven different functional groups: microzooplankton, copepods, euphausiids, pteropods, amphipods, sergestidae (shrimp), chaetognaths, salps, ptenophores, large jellyfish, and a miscellaneous group (mainly larvaceans and polychaetes). Much of the data for these groups was derived from a simulation of the NEMURO biogeochemical model. We found several issues with the assumptions used to translate the NEMURO output data into Ecopath input data.

First, the version of NEMURO used by Aydin *et al.* (2003) was an early realization of that model (Eslinger *et al.*, 2000; Megrey *et al.*, 2000), and we found we were unable to replicate their results using the a version that follows the “official” description (Kishi *et al.*, 2007a). For this study, we developed our own biogeochemical model, based very closely on NEMURO, and substituted the values from a simulation of our model in place of those detailed in the Aydin *et al.* (2003) report.

Second, Aydin *et al.* (2003) interpreted NEMURO’s predatory zooplankton group (ZP) as representing only non-gelatinous omnivores, i.e. euphausiids, pteropods, and amphipods. They gathered data for the gelatinous zooplankton groups (large jellyfish, chaetognaths, salps, and ctenophores) from other sources, and estimated the population of the carnivorous shrimp and miscellaneous groups each as 10% of the ZP value. Overall, this led to a community with a very large mesozooplankton community, more than twice that of the copepod population, despite the fact that copepods should be the dominant mesozooplankton genera (Goldblatt *et al.*, 1999; Harrison *et al.*, 2004). While NEMURO’s ZP state variable does have an omnivorous diet, in our opinion it was intended to represent all unresolved predators of the two smaller zooplankton state variables (which correspond to the microzooplankton and copepod populations); in this Ecopath model, this includes all not only the nine of the remaining zooplankton groups but all other non-planktonic groups. Based on descriptions of the mesozooplankton community in subarctic gyre (Goldblatt *et al.*, 1999), we decided to distribute 50% of the ZP biomass to the omnivorous, non-gelatinous zooplankton groups (euphausiids, pteropods, and amphipods), 40% to the omnivorous, gelatinous groups (salps and ctenophores), and the remaining 10% to the carnivorous groups (shrimp, ctenophores, and miscellaneous).

The final issue with the NEMURO-derived zooplankton biomass data in the Aydin *et al.* (2003) report involved the conversion of units between NEMURO, which tracks state variables through their

Table A.1: A description of the 47 functional groups included in the unsimplified version of the food web model. Species listed are not exhaustive, but represent the dominant members of each functional group.

Group	Includes	Details
Sperm whales	sperm whales (<i>Physeter macrocephalus</i>)	a very large toothed whale, only mature males are found in the subarctic gyre region, and only during the summer months.
Toothed whales	orcas (<i>Orcinus orca</i>)	includes the mammal-eating transient subpopulation and some portion of the piscivorous (and typically more coastal) resident subpopulation
Fin whales	fin whales (<i>Balaenoptera physalus</i>)	a baleen whale, migrates to the gyre during summer months to feed
Sei whales	sei whales (<i>Balaenoptera borealis</i>)	a baleen whale, migrates to the gyre during summer months to feed
Northern fur seals	northern fur seals (<i>Callorhinus ursinus</i>)	a large fur seal.
Elephant seals	northern elephant seals (<i>Mirounga angustirostris</i>)	large seal, migrates biannually between the Alaska Gyre and California breeding beaches.
Dall's porpoises	Dall's porpoises (<i>Phocoenoides dalli</i>)	a porpoise
Pacific white-sided dolphins	Pacific white-sided dolphins (<i>Lagenorhynchus obliquidens</i>)	a dolphin
Northern right whale dolphins	Northern right whale dolphins (<i>Lissodelphis borealis</i>)	a small dolphin
Albatross	primarily Black-footed albatross (<i>Phoebastria nigripes</i>) and Laysan albatross (<i>Phoebastria immutabilis</i>)	large seabirds
Shearwaters	primarily sooty shearwaters (<i>Puffinus griseus</i>) and short-tailed shearwaters (<i>Puffinus tenuirostris</i>)	medium-sized seabirds, the dominant seabird in the Gulf of Alaska region
Storm Petrels	primarily fork-tailed storm petrels (<i>Oceanodroma furcata</i>) and Leach's storm petrels (<i>Oceanodroma leucorhoa</i>)	small seabirds
Kittiwakes	primarily black-legged kittiwakes (<i>Rissa tridactyla</i>)	seabirds in the gull family
Fulmars	northern fulmar (<i>Fulmarus glacialis</i>)	a seabird
Puffins	primarily tufted puffins (<i>Fratercula cirrhata</i>)	a medium-sized seabird
Skuas	primarily south-polar skuas (<i>Stercorarius maccormicki</i>)	a large seabird
Jaegers	primarily Pomarine jaegers	seabird, in the skua family
Sharks	salmon sharks (<i>Lamna ditropis</i>)	small shark, approximately 2m long, homeothermic
Large gonatid squid	armhook squid (family Gonatidae)	medium-sized squid

Table A.2: A description of the 47 functional groups included in the unsimplified version of the food web model (continued).

Group	Includes	Details
Boreal clubhook squid	boreal clubhook squid (<i>Onychoteuthis borealijaponica</i>)	a medium-sized squid
Neon flying squid	neon flying squid (<i>Ommastrephes bartramii</i>)	a slightly larger squid
Sockeye salmon	sockeye salmon (<i>Oncorhynchus nerka</i>)	the most abundant salmon species in the Eastern Gyre, anadromous
Chum salmon	chum salmon (<i>Oncorhynchus keta</i>)	the second-most abundant salmon species in the Easterb Gyre, anadromous
Pink salmon	pink salmon (<i>Oncorhynchus gorbuscha</i>)	smallest Pacific salmon, anadromous, have a two-year breeding cycle, with even- and odd-year populations not interbreeding
Coho salmon	coho salmon (<i>Oncorhynchus kisutch</i>)	a salmon, anadromous
Chinook salmon	Chinook salmon (<i>Oncorhynchus tshawytscha</i>)	the largest Pacific salmon, anadromous
Steelhead	steelhead, or rainbow trout (<i>Oncorhynchus mykiss</i>)	salmonid, anadromous
Pomfret	Pacific pomfret (<i>Brama japonica</i>)	a large perciform fish
Saury	Pacific saury (<i>Cololabis saira</i>)	medium-sized (30-40 cm), highly migratory fish, important commercial fish, especially in Asia
Pelagic forage fish	primarily sticklebacks (<i>Gasterosteus aculeatus</i>)	small (4 cm) schooling forage fish
Micronektonic squid	primarily gonatids such as <i>Berryteuthis anonychus</i> and <i>Gonatus onyx</i>	juvenile squid, few data measurements available
Mesopelagic fish	myctophids, or lanternfishes (family Myctophidae), particularly <i>Stenobrachius leucopsarus</i>	small mesopelagic fish
Large jellyfish	phylum Cnidarian	small jellyfish
Ctenophores	phylum Ctenophora	comb jellies, gelatinous
Salps	family Salpidae	planktonic tunicates, gelatinous
Chaetognaths	phylum Chaetognatha	marine worms, gelatinous
Sergestid shrimp	family Sergestidae	shrimp
Miscellaneous predatory zooplankton	mainly Larvaceans and Polychaetes	planktonic tunicates and annelid worms
Amphipods	order Amphipoda	crustacean zooplankton
Pteropods	Thecosomata	planktonic gastropods
Euphausiids	krill (order Euphausiacea)	crustacean zooplankton
Copepods	subclass Copepoda	small crustacean zooplankton
Microzooplankton	any <200 μm	mainly meroplanktonic larva and copepod nauplii
Large phytoplankton	any <5 μm	includes prasinophytes, prymnesiophytes (coccolithophorids), cryptophytes, and cyanobacteria
Small phytoplankton	primarily diatoms	represent large size class, includes silica cycle
DNH3	detritus, dissolved	detritus pool
POM	detritus, particulate	detritus pool

nitrogen content, and Ecopath, which uses total wet weight. While Aydin *et al.* (2003) detailed the assumptions used to convert the NEMURO data from mmol N m⁻² to g C m⁻², including elemental ratios and mixed layer depth values, no explanation was given for the 0.01 g C/g wet weight conversion factor that was then used to calculate wet weight of both phyto- and zooplankton groups. While this order of magnitude estimate is common in conversions of fish wet weight to carbon content, it is much lower than most measurements for plankton. For example, crustacean zooplankton wet mass to carbon ratios range from 0.06-0.12 g wet mass/gC Harris *et al.* (2000). We compromised with a conversion factor of 0.03 gC/g wet weight, which we applied throughout this study whenever converting between element-based and weight-based units.

The final adjustment we made to the Aydin-48 data concerned the growth efficiency value applied to the ctenophore group. The value of 0.03 used for this group appeared extremely low, even for a gelatinous group. Aydin *et al.* (2003) cited Pauly *et al.* (1996) as the source of this number. However, Pauly *et al.* (1996) derived their carnivorous jelly data from measurements of the cnidarian *Aglantha*, and even for this species they commented that the consumption rate they were using was “very high, perhaps excessively so.” Measured growth efficiencies for ctenophores vary from less than 10% to 45% (Reeve *et al.* , 1978, 1989); we settled on a value of 0.3, in line with that of the other zooplankton groups, in order to resolve Ecopath balance issues that arose as a result of the NEMURO-derived adjustments detailed above.

The final set of Ecopath input data for the 47-group model can be found in Tables A.3 through A.9. Following the simplification process described in Section 2.2, the food web was reduced to 24 groups. The Ecopath input parameters for this 24-group model are found in Tables A.10, A.11, and A.12.

A.2.4.2 Tables of parameters

The following series of tables describe and define all parameters that were used throughout the documentation of the water column ecosystem model.

Table A.3: Ecopath input variables for the 47-group food web, including biomass (B, tons wet weight m^{-2}), production/biomass (PB, yr^{-1}), consumption/biomass (QB, yr^{-1}), ecotrophic efficiency (EE), growth efficiency (GE), and fraction unassimilated (GS)

Group	B		PB		QB		EE	GE	GS
	Value	Ped	Value	Ped	Value	Ped			
Sperm whales	0.000929	0.5	0.0596	0.4	6.61	0.2		0.2	
Toothed whales	2.8e-05	0.5	0.0252	0.4	11.16	0.2		0.2	
Fin whales	0.027883	0.5	0.02	0.4	4.56	0.2		0.2	
Sei whales	0.005902	0.5	0.02	0.4	6.15	0.2		0.2	
Northern fur seals	0.000246	0.5	0.235	0.4	39.03	0.2		0.2	
Elephant seals	0.00043	0.5	0.368	0.4	11.08	0.2		0.2	
Dall's porpoises	0.0059864	0.5	0.1	0.4	27.47	0.2		0.2	
Pacific white-sided dolphins	0.0039625	0.5	0.14	0.4	25.83	0.2		0.2	
Northern right whale dolphins	0.0038973	0.5	0.16	0.4	24.14	0.2		0.2	
Albatross	4e-05	0.5	0.05	0.4	81.59	0.2		0.2	
Shearwaters	0.0004	0.5	0.1	0.4	100.13	0.2		0.2	
Storm Petrels	5.6e-05	0.5	0.1	0.4	152.08	0.2		0.2	
Kittiwakes	5.2e-05	0.5	0.1	0.4	123	0.2		0.2	
Fulmars	7.4e-05	0.5	0.1	0.4	100.26	0.2		0.2	
Puffins	5.8e-05	0.5	0.1	0.4	104.33	0.2		0.2	
Skuas	5.4e-05	0.5	0.075	0.4	96.6	0.2		0.2	
Jaegers	3.8e-05	0.5	0.075	0.4	96.6	0.2		0.2	
Sharks	0.05	0.8	0.2	0.6	10.95	0.4		0.2	
Large gonatid squid	0.03	0.8	2.555	0.6	7.3	0.6		0.2	
Boreal clubhook squid	0.012	0.8	2.555	0.6	7.3	0.6		0.2	
Neon flying squid	0.45	0.8	2.555	0.6	6.205	0.6		0.2	
Sockeye salmon	0.089656	0.5	1.27	0.1	10.13	0.1		0.2	
Chum salmon	0.054136	0.5	1.93	0.1	14.51	0.1		0.2	
Pink salmon	0.023267	0.5	3.37	0.1	18.49	0.1		0.2	
Coho salmon	0.0044535	0.5	2.47	0.1	16.55	0.1		0.2	
Chinook salmon	0.0093031	0.5	0.8	0.3			0.3	0.15	0.2
Steelhead	0.0093	0.5	0.8	0.3			0.3	0.15	0.2
Pomfret	0.21	0.8	0.75	0.4			0.4	0.20	0.2
Saury	0.45	0.8	1.6	0.6	7.9	0.7		0.2	
Pelagic forage fish			0.8	1.5	0.6	5	0.7	0.9	0.2
Micronektonic squid			0.8	3	0.6	15	0.7	0.9	0.2
Mesopelagic fish	4.5	0.8	0.9	0.6	3	0.7		0.2	
Large jellyfish	4	0.8	3	0.7	10	0.7		0.2	
Ctenophores	1.5488	0.5	4	0.7	13.333	0.7		0.3	
Salps	1.5488	0.5	9	0.7	30	0.7		0.3	
Chaetognaths	4.1302	0.5	6.9876	0.7	23.292	0.7		0.3	
Sergestid shrimp	4.1302	0.8	6.9876	0.7	23.292	0.7		0.3	
Miscellaneous predatory zooplankton	4.1302	0.8	6.9876	0.7	23.292	0.7		0.3	
Amphipods	5.1628	0.8	6.9876	0.7	23.292	0.7		0.3	
Pteropods	5.1628	0.8	6.9876	0.7	23.292	0.7		0.3	
Euphausiids	5.1628	0.8	6.9876	0.4	23.292	0.4		0.3	
Copepods	20.919	0.1	23.151	0.1	77.169	0.4		0.3	
Microzooplankton	16.83	0.1	38.833	0.1	129.44	0.4		0.3	
Large phytoplankton	27.029	0.8	41.677	0.1	68.132	0.4			
Small phytoplankton	42.427	0.5	70.621	0.1	101.6	0.4			
DNH3	50	0.1			0.1		0.4		
POM	50	0.1			0.1		0.4		

Table A.4: Diet fraction input for the 47-group food web model.

Predator	Prey	Diet fraction	Pedigree
Sperm whales	Large gonatid squid	0.02287	0.7
	Boreal clubhook squid	0.00915	
Toothed whales	Neon flying squid	0.34299	
	Sockeye salmon	0.00208	
	Chum salmon	0.00125	
	Pink salmon	0.00054	
	Coho salmon	0.0001	
	Chinook salmon	0.00022	
	Steelhead	0.00022	
	Pomfret	0.00486	
	Saury	0.01042	
	Pelagic forage fish	0.126	
	Micronektonic squid	0.375	
	Mesopelagic fish	0.10416	
	Fin whales	0.22725	
	Sei whales	0.04811	
	Northern fur seals	0.002	
	Elephant seals	0.00351	
	Dall's porpoises	0.04879	
Fin whales	Pacific white-sided dolphins	0.03229	0.7
	Northern right whale dolphins	0.03176	
	Albatross	0.00032	
	Shearwaters	0.00326	
	Storm Petrels	0.00046	
	Kittiwakes	0.00042	
	Fulmars	0.00061	
	Puffins	0.00047	
	Skuas	0.00044	
	Jaegers	0.00031	
	Large gonatid squid	0.00305	
	Boreal clubhook squid	0.00122	
	Neon flying squid	0.04573	
	Sockeye salmon	0.0249	
	Chum salmon	0.01504	
	Pink salmon	0.00646	
	Coho salmon	0.00124	
	Chinook salmon	0.00258	
	Steelhead	0.00258	
	Pomfret	0.05833	
	Saury	0.12498	
	Pelagic forage fish	0.264	
	Micronektonic squid	0.05	
	Large gonatid squid	0.001524	
	Boreal clubhook squid	0.000609	
	Neon flying squid	0.022866	
	Sockeye salmon	0.001245	
	Chum salmon	0.000752	
	Pink salmon	0.000323	
	Coho salmon	6.19e-05	
	Chinook salmon	0.000129	
	Steelhead	0.000129	
	Pomfret	0.002917	
	Saury	0.00625	
	Pelagic forage fish	0.076	
	Micronektonic squid	0.025	
	Mesopelagic fish	0.062499	
	Chaetognaths	0.054357	
	Sergestid shrimp	0.041179	
	Misc. predatory zooplankton	0.041746	
	Amphipods	0.083492	
	Pteropods	0.083492	
	Euphausiids	0.20873	
	Copepods	0.287004	

Table A.5: Diet fraction input for the 47-group food web model (continued).

Predator	Prey	Diet fraction	Pedigree
Sei whales	Large gonatid squid	0.001524	0.7
	Boreal clubhook squid	0.000609	
Northern fur seals	Neon flying squid	0.022866	
	Sockeye salmon	0.001245	
	Chum salmon	0.000752	
	Pink salmon	0.000323	
	Coho salmon	6.19e-05	
	Chinook salmon	0.000129	
	Steelhead	0.000129	
	Pomfret	0.002917	
	Saury	0.00625	
	Pelagic forage fish	0.076	
	Micronektonic squid	0.025	
	Mesopelagic fish	0.062499	
	Chaetognaths	0.05435	
	Sergestid shrimp	0.041179	
	Misc. predatory zooplankton	0.041746	
	Amphipods	0.083492	
	Pteropods	0.083492	
	Euphausiids	0.20873	
Elephant seals	Copepods	0.287004	0.7
	Large gonatid squid	0.00915	
	Boreal clubhook squid	0.00366	
	Neon flying squid	0.1372	
	Sockeye salmon	0.02988	
	Chum salmon	0.01804	
	Pink salmon	0.00775	
	Coho salmon	0.00148	
	Chinook salmon	0.0031	
	Steelhead	0.0031	
	Pomfret	0.06999	
	Saury	0.14998	
	Pelagic forage fish	0.267	
	Micronektonic squid	0.15	
	Mesopelagic fish	0.15	
	Large gonatid squid	0.0122	
	Boreal clubhook squid	0.00488	
	Neon flying squid	0.18293	
Dall's porpoises	Sockeye salmon	0.01132	0.7
	Chum salmon	0.00683	
	Pink salmon	0.00294	
	Coho salmon	0.00056	
	Chinook salmon	0.00117	
	Steelhead	0.00117	
	Pomfret	0.056	
	Saury	0.12	
	Pelagic forage fish	0.2	
	Micronektonic squid	0.4	
	Large gonatid squid	0.01372	
	Boreal clubhook squid	0.00549	
	Neon flying squid	0.20579	
	Sockeye salmon	0.01494	
	Chum salmon	0.00902	
	Pink salmon	0.00388	
	Coho salmon	0.00074	
	Chinook salmon	0.00155	
	Steelhead	0.00155	
	Pomfret	0.035	
	Saury	0.07499	
	Pelagic forage fish	0.208	
	Micronektonic squid	0.225	
	Mesopelagic fish	0.2	

Table A.6: Diet fraction input for the 47-group food web model (continued).

Predator	Prey	Diet fraction	Pedigree
Pacific white-sided dolphins	Large gonatid squid	0.00762	0.7
	Boreal clubhook squid	0.00305	
	Neon flying squid	0.11433	
	Sockeye salmon	0.03984	
	Chum salmon	0.02406	
	Pink salmon	0.01034	
	Coho salmon	0.00198	
	Chinook salmon	0.00413	
	Steelhead	0.00413	
	Pomfret	0.09332	
	Saury	0.19997	
	Pelagic forage fish	0.172	
	Micronektonic squid	0.225	
	Mesopelagic fish	0.1	
	Large gonatid squid	0.01524	
	Boreal clubhook squid	0.0061	
Northern right whale dolphins	Neon flying squid	0.22866	0.7
	Sockeye salmon	0.00498	
	Chum salmon	0.00301	
	Pink salmon	0.00129	
	Coho salmon	0.00025	
	Chinook salmon	0.00052	
	Steelhead	0.00052	
	Pomfret	0.01167	
	Saury	0.025	
	Pelagic forage fish	0.053	
	Micronektonic squid	0.25	
	Mesopelagic fish	0.4	
	Large gonatid squid	0.04573	
	Boreal clubhook squid	0.01829	
	Neon flying squid	0.68598	
Albatross	Saury	0.1	0.7
	Pelagic forage fish	0.1	
	Micronektonic squid	0.05	
	Saury	0.275	
	Pelagic forage fish	0.275	
	Micronektonic squid	0.3	
	Amphipods	0.0189	
	Pteropods	0.0189	
	Euphausiids	0.04724	
	Copepods	0.06496	
Shearwaters	Saury	0.05	0.7
	Pelagic forage fish	0.05	
	Micronektonic squid	0.6	
	Amphipods	0.0378	
	Pteropods	0.0378	
	Euphausiids	0.09449	
	Copepods	0.12992	
	Saury	0.4	
	Pelagic forage fish	0.4	
	Amphipods	0.0252	
Storm Petrels	Pteropods	0.0252	0.7
	Euphausiids	0.06299	
	Copepods	0.08661	
	Saury	0.4	
	Pelagic forage fish	0.4	
	Amphipods	0.0252	
	Pteropods	0.0252	
	Euphausiids	0.06299	
	Copepods	0.08661	
	Pelagic forage fish	0.04	
Kittiwakes	Micronektonic squid	0.96	0.7
	Saury	0.4	
	Pelagic forage fish	0.4	
	Amphipods	0.0252	
	Pteropods	0.0252	
	Euphausiids	0.06299	
	Copepods	0.08661	
	Pelagic forage fish	0.04	
	Micronektonic squid	0.96	
	Saury	0.4	
Fulmars	Pelagic forage fish	0.4	0.7
	Micronektonic squid	0.1	
	Saury	0.4	
	Pelagic forage fish	0.4	
	Micronektonic squid	0.0126	
	Amphipods	0.0126	
	Pteropods	0.0126	
	Euphausiids	0.0315	
	Copepods	0.04331	

Table A.7: Diet fraction input for the 47-group food web model (continued).

Predator	Prey	Diet fraction	Pedigree
Skuas	Saury	0.5	0.7
	Pelagic forage fish	0.5	
Jaegers	Saury	0.5	0.7
	Pelagic forage fish	0.5	
Sharks	Large gonatid squid	0.01782	0.8
	Boreal clubhook squid	0.00713	
	Neon flying squid	0.26724	
	Sockeye salmon	0.05324	
	Chum salmon	0.03215	
	Pink salmon	0.01382	
	Coho salmon	0.00264	
	Chinook salmon	0.00552	
	Steelhead	0.00552	
	Pomfret	0.12471	
	Saury	0.26724	
	Pelagic forage fish	0.103	
	Micronektonic squid	0.1	
	Pelagic forage fish	0.01	0.6
	Micronektonic squid	0.33	
	Chaetognaths	0.04484	
Large gonatid squid	Sergestid shrimp	0.03397	
	Misc. predatory zooplankton	0.03444	
	Amphipods	0.06888	
	Pteropods	0.06888	
	Euphausiids	0.1722	
	Copepods	0.23678	
	Pelagic forage fish	0.01	0.6
	Micronektonic squid	0.99	
	Neon flying squid	0.295	0.6
	Saury	0.058	
Neon flying squid	Pelagic forage fish	0.319	
	Micronektonic squid	0.223	
	Mesopelagic fish	0.105	
	Pelagic forage fish	0.10982	0.1
	Micronektonic squid	0.07968	
	Mesopelagic fish	0.10982	
	Ctenophores	0.01609	
	Salps	0.01609	
	Misc. predatory zooplankton	0.00171	
	Amphipods	0.29328	
Sockeye salmon	Pteropods	0.23976	
	Euphausiids	0.10058	
	Copepods	0.03318	
	Pelagic forage fish	0.00802	0.1
	Micronektonic squid	0.03929	
	Mesopelagic fish	0.00802	
	Ctenophores	0.20285	
	Salps	0.20285	
	Chaetognaths	0.00043	
	Misc. predatory zooplankton	0.01474	
Chum salmon	Amphipods	0.07363	
	Pteropods	0.06719	
	Euphausiids	0.08491	
	Copepods	0.29806	

Table A.8: Diet fraction input for the 47-group food web model (continued).

Predator	Prey	Diet fraction	Pedigree
Pink salmon	Pelagic forage fish	0.068096	0.1
	Micronektonic squid	0.034823	
	Mesopelagic fish	0.068096	
	Ctenophores	0.003826	
	Salps	0.003826	
	Misc. predatory zooplankton	8.64e-06	
	Amphipods	0.32162	
	Pteropods	0.440933	
	Euphausiids	0.038951	
	Copepods	0.019816	
Coho salmon	Pelagic forage fish	0.367206	0.1
	Micronektonic squid	0.205691	
	Mesopelagic fish	0.367206	
	Ctenophores	7.31e-05	
	Salps	7.31e-05	
	Amphipods	0.008047	
	Pteropods	0.04623	
	Euphausiids	0.002736	
	Copepods	0.002736	
	Pelagic forage fish	0.367206	
Chinook salmon	Micronektonic squid	0.205691	0.1
	Mesopelagic fish	0.367206	
	Ctenophores	7.31e-05	
	Salps	7.31e-05	
	Amphipods	0.008047	
	Pteropods	0.04623	
	Euphausiids	0.002736	
	Copepods	0.002736	
	Pelagic forage fish	0.367206	
	Micronektonic squid	0.205691	
Steelhead	Mesopelagic fish	0.367206	0.1
	Ctenophores	7.31e-05	
	Salps	7.31e-05	
	Amphipods	0.008047	
	Pteropods	0.04623	
	Euphausiids	0.002736	
	Copepods	0.002736	
	Pelagic forage fish	0.367206	
	Micronektonic squid	0.205691	
	Mesopelagic fish	0.367206	
Pomfret	Ctenophores	7.31e-05	0.5
	Salps	7.31e-05	
	Amphipods	0.008047	
	Pteropods	0.04623	
	Euphausiids	0.002736	
	Copepods	0.002736	
	Saury	0.04	
	Micronektonic squid	0.75	
	Mesopelagic fish	0.08	
	Chaetognaths	0.01	
Saury	Sergestid shrimp	0.01	0.7
	Misc. predatory zooplankton	0.01	
	Amphipods	0.03	
	Pteropods	0.01	
	Euphausiids	0.05	
	Copepods	0.01	
	Chaetognaths	0.05298	
	Sergestid shrimp	0.04014	
	Misc. predatory zooplankton	0.04069	
	Amphipods	0.08138	
Pelagic forage fish	Pteropods	0.08138	0.7
	Euphausiids	0.20344	
	Copepods	0.5	
	Chaetognaths	0.06795	
	Sergestid shrimp	0.05147	
	Misc. predatory zooplankton	0.05218	
	Amphipods	0.10437	
	Pteropods	0.10437	
	Euphausiids	0.26091	
	Copepods	0.35875	

Table A.9: Diet fraction input for the 47-group food web model (continued).

Predator	Prey	Diet fraction	Pedigree
Micronektonic squid	Micronektonic squid	0.05	0.7
	Chaetognaths	0.06455	
	Sergestid shrimp	0.0489	
	Misc. predatory zooplankton	0.04957	
	Amphipods	0.09915	
	Pteropods	0.09915	
	Euphausiids	0.24787	
	Copepods	0.34082	
	Chaetognaths	0.15	0.7
	Sergestid shrimp	0.03	
Mesopelagic fish	Misc. predatory zooplankton	0.03	
	Amphipods	0.24	
	Pteropods	0.031	
	Euphausiids	0.171	
	Copepods	0.348	
Large jellyfish	Ctenophores	0.04356	0.7
	Salps	0.03829	
	Chaetognaths	0.03159	
	Sergestid shrimp	0.02393	
	Misc. predatory zooplankton	0.02426	
	Amphipods	0.04852	
	Pteropods	0.04852	
	Euphausiids	0.12131	
	Copepods	0.62	
	Copepods	0.25	0.7
Ctenophores	Microzooplankton	0.25	
	Large phytoplankton	0.5	
	Copepods	0.25	0.7
Salps	Microzooplankton	0.25	
	Large phytoplankton	0.5	
Chaetognaths	Amphipods	0.04444	0.7
	Pteropods	0.04444	
	Euphausiids	0.11111	
	Copepods	0.8	
	Amphipods	0.04444	0.7
Sergestid shrimp	Pteropods	0.04444	
	Euphausiids	0.11111	
	Copepods	0.8	
	Amphipods	0.04444	0.7
Misc. predatory zooplankton	Pteropods	0.04444	
	Euphausiids	0.11111	
	Copepods	0.8	
	Amphipods	0.04444	0.7
Amphipods	Pteropods	0.04444	
	Euphausiids	0.11111	
	Copepods	0.8	
Pteropods	Copepods	0.4	0.7
	Microzooplankton	0.4	
	Large phytoplankton	0.2	
Euphausiids	Copepods	0.4	0.7
	Microzooplankton	0.4	
	Large phytoplankton	0.2	
Copepods	Copepods	0.4	0.3
	Microzooplankton	0.3	
	Large phytoplankton	0.4	
Microzooplankton	Small phytoplankton	0.3	
	Small phytoplankton	1	0.3

Table A.10: Ecopath input variables for the 24-group simplified food web, including biomass (B, tons wet weight m^{-2}), production/biomass (PB, yr^{-1}), consumption/biomass (QB, yr^{-1}), ecotrophic efficiency (EE), growth efficiency (GE), and fraction unassimilated (GS)

Group	B		PB		QB		EE	GE	GS
	Value	Ped	Value	Ped	Value	Ped			
Albatross	4e-05	0.5	0.05	0.4	81.59	0.2			0.2
Mammals,sharks	0.065451	0.72918	0.18408	0.55279	14.192	0.35279			0.2
Neon flying squid	0.45	0.8	2.555	0.6	6.205	0.6			0.2
Orcas	2.8e-05	0.5	0.0252	0.4	11.16	0.2			0.2
Boreal clubhook squid	0.012	0.8	2.555	0.6	7.3	0.6			0.2
Seabirds 1	0.000166	0.5	0.086145	0.4	98.232	0.2			0.2
Pomfret	0.21	0.8	0.75	0.4		0.4		0.2	0.2
Seabirds 2	0.000566	0.5	0.1	0.4	107.8	0.2			0.2
Gonatid squid	0.03	0.8	2.555	0.6	7.3	0.6			0.2
Salmon	0.19011	0.5	1.6971	0.11957	12.081	0.11957		0.13748	0.2
Baleen whales	0.033785	0.5	0.02	0.4	4.8378	0.2			0.2
Micronektonic squid		0.8	3	0.6	15	0.7	0.9		0.2
Mesopelagic fish	4.5	0.8	0.9	0.6	3	0.7			0.2
Pelagic forage fish		0.8	1.5	0.6	5	0.7	0.9		0.2
Sauries	0.45	0.8	1.6	0.6	7.9	0.7			0.2
Jellyfish	4	0.8	3	0.7	10	0.7			0.2
Predatory zooplankton	12.391	0.7	6.9876	0.7	23.292	0.7			0.3
Large zooplankton	15.488	0.8	6.9876	0.6	23.292	0.6			0.3
Gelatinous zooplankton	3.0977	0.5	6.5	0.7	21.667	0.7			0.3
Copepods	20.919	0.1	23.151	0.1	77.169	0.4			0.3
Microzooplankton	16.83	0.1	38.833	0.1	129.44	0.4			0.3
Small phytoplankton	42.427	0.5	70.621	0.1		0.4			
Large phytoplankton	27.029	0.8	41.677	0.1		0.4			
PON	100	0.1		0.1		0.4			

Table A.11: Diet fraction input for the 24-group food web model.

Predator	Prey	Diet fraction	Pedigree
Albatross	Neon flying squid	0.68598	0.7
	Boreal clubhook squid	0.01829	
	Gonatid squid	0.04573	
	Micronektonic squid	0.05	
	Pelagic forage fish	0.1	
Mammals,sharks	Saury	0.1	
	Neon flying squid	0.250098	0.776393
	Boreal clubhook squid	0.00667251	
	Pomfret	0.105515	
	Gonatid squid	0.016676	
	Salmon	0.0953397	
	Micronektonic squid	0.133994	
	Mesopelagic fish	0.0502069	
	Pelagic forage fish	0.115384	
Neon flying squid	Saury	0.226106	
	Neon flying squid	0.295	0.6
	Micronektonic squid	0.223	
	Mesopelagic fish	0.105	
	Pelagic forage fish	0.319	
Orcas	Saury	0.058	
	Albatross	0.00032	0.7
	Mammals,sharks	0.11835	
	Neon flying squid	0.04573	
	Boreal clubhook squid	0.00122	
	Seabirds 1	0.00136	
	Pomfret	0.05833	
	Seabirds 2	0.00461	
	Gonatid squid	0.00305	
	Salmon	0.0528	
	Baleen whales	0.27536	
	Micronektonic squid	0.05	
Boreal clubhook squid	Pelagic forage fish	0.264	
	Saury	0.12498	
	Micronektonic squid	0.99	0.6
	Pelagic forage fish	0.01	
Seabirds 1	Micronektonic squid	0.427952	0.7
	Pelagic forage fish	0.29494	
	Saury	0.277108	
	Micronektonic squid	0.75	0.5
Pomfret	Mesopelagic fish	0.08	
	Saury	0.04	
	Predatory zooplankton	0.03	
	Large zooplankton	0.09	
	Copepods	0.01	
Seabirds 2	Micronektonic squid	0.281625	0.7
	Pelagic forage fish	0.277032	
	Saury	0.277032	
	Large zooplankton	0.0931553	
	Copepods	0.0711576	
Gonatid squid	Micronektonic squid	0.33	0.6
	Pelagic forage fish	0.01	
	Predatory zooplankton	0.11325	
	Large zooplankton	0.30996	
	Copepods	0.23678	
Salmon	Micronektonic squid	0.0779714	0.1
	Mesopelagic fish	0.106941	
	Pelagic forage fish	0.106941	
	Predatory zooplankton	0.00512718	
	Large zooplankton	0.468088	
	Gelatinous zooplankton	0.131654	
	Copepods	0.103278	

Table A.12: Diet fraction input for the 24-group food web model (continued).

Predator	Prey	Diet fraction	Pedigree
Baleen whales	Neon flying squid	0.022866	0.7
	Boreal clubhook squid	0.000609	
	Pomfret	0.002917	
	Gonatid squid	0.001524	
	Salmon	0.0026399	
	Micronektonic squid	0.025	
	Mesopelagic fish	0.062499	
	Pelagic forage fish	0.076	
	Saury	0.00625	
	Predatory zooplankton	0.137281	
Micronektonic squid	Large zooplankton	0.375714	
	Copepods	0.287004	
	Micronektonic squid	0.05	0.7
	Predatory zooplankton	0.16302	
Mesopelagic fish	Large zooplankton	0.44617	
	Copepods	0.34082	
	Predatory zooplankton	0.21	0.7
Pelagic forage fish	Large zooplankton	0.442	
	Copepods	0.348	
	Predatory zooplankton	0.1716	0.7
Saury	Large zooplankton	0.46965	
	Copepods	0.35875	
	Predatory zooplankton	0.13381	0.7
Jellyfish	Large zooplankton	0.3662	
	Copepods	0.5	
	Predatory zooplankton	0.07978	0.7
	Large zooplankton	0.21835	
Predatory zooplankton	Gelatinous zooplankton	0.08185	
	Copepods	0.62	
	Large zooplankton	0.19999	0.7
	Copepods	0.8	
Large zooplankton	Copepods	0.4	0.566667
	Microzooplankton	0.4	
	Large phytoplankton	0.2	
	Copepods	0.25	0.7
Gelatinous zooplankton	Microzooplankton	0.25	
	Large phytoplankton	0.5	
	Copepods	0.3	0.3
	Microzooplankton	0.3	
Copepods	Small phytoplankton	0.3	
	Large phytoplankton	0.4	
Microzooplankton	Small phytoplankton	1	0.3
	Large phytoplankton		

Table A.13: Biogeochemical process-related parameters: Primary production

Parameter	Symbol	Group	Value
Ammonium inhibition constant	ψ	PS	1.5 (mmol N m ⁻³) ⁻¹
		PL	1.5 (mmol N m ⁻³) ⁻¹
Half-saturation constant for ammonium	K_{NH_4}	PS	0.1 mmol N m ⁻³
		PL	0.3 mmol N m ⁻³
Half-saturation constant for nitrate	K_{NO_3}	PS	1 mmol N m ⁻³
		PL	3 mmol N m ⁻³
Half-saturation constant for silica	K_{Si}	PL	6 mmol Si m ⁻³
Initial slope of P-I curve	α	PS	0.017 (W m ⁻²) ⁻¹ d ⁻¹
		PL	0.016 (W m ⁻²) ⁻¹ d ⁻¹
Light dissipation coefficient of seawater	α_1		0.04 m ⁻¹
Maximum uptake rate at 0 deg C	V_{max}	PS	0.4 d ⁻¹
		PL	0.8 d ⁻¹
Phytoplankton self-shading coefficient	α_2		0.04 m ⁻¹ (mmol N m ⁻³) ⁻¹
Silica to nitrogen ratio	$R_{Si:N}$		2 mmol Si (mmol N) ⁻¹
Carbon to nitrogen ratio	$R_{C:N}$		6.625 mol C (mol N) ⁻¹
Temperature coefficient for photosynthesis	K_{gpp}	PS	0.0693 (deg C) ⁻¹
		PL	0.0693 (deg C) ⁻¹
Empirical Fe:C function coefficient	b_{Fe}	PS	28.5 (mol C m ⁻³) ⁻¹
		PL	42.6 (mol C m ⁻³) ⁻¹
Empirical Fe:C function power	α_{Fe}	PS	0.21
		PL	0.46
Fraction of iron remineralized	f_{rem}	PS	0.5
		PL	0.5
Half-saturation constant for Fe:C	$K_{Fe:C}$	PS	12 μmol Fe (mol C) ⁻¹
		PL	16.9 μmol Fe (mol C) ⁻¹
Timescale for iron uptake	t_{Fe}	PS	1 d
		PL	1 d

Table A.14: Biogeochemical process-related parameters: Iron quota model

Parameter	Symbol	Group	Value
Maximum Fe:N ratio	$R_{Fe:Nmax}$	PS	331.25 μmol Fe (mol N) ⁻¹
		PL	3312.5 μmol Fe (mol N) ⁻¹
Half-saturation constant for iron	K_{Fe}	PS	0.6 μmol Fe m ⁻³
		PL	3.0 μmol Fe m ⁻³
Half-saturation constant for internal Fe:N ratio	$K_{Fe:N}$	PS	66.25 μmol Fe (mol N) ⁻¹
		PL	132.5 μmol Fe (mol N) ⁻¹
Iron uptake factor	$\mu_{Fe:N}$		100 μmol Fe (mol N) ⁻¹
Background ligand concentration	Lig_{bg}		1.0 μmol m ⁻³
Half saturation constant for light effect on ligand-binding	K_{Iscav}		1.0 W m ⁻²
Lower limit of ligand binding under low-light conditions	K_{LigLo}		300 m ³ (μmol) ⁻¹
Upper limit of ligand binding under high-light conditions	K_{LigHi}		0.1 m ³ (μmol) ⁻¹
Iron scavenging coefficient	α_{scav}		50 yr ⁻¹
Fraction of iron remineralized, relative to organic nitrogen	r_{eff}		0.25

Table A.15: Biogeochemical process-related parameters: Respiration

Parameter	Symbol	Group	Value
Respiration rate at 0 deg C	Res_0	PS	0.03 d ⁻¹
		PL	0.03 d ⁻¹
Temperature coefficient for respiration	K_{Res}	PS	0.0519 d ⁻¹
		PL	0.0519 d ⁻¹

Table A.16: Biogeochemical process-related parameters: Extracellular excretion

Parameter	Symbol	Group	Value
Ratio of extracellular excretion to photosynthesis	γ	PS	0.135
		PL	0.135

Table A.17: Biogeochemical process-related parameters: Grazing

Parameter	Symbol	Group	Value
Grazing inhibition coefficient	ψ_{gr}	ZP on PL	4.605 (mmol N m ⁻³) ⁻¹
		ZP on ZS	3.01 (mmol N m ⁻³) ⁻¹
Grazing threshold	B_{thresh}	ZS on PS	0.04 mmol N m ⁻³
		ZL on PS	0.04 mmol N m ⁻³
		ZL on PL	0.04 mmol N m ⁻³
		ZP on PL	0.04 mmol N m ⁻³
		ZL on ZS	0.04 mmol N m ⁻³
		ZP on ZS	0.04 mmol N m ⁻³
		ZP on ZL	0.04 mmol N m ⁻³
Ivlev constant	λ	ZS	1.4 (mmol N m ⁻³) ⁻¹
		ZL	1.4 (mmol N m ⁻³) ⁻¹
		ZP	1.4 (mmol N m ⁻³) ⁻¹
Maximum grazing rate at 0 deg C	g_{max}	ZS on PS	0.8 d ⁻¹
		ZL on PS	0.1 d ⁻¹
		ZL on PL	0.4 d ⁻¹
		ZP on PL	0.2 d ⁻¹
		ZL on ZS	0.4 d ⁻¹
		ZP on ZS	0.2 d ⁻¹
		ZP on ZL	0.2 d ⁻¹
Temperature coefficient for grazing	K_{Gra}	ZS	0.0693 (deg C) ⁻¹
		ZL	0.0693 (deg C) ⁻¹
		ZP	0.0693 (deg C) ⁻¹
		gel. zoo.	0.0693 (deg C) ⁻¹
		pred. zoo.	0.0693 (deg C) ⁻¹
Mixed layer depth, annual average	MLD		80 m
Mixed layer temperature, annual average	T_{avg}		8.26 deg C

Table A.18: Biogeochemical process-related parameters: Egestion and excretion

Parameter	Symbol	Group	Value
Assimilation efficiency	α_{eg}	ZS	0.7
		ZL	0.7
		ZP	0.7
Growth efficiency	β_{eg}	ZS	0.3
		ZL	0.3
		ZP	0.3

Table A.19: Biogeochemical process-related parameters: Decomposition

Parameter	Symbol	Group	Value
Decomposition (or nitrification) rate	V_{Dec}	NH ₄ to NO ₃	0.03 d ⁻¹
		PON to NH ₄	0.1 d ⁻¹
		PON to DON	0.1 d ⁻¹
		DON to NH ₄	0.02 d ⁻¹
		Opal to SiOH ₄	0.04 d ⁻¹
Temperature coefficient for decomposition	K_{Dec}	NH ₄ to NO ₃	0.0693 (deg C) ⁻¹
		PON to NH ₄	0.0693 (deg C) ⁻¹
		PON to DON	0.0693 (deg C) ⁻¹
		DON to NH ₄	0.0693 (deg C) ⁻¹
		Opal to SiOH ₄	0.0693 (deg C) ⁻¹

Table A.20: Biogeochemical process-related parameters: Mortality

Parameter	Symbol	Group	Value
Mortality rate at 0 deg C	Mor_0	PS	0.0585 d ⁻¹
		PL	0.029 d ⁻¹
		ZS	0.0585 d ⁻¹
		ZL	0.0585 d ⁻¹
		ZP	0.0585 d ⁻¹
Temperature coefficient for mortality	K_{Mor}	PS	0.0693 (deg C) ⁻¹
		PL	0.0693 (deg C) ⁻¹
		ZS	0.0693 (deg C) ⁻¹
		ZL	0.0693 (deg C) ⁻¹
		ZP	0.0693 (deg C) ⁻¹

Table A.21: Derived parameters used in the equations in Appendix A.2. These parameters vary over time as a function of the state variables from both the physical and biological models.

Parameter Name	Symbol	Definition
Nitrogen limitation	L_N	$\frac{NO_3}{K_{NO_3} + NO_3} \cdot \exp(-\psi NH_4) + \frac{NH_4}{K_{NH_4} + NH_4}$
Silica limitation	L_{Si}	$\frac{SiOH_4}{K_{SiOH_4} + SiOH_4}$
Iron limitation	L_{Fe}	$\frac{R_{Fe:C}^2}{K_{Fe:C}^2 + R_{Fe:C}^2}$
Iron limitation (quota model)	L_{Fe}	$\frac{B_{Fe}}{K_{Fe} + B_{Fe}}$
Iron deficiency	D_{Fe}	$\frac{R_{Fe:N}^2}{K_{Fe:N}^2 + R_{Fe:N}^2}$
f-ratio	f	$\frac{\frac{NO_3}{K_{NO_3} + NO_3} \cdot \exp(-\psi NH_4)}{\frac{NO_3}{K_{NO_3} + NO_3} \cdot \exp(-\psi NH_4) + \frac{NH_4}{K_{NH_4} + NH_4}}$
Total nutrient limitation	L_{nut}	$\min(L_N, L_{Si}, L_{Fe})$
Total nutrient limitation (quota model)	L_{nut}	$\min(L_N, L_{Si}, D_{Fe})$
Light limitation	L_{light}	$1 - \exp\left(\frac{\alpha I_z}{V_{max}}\right)$
Empirical Fe:C ratio	R_{0i}	$b_{Fe,i} F e_z^{a_{Fe,i}}$
Realized Fe:C ratio	R_i	$\frac{B_{Fe,i}}{B_i \cdot R_{C:N}}$
Realized Fe:N ratio	$R_{Fe:N}$	$\frac{B_{Fe,i}}{B_i}$
Ligand-binding parameter	K_{Lig}	$10^{\left(\log_{10}(K_{LigLo}) - \frac{I_z}{K_{Isca} + I_z}\right)\left(\log_{10}(K_{LigLo}) - \log_{10}(K_{LigHi})\right)}$

Table A.22: Group-related, Ecopath-derived parameters for the water column ecosystem model, including mass-balanced biomass (B^*), growth efficiency (GE), non-pedatory mortality flux (M_0), and unassimilated fraction (GS). Where values vary across ensemble members, mean, standard deviation, minimum, and maximum values, calculated across the 500 ensemble members, are given

Table A.23: Flux-related, Ecopath-derived parameters for the water column ecosystem model, including mass-balanced prey-to-predator flux (Q^*), functional response top-down parameter (X), functional response bottom-up parameter (D), and functional response exponent (θ). Where values vary across ensemble members, mean, standard deviation, minimum, and maximum values, calculated across the 500 ensemble members, are given

Predator	Prey	Q^* (mmol N m ⁻² s ⁻¹)				X	D				θ
		mean	std	min	max		mean	std	min	max	
Albatross	Neon flying squid	2.57e-14	8.76e-15	9.84e-15	5.46e-14	2	1e+03	0	1e+03	1e+03	2
Albatross	Boreal clubhook squid	7.43e-16	4.24e-16	1.08e-16	2.51e-15	2	1e+03	0	1e+03	1e+03	2
Albatross	Gonatid squid	1.88e-15	1.03e-15	3.42e-16	6.64e-15	2	1e+03	0	1e+03	1e+03	2
Albatross	Micronektonic squid	1.96e-15	1.15e-15	2.92e-16	7.07e-15	2	1e+03	0	1e+03	1e+03	2
Albatross	Pelagic forage fish	4e-15	2.27e-15	5.49e-16	1.33e-14	2	1e+03	0	1e+03	1e+03	2
Albatross	Saury	4.01e-15	2.31e-15	4.61e-16	1.48e-14	2	1e+03	0	1e+03	1e+03	2
Mammals,sharks	Neon flying squid	2.06e-12	1.32e-12	3.2e-13	7.83e-12	2	1e+03	0	1e+03	1e+03	2
Mammals,sharks	Boreal clubhook squid	5.42e-14	3.6e-14	4.95e-15	2.02e-13	2	1e+03	0	1e+03	1e+03	2
Mammals,sharks	Pomfret	8.2e-13	4.73e-13	1.35e-13	2.9e-12	2	1e+03	0	1e+03	1e+03	2
Mammals,sharks	Gonatid squid	1.41e-13	9.48e-14	1.74e-14	5.69e-13	2	1e+03	0	1e+03	1e+03	2
Mammals,sharks	Salmon	7.9e-13	4.32e-13	1.51e-13	2.64e-12	2	1e+03	0	1e+03	1e+03	2
Mammals,sharks	Micronektonic squid	1.14e-12	7.98e-13	1.49e-13	5.9e-12	2	1e+03	0	1e+03	1e+03	2
Mammals,sharks	Mesopelagic fish	4.18e-13	2.85e-13	3.32e-14	1.76e-12	2	1e+03	0	1e+03	1e+03	2
Mammals,sharks	Pelagic forage fish	9.59e-13	6.49e-13	1.03e-13	3.9e-12	2	1e+03	0	1e+03	1e+03	2
Mammals,sharks	Saury	1.87e-12	1.27e-12	2.17e-13	7.88e-12	2	1e+03	0	1e+03	1e+03	2
Neon flying squid	Neon flying squid	7.35e-12	4.91e-12	5.37e-13	3.16e-11	2	1e+03	0	1e+03	1e+03	2
Neon flying squid	Micronektonic squid	6.51e-12	4.89e-12	4.39e-13	3.14e-11	2	1e+03	0	1e+03	1e+03	2
Neon flying squid	Mesopelagic fish	3e-12	2.3e-12	1.2e-13	1.25e-11	2	1e+03	0	1e+03	1e+03	2
Neon flying squid	Pelagic forage fish	9.49e-12	7.14e-12	5.08e-13	4.07e-11	2	1e+03	0	1e+03	1e+03	2
Neon flying squid	Saury	1.56e-12	1.2e-12	8.73e-14	8.18e-12	2	1e+03	0	1e+03	1e+03	2
Orcas	Albatross	1.17e-18	6.34e-19	1.7e-19	3.52e-18	2	1e+03	0	1e+03	1e+03	2
Orcas	Mammals,sharks	4.54e-16	2.58e-16	5.37e-17	1.46e-15	2	1e+03	0	1e+03	1e+03	2
Orcas	Neon flying squid	1.76e-16	8.56e-17	3.17e-17	5.03e-16	2	1e+03	0	1e+03	1e+03	2
Orcas	Boreal clubhook squid	4.79e-18	2.31e-18	1.08e-18	1.43e-17	2	1e+03	0	1e+03	1e+03	2
Orcas	Seabirds 1	5.26e-18	2.98e-18	8.76e-19	1.79e-17	2	1e+03	0	1e+03	1e+03	2
Orcas	Pomfret	2.3e-16	9.86e-17	5.73e-17	5.37e-16	2	1e+03	0	1e+03	1e+03	2
Orcas	Seabirds 2	1.76e-17	9.23e-18	2.8e-18	5.51e-17	2	1e+03	0	1e+03	1e+03	2
Orcas	Gonatid squid	1.18e-17	5.71e-18	2.07e-18	3.29e-17	2	1e+03	0	1e+03	1e+03	2
Orcas	Salmon	2.04e-16	7.17e-17	7.5e-17	4.4e-16	2	1e+03	0	1e+03	1e+03	2
Orcas	Baleen whales	1.03e-15	4.88e-16	2.08e-16	3e-15	2	1e+03	0	1e+03	1e+03	2
Orcas	Micronektonic squid	1.94e-16	1.06e-16	3.32e-17	6.35e-16	2	1e+03	0	1e+03	1e+03	2
Orcas	Pelagic forage fish	1.01e-15	4.62e-16	2.13e-16	2.56e-15	2	1e+03	0	1e+03	1e+03	2
Orcas	Saury	4.64e-16	2.35e-16	7.27e-17	1.42e-15	2	1e+03	0	1e+03	1e+03	2
Boreal clubhook squid	Micronektonic squid	1.08e-12	6.07e-13	1.09e-13	2.86e-12	2	1e+03	0	1e+03	1e+03	2
Boreal clubhook squid	Pelagic forage fish	1.45e-14	1.44e-14	5.85e-16	1.18e-13	2	1e+03	0	1e+03	1e+03	2

Table A.24: Flux-related, Ecopath-derived parameters for the water column ecosystem model (continued).

Predator	Prey	Q* ($\text{mmol N m}^{-2} \text{s}^{-1}$)				X	D				θ
		mean	std	min	max		mean	std	min	max	
Seabirds 1	Micronektonic squid	8.28e-14	3.57e-14	1.96e-14	1.94e-13	2	1e+03	0	1e+03	1e+03	2
Seabirds 1	Pelagic forage fish	6.01e-14	2.99e-14	1.07e-14	1.71e-13	2	1e+03	0	1e+03	1e+03	2
Seabirds 1	Saury	5.47e-14	2.84e-14	9.13e-15	1.47e-13	2	1e+03	0	1e+03	1e+03	2
Pomfret	Micronektonic squid	7.36e-12	3.42e-12	1.13e-12	1.81e-11	2	1e+03	0	1e+03	1e+03	2
Pomfret	Mesopelagic fish	9.05e-13	6.44e-13	7.34e-14	4.41e-12	2	1e+03	0	1e+03	1e+03	2
Pomfret	Saury	4.57e-13	3.17e-13	3.06e-14	2.2e-12	2	1e+03	0	1e+03	1e+03	2
Pomfret	Predatory zooplankton	3.41e-13	2.49e-13	2.37e-14	1.59e-12	2	1e+03	0	1e+03	1e+03	2
Pomfret	Large zooplankton	9.92e-13	6.56e-13	6.5e-14	3.67e-12	2	1e+03	0	1e+03	1e+03	2
Pomfret	Copepods	1.13e-13	6.98e-14	1.28e-14	5.13e-13	2	1e+03	0	1e+03	1e+03	2
Seabirds 2	Micronektonic squid	2.02e-13	9.16e-14	4.44e-14	6.04e-13	2	1e+03	0	1e+03	1e+03	2
Seabirds 2	Pelagic forage fish	2.01e-13	1.01e-13	3.58e-14	6.42e-13	2	1e+03	0	1e+03	1e+03	2
Seabirds 2	Saury	1.98e-13	9.4e-14	4.29e-14	5.6e-13	2	1e+03	0	1e+03	1e+03	2
Seabirds 2	Large zooplankton	7.15e-14	3.48e-14	1.22e-14	2.01e-13	2	1e+03	0	1e+03	1e+03	2
Seabirds 2	Copepods	5.44e-14	2.32e-14	1.66e-14	1.65e-13	2	1e+03	0	1e+03	1e+03	2
Gonatid squid	Micronektonic squid	9.02e-13	5.9e-13	5.53e-14	3.25e-12	2	1e+03	0	1e+03	1e+03	2
Gonatid squid	Pelagic forage fish	2.94e-14	2.22e-14	1.26e-15	1.37e-13	2	1e+03	0	1e+03	1e+03	2
Gonatid squid	Predatory zooplankton	3.3e-13	2.3e-13	1.11e-14	1.11e-12	2	1e+03	0	1e+03	1e+03	2
Gonatid squid	Large zooplankton	8.73e-13	5.58e-13	5.5e-14	3.05e-12	2	1e+03	0	1e+03	1e+03	2
Gonatid squid	Copepods	6.87e-13	4.2e-13	6.89e-14	2.22e-12	2	1e+03	0	1e+03	1e+03	2
Salmon	Micronektonic squid	2.25e-12	1.19e-12	3.82e-13	6.51e-12	2	1e+03	0	1e+03	1e+03	2
Salmon	Mesopelagic fish	2.96e-12	1.46e-12	5.14e-13	7.65e-12	2	1e+03	0	1e+03	1e+03	2
Salmon	Pelagic forage fish	3.07e-12	1.61e-12	4.94e-13	9.36e-12	2	1e+03	0	1e+03	1e+03	2
Salmon	Predatory zooplankton	1.46e-13	8.08e-14	2.17e-14	4.81e-13	2	1e+03	0	1e+03	1e+03	2
Salmon	Large zooplankton	1.24e-11	4.48e-12	3.1e-12	2.49e-11	2	1e+03	0	1e+03	1e+03	2
Salmon	Gelatinous zooplankton	3.67e-12	1.88e-12	4.84e-13	1.03e-11	2	1e+03	0	1e+03	1e+03	2
Salmon	Copepods	2.93e-12	1.08e-12	8.73e-13	6.95e-12	2	1e+03	0	1e+03	1e+03	2

Table A.25: Flux-related, Ecopath-derived parameters for the water column ecosystem model (continued).

Predator	Prey	Q* ($\text{mmol N m}^{-2} \text{s}^{-1}$)				X	D				θ
		mean	std	min	max		mean	std	min	max	
Baleen whales	Neon flying squid	4.62e-14	2.29e-14	7.95e-15	1.32e-13	2	1e+03	0	1e+03	1e+03	2
Baleen whales	Boreal clubhook squid	1.17e-15	6.03e-16	2.71e-16	3.24e-15	2	1e+03	0	1e+03	1e+03	2
Baleen whales	Pomfret	5.82e-15	2.65e-15	1.38e-15	1.56e-14	2	1e+03	0	1e+03	1e+03	2
Baleen whales	Gonatid squid	3.12e-15	1.56e-15	6.28e-16	9.66e-15	2	1e+03	0	1e+03	1e+03	2
Baleen whales	Salmon	5.33e-15	1.86e-15	1.81e-15	1.17e-14	2	1e+03	0	1e+03	1e+03	2
Baleen whales	Micronektonic squid	5e-14	2.71e-14	9.15e-15	1.4e-13	2	1e+03	0	1e+03	1e+03	2
Baleen whales	Mesopelagic fish	1.25e-13	6.71e-14	1.93e-14	3.59e-13	2	1e+03	0	1e+03	1e+03	2
Baleen whales	Pelagic forage fish	1.48e-13	7.72e-14	2.25e-14	4.47e-13	2	1e+03	0	1e+03	1e+03	2
Baleen whales	Saury	1.29e-14	7.32e-15	1.6e-15	4.04e-14	2	1e+03	0	1e+03	1e+03	2
Baleen whales	Predatory zooplankton	2.76e-13	1.46e-13	5.12e-14	8.78e-13	2	1e+03	0	1e+03	1e+03	2
Baleen whales	Large zooplankton	7.11e-13	2.76e-13	2.25e-13	1.78e-12	2	1e+03	0	1e+03	1e+03	2
Baleen whales	Copepods	5.75e-13	2.09e-13	1.72e-13	1.25e-12	2	1e+03	0	1e+03	1e+03	2
Micronektonic squid	Micronektonic squid	1.01e-11	1.49e-11	4e-13	1.35e-10	2	1e+03	0	1e+03	1e+03	2
Micronektonic squid	Predatory zooplankton	3.17e-11	4.28e-11	1.57e-12	4.82e-10	2	1e+03	0	1e+03	1e+03	2
Micronektonic squid	Large zooplankton	8.07e-11	9.26e-11	5.6e-12	9.08e-10	2	1e+03	0	1e+03	1e+03	2
Micronektonic squid	Copepods	6.58e-11	8.2e-11	5.39e-12	8.47e-10	2	1e+03	0	1e+03	1e+03	2
Mesopelagic fish	Predatory zooplankton	3.38e-11	2.58e-11	2.18e-12	1.83e-10	2	1e+03	0	1e+03	1e+03	2
Mesopelagic fish	Large zooplankton	6.77e-11	4.58e-11	3.91e-12	2.31e-10	2	1e+03	0	1e+03	1e+03	2
Mesopelagic fish	Copepods	5.61e-11	3.82e-11	4.06e-12	2.06e-10	2	1e+03	0	1e+03	1e+03	2
Pelagic forage fish	Predatory zooplankton	1.03e-11	9.67e-12	8.2e-13	7.52e-11	2	1e+03	0	1e+03	1e+03	2
Pelagic forage fish	Large zooplankton	2.78e-11	2.35e-11	1.84e-12	1.48e-10	2	1e+03	0	1e+03	1e+03	2
Pelagic forage fish	Copepods	2.22e-11	1.92e-11	1.66e-12	1.58e-10	2	1e+03	0	1e+03	1e+03	2
Saury	Predatory zooplankton	6.17e-12	4.45e-12	3.37e-13	2.5e-11	2	1e+03	0	1e+03	1e+03	2
Saury	Large zooplankton	1.72e-11	1.1e-11	1.74e-12	5.81e-11	2	1e+03	0	1e+03	1e+03	2
Saury	Copepods	2.44e-11	1.45e-11	2.52e-12	7.74e-11	2	1e+03	0	1e+03	1e+03	2
Jellyfish	Predatory zooplankton	3.55e-11	2.93e-11	2.15e-12	1.75e-10	2	1e+03	0	1e+03	1e+03	2
Jellyfish	Large zooplankton	9.09e-11	6.77e-11	4.18e-12	4.12e-10	2	1e+03	0	1e+03	1e+03	2
Jellyfish	Gelatinous zooplankton	3.58e-11	3.17e-11	1.92e-12	1.99e-10	2	1e+03	0	1e+03	1e+03	2
Jellyfish	Copepods	2.67e-10	1.92e-10	2.03e-11	1.01e-09	2	1e+03	0	1e+03	1e+03	2

Table A.26: Flux-related, Ecopath-derived parameters for the water column ecosystem model (continued).

Predator	Prey	Q* ($\text{mmol N m}^{-2} \text{s}^{-1}$)				X		D		θ	
		mean	std	min	max	mean	std	min	max		
Predatory zooplankton	Large zooplankton	3.92e-10	2.36e-10	2.98e-11	1.51e-09	1e+03	44.8	26.3	11.3	177	2
Predatory zooplankton	Copepods	1.65e-09	7.99e-10	2.88e-10	4e-09	1e+03	10.6	5.02	3.92	25.6	2
Large zooplankton	Copepods	1.5e-09	7.67e-10	2.24e-10	5.01e-09	1e+03	19.4	7.89	6.78	45.8	2
Large zooplankton	Microzooplankton	1.47e-09	7.21e-10	2.13e-10	3.63e-09	1e+03	19.5	7.79	7.6	45.2	2
Large zooplankton	Large phytoplankton	7.55e-10	3.98e-10	1.25e-10	2.61e-09	1e+03	21.9	14.9	6.45	88.6	2
Gelatinous zooplankton	Copepods	1.96e-10	1.1e-10	2.84e-11	6e-10	1e+03	30.8	16.7	10	114	2
Gelatinous zooplankton	Microzooplankton	1.98e-10	1.08e-10	3.08e-11	6.14e-10	1e+03	31	17.5	10.3	102	2
Gelatinous zooplankton	Large phytoplankton	3.91e-10	2.08e-10	6.52e-11	1.07e-09	1e+03	13	6.39	6.02	39.5	2
Copepods	Microzooplankton	4.61e-09	9.88e-10	2.54e-09	7.3e-09	1e+03	14.8	3.24	8.44	26.9	2
Copepods	Small phytoplankton	4.95e-09	1.42e-09	2.39e-09	1.07e-08	1e+03	3.54	0.939	1.58	6.36	2
Copepods	Large phytoplankton	6.61e-09	1.75e-09	3.18e-09	1.26e-08	1e+03	10.5	2.56	5.07	19.1	2
Microzooplankton	Small phytoplankton	2.46e-08	6e-09	1.46e-08	3.83e-08	1e+03	4.52	1.06	2.89	6.72	2

APPENDIX B

Software documentation for mixed_layer model with biological modules

B.1 Overview

This section provides detailed documentation of the Matlab code package developed for this dissertation, which will be made available for public download. The central component of this code is the mixed_layer package, which implements the one-dimensional physical model within which all simulations discussed in this thesis were run. The mixed_layer package also provides a variety of interchangeable biological modules that can be run within this physical model, including the biogeochemical-only module used to calculate initial Ecopath values for the planktonic groups (`nemurokak.m`) and the full end-to-end ecosystem model (`wce.m`).

In Section B.2, we provide a short user's manual for the `mixed_layer.m` code. This is not intended as a thorough tutorial, but should give a basic overview of how the code is designed to be used for both simple and complex simulations. Section B.3 provides detailed documentation of each individual Matlab function provided in the package.

B.2 The mixed_layer (with biology) toolbox

B.2.1 Code organization and installation

The distributed code includes four folders:

- `mixed_layer`: This folder holds the main `mixed_layer` function, as well as helper functions for reading the output of `mixed_layer` simulations. This folder also holds three subfolders. The `biomodules` folder includes the various biological modules that can be paired with `mixed_layer`. The `private` folder holds several private subfunctions exclusive to the `mixed_layer.m` parent function. The `defaultdata` folder includes physical forcing datasets that the model uses as defaults.
- `setup`: This folder holds setup scripts used to parameterize the `mixed_layer` model with water column ecosystem module for the Eastern Subarctic Gyre ecosystem simulations.
- `utilities`: This folder holds all children functions required to run any of the abovementioned functions. This includes subfunctions associated with the various biological routines as well as several general utilities that I have developed as part of my own Matlab library.
- `fex`: This folder includes functions I acquired via the MatlabCentral File Exchange (<http://www.mathworks.com/matlabcentral/fileexchange/>). They are written and maintained by third parties, and therefore I do not document them here, but simply provide a reference to each.

In addition to the code provided in these folders, the `mixed_layer` model requires three third-party Matlab toolboxes and the NCO utilities to run:

- Rich Signell's RPSstuff toolbox: <http://woodshole.er.usgs.gov/operations/sea-mat/RPSstuff-html/index.html>
- Phil Morgan's seawater toolbox: <http://www.marine.csiro.au/datacentre/processing.htm>
- mexnc and snctools: <http://mexcdf.sourceforge.net/>. Matlab introduced native netCDF file support in version R2009a, about halfway through the development process of this code. In most areas, I have attempted to migrate the important netCDF-related coding to this native interface, rather than the external mexnc package on which I had previously relied. However, due in part to attempts to keep back-compatibility and in part to time restrictions, there are several helper functions that still rely on the external toolbox. Note that the third-party NetCDF Toolbox (designed for Matlab v5/6) is not compatible with the `mixed_layer` code, and may cause filename clashes if it is installed.

- NetCDF Operators (NCO): <http://nco.sourceforge.net/>. These command-line programs (specifically ncrcat), need to be installed and accessible to Matlab via calls to the operating system (i.e. `system('ncrcat --version')` should return a valid result within Matlab).

To use this software, the four folders listed above (mixed_layer, setup, utilities, and fex), as well as the three outside toolboxes, must be added to the Matlab search path (via `addpath`, `pathtool`, File > Set Path, etc).

As one final note, within the mixed_layer code (in the initialize.m subfunction), I use the smooth.m function, which is from Matlab's Curve Fitting toolbox. This function is used to calculate running means in place of a simple filter.m call because it deals with edge cases in a more desirable manner; however, replacing the former with the latter is an easy modification in one does not have access to the Curve Fitting Toolbox. Beyond that, no additional Mathworks toolboxes should be required to run the code.

Below is a brief description of all functions included in this package; see Section B.3 for the complete description and calling syntax of each. Figure B.1 on page 109 diagrams the calling tree for the entire program.

Folder: fex

consolidator	written by John D'Errico, http://www.mathworks.com/matlabcentral/fileexchange/8354
mergestruct	written by Jos van der Geest, http://www.mathworks.com/matlabcentral/fileexchange/7842 (note: named catstruct originally, changed due to name conflict with my own function)
ode4	written by The Mathworks, http://www.mathworks.com/support/tech-notes/1500/1510.html#fixed
parseArgs	written by Aslak Grinsted, http://www.mathworks.com/matlabcentral/fileexchange/3696
parse_pv_pairs	written by John D'Errico, http://www.mathworks.com/matlabcentral/fileexchange/9082
readtext	written by Peder Axensten, http://www.mathworks.com/matlabcentral/fileexchange/10946
round2	written by Robert Bernis, http://www.mathworks.com/matlabcentral/fileexchange/4261

subaxis	written by Aslak Grinsted, http://www.mathworks.com/matlabcentral/fileexchange/3696
tlabel	written by Carlos Adrian Vargas Aguilera, http://www.mathworks.com/matlabcentral/fileexchange/19314
uniquetol	written by Siyi Deng, http://www.mathworks.com/matlabcentral/fileexchange/27498
wreshape	written by John D'Errico, no longer available on File Exchange

Folder: mixed_layer

mixed_layer	Runs a 1-D physical model of a water column
plotmixed	Plots results of the mixed_layer model
readmixed	Read mixed_layer output into a structure
recovercrashed	Create netcdf output for a partially-run mixed_layer sim

Folder: mixed_layer/biomodules

biomodule	Template biological module for mixed layer model
nemurokak	NEMURO, with iron and grazing modifications
np	Nutrient-phytoplankton biological module
npz	Nutrient-phytoplankton-zooplankton biological module
npzd	Nutrient-phytoplankton-zooplankton-detritus biological module
tracer	Generic tracer
tracerforced	Generic tracer with deep-water concentration held constant
wce	Water column ecosystem biological module

Folder: mixed_layer/private

archivemldata	Write mixed_layer results to file
binary2netcdf	Convert temporary binary output file to netcdf
calcheat	Calculate heating factors
clearsky	Calculate clear-sky irradiance
initbiorelax	Sets up relaxation for biological variables
initialize	Initialize parameters for mixed_layer model
initinterpdata	Initialize datasets for later interpolation

mixtracer	Calculates diffusive mixing of a tracer in the mixed_layer model
mixturb_my	Calculate and mix terms related to turbulence and energy
mycoef	Calculate mixing coefficients
parseinput	Parse and check all input variables
solve_velocities	Steps the equations of motion forward to solve for new
verticalflux	Calculates vertical movement within mixed layer model

Folder: setup

esabgcsetup	Step 2 of ESA mixed_layer runs: biogeochemistry
esafoodwebsetup	Step 3 of ESA mixed_layer runs: food webs
esaphysicssetup	Step 1 of ESA mixed_layer runs: physics
formatfornemurokak	Reformat data for nemurokak run
formatforwce	Reformat input data for wce run
runmixedlayer	Run mixed_layer model for multiple inputs

Folder: utilities

aggregate	Aggregate values into cell array
calcclusteredparams	Calculates new Ewe input params for clustered model
cell2matfill	Converts a cell array to a matrix filling in empty cells
cellstr2	Create cell array of strings from character array.
climatology	Creates climatology from timeseries
cptcmap	Apply a .cpt file as colormap to an axis
createensemble2	Create an ensemble of Ecopath models
ecopathinputcheck	Checks and fixes input in an Ewe input structure
ecopathinputinfo	Table of dimesions and units for ecopath input fields
ecopathlite	Rewrite of Ecopath algorithms
endonly	Grab only last row of a 3-dimensional array
eweunitconvert	Convert Ewe input structure between units
fluxread	Read and reformat flux data from nemurokak or wce run
integratebio	Integrate biology in mixed_layer module
ivlev2forage	Choose D to match foraging arena func. res. to Ivlev
listfluxes	Return indices of fluxes in nemurokak or wce model

minmax	Returns minimum and maximum value in the given array
nanmean	Mean value, ignoring NaNs.
ncvarsget	Read several variables from a netcdf file
nemuroecopathdata	Calculates B,P/B,etc for NEMURO run
nemuroflexinput	Returns paramters for a nemuroflex simulation
nemuroinputparser	Checks and returns user input and defaults for NEMURO
nemurokakode	My version of NEMURO
nemvarnames	Returns cell array holding NEMURO variable names
ode4splitsnonneg	Like ode4, but returns intermediate components, no negative
odewrap	Wrapper for ODE solvers with more flexible input and output
parsepv	Parses parameter/value pairs
photosynthesis	Calculate growth due to photosynthesis
regexpfound	Determine whether a regular expression is in a string
sh2dewpoint	Calculate dewpoint temperature based on specific humidity
sortewein	Sort groups in Ewe input structure by trophic level
suplabel	Create title, xlabel, and ylabel for group of axes
trophiclevel	Estimates trophic level of food web members
wceode	Water column ecosystem model, main ODE function

B.2.2 Usage guide

While I made every attempt possible to fully document all the code associated with this thesis such that others besides myself could work with this model, the setup process is still a somewhat complicated. A single iteration of the model with simple biology (e.g. a single nutrient, single phytoplankton module) requires a large collection of input variables and forcing datasets. Adding the module for the water column ecosystem requires hundreds of additional input variables, and running a full ensemble adds several more setup steps. This section provides instructions for taking the publicly-available code and running a few simulations, ranging from a simple nutrient-phytoplankton model to the full climatologically-forced Eastern Subarctic Gyre ensemble described in Chapter 3.

Of the many functions provided, users should only directly access those in the mixed_layer (top level) and setup folders. The mixed_layer.m function is the primary tool. Relying on all the default values for the input variables, one can run an example physics-only simulation. The physical forcings included in this default dataset describe a one-year period (1976-77) for the Scotian Shelf region, off

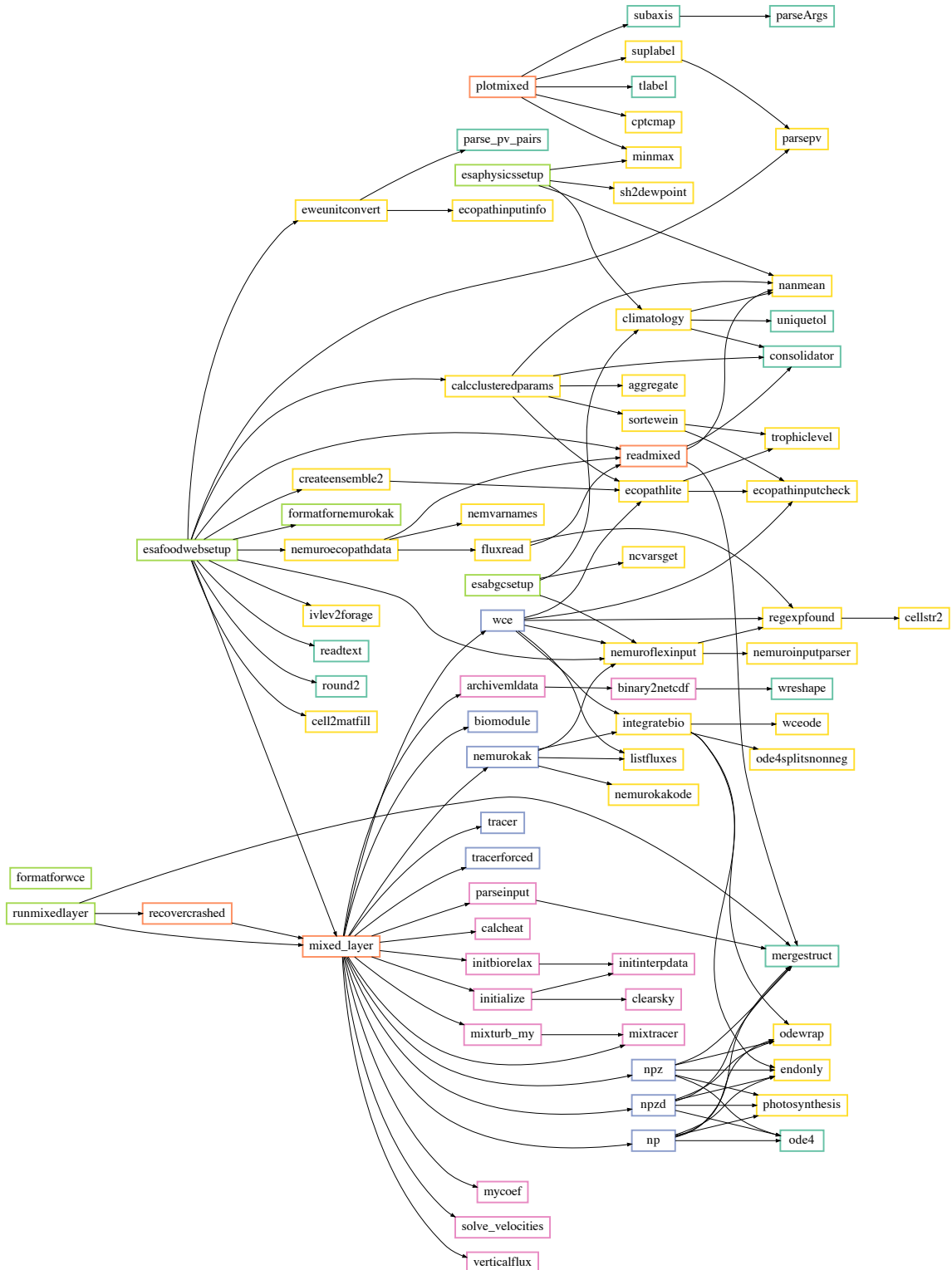


Figure B.1: Calling tree for all functions provided in the mixed_layer code package. Colors indicate which functions are found in each folder: mixed_layer (orange), private (pink), biomodules (blue), setup (green), utilities (yellow) or fex (turquoise).

the coast of Nova Scotia, Canada; they were compiled by Charlie Stock for a study of phytoplankton blooms (Song *et al.*, 2011). The command `mixed_layer('test')` will run the simulation and save the output to the file `test.nc`. A few status messages will be printed to the command line while the simulation is running to notify users of the model's progress. The warnings regarding missing input data simply point out that the forcing datasets are missing an hour on each end (the model starts at midnight, and the data at 1:00am); this type of warning will always be issued if input forcing data grids don't extend completely to the edges of the model's temporal and spatial grids, such that model values must be extrapolated.

Data from the netCDF output file can be read into Matlab most easily via the `readmixed.m` function. This function can also be used to list the names of the output variables included in the file via `readmixed('test', 'list')`.

One can also analyze the output files outside of Matlab using various netCDF utilities, but my use of non-standard coordinate variables may cause some confusion in external software designed for oceanographic data. Originally, I wrote the code to output to Matlab's .mat files, but migrated to the use of netCDF so one could access partial slices of often very large output files. Because of this, the netCDF files generated do not follow COARDS standards (as used by climate models), particularly with regards to the time dimension.

Simple plots of the various output variables can be generated via the `plotmixed` routine, which will plot each variable versus time and, if applicable, depth.

Biology can be added to the `mixed_layer` model via the `'biofun'` input variable, which holds a `function_handle` corresponding to one of the functions in the `mixed_layer/biomodules` folder (these functions follow a very specific format; see `biomodules/biomodule.m` for an overview if you intend to add to this library). For example, the `np` module adds a nutrient-phytoplankton model based on a simple box model described in Sarmiento & Gruber (2006). To run the model with this module, a few more input variables are needed:

```

nut = [...      % A rough starting
        0    20    % nutrient profile
       -150   40];

phyto = [...    % Seed a small population
           0   0.1    % of phytoplankton throughout
          -150  0.1]; % the water colum

kn = 0.1;      % Half-saturation constant
lambda = 0.05/86400; % Loss rate, /d
mu = 0.5;

% Run model

```

```
mixed_layer('nptest', 'biofun', @np, 'n', nut, 'p', phyto, 'kn', kn, ...
    'loss', lambda, 'remin', mu);
```

In the setup folder, three scripts are provided to compile input variables for the mixed_layer function specific to the Eastern Subarctic Pacific region: esaphysicssetup, esabgcsetup, and esafoodwebsetup, which gather the physical, biogeochemical, and food web-related variables, respectively. The data output by each of these three functions can then be passed to either formatfornemuro.m or formatforwce.m to create a structure of input data that can be fed into mixed_layer.m. The following script will run a 5-year simulation of the water column ecosystem model, with climatological forcing, for a single food web ensemble member.

```
Nyf = esaphysicssetup(2, 'nyf');
Nyf.eyear = 1904;

Bgc = esabgcsetup;

Fw = esafoodwebsetup(Nyf, Bgc, 500, 'runnemuro', true, ...
    'cvtparams', {'wwCfrac', 0.03});

In = formatforwce(Nyf, Bgc, Fw);

mixed_layer('wceexample', In(1));
```

To run an entire ensemble, one can repeat the mixed_layer call from the above example for each index in the In structure variable. Alternatively, one can use the runmixedlayer.m function, which performs this looping as well as some simple file organization:

```
Nyf = esaphysicssetup(2, 'nyf');
Nyf.eyear = 1904;

Bgc = esabgcsetup;

Fw = esafoodwebsetup(Nyf, Bgc, 500, 'runnemuro', true, ...
    'cvtparams', {'wwCfrac', 0.03});

In = formatforwce(Nyf, Bgc, Fw);

runmixed(In(1:50), 'wceexample', '.', false, 1);
```

The code above will create a folder in the current directory called wceexample, and will place sequentially-named output files for a 50-member ensemble in this folder. If one has the Parallel Computing Toolbox, the 4th and 5th input variables to this function can be set so that the 50 simulations are run in parallel to each other (note that this only parallelizes the looping of calls to mixed_layer, and not any of the calculations within mixed_layer itself).

B.3 Function reference

The following sections document all functions provided within the mixed_layer code distribution. Each section provides calling syntax, a brief description of the function, and a description of all input and output variables required by and returned by the function. These descriptions can also be accessed via the `help` command from the Matlab command line (for functions residing in either the mixed_layer/biomodules or mixed_layer/private folders, one must change directories to those locations to access the help).

B.3.1 aggregate

```
[xcon, yagg] = aggregate(x, y)
[xcon, yagg] = aggregate(x, y, fun)
```

This function groups together values of `y`, based on category values in `x`. It performs more or less like `accumarray(x,y,[a b]. @(x) {x})`, except allows `x` to be any value, not just indices, and `y` can have any number of columns.

Input variables:

```
x:      n x 1 array, categories, can be either numeric or a cell array
       of strings

y:      n x m array, values to be grouped

fun:    function handle. If included, this function is applied to the
       grouped values of y
```

Output variables:

```
xcon:   unique values of x

yagg:   cell array of y values corresponding to each x.
```

B.3.2 archivemldata

```
avg = archivemldata(Grd, Arch, outfile, it, data)
[avg, fid] = archivemldata(Grd, Arch, outfile, it, data)
```

New version should be compatible with all versions of Matlab, as long as sntctools is installed and mexnc points to the proper backend (either newer internal stuff or the proper mex version).

Input variables:

```
Grd:      1 x 1 structure holding spatial and temporal grid data for
          mixed_layer simulation

Arch:     1 x 1 structure holding data related to archiving

outfile:   name of output file

it:        index of current model time step

data:      nvar x 4 cell array of data to be written to file. Column
          1 holds the actual data values for the current model time
          step, which must be either nz x 1 vectors, nzp x 1 vectors,
          or scalars. Columns 2-4 are strings with the variables'
          short names, long names, and units, respectively.
```

Output variables:

```
avg:      nvar x 1 cell array, holding the newly-averaged values each
          variable. Averages are performed over each archiving
          period.
```

B.3.3 binary2netcdf

```
binary2netcdf(binfile, ncfile, sdate, edate, mdate, z, zp, vartable, ...
               ntpерread)
```

This function creates the netcdf output file for mixed_layer. It requires Matlab R2009a or later, which has netcdf support. binary2netcdf_snc can replace this function for older Matlab versions, but that version is currently absurdly slow.

Input variables:

```
binfile:    name of binary output file

ncfile:     name of netcdf file

sdate:      vector of datenumbers, time grid (beginning)

edate:      vector of datenumbers, time grid (end)

mdate:      vector of datenumbers, time grid (middle)

z:          depth grid

zp:         depth grid, edges

vartable:   n x 3 cell array, all variables from simulation
```

```

ntperfile:    number of time steps to be written to each small
              temporary file

verbose:      flag indicating whether to print progress to screen

```

B.3.4 biomodule

```

[bioinit, ismixed, bottomval, Biovars, names] = ...
    biomodule('init', In, Grd);
[newbio, diag] = ...
    biomodule('sourcesink', oldbio, meanqi, temp, z, dz, Biovars, t, dt);
wsink = ...
    biomodule('vertmove', oldbio, meanqi, temp, z, dz, Biovars, t, dt);

```

This is a template for a biological module for the mixed layer model. The module is called in three different modes during the mixed_layer simulation: 'init', 'sourcesink', and 'vertmove'.

The initialize ('init') mode sets up several different variables associated with the biology of the model, including:

- setting initial depth profiles of all biological state variables
- determining whether each state variable will be mixed via the diffusive mixing scheme used in the model
- setting any deep water forcing of each state variable
- adding any additional variables that will be needed to run the 'sourcesink' and/or 'vertmove' modes of the module.
- setting the names of any diagnostic variables that will be calculated in the 'sourcesink' mode.

The source and sink mode ('sourcesink') calculates the change in biomass of each state variable over a single time step of the model. This mode receives as input the biomass of all biological state variables, the mean solar radiation, and the temperature profile at the current time step, as well as the time and depth grid variables. If you require additional variables to calculate changes in biomass, these variables should be included in the Biovars structure created during initialization.

The vertical movement ('vertmove') mode calculates speed of vertical movement for each state variable. This can be used to introduce sinking or any other vertical movement unrelated to turbulent mixing.

Input variables for 'init' mode:

In: 1 x 1 structure holding user-supplied info.

See each individual function in this folder for the particular variables required by each module.

Grd: 1 x 1 structure, see mixed_layer code for fields

Output variables for 'init' mode:

bioinit: ndepth x nbsv array, initial depth profiles for all biological state variables
ismixed: 1 x nbsv logical array, indicates whether each biological state variable undergoes physical mixing.
bottomval: 1 x nbsv array, value used to force bottom layer during mixing. NaN indicates no forcing.
Biovarts: 1 x 1 structure holding additional parameters
names: 1 x nbsv cell array of strings, names for each state variable, Names must begin with a letter and contain only letters, numbers, and underscores.
diagnames: 1 x ndiag cell array of strings, names for each diagnostic variable. Names must begin with a letter and contain only letters, numbers, and underscores.

Input variables for 'sourcesink' and 'vertmove' mode:

oldbio: ndepth x nbsv array, profiles of biological state variables at current time step
meanqi: mean incoming solar radiation (W m⁻²)
temp: ndepth x 1 array, temperature profile (deg C)
z: ndepth x 1 array, depth grid for model (m)
dz: depth grid cell size (m)
t: current time (s)
dt: time step (s)

Output variables for 'sourcesink' mode:

newbio: ndepth x nbsv array, profiles of biological state variables after stepping forward by one time step
diag: ndepth x ndiag array, values of each diagnostic variable at each depth

Output variables for 'vertmove' mode:

wsink: ndepth x nbsv array, velocity of vertical movement, where positive values indicate movement towards the surface (m/s)

B.3.5 calcclusteredparams

```
[New, ped, old2new] = calcclusteredparams(Full, pedigree, idx, pedtype)
```

Given an Ewe input structure and a list of clustering indices, this function calculates the new parameter values by summing biomass in each clustered group, and performing a biomass-weighted average on all other parameters.

Input variables:

```
Full:      Ewe input structure for original food web  
  
pedigree:  ng x 4 array pedigree values for B, P/B, Q/B, and DC  
  
idx:       ng x 1 array of indices, where each index represents the  
           cluster number into which this group will be added. Values  
           must be integers from 1 to nc, where nc is the number of  
           clusters,  
  
pedtype:   method to use when calculating new pedigree  
           'propagate': uses propagation of error through the  
             summing/averaging calculations, assuming  
             that pedigree represents 95% confidence  
             interval (i.e. 2 std) in a normal  
             distribution  
           'average': performs a simple biomass-weighted average  
             over clustered groups. This will result in  
             higher pedigree values than the propagation  
             method, which may be preferable since the  
             values are not based on measurements but  
             rather rough guesses.
```

Output variables:

```
New:      new Ewe input structure for clustered model, with nc groups  
  
ped:      pedigree matrix for clustered model  
  
old2new:  ng x 1 array of indices showing which group each old one is  
           now part of (doesn't match idx because groups are resorted  
           by trophic level)
```

B.3.6 calcheat

```
[Qi, Qs, Ql, Qlw, adv_fac] = calcheat(Qi, atmp, dpnt, Tsrf, wspeed10, ...  
                                         Qo, meanQi, alb)
```

All variables are vectors of the same size unless otherwise indicated.

Input variables:

```
Qi:           incident solar radiation (W m^-2)
atmp:         air temperature (deg C)
dpnt:         dewpoint temperature (deg C)
Tsrf:         scalar, sea surface temperature (deg C)
wspeed10:     wind speed 10 m above ocean surface (m/s)
Qo:           clear-sky irradiance (W m^-2)
meanQi:       mean observed daily irradiance (W m^-2)
alb:          scalar, albedo, i.e. fraction of incoming radiation
               reflected from the sea surface
```

Output variables:

```
Qi:           incident solar radiation (W m^-2)
Qs:           sensible heat flux (W m^-2)
Ql:           latent heat flux (W m^-2)
Qlw:          longwave heat flux (W m^-2)
adv_fac:      advection factor, i.e. any net heating or cooling due to
               advection. Currently hardcoded to 0.
```

B.3.7 cell2matfill

```
a = cell2matfill(c, empty)
```

Input variables:

```
c:            cell array, where each cell holds either a numeric scalar or
empty array
empty:        value used to replace empty arrays
```

Output variables:

```
a:            numeric array, same size as c
```

B.3.8 cellstr2

C = CELLSTR2(S) places each row of the character array S into separate cells of C.

Use CHAR to convert back.

Another way to create a cell array of strings is by using the curly braces:

```
C = {'hello' 'yes' 'no' 'goodbye'};
```

This is a modified version of the cellstr function that does not deblank the strings. -Kelly Kearney

See also STRINGS, CHAR, ISCELLSTR.

B.3.9 clearsky

```
Qo = clearsky(start_date,t,Lat)
```

This function calculates the clear-sky irradiance using the formula of Seckel and Beaudry (1973) as reported in Reed (1977). This is used in the calculation of net longwave heat flux.

Input variables:

start_date: 1 x 6 date vector of time corresponding to t = 0

t: vector of time values to calculate clear-sky irradiance for, in seconds since start_date

Lat: scalar, latitude of location of interest

Output variables:

Qo: vector same length as t, clear-sky irradiance (W m⁻²)

B.3.10 climatology

```
[timec, datac] = climatology(time, data)
[timec, datac] = climatology(time, data, dt)
[timec, datac] = climatology(time, data, 'noleap')
[timec, datac] = climatology(time, data, 'expand')
[timec, datac, lower, upper] = climatology(...)
```

This function creates a climatology by calculating the average yearly cycle of data.

Input variables:

```
time:      time data, in any Matlab date format (datenumbers, date
           vectors, or date strings)

data:      nt x m array of data timeseries values.

dt:        time interval tolerance for output climatology. Timeseries
           values within this distance from each other are considered
           the same (see unquietol.m for details). Highly recommended
           for noisy data.

'noleap':  if included, indicates that time data is in days since a
           pivot year, with no leap year (i.e. all 365-day years).

'expand':   if included, the climatology is expanded to all input time
           points, rather than just including the one-year cycle
```

Output variables:

```
timec:    climatology time values, in either date numbers or days
           since pivot year, no leap, depending on input format.

datac:    climatology data

lower:    lower quartile of climatology data

upper:    upper quartile of climatology data
```

B.3.11 cptcmap

```
cptcmap(name);
cptcmap(name, ax);
cptcmap(... param, val, ...);
[cmap, lims, ticks, bfncol, ctable] = cptcmap(...)
```

This function creates and applies a colormap defined in a color palette table (.cpt file). For a full description of the cpt file format, see the Generic Mapping Tools documentation (<http://gmt.soest.hawaii.edu/>). Color palette files provide more flexible colormapping than Matlab's default schemes, including both discrete and continuous gradients, as well as easier direct color mapping.

Limitations: X11 color names not supported, patterns not supported, CMYK not supported yet

Input variables:

```
name:      .cpt file name. You may either specify either the full
           path, or just the file name. In the latter case, the
```

function will look for the file in the folder specified by the cptpath variable in the first line of code; by default this folder is located in the same location as cptcmap.m and is called cptfiles.

ax: handle of axis or axes where colormap should be applied (colormaps will effect the entire figure(s), but axis clim adjustments for direct scaling will only affect the specified axes). If no axis is specified and no output variables are supplied, colormap will be applied to the current axis. If no axis is specified and output variables are supplied, the colormap will not be applied to any axes.

'showall': When this option is used, a figure is created displaying colorbars for all colormaps contained in the .cpt folder. Color limits of each colormap are listed along with the names of each. A small tick mark indicates the location of 0, where applicable. NOTE: the number of columns to use for display is hard-coded. As you start collecting more color palettes, the figure may get too cluttered and you may have to adjust this (variable ncol is the plotcmaps subfunction).

Optional input variables (passed as parameter/value pairs):

'mapping': 'scaled' or 'direct'. Scaled mapping spreads the colormap to cover the color limits of the figure. Direct mapping resets the color limits of the axes so that colors are mapped to the levels specified by the .cpt file. ['scaled']

'ncol': number of colors in final colormap. If not included or NaN, this function will try to choose the fewest number of blocks needed to display the colormap as accurately as possible. I have arbitrarily chosen that it will not try to create more than 256 colors in the final colormap when using this automatic scheme. However, you can manually set ncol higher if necessary to resolve all sharp breaks and gradients in the colormap.

'flip': if true, reverse the colormap order [false]

Output variables:

cmap: ncol x 3 colormap array

lims: 1 x 2 array holding minimum and maximum values for which the colormap is defined.

ticks: vector of tick values specifying where colors were defined in the original file

bfncol: 3 x 3 colormap array specifying the colors defined for background (values lower than lowest color limit), foreground (values higher than highest color limit), and

NaN values. These do not affect the resulting colormap, but can be applied by the user to replicate the behavior seen in GMT.

ctable: n x 8 color palette table, translated to Matlab color space. Column 1 holds the lower limit of each color cell, columns 2-4 the RGB values corresponding to the lower limit, column 5 the upper limit of the color cell, and columns 6-8 the RGB values of the upper limit. When the lower and upper colors are the same, this defines a solid-colored cell; when they are different, colors are linearly interpolated between the endpoints.

Example:

```
[lat, lon, z] = satbath(10);
pcolor(lon, lat, z);
shading flat;
cptcmap('GMT_globe', 'mapping', 'direct');
colorbar;
```

B.3.12 createensemble2

```
[Lim, Set] = createensemble2(Ewein, pedigree, nset)
[Lim, Set, count] = createensemble2(Ewein, pedigree, nset)
```

Same as createensemble, but in this case it keeps generating ensembles until it finds the designated number of balanced ones. Only balanced parameters are returned, since otherwise arrays could be unmanageably large. Could take a while...

Input variables:

Ewein: Ewe input structure, in any set of consistent units
pedigree: ngroup x 4 array of pedigree values (B, PB, QB, DC)
nset: number of balanced ensemble members to generate.

Output variables:

Lim: 1 x 1 structure with the following fields

bb: ng x 2 array, lower and upper limits for biomass
pb: ng x 2 array, lower and upper limits for production/biomass
qb: ng x 2 array, lower and upper limits for consumption/biomass
dc: ng x ng x 2, prey x pred x lower/upper limits for diet fractions. Final dc values are renormalized to 1 after being chosen from these intervals.

```

Set:      1 x 1 structure with the following fields

bb: ng x nset, biomass values for each potential food web
pb: ng x nset, production/biomass values for each potential
    food web
qb: ng x nset, consumption/biomass values for each
    potential food web
dc: ng x ng x nset, diet composition for each potential
    food web
ee: ng x nset, ecotrophic efficiency of resulting food web
q0: ng x ng x nset, flux due to consumption between all
    groups

count:    # of iterations required to acquire requested number of
          balanced simulations

```

B.3.13 ecopathinputcheck

```

B = ecopathinputcheck(A)
B = ecopathinputcheck(A, warnoff)

```

This function checks an Ewe input structure for proper dimensions and to verify certain values. If incorrect values are found (for example, non-zero values for a primary producer's consumption/biomass ratio), the values are corrected.

Input variables:

```

A:           Ewe input structure

warnoff:     logical scalar. If true, no warnings are issued when
             corrections are made to the structure. Default: false.

```

Output variables:

```

B:           structure identical to A but with corrections made if
             necessary.

```

B.3.14 ecopathinputinfo

```

fieldTable = ecopathinputinfo;

```

This function returns a table with information on the dimensions and units used for each field in a Ewe input structure.

Output variables:

```

fieldTable: n x 3 cell array of strings
    column 1: names of each input variable
    column 2: dimensions of variable (ngroup = number of
               functional groups in the model, ndet = number
               of non-live detritus groups, ngear = number of
               fishing fleets in the model)
    column 3: units of each variable (M = mass, A = area or
               volume, T = time)

```

B.3.15 ecopathlite

```

ecopathlite(S)
C = ecopathlite(S)

```

This function reproduces the main calculations performed by the Ecopath portion of the EwE model (www.ecopath.org). If no output variable is provided, the results are printed to tables in the command window. (Note: this part is out of date, must use output option for now).

Ecopath is used to parameterize the initial conditions of an ecosystem model. This function is not really meant to be used to set up and balance a model for the first time, since it does not provide any feedback on the results (e.g. whether EE values are > 1, etc); use the original Ecopath software for this.

Note that the units listed below are those used in the original Ecopath software. They can be changed as long as all parameters are changed consistently.

Input variable:

```

S: structure with the following fields. Values of the fields b, pb,
   qb, ee, ge, gs, and/or dtImp that defined as NaN indicate
   unknown values, which will be filled in by the ecopath algorithm.

ngroup:           1 x 1 array, number of functional groups in the
                  model

nlive:            1 x 1 array, number of live (non-detrital) groups
                  in the model

ngear:            1 x 1, number of fishing gear types in the model

areafrac:         ngroup x 1 array, fraction of habitat area occupied
                  by each group (no units, 0-1)

b:                ngroup x 1 array, biomass (t km^-2)

pb:               ngroup x 1 array, production over biomass ratios
                  (yr^-1)

```

qb: ngroup x 1 array, consumption over biomass ratios
 (yr^{-1})

 ee: ngroup x 1 array, ecotrophic efficiencies (no units, 0-1)

 ge: ngroup x 1 array, gross efficiency, i.e. production over consumption ratio (no units)

 gs: ngroup x 1 array, fraction of consumed food that is not assimilated (no units)

 dtImp: ngroup x 1 array, detritus import (should be zero for all non-detrital groups) (t $\text{km}^{-2} \text{yr}^{-1}$)

 bh: ngroup x 1 array, habitat biomass, i.e. biomass per unit area (b/areafrac) (t km^{-2})

 pp: ngroup x 1 array, fraction of diet consisting of primary production, pp = 2 indicates detritus

 dc: ngroup x ngroup array, diet composition, dc(i,j) tells fraction predator j's diet consisting of prey i

 df: ngroup x (ngroup - nlive) array, fraction of each group that goes to each detrital group due to other mortality and egestion

 immigr: ngroup x 1 array, immigration into area (t $\text{km}^{-2} \text{yr}^{-1}$)

 emig: ngroup x 1 array, emigration out of area (t $\text{km}^{-2} \text{yr}^{-1}$)

 emigRate: ngroup x 1 array, emigration per unit biomass
 (yr^{-1})

 ba: ngroup x 1 array, biomass accumulation (t $\text{km}^{-2} \text{yr}^{-1}$)

 baRate: ngroup x 1 array, biomass accumulation per unit biomass
 (yr^{-1})

 landing: ngroup x ngear array, landings of each group by each gear type (t $\text{km}^{-2} \text{yr}^{-1} ?$)

 discard: ngroup x ngear array, discards of each group by each gear type (t $\text{km}^{-2} \text{yr}^{-1} ?$)

 discardFate: ngear x (ngroup - nlive) array, fraction of discards from each gear type that go to each detritus group

Output variables:

C: structure with the following fields, all ngroup x 1 arrays unless otherwise specified

trophic:	trophic level
areafrac:	fraction of total area occupied by group
bh:	habitat biomass (biomass/area)
b:	total biomass
pb:	production/biomass ratio
qb:	consumption/biomass ratio
ee:	ecotrophic efficiency
ge:	growth efficiency, i.e. production/consumption
ba:	biomass accumulation
baRate:	biomass accumulation rate
migration:	net migration
flowtodet:	(ngroup + ngear) x 1 array, flow to detritus from each group and each gear type
fishMortRate:	mortality rate due to fishing
predMortRate:	mortality rate due to predation
migrationRate:	net migration rate
otherMortRate:	mortality rate due to anything else
predMort:	predation mortality
q0:	ngroup x ngroup array, initial consumption rates by each predator on each prey
q0sum:	total consumption rate by each predator
respiration:	respiration
searchRate:	ngroup x ngroup array, search rates of each predator for each prey
detexport:	(ngroup-nlive) x 1 array, amount of detritus exported from the system

B.3.16 endonly

```
[anew, bnew, ...] = endonly(a,b);
```

Returns only last row of a n x m x p array (i.e. squeeze(a(end,:,:))). I wrote this function simplify grabbing the last time step result from an ODE solver. Result will be a m x p array.

Input variables:

```
a,b, ...: three-dimensional arrays. Arrays do not have to be the same size as each other.
```

Output variables:

```
anew...: two-dimensional arrays holding first row of each input array, respectively
```

B.3.17 esabgcsetup

```
A = esabgcsetup
```

This function returns the biogeochemical parameters for a mixed_layer run with the @nemurokak or @wce modules. This includes biogeochemical parameters (including iron-related ones, starting profiles for all nutrients, and rerouting fluxes.

I think I've now made units consistant between both modules (mol/m^3). However, just due to the way NEMURO was originally written, some of the variables here are still in mol/l; those are properly converted in the formatforxxx.m routines.

Output variables:

```
A: 1 x 1 structure with the following fields
```

```
Np: structure of NEMURO-related paramters (see nemuroinputparser)

binit: nz x 11 array, initial profile data for 11 standard nemuro variables (mol/l)

zinit: nz x 1 array, depths corresponding to initial profile data in binit (m)

reroute: nr x 5 cell array, rerouting of fluxes

grmax: 1 x 11 array, maximum grazing rates for nemuro variables (s^-1)
```

```
thresh:      1 x 11 array, grazing threshold values for nemuro
variables (mol m^-3)
```

TODO: finish this list

B.3.18 esafoodwebsetup

```
A = esafoodwebsetup(Phys, Bgc, nset)
A = esafoodwebsetup(Phys, Bgc, nset, 'norun')
```

This is probably the most complicated step of the setup process. It includes the entire process to go from the published Aydin 2003 ESA Ecopath model to an ensemble of balanced models that can be used in the @wce module. Steps include:

- Make some manual changes to the original food web, including removing the bacteria group and adjusting ctenophore GE.
- Adjust NEMURO-derived parameters to match my own version (@nemurokak)
- Reduce the number of functional groups via hierarchical clustering routine based on shared predator and prey groups
- Generate an ensemble based on the pedigree uncertainty of B, P/B, Q/B, and DC and keep only the members that balance
- Calibrate the X and D parameters of NEMURO-derived groups to match the Ivlev growth curves as closely as possible.

Although the most time-consuming setup step, this should only need to be rerun if I make major changes to my biogeochemistry that will effect the nemuro-only calibration steps. Otherwise, all experiments use the same set of input food webs.

Input variables:

```
Phys:           physical input (see esaphysicssetup) for a normal-year run
Bgc:           biogeochemical input (see esabgcsetup)
nset:          numbers of potential food webs to create; likely only a
               small fraction of these will be balanced
```

Optional input:

```
adjustmanually: flag to indicate whether to perform the manual
                parameter adjustments [true]
adjustnemuro:   flag to indicate when to perform the match-to-nemuro
                adjustments [true]
runnemuro:     flag to indicate whether to rerun a 3-year normal-year
                nemuro run. If true, the run will be done using the
                Phys and Bgc input. Otherwise, nemuro adjustments will
```

be performed using the esafwCalibration.nc file found in the calling directory, and this file must contain a nemuro simulation whose last year is 1902. [true]

cvtparams: cell array of conversion parameters used when adjusting food web to match nemuro run (need to convert from molN/m^3/s to g ww/m^3/yr [{'wwCfrac', 0.02}])

Output variables:

A: structure with fields:

EweinFull: original food web with bacteria group removed, in t ww/km^2/yr, includes ngf groups

EweinFullAdj: above food web with parameters adjusted to match NEMURO, as well as a manual adjustment to ctenophore growth efficiency, in t ww/km^2/yr.

EweinSimp: above food web simplified to include fewer functional groups, in t ww/km^2/yr, includes ngs groups

EweinEns: ensemble generated from EweinSimp and its associated pedigree, in molN/m^2/s. Each food web includes X, D, and theta parameters such that the nemuro-derived functional responses mimic Ivlev grazing.

full2sim: ngf x 1 array, indicating which simplified group each of the original groups were added to

Lim: structure listing the uncertainty bounds used for the ensemble generation (see createensemble.m), in t ww/km^2/yr

Set: structure listing the parameters associated with each ensemble member (see createensemble.m), in t ww/km^2/yr

CalDetailsSimp: matchmk output structure resulting from functional response calibration of EweinSimp (see matchmk.m)

CalDetailsEns: matchmk output structure resulting from functional response calibration of EweinEns (see matchmk.m)

nemidx: 1 x 11 array indicating which of the simplified groups correspond to NEMURO state variables, where the indices correspond to the 11 original state variables (see nemvarnames.m)

pedigreeFull: ngf x 4 array of pedigree values for B, P/B,

```

Q/B, and DC variables for the original model

pedigreeSimp:    ngf x 4 array of pedigree values for B, P/B,
                  Q/B, and DC variables for the simplified model

```

B.3.19 esaphysicssetup

```
A = esaphysicssetup(iloc, type)
```

The esaCoreGeccoData datasets have CORE- and GECCO-extracted forcings for 4 locations within the ESA region:

- 1: 50 N -165 W
- 2: 50 N -145 W (OSP)
- 3: 50 N -135 W
- 4: 55 N -145 W

This file extracts those forcings, for either the normal-year or interannual datasets, and also makes a few modifications to the default physical parameters.

Input variables:

```
iloc:    1-4, corresponding to desired location
type:    'nyf' or 'iaf', specifying normal-year or interannual datasets
```

Output variables:

```
A:      1 x 1 structure with mixed_layer input variables:
        dz, zbot, syear, eyear, Lat, wind_input, heat_input, ts_input,
        srelax, srelaxtime, velocity_dissipation
```

B.3.20 eweunitconvert

```
[new1, new2, ...] = eweunitconvert(oldunit, newunit, old1, old2, ..., ...
                                     param, val, ...)
```

Input variables:

```
oldunit:    string specifying the units used in the old variable, in
            the format M/A/T
            M (mass):          'tons wet weight', 't ww', 'mmol N',
                               'mmol n', 'mol N', 't C', 'g C'
            A (area/volume):   'km^2', 'm^2', 'km^3', 'm^3'
            T (time):          'year', 'yr', 'sec', 's'

newunit:    string specifying the units for the new variables, using
            the same format as oldunit
```

```
old#:      variables to be converted. These can be either Ewe input  
           structures, NemEp structures (see nemuroecopathdata) or  
           numeric arrays. All numeric arrays are assumed to start  
           with the same unit type, specified by the 'varunit'  
           parameter
```

Optional input variables (passed as parameter/value pairs), defaults in parentheses

```
wwCfrac:    ratio of carbon over wet weight (0.05)  
  
c2n:        nitrogen/carbon ratio (16/106)  
  
cmw:        molecular weight of carbon (12.0107)  
  
depth:      depth of water column used for any area to volume  
           conversions, in km (NaN)  
  
varunit:    type of unit used by input variables. Can be either  
           'M/A/T' (flux rate), 'M/A' (concentration), or '1/T' (rate)  
           ('M/A/T')
```

Output variables:

```
new#:      converted versions of all old# input variables
```

B.3.21 fluxread

```
Flux = fluxread(file, Opt)
Flux = fluxread(file, Opt, 'matrix')
Flux = fluxread(file, Opt, 'cell')
Flux = fluxread(Data, '[cell]matrix')
Flux = fluxread(..., flux1, flux2, ...);
```

This function reads in the flux data associated with a wce or nemurokak run of the mixed_layer model. To save time and space, all predation fluxes are read only at the surface.

Input variables:

```
file:      name of output netcdf file (with or without .nc extension)

Opt:       1 x 1 one structure holding options for reading and
           averaging data:

tstart:    date number corresponding to earliest value to
           read in time dimension. If NaN, will read from
           beginning. [NaN]

tend:      date number corresponding to latest value to
           read in time dimension. If NaN, data will be
```

```

                    read to end of time dimension. [NaN]

tstride:      sampling interval (stride) along time
               dimension. [1]

monthavg:    True indicates to average data over each month.
               Sampling based on above parameters will be done
               prior to averaging. [false]

Data:        Data structure returned by readmixed. Can be used instead
               of file and Opt if data is already in memory and you just
               want to reshape the fluxes

'matrix':   if included, reshape flux data into ngroup x ngroup x ntime
               x ndepth matrices, If not included fluxes will be left in
               same format as in netcdf file. This can greatly increase
               the size of the data since the fluxes are sparsely
               distributed between groups, so not recommended for large
               files (use cell instead).

'cell':     if included, store flux data in ngroup x ngroup cell array,
               where cells hold ntime x ndepth data, or empty cells if no
               flux occurs between two groups

flux#:       Types of fluxes to read in. Can be any of the wce flux
               types: 'dec', 'ege', 'exc', 'gpp', 'gra', 'mor', 'pre', 'exx',
               'res'. If not included, all flux types are read.

```

B.3.22 formatfornemurokak

```

In = formatfornemuro(Phys, Bgc)
In = formatfornemuro(Phys, Bgc, fe)

```

Just a little bookkeeping script to try to wrangle all the input data for mixed_layer nemuro simulations. Takes data from esaphysicssetup.m and exabgcsetup (which are designed to be more human-manageable so that one can make easy modifications to the default values) and reformats it as required for mixed_layer with the nemurokak biological module.

Input variables:

```

Phys:      structure, output of esaphysicssetup.m

Bgc:      structure, output of esabgcsetup.m

fe:       string indicating which iron flux data to use:
          'constant': apply the constant flux over the whole run
          'climatology': use the climatological cycle derived from the
                          constant value paired with dry/wet-deposition
                          scaling
          'timeseries': use the full timeseries derived from the

```

constant value paired with dry/wet-deposition
scaling

Output variables:

In: structure holding all inputs required for mixed_layer with the nemurokak module

B.3.23 formatforwce

```
In = formatforwce(Phys, Bgc, Fw)
In = formatforwce(Phys, Bgc, Fw, fe)
```

Input variables:

Phys: see esaphysicssetup

Bgc: see esabgcsetup

Fw: see esafoodwebsetup

fe: string indicating which iron flux data to use:

'constant': apply the constant flux over the whole run
'climatology': use the climatological cycle derived from the
constant value paired with dry/wet-deposition
scaling
'timeseries': use the full timeseries derived from the
constant value paired with dry/wet-deposition
scaling

Output variables:

In: structure holding all inputs required for mixed_layer with the wce module

B.3.24 initbiorelax

Fields added to Bio structure:

hasrelax: nbsv x 1 logical array, true if relaxation data provided

Relax: 1 x nbsv 1 x 1 structure of data for bio relaxation
interpolation. Fields empty for non-relaxed variables.

t: nt x 1 array, times corresponding to
columns of data (s from sim start time)

z: nz x 1 array, depths corresponding to the
rows of data (m, neg down)

data: nz x nt array, biological relaxation profiles

(in units defined bio biological module)

B.3.25 initialize

This function initializes the values of most constant parameters used throughout the mixed-layer model. It also preallocates and sets the initial conditions for many variables that will be modified throughout the model simulation.

Input variables:

In: structure holding user-supplied input variables

Output variables:

Grd: structure holding temporal and spatial grid parameters:

z: nz x 1 array, depth coordinate at the center of each grid cell (m)

zp: (nz+1) x 1 array, depth coordinate at the edges of each grid cell (m)

nz: number of vertical levels

tmax: simulation length (s)

nt: total number of internal time iterations

time: 1 x nt array, time elapsed from model start time to the beginning of each time interval (s)

start_date: 1 x 6 array, date vector for simulation start date. This will always be Jan 1 of the specified start year.

end_date: 1 x 6 array, date vector for simulation end date. This will always be Dec 31 of the specified end year.

Ht: structure holding variables related to heat forcing

t: nth x 1 array, time corresponding to Ht.data (s from simulation start)

data: nth x 3 array, heat forcing data. Column 1 = incoming solar radiation (W m^{-2}), Column 2 = air temperature (deg C), Column 3 = dewpoint temperature (deg C)

Qo: nt x 1 array, estimate of clear sky irradiancne,
 based on the "Smithsonian Formula" from Seckel and
 Beaudry, as reported in Reed, 1977, JPO, 7, pp.
 482-485. It is good for latitudes between 20S and
 60N.

meanQi: nt x 1 array, mean observed daily irradiance (W
 m^{-2})

Ts: structure holding variables related to temperature and salinity

T: nz x 1 array, temperature profile (deg C)

S: nz x 1 array, salinity profile (psu)

Sig: nz x 1 array, density profile. Note that water is
 currently treated as incompressible ($kg\ m^{-3}$)

Srelax: 1 x 1 structure of data for salt relaxation
 interpolation. Not included if no salt relaxation
 data was provided.

t: nts x 1 array, times corresponding to
 columns of data (s from sim start time)

z: nzs x 1 array, depths corresponding to the
 rows of data (m, neg down)

data: nzs x nts array, salt relaxation profiles
 (psu)

Trelax: 1 x 1 structure of data for temperature relaxation
 interpolation. Not included if no temperature
 relaxation data was provided.

t: ntt x 1 array, times corresponding to
 columns of data (s from sim start time)

z: nzt x 1 array, depths corresponding to the
 rows of data (m, neg down)

data: nzt x ntt array, temperature relaxation
 profiles (deg C)

Mmntm: structure holding variables related to momentum, mixing, and
 turbulence

Kh: (nz+1) x 1 array, tracer mixing coefficient (m^2
 s^{-1})

small: arbitrarily small value, used as proxy for 0 to
 prevent things from blowing up

U: nz x 1 array, east-west current velocity (m/s)

V: nz x 1 array, north-south current velocity (m/s)

q2: (nz+1) x 1 array, twice the turbulent kinetic
 energy ($m^2\ s^{-2}$)

q2l: (nz+1) x 1 array, turbulent kinetic energy * length scale term ($m^3 s^{-2}$)
 len: (nz+1) x 1 array, turbulence length scale (m)
 gh: (nz+1) x 1 array, Richardson number (no units)
 sh: (nz+1) x 1 array, MY 2.5 intermediate quantity, a function of the Richardson number
 sm: (nz+1) x 1 array, MY 2.5 intermediate quantity, a function of the Richardson number
 Km: (nz+1) x 1 array, vertical kinematic viscosity, i.e. momentum mixing coefficient ($m^2 s^{-1}$)
 Kq: (nz+1) x 1 array, turbulence mixing coefficient ($m^2 s^{-1}$)
 boygr: (nz+1) x 1 array, buoyancy generation term
 shear: (nz+1) x 1 array, shear term
 lc_q2: (nz+1) x 1 array, dissipation constant for turbulent kinetic energy (no units)
 lc_q2l: (nz+1) x 1 array, dissipation constant for kinetic-energy-length-scale (no units)
 kmol: Background diffusivity ($m^2 s^{-1}$)
 cor: coriolis forcing based on latitude (s^{-1})
 pgx: acceleration due to a pressure gradient in the EW direction ($m s^{-2}$)
 pgy: acceleration due to a pressure gradient in the NS direction ($m s^{-2}$)
 kappa: parameter related to bottom friction, von Karman's constant (no units)
 z0b: roughness parameter, related to bottom friction (m)
 Cbot: bottom friction coefficient (POM parameterization) (no units)
 Wnd: structure holding variables related to wind forcing
 t: ntw x 1 array, times corresponding to wind data (s from sim start time)
 data: ntw x 3 array of wind forcing data. Column 1 =

surface wind stress in east-west (u) direction (N m^-2), column 2 = surface wind stress in the north-south (v) direction (N m^-2), column 3 = wind speed at 10 m above sea level (m/s)

Arch: structure holding variables related to archive (i.e. output).
The archiving period refers to the In.tarch input.

startdate: nbin x 6 array, date vectors corresponding to start of each archiving time step

enddate: nbin x 6 array, date vectors corresponding to end of each archiving time step

middate: nbin x 6 array, date vectors corresponding to middle of each archiving time step

fraction: 1 x nt array, fraction that each model time step contributes to its archiving time step

islast: 1 x nt logical array, true if time step corresponds to the end of an archiving time step

bin: 1 x nt array, index of archiving time step to which each model time step corresponds

nbin: number of archiving time steps

fileidx: nt x 2 array, column one holds the index of the temporary output file to which results will be written for each time step, column 2 tells the index of that time step within the file

isnewfile: nt x 1 array, true if model time step is the first to be written to a new temporary output file

endtime: n x 1, end time of each archiving period (s)

filedates: nfile x 2 array, indices of first and last archive step included in each temporary output file

Charlie Stock
cstock@alum.mit.edu

modified by Kelly Kearney

B.3.26 initinterpdata

```
[A, str] = initinterpdata(type, data, Grd)
```

This function sets up forcing datasets for use for later interpolation. It verifies that data is in the proper format (vs depth, time, or both), repeats climatological data if necessary, and extends data to the edges of the model temporal and spatial grids if necessary (using nearest-neighbor extrapolation).

Input variables:

```
type: One of the following strings:  
      'time': data describes one or more variables vs time  
      'depth': data describes one or more variables vs depth  
      'both': data describes a single variable vs both time and  
              depth  
  
data: Input data  
      'time': nt x (6+nvar) array. Columns 1-6 hold date vectors  
              corresponding to each row of data, remaining  
              column(s) hold variable data. If the simulation  
              time spans multiple years and the data only spans a  
              single year, the data will be treated as a  
              climatology and repeated for all simulation years  
      'depth': nz x (1+nvar) array. Column 1 holds depth values  
              corresponding to each row of data (m, negative  
              down), remaining column(s) hold variable data  
      'both': (nt+1) x (nz+6) array. Columns 1-6 hold date  
              vectors corresponding to each row of data, row 1  
              holds depth values corresponding to each column of  
              data (cells (1,1:6) are ignored), remaining cells  
              hold variable data. If the simulation time spans  
              multiple years and the data only spans a single  
              year, the data will be treated as a climatology and  
              repeated for all simulation years.  
  
Grd: Struct holding spatial and temporal grid data for mixed_layer  
      simulation
```

Output variables:

```
A: 1 x 1 structure with the following fields:  
  
t: nt x 1 vector, time (seconds from simulation start  
time) ('time' or 'both' only)  
  
z: nz x 1, depth (m, negative down) ('depth' or 'both'  
only)  
  
data: nt x nvar ('time'), nz x nvar ('depth'), or nz x nt  
('both') array of variable values  
  
str: string, describing time and/or depth interval where  
      extrapolation was necessary
```

B.3.27 integratebio

```
[newbio, dbdt, Split, Diag, bad] = integratebio(fun, t, dt, oldbio, ...
                                                Param, solver1, solver2, ...)
```

This function is a wrapper for different ODE solvers, used to integrate biological variables in a few mixed_layer modules. It allows one to try multiple different solvers, which can sometimes be useful when values get low or start changing quickly (such that they are difficult to solve with the set time step).

Input variables:

```
fun:      function handle of ODEs for biology. Must be of the form
          [db,Splitdb,Diag] = fun(t,b,P).

t:        current time of integration

dt:       time step

oldbio:  nz x nbsv array of biological state variables

Param:   structure of additional parameters for ODEs

solver:  ODE solvers to use, in order. If any tracers go negative,
         become NaNs, or become infinite, the next solver will be tried,
         until the last solver is reached. Can be 'euler', 'ode4', or
         'ode45', or 'implicit'. *NOTE* Implicit doesn't really work,
         doesn't conserve mass
```

Output variables:

```
newbio:  biological state variable values at time t+dt

dbdt:    dB/dt for each state variable.

Split:   structure with contribution toward dB/dt from each flux type in
         the ODE function. For euler and ode4, these will add to dbdt;
         for ode45 they represent the splits when the ODE function is
         evaluated at time t (since getting weights throughout the
         variable steps is not presently possible)

Diag:    additional diagnostic variables returned by the ODE function.
         For euler and ode4, the diagnostics are those associated with
         the beginning of the time step. Extra diagnostics cannot be
         returned from the ode45 solver at this time.

bad:     nz x nbsv logical array, true if the final solver attempted
         still failed to integrate without hitting a negative, NaN, or
         Inf value.
```

B.3.28 ivlev2forage

```
A = ivlev2forage(m, d, tau, bi, bj, qij, dz, tfac)
```

This function attempts to choose the best parameters in order to make a foraging arena functional response match a threshholded Ivlev functional repsonse.

```
Ivlev:           I = m * (1 - exp(-d * (N - tau)))
Type 2:         I = m * (N / (k + N))
Type 3:         I = m * (N^2 / (k^2 + N^2))
Foraging arena: I = Q/Bj .* (D .* (N/Bi)^theta)/(D - 1 + (N/Bi)^theta)
```

Currently, the "best match" is defined as the value of D that gets closest to the same half-saturation constant ($k = \ln 2/(d) + \tau$) and maximum grazing rate (m) as in the Ivlev version.

In previous versions of this function, I tried to do a full sum-of-squares curve fit over an arbitrary domain, but found that just fitting to k and m was much more time-efficient and provided results of a similar quality.

Input variables:

```
m:      maximum ingestion rate of target Ivlev function (at 0deg C)
(s^-1)

d:      Ivlev parameter for target Ivlev function (molN/m^3)^-1

tau:    prey threshhold value for target Ivlev function (molN/m^3)

bi:     mass-balanced prey biomass (molN/m^2)

bj:     mass-balanced predator biomass (molN/m^2)

qij:    mass-balanced consumption (molN/m^2/s)

dz:     depth over which to assume consumption occurs (m)

tfac:   average temperature factor (i.e. exp(kT)) experienced over the
time and space from which bi, bj, and qij were derived
```

Output variables:

```
Dfit:   value of D for which fraction error of foraging-arena
equivalent m and k is smallest compared to the Holling Type 3
response whose half-sat is equal to ln(2)/d + tau and whose
maximum ingestion rate equals that of the Ivlev form

mfit:   maximum ingestion rate achieved with Dfit (/s)

kfit:   half-saturation value achieved with Dfit (theta = 2) (molN/m^3)
```

```

bi:      mass-balanced prey biomass, in volumetric units (molN/m^3)

bj:      mass-balanced predator biomass, in volumetric units (molN/m^3)

qij:     mass-balanced consumption rate of prey by predator at 0deg C
        (molN/m^3/s)

k:       half-saturation constant of Holling Type 3 function closest to
        target Ivlev ( $\ln(2)/d + \tau$ ) (molN/m^3)

fun:    cell array of function handles to calculate Ivlev, Holling Type
        2, Holling Type 3, and foraging arena functional responses,
        respectively.

```

B.3.29 listfluxes

```

list = listfluxes('nemurokak', Idx)
list = listfluxes('wce', Idx, links)

```

Input variables:

```

Idx:      1 x 1 structure with fields (ps, pl, zs, zl, etc) indicating
        the index of the biological state variables corresponding to
        each nemuro-derived variable (see wce and nemurokak setup)

links:   ng x ng array indicating type of predator/prey interaction
        1 = zooplankton eat zooplankton
        2 = nekton eat zooplankton
        3 = nekton eat nekton
        4 = zooplankton eat phytoplankton
        Note: For mortality flux indices, this function assumes that
        all living critters are involved in at least one predator-prey
        interaction. If not true, I'll need to update this.

```

Output variables:

```

list:   n x 3 cell array, where column 1 indicates the type of flux,
        column 2 source group index, and column 3 the sink group index

```

B.3.30 minmax

```

[minval maxval] = minmax(a)
lims = minmax(a);
lims = minmax(a, type);
lims = minmax(a, w);

```

Computes the minimum and maximum value in entire array (all dimensions).

Input variables:

```
a: numeric array

type: 'all': absolute minimum and maximum (default)
      'noout': discards outliers
      'center': centers on zero
      'centernoout': centers on 0 and eliminates outliers

w: for no-outlier version, factor defining an outlier. Point is
  considered an outlier if larger than q3+w*(q3-q1) or smaller
  than q1-w*(q3-q1) [1.5]
```

Output variables:

```
minval: minimum value in a

maxval: maximum value in a
```

B.3.31 mixed_layer

```
mixed_layer(outputfile)
mixed_layer(outputfile, param1, val1, param2, val2, ...)
Input = mixed_layer(...)
Stop = mixed_layer(..., 'stopafterinit', true)
```

This program simulates the seasonal evolution of a 1D water column. It is forced by observed solar radiation and wind forcing. Numerically, a 1D diffusion equation is solved implicitly, allowing for long time steps without loss of stability.

The supporting functions for this model reside in the private directory. In addition, the model relies on a few 3rd-party toolboxes:

Rich Signell's RPSstuff toolbox (wstress.m)
<http://woodshole.er.usgs.gov/operations/sea-mat/RPSstuff-html/index.html>

Phil Morgan's seawater toolbox (sw_dens0.m and sw_smow.m)
<http://www.marine.csiro.au/datacentre/processing.htm>.

mexnc and snctools (pre-Matlab R2009a only)
<http://mexcdf.sourceforge.net/>

The mixed_layer model is set up to allow interchangeable biological modules to be run within it. Please see biomodule.m (in the biomodules directory) for a template function and more information.

The output filename input is required for the model to run. All other inputs are optional and passed as parameter/value pairs. One or more of these parameters can also be passed in structure format, where the fieldnames correspond to one or more of the parameter names. The default

values for these parameters set up the model for a specific example scenario. Some variables (such as albedo and the attenuation coefficients) can be relied on for other models, while others (such as years, depths, or various input data sets) would make little sense when combined with other data. Unless indicated, all variables hold numerical arrays. Variables are scalars unless dimensions are specified. Default values are in brackets.

Input variables:

REQUIRED:

outputfile: string, name of netcdf output file, where all model results will be saved. If no extension is provided, .nc will be appended.

MODEL GRID:

dz: the thickness of each grid cell (m). Can be a vector of thicknesses, prescribing the thickness of each individual layer, although math is not as certain for this. [5]

zbot: the depth of the modeled water column (m, negative) [-150]

dt: the model time step (seconds) [10800]

syear: starting year for simulation (will start on Jan 1 of this year), or 1 x 6 date vector of starting date [1976]

eyear: ending year for simulation (will end on Dec 31 of this year), or 1 x 6 date vector of ending date [1976]

PHYSICAL PARAMETERS:

krad1: the attenuation coefficient (m^{-1} , value should be positive) for visible radiation (~between 350 nm and 700 nm wavelength). This is approximately equivalent to the photosynthetically available radiation (PAR). [0.15]

prad1: the fraction of incoming solar radiation that falls into visible wavelengths ~ PAR. By default, it is assumed that roughly 45% of the incoming solar radiation falls into this category (Baker and Frouin, 1987, L&O, 32:6, pp. 1370-1377). [0.45]

krad2: the attenuation coefficient (m^{-1} , value should be positive) for non-visible (mainly infra-red) solar radiation. Water absorbs this radiation very quickly. [1.67]

alb: the albedo, or the fraction of incoming radiation reflected

from the sea surface. The default value is 0.079, which is typical for 43 N latitude. (Payne, R.E., 1972, Journal of Atmospheric Sciences, 29:5, pp. 959-969). *If your heat forcing was measured below the water surface, set the albedo to 0. [0.079]

Lat: latitude where simulation takes place (used for Coriolis force calculations) [45]

whgt: elevation above sea level where wind forcing data was measured (m). [10]

pgx: acceleration due to a pressure gradient in the east-west direction ($m\ s^{-2}$) [1e-5]

pgy: acceleration due to a pressure gradient in the north-south direction ($m\ s^{-2}$) [0]

kmol: molecular diffusivity (m^2/s) [1e-4]

velocity_dissipation: dissipation constant (s^{-1}). This term removes energy from past storm events over a specified time-scale as though energy was being transferred to more quiescent surrounding waters. [3.858e-6, i.e. 1/(3 day)]

EXTERNAL FORCING:

wind_input: Wind forcing data. This is an $n \times 8$ matrix, with columns representing year, month, day, hour, minute, second, east-west wind speed (i.e. u), north-south wind speed (i.e. v). Speeds in m/s. By default, a dateset representing 1976 observations on the Scotia Shelf is used.

heat_input: Heat forcing data. This is an $n \times 9$ matrix, with columns representing year, month, day, hour, minute, second, incident solar radiation (Qi), air temperature, and dew point temperature. Radiation is in W/m^2 and all temperatures are in deg C. By default, a dateset representing 1976 observations on the Scotia Shelf is used.

ts_input: Initial temperature and salinity profiles for simulation. Data is an $n \times 3$ matrix with columns representing depth (m, negative down), temperature (deg C), and salinity (psu). By default, a dateset representing 1976 observations on the Scotia Shelf are used.

srelax: Relaxtion data for salinity. Columns 1-6 of this array hold a year, month, day, hour, minute, and second corresponding to the dates of the relaxation forcing, and row 1 of the array hold depths (negative down, m). Columns 1-6 in row 1 are just placeholders and will be ignored.

The remaining cells hold salinity data (ppt) for the given times and depths towards which the modeled salinity will be relaxed. If all the relaxation data is from the same year, the data will be treated as climatological data and will be repeated for every simulated year. If empty, no relaxation will be done. [empty]

srelaxtime: Timescale for salinity relaxation (s) [2592000, i.e. 30 d]

trelax: Relaxation data for temperature. Format is the same as for srelax, with temperature data in deg C. If all the relaxation data is from the same year, the data will be treated as climatological data and will be repeated for every simulated year. If empty, no relaxation will be done. [empty]

trelaxtime: Timescale for temperature relaxation (s) [2592000]

tracerw: Vertical velocity data. Format can be either a single scalar value, indicating constant vertical advection over space and time, or the same as for srelax, with velocity data in m/s. This data can be used to simulate upwelling (positive) or downwelling (negative) velocities. The movement associated with this is applied to temperature, salinity, and all mixed biological state variables. NOTE: This hasn't really been tested, and probably shouldn't be used unless I put some more work into it.

ARCHIVING:

tarch: the archiving interval (seconds). Data is averaged over tarch seconds. Can also be one of these indicators, which represent non-even archiving intervals:
-1: monthly
If tarch isn't scalar, then multiple output files will be created; beginarchive and endarchive must be the same size as tarch. [86400]

beginarchive: datenumber indicating what model date to begin recording to an output file, or NaN to indicate that archiving begins immediately. [NaN]

endarchive: datenumber indicating what model date to stop recording output to an output file, or NaN to indicate archiving until the simulation ends. [NaN]

outputextension: cell array of strings, same size as tarch, beginarchive, and endarchive. This string is appended to the outputfile string if multiple files are indicated by the other archiving variables.

tempfilesz: number of data points (i.e. time steps) to read in at a time when converting from the temporary binary output file

to a netcdf file. If NaN, all data is read at once. Using smaller amounts may speed up the read/write process, and can avoid memory errors, especially if a simulation returns a large number of biology-associated variables. For variable-heavy runs, reading a few hundred time steps at a time is probably a good idea. [NaN]

stopafterinit: logical scalar. If true, simulation is terminated after the initialization process, and no forward integration is performed. This is for debugging purposes. Using this option also leads to different output if mixed_layer is called with an output variable (see below) [false]

tempdir: string, folder where temporary file will be stored. If empty, the default temporary directory will be used. []

cleanup: logical scalar. If true, temporary files will be deleted after the netcdf file is created. Files will always be kept if the simulation crashes. [true]

BIOLOGY:

biofun: Function handle to biological module. If empty, the model will run without any biology. [empty]

*var*relax: Relaxation data for any biological state variable, where *var* corresponds to the short name of the variable. Format is the same as for srelax. If not included or empty, no relaxation will be done.

*var*flux: Additional flux into (or out of) any biological state variable, where *var* corresponds to the short name of the variable. Format is the same as for srelax, in units of stateVariableUnit/s.

brelaxtime: Timescale for relaxation of biological state variables. (s) [2592000]

openbottom: Logical scalar. The value changes the way the biological tracer variables interact in the bottom cell. If false, a no-flux condition is set at the bottom; mixing and vertical movement will be conservative for biological tracers. If true, the values of biological variables are held constant in the bottom cell, and material sinks through the bottom boundary; mass is not conserved under these conditions. [false]

OTHER

verbose: logical scalar. If true, progress statements will be printed to the screen. If false, nothing will be printed. [true]

Output variables:

- Input: 1 x 1 structure holding the input variables used for the run. Returning this variable allows you to see all inputs used, including those set by defaults.
- Stop: 1 x 1 structure holding the variables used within a mixed_layer run. This is returned only if the 'stopafterinit' flag is set to true, and is useful for debugging purposes.

B.3.32 mixtracer

```
newtracer = mixtracer(tracer, mixcoef, dt, dz, sbc, bbc, bottomval,  
                      source, dissipate)
```

This function calculates an implicit solution to integrate the diffusion equation over one time step. The diffusion equation in this case is $du/dt = d/dz(K * du/dz) - cu$, where u is any tracer, K is the mixing coefficient for that tracer, and c is a constant dissipation term.

Input variables:

- tracer: n x 1 array of tracer concentrations at each depth at the current time step (units vary based on tracer)
- mixcoef: n x 1 array, mixing coefficient for tracer at each depth ($m^2 s^{-1}$)
- dt: time increment (s)
- dz: depth increment (m)

Optional input variables (passed as parameter/value pairs):

- sflux: flux of tracer across the surface interface, i.e. $K * du/dz$ at the surface, where u is tracer concentration and K is the mixing coefficient (tracer unit s^{-1})
- bflux: flux of tracer across the bottom interface, i.e. $K * du/dz$ along the bottom, where u is tracer concentration and K is the mixing coefficient (tracer unit s^{-1})
- sval: tracer value at the surface, used to force the surface grid cell.
- bval: tracer value along the bottom, used to force the bottom grid cell
- source: n x 1 array, source (or sink) flux of tracer at each depth

```

        (tracer unit s^-1)

dissipate: dissipation constant (s^-1)

Output variables:

newtracer: n x 1 array, tracer concentrations at next time step
           (tracer unit)

```

B.3.33 mixturb_my

B.3.34 mycoef

```
[b1, sh, sm, Kq, Km, Kh] = mycoef(nz, sh, gh, sm, len, q2)
```

This routine calculates the mixing coefficients for turbulence, scalars and momentum. A typical value for molecular diffusion (kmol) is added to the calculated values to serve as a lowe limit for diffusion.

B.3.35 nanmean

M = NANMEAN(X) returns the sample mean of X, treating NaNs as missing values. For vector input, M is the mean value of the non-NaN elements in X. For matrix input, M is a row vector containing the mean value of non-NaN elements in each column. For N-D arrays, NANMEAN operates along the first non-singleton dimension.

NANMEAN(X,DIM) takes the mean along the dimension DIM of X.

See also MEAN, NANMEDIAN, NANSTD, NANVAR, NANMIN, NANMAX, NANSUM.

B.3.36 ncvarsget

```
Data = ncvarsget(file, var1, var2, ...)
```

This function reads multiple variables from a netcdf file. It is just a wrapper function for nc_varget.

Input variables:

```
file: name of netcdf file
```

var: name of variable to read in, which must correspond exactly to a variable in the file. If no variable names are listed, all variables are read.

Output variables:

Data: 1 x 1 structure, with fieldnames corresponding to requested variables, each holding the data value for that variable

B.3.37 nemuroecopathdata

```
Data = nemuroecopathdata(file, Opt, depth)
```

This function calculates Ecopath-related variables based on the output of a NEMURO simulation, using the depth-integrated values.

Input variables:

file: output file for mixed_layer with nemuro biology (units mol/m³/s)

Opt: structure of options for reading in file (see readmixed)

depth: depth to integrate over. If not included, will integrate over the entire water column

Output variables:

Data: 1 x 1 structure with the following fields

b: mol N m⁻²

qb: s⁻¹

q0: mol N m⁻² s⁻¹

q0sum: mol N m⁻² s⁻¹

pb: s⁻¹

ge: no unit

gs: no unit

dc: no unit

m0: mol N m⁻² s⁻¹

m2: mol N m⁻² s⁻¹

B.3.38 nemuroflexinput

```
Params = nemuroflexinput('param1', val1, 'param2', val2, ...)
Params = nemuroflexinput(setname)
Params = nemuroflexinput(setname, 'param1', val1, 'param2', val2, ...)
```

This function collects all the input variables from a nemuro parameter structure into critter x 1 (for group-related) or critter x critter (for flux-related) arrays. Originally this was in preparation for the flexible-nemuro biological module, hence the name, but it's now used as a convenient organization step for several biological modules.

Input variables:

setname: string corresponding to one of the set names in nemuroParamSets.mat. These indicate various sets of NEMURO parameters that have been published in the literature. Any unspecified variables (see below) will be set to a default value from the specified set. If no set is specified, the 'NEMURO Version 1.f90' set, from the original source code representing the A7 location, will be used.

Optional input variables:

All variables should be scalars. Values can be entered as parameter/value pairs or as fields in a structure. Default values come from parameter set indicated by setname. See nemuroinputparser.m for full list of variables for native variables. For non-native variables (i.e. live groups other than those included in the original NEMURO), variables should follow the format:

```
var_#:      where # is the index of the critter

        for producers: alpha, Iopt, Vmax, Kno3, Knh4, Kgpp, pusai,
                        res0, Kres, gamma, needsi, Ksi

        for grazers:   lambda, Kgra, alphaeg, beta

        for both:      mor0, Kmor, settle

var_#1_#2: where #1 is the index of the prey and #2 is the index of
            the predator

        for grazers:   grmax, thresh, grpusai
```

Output variables:

Params: 1 x 1 structure with the following fields:

alpha1:	Light Dissipation coefficient of sea water (/m)
---------	---

alpha2: phytoplankton self-shading coefficient
 (l/molN/m)

 usesteele: logical scalar indicating whether to use
 Steele (1) or Platt (0)
 photosynthesis-irradiance curves

 RSiN: Si/N ratio (molSi/molN)

 alpha: nbsvx1 array, initial slope of
 photosynthesis-irradiance curve (Platt
 only) (/ly/min)/s

 Iopt: nbsvx1 array, optimal light intensity
 (Steele only) (ly/min)

 Vmax: nbsvx1 array, maximum photosynthetic rate
 @0degC (/s)

 Kno3: nbsvx1 array, half-saturation constant for
 uptake of NO₃ (molN/l)

 Knh4: nbsvx1 array, hal-saturation constant for
 uptake of NH₄ (molN/l)

 Kgpp: nbsvx1 array, temperature coefficient for
 photosynthetic rate (/degC)

 pusai: nbsvx1 array, ammonium inhibition
 coefficient (l/molN)

 res0: nbsvx1 array, respiration rate @0degC (/s)

 Kres: nbsvx1 array, temperature coefficient for
 respiration (/degC)

 mor0: nbsvx1 array, mortality rate @0degC
 (1/(molN s))

 Kmor: nbsvx1 array, temperature coefficient for
 mortality (/degC)

 gamma: nbsvx1 array, ratio of extracellular
 excretion to photosynthesis (no units)

 lambda: nbsvx1 array, Ivlev constant (l/molN)

 Kgra: nbsvx1 array, temperature coefficient for
 grazing (/degC)

 Kxi: nbsvx1 array, half-saturation coefficient
 for silica (molSi/l)

 alphaeg: nbsvx1 array, assimilation efficiency (no

	units)
beta:	nbsvx1 array, growth efficiency (no units)
needsi:	nbsvx1 logical array, true if requires silica for growth
grmax:	nbsvxnbsv array, maximum rate of grazing by predator j on prey i @0degC (/s)
thresh:	nbsvxnbsv array, threshold value for grazing (molN/l)
grpusai:	nbsvxnbsv array, preference coefficient for prey i by predator j (l/molN)
vdec:	nbsvxnbsv array, decomposition (or nitrification) rate of i into j @0degC (/s)
Kdec:	nbsvxnbsv array, temperature coefficient for decomposition (/degC)
inhibitedby:	nbsvxnbsv cell array, indices of prey groups preferred over prey i by predator j
settle:	nbsvx1 array, settling velocity (m/s)
egecosink:	nbsvx1 array, fraction of food egested by each grazer that does not sink (i.e. goes to DON instead of PON).

B.3.39 nemuroinputparser

```
Params = nemuroinputparser('param1', val1, 'param2', val2, ...)
Params = nemuroinputparser(setname)
Params = nemuroinputparser(setname, 'param1', val1, 'param2', val2, ...)
[Params, Extra] = nemuroinputparser(...)
```

Input variables:

setname: string corresponding to one of the set names in
nemuroParamSets.mat. These indicate various sets of NEMURO
parameters that have been published in the literature. Any
unspecified variables (see below) will be set to a default
value from the specified set. If no set is specified, the
'NEMURO Version 1.f90' set, from the original source code
representing the A7 location, will be used.
'Eslinger et al. Simulation Parameter'
'Eslinger et al. Station P'
'Eslinger et al. A7'
'Eslinger et al. Bering'

```

'NEMURO Version 1.f90'
'Fujii et al. Papa'
'Fujii et al. A7'
'Fujii et al. KNOT'
'Kishi et al. A7'

```

Optional input variables:

All variables should be scalars. Values can be entered as parameter/value pairs or as fields in a structure. Default values come from parameter set indicated by setname.

alpha1:	Light Dissipation coefficient of sea water	[/m]
alpha2:	PS+PL Selfshading coefficientS+PL	[l/molN/m]
IoptS:	PS Optimum Light Intensity S	[ly/min]
IoptL:	PL Optimum Light Intensity	[ly/min]
LLN:	Number of sublayer for calculating of Lfc	
VmaxS:	PS Maximum Photosynthetic rate @0degC	[/s]
KNO3S:	PS Half satuation constant for Nitrate	[molN/l]
KNH4S:	PS Half satuation constant for Ammonium	[molN/l]
PusaiS:	PS Ammonium Inhibition Coefficient	[l/molN]
KGppS:	PS Temp. Coeff. for Photosynthetic Rate	[/degC]
MorPS0:	PS Mortality Rate @0degC	[/s]
KMorPS:	PS Temp. Coeff. for Mortality	[/degC]
ResPS0:	PS Respiration Rate at @0degC	[/s]
KResPS:	PS Temp. Coeff. for Respiration	[/degC]
GammaS:	PS Ratio of Extracell. Excret. to Photo.	[(nodim)]
VmaxL:	PL Maximum Photosynthetic rate @0degC	[/s]
KNO3L:	PL Half satuation constant for Nitrate	[molN/l]
KNH4L:	PL Half satuation constant for Ammonium	[molN/l]
KSIL:	PL Half satuation constant for Silicate	[molSi/l]
PusaiL:	PL Ammonium Inhibition Coefficient	[l/molN]
KGppL:	PL Temp. Coeff. for Photosynthetic Rate	[/degC]
MorPL0:	PL Mortality Rate @0degC	[/s]
KMorPL:	PL Temp. Coeff. for Mortality	[/degC]
ResPL0:	PL Respiration Rate at @0degC	[/s]
KResPL:	PL Temp. Coeff. for Respiration	[/degC]
GammaL:	PL Ratio of Extracell. Excret. to Photo.	[(nodim)]
GRmaxS:	ZS Maximum Rate of Grazing PS @0degC	[/s]
KGraS:	ZS Temp. Coeff. for Grazing	[/degC]
LamS:	ZS Ivlev constant	[l/molN]
PS2ZSstar:	ZS Threshold Value for Grazing PS	[molN/l]
AlphaZS:	ZS Assimilation Efficiency	[(nodim)]
BetaZS:	ZS Growth Efficiency	[(nodim)]
MorZS0:	ZS Mortality Rate @0degC	[/s]
KMorZS:	ZS Temp. Coeff. for Mortality	[/degC]
GRmaxLps:	ZL Maximum Rate of Grazing PS @0degC	[/s]
GRmaxLpl:	ZL Maximum Rate of Grazing PL @0degC	[/s]
GRmaxLzs:	ZL Maximum Rate of Grazing ZS @0degC	[/s]
KGraL:	ZL Temp. Coeff. for Grazing	[/degC]
LamL:	ZL Ivlev constant	[l/molN]
PS2ZLstar:	ZL Threshold Value for Grazing PS	[molN/l]
PL2ZLstar:	ZL Threshold Value for Grazing PL	[molN/l]
ZS2ZLstar:	ZL Threshold Value for Grazing ZS	[molN/l]

AlphaZL:	ZL Assimilation Efficiency	[(nodim)]
BetaZL:	ZL Growth Efficiency	[(nodim)]
MorZL0:	ZL Mortality Rate @0degC	[/s]
KMorZL:	ZL Temp. Coeff. for Mortality	[/degC]
GRmaxPpl:	ZP Maximum rate of grazing PL @0degC	[/s]
GRmaxPzs:	ZP Maximum rate of grazing ZS @0degC	[/s]
GRmaxPzl:	ZP Maximum rate of grazing ZL @0degC	[/s]
KGraP:	ZP Temp. Coeff. for grazing	[/degC]
LamP:	ZP Ivlev constant	[l/molN]
PL2ZPstar:	ZP Threshold Value for Grazing PL	[molN/l]
ZS2ZPstar:	ZP Threshold Value for Grazing ZS	[molN/l]
ZL2ZPstar:	ZP Threshold Value for Grazing ZL	[molN/l]
PusaiPL:	ZP Preference Coeff. for PL	[l/molN]
PusaiZS:	ZP Preference Coeff. for ZS	[l/molN]
AlphaZP:	ZP Assimilation Efficiency	[(nodim)]
BetaZP:	ZP Growth Efficiency	[(nodim)]
MorZP0:	ZP Mortality Rate @0degC	[/s]
KMorZP:	ZP Temp. Coeff. for Mortality	[/degC]
Nit0:	NH4 Nitrification Rate @0degC	[/s]
KNit:	NH4 Temp. coefficient for Nitrification	[/degC]
VP2NO:	PON eecomp. Rate to Ammonium @0degC	[/s]
KP2N:	PON Temp. Coeff. for Decomp. to Ammon.	[/degC]
VP2DO:	PON Decomp. Rate to DON @0degC	[/s]
KP2D:	PON Temp. Coeff. for Decomp. to DON	[/degC]
VD2NO:	DON Decomp. Rate to Ammonium @0degC	[/s]
KD2N:	DON Temp. Coeff. for Decomp. to Ammon.	[/degC]
VO2SO:	Opal Decomp. Rate to Silicate @0degC	[/s]
KO2S:	Opal Temp. Coeff. for Decomp.to Silicate	[/degC]
RSiN:	Si/N ratio	[molSi/molN]
RCN:	C/N ratio	[molC/molN]
setVPON:	Settling velocity of PON	[m/s]
setVOpal:	Settling velocity of Opal	[m/s]
TNO3d:	Nitrate Concentraion in the Deep Layer	[molN/l]
TSiOH4d:	Silicate Concentraion in the Deep Layer	[molSi/l]
usesteele:	logical scalar indicating whether to use Steele (1) or Platt (0) light curves	

Output variables:

Params:	1 x 1 structure with fields corresponding to variables listed above, with default values if user did not provide a value via input.
Extra:	1 x 1 structure including any parameter-value pairs included by the user that are not included in the above list (used by nemuroflexinput)

B.3.40 nemurokak

See biomodule.m for full syntax details.

This module runs a lower-trophic level biogeochemical model based on the NEMURO model. It includes modifications for explicit iron limitation, as well as options to switch between single-resource and multi-resource grazing functional responses.

User-specified input variables (passed to mixed_layer as parameter/value pairs):

```

NemParam: 1 x 1 structure of nemuro input variables (see
nemuroinputparser.m)

bnem0:      nz x 13 array of initial values for each state variables.
Column 1 holds depths (m, negative down) and columns 2-13
correspond to the 12 state variables (mol/m^3):
 1: PS   4: ZL   7: NH4  10: SiOH4
 2: PL   5: ZP   8: PON  11: Opal
 3: ZS   6: NO3  9: DON  12: Fe

ivlev:      String, specifying which grazing scheme to use ['orig']
'orig':     single-resource for all except ZP, which has
            "gourmet" function
'single':   single-resource for all
'multi':    multi-resource for all

grmax:      (ivlev = 'multi' only) 11 x 1 array, maximum razing rates
for each of the live state variables (with placeholders for
the remaining originals) (/s)

thresh:     (ivlev = 'multi' only) 11 x 1 array, theshold feeding
values for each of the live state variables (mol/m^3)

p:          (ivlev = 'multi' only) 11 x 11 array of prey preference
values, with values ranging from 0-1. 1 indicates the most
preferred prey.

Kfe:        1 x 2 array, half-saturation constants for iron uptake for
small and large phytoplankton, respectively (molFe/m^3)
[6e-7 3e-6]

kfe2n:      1 x 2 array, half-saturation constants for internal Fe:N
ratio for small and large phytoplankton, respectively
(molFe/molN) [[6.625e-05 0.0001325], i.e. [10 20]
umolFe/molC assuming Redfield]

fe2nmax:    1 x 2 array, maximum internal Fe:N ratio for small and
large phytoplankton, respectively (molFe/molN)
[[0.00033125 0.0033125], i.e. [50 500] umolFe/molC assuming
Redfield]

fe2nupfac:  scalar, Fe:N uptake ratio (molFe/molN) [100e-6]

ligbkg:     Ligand background concentration (mol/m^3) [1.0e-6]

alphascav:  Iron scavenging coefficient (s^-1) [1.5855e-06, i.e. 50

```

```

        yr^-1]

remineff: Fraction of particulate iron remineralization relative to
          organic (N) material (no unit) [0.25]

kiscav:   Half-saturation constant for light's influence on ligand
          binding (W/m^2) [1.0]

kliglo:   Lower limit of ligand binding under low-light conditions
          (m^3/mol) [3.0e8]

klighi:   Upper limit of ligand binding under high-light conditions
          (m^3/mol) [1.0e5]

reroute:  n x 5 cell array. This allows you to reroute fluxes from
          the original path defined in the nemuro model. Each row
          describes a change, with column as follows:
          col 1: name of flux (gpp, gra, pre, res, exx, exc, ege,
                  mor, dec)
          col 2: name of original source group
          col 3: name of original sink group
          col 4: name of new sink group
          col 5: fraction of flux to reroute

odesolver: cell array of strings, indicating which solvers to use. If
           the first one fails to integrate a timestep (i.e. causes
           something to become negative, NaN, or Inf), the next one is
           tried. See integratebio.m for choices. [{'euler'}]

```

B.3.41 nemurokakode

```
[db, Flx, Diag] = nemurokakode(time, bio, A)
```

Source/sink ODE function for the nemurokak biological module. See biomodules/nemurokak.m for details; this function is designed to be called by ODE solvers.

B.3.42 nemvarnames

```

vars = nemvarnames
vars = nemvarnames('long')
vars = nemvarnames('iron')

```

Yes, I am that lazy

Input variables:

```
'long': Return long names (e.g. 'Small Phytoplankton' as opposed to
        'PS')
```

```
'iron': Include the iron-related that I added to the original 11  
variables.
```

Output variables:

```
vars: {'PS', 'PL', 'ZS', 'ZL', 'ZP', 'NO3', 'NH4', 'PON', 'DON', 'SiOH4',  
'Opal'}, or a variation on that theme.
```

B.3.43 np

See biomodule.m for full syntax details.

This module adds a simple nutrient-phytoplankton model to the mixed_layer model. The model is based on the NP model described in Sarmiento and Gruber (2008) Chapter 4, where

$$\begin{aligned} \frac{dP}{dt} &= P * (V_{max} * N / (K_n + N) - \lambda_{dap}) \\ \frac{dN}{dt} &= P * (-V_{max} * N / (K_n + N) + m_{up} * \lambda_{dap}) \end{aligned}$$

The maximum growth rate V_{max} is determined by temperature and light limitation, following Eppley (1972) and Platt and Jasby (1976), respectively. The half-saturation constant (K_n), loss rate (λ_{dap}), and fraction of remineralization (m_{up}) are provided by the user.

User-specified input variables (passed to mixed_layer as parameter/value pairs)

```
n: n x 2 depth profile of initial nutrients, where column 1 gives  
the depth values (negative down) and column 2 holds the  
concentrations of nutrients (mmol N m^-3)

p: n x 2 depth profile of phytoplankton, where column 1 gives the  
depth values (negative down) and column 2 holds the  
concentrations of phytoplankton (mmol N m^-3)

kn: half-saturation for nutrient uptake by phytoplankton (mmol N  
m^-3)

loss: loss rate for phytoplankton (s^-1)

remin: fraction of phytoplankton loss that is remineralized
```

B.3.44 npz

See biomodule.m for full syntax details.

This module adds a simple nutrient-phytoplankton-zooplankton model to the mixed_layer model. The model is based on the NPZ model described

in Sarmiento and Gruber (2008) Chapter 4, where

```
dZ/dt = Z * (gammaz * g * P/(Kp + P) - lambdaz)
dP/dt = P * (Vmax * N/(Kn + N) - lambdap - g*Z/(Kp + P))
dN/dt = P * (-Vmax * N/(Kn + N) + mup * lambdap) +
         Z * muz * ((1 - gammaz) * g * P/(Kp + P) + lambdaz)
```

The maximum growth rate Vmax is determined by temperature and light limitation, following Eppley (1972) and Platt and Jasby (1976), respectively. The half-saturation constants (Kn, Kp), loss rates (lambdap, lambdaz), and fractions of remineralization (mup, muz) are provided by the user.

User-specified input variables (passed to mixed_layer as parameter/value pairs)

```
n:           n x 2 depth profile of initial nutrients, where column 1
             gives the depth values (negative down) and column 2 holds
             the concentrations of nutrients (mmol N m^-3)

p:           n x 2 depth profile of phytoplankton, where column 1 gives
             the depth values (negative down) and column 2 holds the
             concentrations of phytoplankton (mmol N m^-3)

z:           n x 2 depth profile of zooplankton, where column 1 gives
             the depth values (negative down) and column 2 holds the
             concentrations of zooplankton (mmol N m^-3)

kn:          half-saturation for nutrient uptake by phytoplankton (mmol
             N m^-3)

kp:          half-saturation for phytoplankton uptake by zooplankton
             (mmol N m^-3)

lambdap:     loss rate for phytoplankton (s^-1)

lambdaz:     loss rate for zooplankton (s^-1)

mup:         fraction of phytoplankton loss that is remineralized

muz:         fraction of zooplankton loss that is remineralized

g:           maximum zooplankton growth rate (s^-1)

gammaz:      zooplankton assimilation efficiency (0-1)
```

B.3.45 npzd

See biomodule.m for full syntax details.

This module adds a nutrient-phytoplankton-zooplankton-detritus model.

The dynamics for phytoplankton and zooplankton growth are the same as the NPZ model. Egestion and mortality go to a detritus pool, which is remineralized at a constant rate to the nutrient pool. Excretion goes directly to the nutrient pool.

User-specified input variables (passed to mixed_layer as parameter/value pairs)

n:	n x 2 depth profile of initial nutrients, where column 1 gives the depth values (negative down) and column 2 holds the concentrations of nutrients (mmol N m ⁻³)
p:	n x 2 depth profile of phytoplankton, where column 1 gives the depth values (negative down) and column 2 holds the concentrations of phytoplankton (mmol N m ⁻³)
z:	n x 2 depth profile of zooplankton, where column 1 gives the depth values (negative down) and column 2 holds the concentrations of zooplankton (mmol N m ⁻³)
d:	n x 2 depth profile of detritus, where column 1 gives the depth values (negative down) and column 2 holds the concentrations of detritus (mmol N m ⁻³)
kn:	half-saturation for nutrient uptake by phytoplankton (mmol N m ⁻³)
kp:	half-saturation for phytoplankton uptake by zooplankton (mmol N m ⁻³)
lambdap:	loss rate for phytoplankton (s ⁻¹)
lambdaz:	loss rate for zooplankton (s ⁻¹)
g:	maximum zooplankton growth rate (s ⁻¹)
gammaz:	zooplankton assimilation efficiency (0-1)
dsink:	detritus sinking velocity, negative (m/s)
kremin:	remineralization rate constant (s ⁻¹)
egestz:	fraction of zooplankton ingestion that is egested

B.3.46 ode4splitsnonneg

```
[y, dy, Splits, Diag, failflag] = ode4splits(odefun,tspan,y0,p1, p2, ...)
```

This function extends the ode4 function to calculate diagnostic variables and additive components as the ODE is solved. For the additive

components aspect, I assume that the ODE function is of the form $dy/dt = dy_1 + dy_2 + dy_3 + \dots$. This is particularly designed for biological modules in mixed_layer, where the total change is a sum of processes (production, grazing, predation loss, etc).

Input variables:

```

odefun:      function handle to ode, of form [db,Splitdb,Diag] =
              fun(t,b,P)

tspan:       vector of time steps to integrate over

y0:          vector or 2D array of initial conditions

p#:          additional parameters to pass to the ODE function

```

Output variables:

```

y:            new values at each time step

dy:           dy/dt over each time step

Splits:       structure of dy additive components at each time step

Diag:         structure of diagnostic variables at each time step

failflag:     true if any component becomes negative within the
              Runge-Kutta calculations.

```

B.3.47 odewrap

```

[t,y] = odewrap(solver, fun, tspan, y0)
[t,y] = odewrap(solver, fun, tspan, y0, options)
[t,y] = odewrap(solver, fun, tspan, y0, options, in1, in2, ...)
[t,y] = odewrap(solver, fun, tspan, y0, [],      in1, in2, ...)
[t,y, dy, out1, out2, ...] = odewrap(...)

```

This function is a wrapper for Matlab's ODE solvers. It adds the flexibility of allowing the solvers to evaluate functions of the form

```
[dydt, out1, out2, ...] = odefun(t, y, in1, in2, ...),
```

where both y and dydt can be matrices rather than vectors. It can be used to run any of the variable-step solvers provided with Matlab, as well as the fixed-step solvers that can be downloaded from the Mathworks website (see "Tech Note 1510: Differential Equations in Matlab").

This function is not intended to support systems that require mass matrix or Jacobian properties, or those that utilize Events.

Input variables:

```

solver:    function handle to ODE solver

fun:       function handle that evaluates the differential equation.
           This function should be of the form dydt = fun(t, y), where
           t is a scalar time value, and y and dydt are matrices of
           identical size. See params input to pass additional input
           to the differential equation.

tspan:     vector specifying interval of differentiation. If a
           variable-step solver is used and tspan includes two
           elements [t0 tf], the solver returns the solution evaluated
           at every integration step. Otherwise, a solution will be
           returned at each specified time value. For fixed-step
           solvers, values will only be returned at the specified
           values, regardless of the length of tspan.

y0:        matrix of initial conditions.

options:   structure of optional parameters that change the default
           integration properties. Only applicable to variable-step
           solvers (use empty array if you need to pass additional
           parameters to a fixed-step solver). This function is not
           designed to solve systems where mass matrix or Jacobian
           properties are needed. Those properties may work, but if
           so it is by accident.

in#:      additional parameters required by fun. These can be any
           size or data type, depending on the specific function being
           evaluated. Parameters are held constant throughout the
           integration time span.

```

Output variables:

```

t:         vector of times values corresponding to solution

y:         array of solutions. This will be a length(t) x size(y0)
           array.

dy:        array of dy/dt values at each of the solution times

out#:     additional output variables returned by the differential
           equation function. These may be any size or data type,
           depending of the specific function being evaluated.

```

B.3.48 parseinput

B.3.49 parsepv

```
NewParam = parsepv(Param, pvpairs)
[NewParam, extra] = parsepv(Param, pvpairs, 'returnextra')
```

This function is an extension of `parse_pv_pairs`. It allows the option of returning unrecognized parameter/value pairs, rather than erroring.

Input variables:

Param: 1 x 1 structure holding default parameters (fieldnames) and values

pvpairs: 1 x n cell array of parameter/value pairs

'returnextra': if this string is included, the function will return a cell array holding any unrecognized parameters and the corresponding values. Otherwise, it will error if a parameter is not recognized.

Output variables:

NewParam: 1 x 1 struct identical to Param but with defaults replaced by the values from pvpairs

extra: 1 x m cell array of any unrecognized parameter/value pairs

B.3.50 photosynthesis

```
ps = photosynthesis(nutrients, phyto, kn, z, irr, temp, dz)
```

Using photosynthesis model from Sarmiento and Gruber 2006, Chapter 4. Net uptake and assimilation of nitrogen is defined as $V_p(T) * \text{gammap}(I, N)$, where $V_p(T)$ is the maximum temperature-dependant growth rate (time^{-1}), and $\text{gammap}(I, N)$ is a value between 0 and 1 that describes the limitation of growth due to light and nutrients.

Input variables:

phyto: ndepth x np, concentration of producers (mmol N m^{-3})

nutrients: ndepth x 1, concentration of nutrients (mmol N m^{-3})

kn: 1 x np, half-saturation constants for each producer (mmol N m^{-3})

z: ndepth x 1, depths (m, positive down)

```
    irr:          mean irradiance at surface (W m^-2)
    dz:           ndepth x 1 or 1 x 1 array, thickness of each layer (m)
```

Output variables:

```
    ps:            ndepth x np, nutrient uptake rate (or rate of accumulation
                   of biomass due to photosynthesis) per unit biomass of
                   producer (s^-1)
```

B.3.51 plotmixed

```
h = plotmixed(file, field1, field2, ...)
h = plotmixed(file, splitdepth, ...)
```

Input variables:

```
    file:          mixed_layer output file
    field:         output variables to be plotted, corresponding to a variable
                   names in the output file, or an arbitrary matrix of size
                   ndepth x ntime, ndepth+1 x ntime, or 1 x ntime.
```

splitdepth: depth to separate surface and deep layers. The surface layers will be displayed in the upper quarter of the figure; the bottom layers in the lower three quarters.

Output variables:

```
    h:             structure with handles to figures and axes
```

B.3.52 readmixed

```
Data = readmixed(file)
Data = readmixed(file, 'var1', 'var2', ...)
Data = readmixed(file, Opt, 'var1', 'var2', ...)
readmixed(file, 'list')
```

Input variables:

```
    file:          name of output netcdf file (with or without .nc extension)
    var#:         name of variables to be read. If not included, all
                  variables will be read. If the string 'dimensions' is
                  included, this corresponds to all the dimensional
                  variables: 'depth', 'depth_edge', 'startdate', 'middate',
                  'enddate'.
```

Opt: 1 x 1 one structure holding options for reading and averaging data:

tstart: date number corresponding to earliest value to read in time dimension. If NaN, will read from beginning. [NaN]

tend: date number corresponding to latest value to read in time dimension. If NaN, data will be read to end of time dimension. [NaN]

tstride: sampling interval (stride) along time dimension. [1]

tbin: Bin edges, as in histc. Data will be averaged over each bin. Sampling based on above parameters will be done prior to averaging.

monthavg: True indicates to average data over each month (a shortcut to listing months as tbin). Sampling based on above parameters will be done prior to averaging. [false]

tmid: Values of the 'middate' variable in the file. If you're doing multiple reads of a large file using tstart or tend, it can speed things up if readmixed doesn't need to read in this variable each time to analyze where to start and stop.

surfonly: Only read the surface depth values, i.e. first cell in the depth dimension [false]

'list': When called with just the file name and this string, this will simply list the names and dimensions of all variables in the file.

Output variables:

Data: 1 x 1 structure holding data from specified file. Field names correspond to variable names.

B.3.53 recovercrashed

`recovercrashed(varargin)`

This function recovers the data from a crashed mixed_layer run. It assumes that the crashed one was the most recently run mixed_layer simulation, and that the mltemp.bin and mltemp.mat files in the current directory are associated with it.

Run with the same input as was used for mixed_layer.

B.3.54 regexpfound

```
found = regexpfound(str, expression);
found = regexpfound(cells, expression);
```

This function returns a logical array indicating whether the expression was found in the input string or cell array. It acts similar to `regexp` but with output of a logical array rather than the typical cell array.

Input variables:

```
str:          vector character array
cells:        cell array of strings
expression:   regular expression to match
```

Output variables:

```
found:        logical array same size as cells (1 x 1 if input was a
              string), true if expression was found 1 or more times in
              the string
```

B.3.55 runmixedlayer

```
runmixedlayer(In, name, usepar, nlabs, folder, p1, v1, ...)
```

This function runs `mixed_layer` for multiple input sets. It provides a log file to note any errors. It will skip over any sets where it finds an existing file of the specified name, so can be used to complete partly-run ensembles.

Input variables:

```
In:          n x 1 structure holding mixed_layer input fields. Each
              structure element corresponds to one set of input
              variables.

name:        base name for run. A folder with this name will be placed
              under the folder specified below, and will contain the
              logfile name.log as well as all .nc files produced by the
              run.

folder:      location where new results folder will be placed (new
              folder will be names <folder>/<name>/

usepar:      true to run simulations in parallel via matlabpool and
              parfor, false to run one at a time
```

```

nlabs:      number of labs to run if running in parallel

p#/v#:      any additional mixed_layer input variables that will be
            applied to all runs, passed as parameter/value pairs

```

B.3.56 sh2dewpoint

```
dp = sh2dewpoint(sh, p, t)
```

Calculations are as follows:

```

pH20 = SH * mr                                <-- relationship between mole
                                                fraction and partial pressure
es = A * exp(beta * T)                         <-- simplified Clausius-Clapeyron
RH = pH20/es * 100                             <-- definition of relative humidity
gamma = a.*T./(b + T) + log(RH);
Td = (b .* gamma)./(a - gamma);                <-- August-Roche-Magnus
                                                approximation

```

where pH20 = partial pressure of water vapor
 SH = specific humidity
 mr = mole ratio of water to dry air (18.015/28.97)
 es = saturation vapor pressure (Pa)
 A = 611 Pa
 beta = 0.067 deg C
 RH = relative humidity
 T = temperature (deg C)
 a = 17.271
 b = 237.7 deg C
 Td = dewpoint temperature (deg C)

Valid for 0 degC < T < 60 degC, 1% < RH < 100%, 0 degC < Td < 50 degC

Input variables:

```

sh: specific humidity (g H20/g air)

p:  pressure (Pa)

t:  temperature (deg C)

```

Output variables:

```
dp: dewpoint temperature (deg C)
```

B.3.57 solve_velocities

velocity values

```
newvel = solve_velocities(oldvel, mixcoef, dt, dz, cor, pgx, pgy, ...
                          sbc, bbc, bottomval, source, dissipate)
```

The routine uses a semi-implicit Crank-Nicolson scheme to solve:

```
du/dt = fv + d/dz(K*du/dz) - pgx - eps*u  
dv/dt = -fu + d/dz(K*dv/dz) - pgy - eps*v
```

Where u and v are the velocities, f is the coriolis parameter, K is a mixing coefficient, pgx and pgy are pressure gradients in the x and y directions respectively, and eps is a dissipation term that mimics the horizontal divergence.

Input variables (n = number of vertical layers)

```
oldvel:      2n x 1 array of velocities at each depth at the current  
             time step, first n entries are u values, next n entries are  
             v values (m s^-1)  
  
mixcoef:    n x 1 array, mixing coefficient for tracer at each depth  
             (m^2 s^-1)  
  
dt:          time increment (s)  
  
dz:          depth increment (m)  
  
cor:         coriolis parameter (s^-1)  
  
pgx:        pressure acceleration in the x direction (m s^-2)  
  
pgy:        pressure acceleration in the y direction (m s^-2)
```

Optional input variables (passed as parameter/value pairs):

```
sflux:       "velocity flux" i.e., momentum flux/density, into the  
             top depth bin = 1/dz(1) * K * du/dz (m s^-2)  
  
bflux:       "velocity flux" i.e., momentum flux/density, into the top  
             depth bin = 1/dz(1) * K * dv/dz (m s^-2)  
  
sval:        velocity value at the surface, used to force the surface  
             grid cell (m/s)  
  
bval:        velocity value along the bottom, used to force the bottom  
             grid cell (m/s)  
  
source:      n x 1 array, source (or sink) flux of tracer at each grid  
             cell (m s^-2)  
  
dissipate:   dissipation constant (s^-1)
```

Output variables:

```
newvel:      n x 1 array, tracer concentrations at next time step
```

(tracer unit)

Local variables:

- theta: Numerical parameter determining the relative weighting of future versus present conditions in the numerical calculation. A value of 0 is an explicit scheme, a value of 1 is a fully implicit scheme, the default value of 0.5 is the Crank-Nicolson scheme, which offers a robust blend of stability and accuracy.
- dtheta: Added this parameter to control the relative weighting of future versus present conditions for the diffusive step.

B.3.58 sortewein

```
[New, isrt] = sortewein(Ewein)
```

This function rearranges the groups in a Ewe input structure so that they are in descending order by trophic level (and also makes sure detritus groups are listed last).

Input variables:

Ewein: Ewe input structure

Output variables

New: Ewein input structure with groups sorted by trophic level

isrt: index vector showing old positions of new groups, such that
old(isrt) = new

B.3.59 suplabel

```
[h1, h2, ...] = suplabel(param, val, ...)
```

This function adds a title, xlabel, and/or ylabel to a group of axes.

Input variables:

figure: handle of figure where axes are located. This is ignored if specific axes handles are given. Default is current figure.

axes: handles(s) of axes that will be labeled. If omitted, all visible axes in the specified figure (or current figure if no figure is specified) are used.

```

title:      title string

xlabel:     xlabel string

ylabel:     ylabel string

buffert:    distance (normalized) between title string and top of axes
[0.02] .

bufferx:   distance (normalized) between xlabel string and bottom of
axes [0.05]

buffery:   distance (normalized) between ylabel string and left of
axes [0.05]

```

Output variables:

```

h:          handles to labels added, in order listed in input. If one
extra handle is requested (e.g. listed 2 label types but
you ask for 3 output variables), the handle to the axis
used to position the labels will be returned as well (this
axis is always an invisible axis with normalized position
[0 0 1 1]).
```

B.3.60 tracer

See `biomodule.m` for full syntax details.

This module adds a simple tracer variable to the `mixed_layer` model. The tracer has no sources or sinks.

User-specified input variables (passed to `mixed_layer` as parameter/value pairs):

```

tracer: n x 2 depth profile of tracer, where column 1 gives the depth
values (negative down) and column 2 holds the initial
concentrations of a generic tracer (mmol m^-3)

```

B.3.61 tracerforced

See `biomodule.m` for full syntax details.

This module adds a single tracer variable to the `mixed_layer` model. The tracer has no sources or sinks, but is forced during mixing so that the bottom grid cell maintains the same tracer concentration as was supplied in the initial profile.

User-specified input variables (passed to `mixed_layer` as parameter/value

pairs):

```
tracer: n x 2 depth profile of tracer, where column 1 gives the depth  
values (negative down) and column 2 holds the initial  
concentrations of a generic tracer (mmol m^-3)
```

B.3.62 trophiclevel

```
level = trophiclevel(dc, pp, nlive, ngroup)  
level = trophiclevel(A)
```

This function calculates the trophic levels of each member of a food web, based on their diets and whether they are primary producers/detrital. The calculations derive from EstimateTrophicLevels in the EwE model. Primary producers and detrital groups receive a trophic level of 1, while consumers are assigned $1 + w$, where w is the weighted average of their prey's trophic levels.

Input variables:

```
dc:      ngroup x ngroup array, diet composition, dc(i,j) tells fraction  
        of predator j's diet consisting of prey i  
  
pp:      ngroup x 1 array, 1 = is primary producer, 0 = is not primary  
        producer, 2 = is detrital  
  
nlive:   scalar, number of live, non-detrital groups  
  
ngroup:  scalar, number of functional groups in model
```

Output variables:

```
level:  ngroup x 1 array, trophic levels of each functional group
```

B.3.63 verticalflux

```
newtracer = verticalflux(tracer, wsink, dt, dz, openbot)
```

Calculated changes in tracer concentration due to non-mixing processes.

Input variables:

```
tracer:      nz x 1 array, concentration of tracer  
  
wsink:       nz x 1 array, vertical velocities (m/s)  
  
dt:          scalar, model time step (s)  
  
dz:          scalar, depth interval (m)
```

```
openbot: logical scalar, true if open bottom (i.e. things sink out)
```

Output variables:

```
newtracer: nz x 1 array, new value of tracer concentrations after one  
time step
```

B.3.64 wce

See biomodule.m for full syntax details.

This module simulates a mixed planktonic-nektonic ecosystem, based on a combination of models derived mainly from NEMURO and Kerim Aydin's version of Ecosim, with a little bit of COBALT thrown in for flavor.

A note on units: The biomass of all critters is saved to file in mol N[Si][Fe]/m^3. For nektonic critters, all biomass is placed in the surface cell, and actually represents the total over the entire water column; multiply by the thickness of the surface layer to get the true biomass, in mol N/m^2.

User-specified input variables (passed to mixed_layer as parameter/value pairs):

```
Ewein: 1 x 1 Ewe input structure. Must include all ecopath fields  
(see ecopathlite) in units of mol N/m^2/s, as well as the  
following fields:
```

x: Vulnerability parameter. Can be either a ngroup x 1 vector of log-transformed anomaly-from-base values (same as P4/P5 inputs in aydin-ecosim, range from -Inf to Inf w/ default of 0, xi in equation below), or an ngroup x ngroup array of non-transformed values for each predator-prey pair (range from 1 to Inf w/ default of 2, Xij in equation below).

$$X_{ij} = \exp(x_i + x_j) + 1$$

d: Handling time parameter, same format as x.

theta: Switching parameter. Same format as x but with slightly different transform

$$TH_{ij} = \exp(0.5 * (th_i + th_j))$$

TH = 1 yields a type 2 functional response
TH = 2 yields a type 3 functional response

NemParam: 1 x 1 structure of NEMURO parameters (see

```

nemuroinputparser)

types: ngroup x 1 cell array of strings, indicating what type of
critter each functional group is.
'n': nekton, not affected by physical mixing, feed over
entire water column
'z': zooplankton, mixed, feed only in the layer where
they are located
Can also be any of the 11 nemuro state variables ('ps',
'pl', 'zs', 'zl', 'zp', 'no3', 'nh4', 'pon', 'don',
'sioh4', 'opal'), all of which are planktonic.

bnem0: n x 12 array. Column 1 holds depth values (m, negative
down) and the remaining columns hold the initial biomass
values for nemuro-derived variables (mol/l). Currently
only the non-living profiles are used, but the entire
matrix is used as input for consistency with the NEMURO
module.

nomix: logical scalar, if true biological variables are not subject
to mixing (for debugging purposes) [false]

ecosimpp: logical scalar, if true ecosim primary production function
is used, decoupling biology from nutrient constraints (for
debugging purposes) [false]

mld: mixed layer depth, used for initial plankton distributions
and per-area-to-per-volume rate conversions (m, negative
down) [-50]

temp: temperature associated with initial mass-balanced values,
used for grazing functional response (deg C) [0]

kgra: nexz x 1 array, temperature coefficient associated with
non-nemuro zooplankton groups (i.e. those with type 'z').
Default is 0.0693 deg C^-1 for all, i.e. a Q10 of 2.

Kfe: 1 x 2 array, half-saturation constants for iron uptake for
small and large phytoplankton, respectively (molFe/m^3)
[6e-7 3e-6]

kfe2n: 1 x 2 array, half-saturation constants for internal Fe:N
ratio for small and large phytoplankton, respectively
(molFe/molN) [[6.625e-05 0.0001325], i.e. [10 20]
umolFe/molC assuming Redfield]

fe2nmax: 1 x 2 array, maximum internal Fe:N ratio for small and
large phytoplankton, respectively (molFe/molN)
[[0.00033125 0.0033125], i.e. [50 500] umolFe/molC assuming
Redfield]

fe2nupfac: scalar, Fe:N uptake ratio (molFe/molN) [100e-6]

ligbkg: Ligand background concentration (mol/m^3) [1.0e-6]

```

alphascav: Iron scavenging coefficient (s^{-1}) [1.5855e-06, i.e. 50 yr^{-1}]
 remineff: Fraction of particulate iron remineralization relative to organic (N) material (no unit) [0.25]
 kiscav: Half-saturation constant for light's influence on ligand binding (W/m^2) [1.0]
 kliglo: Lower limit of ligand binding under low-light conditions (m^3/mol) [3.0e8]
 klighi: Upper limit of ligand binding under high-light conditions (m^3/mol) [1.0e5]
 m0exp: Exponent for mortality function, of form $M0 = aB^{(m0exp)}$. A value of 1 leads to linear mortality and 2 to quadratic mortality. Can also be a nlive x 1 array of values to allow different functions for each critter. [2]
 reroute: n x 5 cell array. This allows you to reroute fluxes from the original path defined in the nemuro model. Each row describes a change, with column as follows:
 col 1: name of flux (gpp, gra, pre, res, exx, exc, ege, mor, dec)
 col 2: name of original source group
 col 3: name of original sink group
 col 4: name of new sink group
 col 5: fraction of flux to reroute
 odesolver: cell array of strings, indicating which solvers to use. If the first one fails to integrate a timestep (i.e. causes something to become negative, NaN, or Inf), the next one is tried. See integratebio.m for choices. [{'euler'}]

B.3.65 wceode

```
[db, Flx, Diag] = wceode(time, bio, A)
```

Source/sink ODE function for wce module. See biomodules/wce for details; this function is designed to be called by ODE solvers.

Bibliography

- Aita, M N, Yamanaka, Y, & Kishi, M J. 2007. Interdecadal variation of the lower trophic ecosystem in the northern Pacific between 1948 and 2002, in a 3-D implementation of the NEMURO model. *Ecological Modelling*, **202**(1-2), 81–94.
- Aydin, K, Gaichas, S, Ortiz, I, Kinzey, D, & Friday, N. 2007. A Comparison of the Bering Sea, Gulf of Alaska, and Aleutian Islands Large Marine Ecosystems Through Food Web Modeling. *NOAA Technical Memorandum*.
- Aydin, Kerim Y, McFarlane, Gordon A, King, Jacquelynne R, & Megrey, Bernard A. 2003. The BASS/MODEL report on trophic models of the Subarctic Pacific Basin ecosystems. *PICES Scientific Report*, **25**(25).
- Aydin, Kerim Y, McFarlane, Gordon A, King, Jacquelynne R, Megrey, Bernard A, & Myers, Katherine W. 2005. Linking oceanic food webs to coastal production and growth rates of Pacific salmon (*Oncorhynchus spp.*), using models on three scales. *Deep Sea Research Part II: Topical Studies in Oceanography*, **53**, 757–780.
- Beamish, R J, Leask, K D, Ivanov, O A, Balanov, A A, Orlov, A M, & Sinclair, B. 1999. The ecology, distribution, and abundance of midwater fishes of the Subarctic Pacific gyres. *Progress in Oceanography*, **43**, 399–442.
- Beamish, Richard J, & Bouillon, Daniel R. 1993. Pacific salmon production trends in relation to climate. *Canadian Journal of Fisheries and Aquatic Science*, **50**, 1002–1016.
- Beverton, R.J.H., & Holt, S.J. 1957. On the dynamics of exploited fish populations. *MAFF Fisheries Investigation of London Series 2*, **19**, 1—533.
- Boyd, P, & Harrison, P J. 1999. Phytoplankton dynamics in the NE subarctic Pacific. *Deep Sea Research Part II: Topical Studies in Oceanography*, **46**(11-12), 2405–2432.
- Brodeur, R, McKinnell, S, Nagasawa, K, Pearcy, W, Radchenko, V, & Takagi, S. 1999. Epipelagic nekton of the North Pacific subarctic and Transition Zones. *Progress in Oceanography*, **43**(2-4), 365–397.
- Brodeur, Richard D, & Ware, Daniel M. 1992. Long-term variability in zooplankton biomass in the subarctic Pacific Ocean. *Fisheries Oceanography*, **1**(1), 32–38.
- Brussaard, C.P.D. 2004. Viral Control of Phytoplankton Populations-a Review. *Journal of Eukaryotic Microbiology*, **51**(2), 125–138.
- Chassot, E, Mélin, F, Le Pape, O, & Gascuel, D. 2007. Bottom-up control regulates fisheries production at the scale of eco-regions in European seas. *Marine Ecology Progress Series*, **343**(Aug.), 45–55.
- Christensen, Villy, & Walters, Carl J. 2004. Ecopath with Ecosim: methods, capabilities and limitations. *Ecological Modelling*, **172**, 109–139.

- Christensen, Villy, Walters, Carl J, & Pauly, Daniel. 2005 (Nov.). *Ecopath with Ecosim: A User's Guide*. Fisheries Centre, University of British Columbia, Vancouver, Canada.
- Denman, K L, & Pena, M A. 1999. A coupled 1-D biological/physical model of the northeast subarctic Pacific Ocean with iron limitation. *Deep Sea Research Part II: Topical Studies in Oceanography*, **46**(11-12), 2877–2908.
- Denman, K L, Brasseur, G, Chidthaisong, A, Caias, P, Cox, P M, Dickinson, R E, Hauglustaine, D, Heinze, C, Holland, E, Jacob, D, & Others. 2007. Couplings between changes in the climate system and biogeochemistry Climate Change 2007: The Physical Science Basis. Contribution of Working Group I to the Fourth Assessment Report of the Intergovernmental Panel on Climate Change ed S Solomon et al. Cambridge University Press, Cambridge, United Kingdom and New York, NY, USA.
- Denman, KL L, & Miyake, M. 1973. Upper layer modification at Ocean Station Papa: observations and simulation. *Journal of Physical Oceanography*, **3**, 185–196.
- Eslinger, David L., Kashiwai, Makoto B., Kishi, Michio J., Megrey, Bernard A., Ware, Daniel M., & Werner, Francisco E. 2000. MODEL Task Team Workshop Report-Final report of the international Workshop to develop a prototype lower trophic level model for comparison of different marine ecosystems in the North pacific. *PICES Scientific report*, **15**.
- Fan, Song-Miao. 2008. Photochemical and biochemical controls on reactive oxygen and iron speciation in the pelagic surface ocean. *Marine Chemistry*, **109**(1-2), 152–164.
- Fasham, M J R, Ducklow, H W, & McKelvie, S M. 1990. A nitrogen-based model of plankton dynamics in the oceanic mixed layer. *Journal of Marine Research*, **48**(3), 591–639.
- Fiechter, J, Moore, A M, Edwards, C A, Bruland, K W, Di Lorenzo, E, Lewis, C V W, Powell, T M, Curchitser, E N, & Hedstrom, K. 2009. Modeling iron limitation of primary production in the coastal Gulf of Alaska. *Deep Sea Research Part II: Topical Studies in Oceanography*, **56**(24), 2503–2519.
- Fitzwater, S E, Knauer, G A, & Martin, J H. 1982. Metal contamination and its effect on primary production measurements. *Limnology and Oceanography*, 544–551.
- Francis, Robert C, Hare, Steven R, Hollowed, Anne B, & Wooster, Warren S. 1998a. Effects of interdecadal climate variability on the oceanic ecosystems of the NE Pacific. *Fisheries Oceanography*, **7**(1), 1–21.
- Francis, Robert C., Hare, Steven R., Hollowed, Anne B., & Wooster, Warren S. 1998b. Effects of interdecadal climate variability on the oceanic ecosystems of the NE Pacific. *Fisheries Oceanography*, **7**(1), 1–21.
- Frank, Kenneth T, Petrie, Brian, Shackell, Nancy L, & Choi, Jae S. 2006. Reconciling differences in trophic control in mid-latitude marine ecosystems. *Ecology Letters*, **9**(10), 1096–105.
- Friedland, Kevin D., Stock, Charles, Drinkwater, Kenneth F., Link, Jason S., Leaf, Robert T., Shank, Burton V., Rose, Julie M., Pilskalm, Cynthia H., & Fogarty, Michael J. 2012. Pathways between Primary Production and Fisheries Yields of Large Marine Ecosystems. *PLoS ONE*, **7**(1), e28945.
- Friehe, C A, & Schmitt, K F. 1976. Parameterization of air-sea interface fluxes of sensible heat and moisture by the bulk aerodynamic formulas. *Journal of Physical Oceanography*, **6**(6), 801–809.
- Fujii, M, Yamanaka, Y, Nojiri, Y, Kishi, M J, & Chai, F. 2007. Comparison of seasonal characteristics in biogeochemistry among the subarctic North Pacific stations described with a NEMURO-based marine ecosystem model. *Ecological Modelling*, **202**(1-2), 52–67.

- Fulton, E A. 2010. Approaches to end-to-end ecosystem models. *Journal of Marine Systems*, **81**(1-2), 171–183.
- Fulton, Elizabeth a., Smith, Anthony D.M., & Johnson, Craig R. 2003. Mortality and predation in ecosystem models: is it important how these are expressed? *Ecological Modelling*, **169**(1), 157–178.
- Fulton, Elizabeth a., Smith, Anthony D.M., & Johnson, Craig R. 2004a. Biogeochemical marine ecosystem models I: IGBEM- a model of marine bay ecosystems. *Ecological Modelling*, **174**(3), 267–307.
- Fulton, Elizabeth a., Parslow, John S., Smith, Anthony D.M., & Johnson, Craig R. 2004b. Biogeochemical marine ecosystem models II: the effect of physiological detail on model performance. *Ecological Modelling*, **173**(4), 371–406.
- Garcia, H E, Locarnini, R A, Boyer, T P, & Antonov, J I. 2006. *World Ocean Atlas 2005. Vol. 4, Nutrients (phosphate, nitrate, silicate)*. NOAA Atlas NESDIS 64. U.S. Government Printing Office, Washington, D.C.: National Oceanic and Atmospheric Administration.
- Gentleman, Wendy, Leising, Andrew, Frost, Bruce, Strom, Suzanne, & Murray, James. 2003. Functional responses for zooplankton feeding on multiple resources: a review of assumptions and biological dynamics. *Deep-Sea Research II*, **50**, 2847–2875.
- Goldblatt, R, Mackas, D, & Lewis, a. 1999. Mesozooplankton community characteristics in the NE subarctic Pacific. *Deep Sea Research Part II: Topical Studies in Oceanography*, **46**(11-12), 2619–2644.
- Hansen, Per Juel, Bjornsen, Peter Koefoed, & Hansen, Benni Winding. 1997. Zooplankton grazing and growth: scaling within the 2-2000 um body size range. *Limnology and Oceanography*, **42**(4), 687–704.
- Harris, Roger, Wiebe, Peter, Lenz, Jurgen, Skjoldal, Hein Rune, & Huntley, Mark. 2000. *Zooplankton Methodology Manual*. Elsevier Academic Press.
- Harrison, P J, Whitney, F A, Tsuda, A, Saito, H, & Tadokoro, K. 2004. Nutrient and plankton dynamics in the NE and NW gyres of the subarctic Pacific Ocean. *Journal of Oceanography*, **60**(1), 93–117.
- Kearney, Kelly A., Stock, Charles, Aydin, Kerim, & Sarmiento, Jorge L. 2012. Coupling planktonic ecosystem and fisheries food web models for a pelagic ecosystem: Description and validation for the subarctic Pacific. *Ecological Modelling*, **237-238**(July), 43–62.
- Keyl, F, & Wolff, M. 2008. Environmental variability and fisheries: what can models do? *Reviews in Fish Biology and Fisheries*, **18**(3), 273–299.
- Kishi, M, Kashiwai, M, Ware, D, Megrey, B, Eslinger, D, Werner, F, Noguchiaita, M, Azumaya, T, Fujii, M, & Hashimoto, S. 2007a. NEMURO- a lower trophic level model for the North Pacific marine ecosystem. *Ecological Modelling*, **202**(1-2), 12–25.
- Kishi, M J, Kashiwai, M, Ware, D M, Megrey, B A, Eslinger, D L, Werner, F E, Noguchi-Aita, M, Azumaya, T, Fujii, M, Hashimoto, S, & Others. 2007b. NEMURO—a lower trophic level model for the North Pacific marine ecosystem. *Ecological Modelling*, **202**(1-2), 12–25.
- Kishi, M J, Ito, S, Megrey, B A, Rose, K A, & Werner, F E. 2010. A review of the NEMURO and NEMURO. FISH models and their application to marine ecosystem investigations. *Journal of Oceanography*, 1–14.
- Large, W G, & Pond, S. 1981. Open ocean momentum flux measurements in moderate to strong winds. *Journal of physical oceanography*, **11**(3), 324–336.

- Large, W G, & Yeager, S G. 2009. The global climatology of an interannually varying air-sea flux data set. *Climate dynamics*, **33**(2), 341–364.
- Larkin, P.A. 1996. Concepts and issues in marine management. *Review in Fish Biology and Fisheries*, **6**, 139–164.
- Lehodey, P, Senina, I, & Murtugudde, R. 2008. A spatial ecosystem and populations dynamics model (SEAPODYM)-Modeling of tuna and tuna-like populations. *Progress in Oceanography*, **78**(4), 304–318.
- Link, Jason. 2010a. *Ecosystem-based Fisheries Management: Confronting Tradeoffs*. Cambridge University Press.
- Link, Jason S. 2010b. Adding rigor to ecological network models by evaluating a set of pre-balance diagnostics : A plea for PREBAL. *Ecological Modelling*, **221**(12), 1580–1591.
- Link, J.S., Ihde, T.F., Harvey, C.J., Gaichas, S.K., Field, J.C., Brodziak, J.K.T., Townsend, H.M., & Peterman, R.M. 2012. Dealing with uncertainty in ecosystem models: The paradox of use for living marine resource management. *Progress In Oceanography*, Apr.
- Mantua, Nathan J, Hare, Steven R, Zhang, Yuan, Wallace, John M, & Francis, Robert C. 1997. A Pacific interdecadal climate oscillation with impacts on salmon production. *Bulletin of the American Meteorological Society*, **78**(6), 1069–1079.
- Marchetti, Adrian, Sherry, Nelson D., Kiyosawa, Hiroshi, Tsuda, Atsushi, & Harrison, Paul J. 2006. Phytoplankton processes during a mesoscale iron enrichment in the NE subarctic Pacific: Part I—Biomass and assemblage. *Deep Sea Research Part II: Topical Studies in Oceanography*, **53**(20-22), 2095–2113.
- Martin, J H, Gordon, R M, Fitzwater, S, & Broenkow, W W. 1989. VERTEX: phytoplankton/iron studies in the Gulf of Alaska. *Deep Sea Research Part A. Oceanographic Research Papers*, **36**(5), 649–680.
- Martin, John H, & Fitzwater, Steve E. 1988. Iron deficiency limits phytoplankton growth in the north-east Pacific subarctic. *Nature*, **331**(28), 341—343.
- Maury, Olivier. 2010. An overview of APECOSM, a spatialized mass balanced "Apex Predators ECOSystem Model" to study physiologically structured tuna population dynamics in their ecosystem. *Progress In Oceanography*, **84**(1-2), 113–117.
- May, Robert, & McLean, Angela. 2007. *Theoretical Ecology : Principles and Applications*. 3 edn. Oxford University Press, UK.
- Megrey, B A, Rose, K A, Klumb, R A, Hay, D E, Werner, F E, Eslinger, D L, & Smith, S L. 2007. A bioenergetics-based population dynamics model of Pacific herring (*Clupea harengus pallasi*) coupled to a lower trophic level nutrient-phytoplankton-zooplankton model: Description, calibration, and sensitivity analysis. *Ecological Modelling*, **202**(1-2), 144–164.
- Megrey, BA, Kishi, MJ, Kashiwai, M., Ware, DM, Eslinger, DL, & Werner, FE. 2000. PICES Lower trophic level modeling workshop, Nemuro. *PICES Press*, **8**(2), 18–22.
- Mellor, G, & Blumberg, A. 2004. Wave breaking and ocean surface layer thermal response. *Journal of physical oceanography*, **34**(3), 693–698.
- Mellor, G L. 2001. One-dimensional, ocean surface layer modeling: A problem and a solution. *Journal of Physical Oceanography*, **31**(3), 790–809.
- Mellor, G L, & Yamada, T. 1982. Development of a turbulence closure model for geophysical fluid problems. *Reviews of geophysics and space physics*, **20**(4), 851–875.

- Mellor, George L. 2004. *User's guide for a three-dimensional, primitive equation, numerical ocean model*. Atmospheric and Oceanic Sciences Program, Princeton University.
- Moustahfid, H, Tyrrell, M C, Link, J S, Nye, J A, Smith, B E, & Gamble, R J. 2010. Functional feeding responses of piscivorous fishes from the northeast US continental shelf. *Oecologia*, **163**, 1059–1067.
- Moxim, Walter J., Fan, Song-Miao, & Levy, Hiram. 2011. The meteorological nature of variable soluble iron transport and deposition within the North Atlantic Ocean basin. *Journal of Geophysical Research*, **116**(D3), 1–26.
- Nagata, T. 2000. Production mechanisms of dissolved organic matter. *Pages 121–152 of: Kirchman, D L (ed), Microbial Ecology of the Oceans*. New York: John Wiley and Sons, Inc.
- Ohman, M D, & Hirche, H J. 2001. Density-dependent mortality in an oceanic copepod population. *Nature*, **412**(6847), 638–641.
- Pauly, D, & Christensen, V. 1995. Primary production required to sustain global fisheries. *Nature*, **374**(March), 255–257.
- Pauly, D, Christensen, V, & Haggan, N. 1996. Mass-balance models of north-eastern Pacific ecosystems. *Fisheries Centre Research Reports*, **4**(1), 131.
- Pikitch, E K, Santora, C, Babcock, E A, Bakun, A, Bonfil, R, Conover, D O, Dayton, P, Doukakis, P, Fluharty, D, Heneman, B, Houde, E D, Link, J, Livingston, P A, Mangel, M, McAllister, M K, Pope, J, & Sainsbury, K J. 2004. Ecosystem-based fishery management. *Science*, **305**(5682), 346—347.
- Plaganyi, Eva E. 2007. Models for an Ecosystem Approach to Fisheries. *FAO Fisheries Technical Paper*, **477**, 108.
- Platt, T, & Jassby, A D. 1976. The relationship between photosynthesis and light for natural assemblages of coastal marine phytoplankton. *Journal of Phycology*, **12**(4), 421–430.
- Polovina, Jeffrey J. 1984. Model of a Coral Reef Ecosystem I. The ECOPATH Model and Its Applications to French Frigate Shoals. *Coral Reefs*, **3**, 1–11.
- Polovina, Jeffrey J, Mitchum-i, Gary T, Evansd, T, Mitchum, Gary T, & Evans, Geoffrey T. 1995. Decadal and basin-scale variation in mixed layer depth and the impact on biological production in the Central and North Pacific, 1960-88. *Deep-Sea Research*, **42**(10), 1701–1716.
- Reeve, M R, Walter, M A, & Ikeda, T. 1978. Laboratory studies of ingestion and food utilization lobate and tentaculate ctenophores. *Limnology and Oceanography*, **23**(4), 740–751.
- Reeve, Michael R., Syms, Mary Ann, & Kremer, Patricia. 1989. Growth dynamics of a ctenophore (Mnemiopsis) in relation to variable food supply. I. Carbon biomass, feeding, egg production, growth and assimilation efficiency. *Journal of Plankton Research*, **11**(3), 535–552.
- Ricker, W.E. 1954. Stock and recruitment. *Journal of the Fisheries Board of Canada*, **11**(5), 559–623.
- Ryther, J H. 1969. Photosynthesis and fish production in the sea. *Science*, **166**(3901), 72–6.
- Sarmiento, Jorge, & Gruber, Nicolas. 2006. *Ocean Biogeochemical Dynamics*. Princeton University Press.
- Simpson, J J, & Paulson, C A. 1979. Mid-ocean observations of atmospheric radiation. *Quarterly Journal of the Royal Meteorological Society*, **105**(444), 487–502.

- Song, Hongjun, Ji, Rubao, Stock, Charles, Kearney, Kelly, & Wang, Zongling. 2011. Interannual variability in phytoplankton blooms and plankton productivity over the Nova Scotian Shelf and in the Gulf of Maine. *Marine Ecology Progress Series*, **426**, 105–118.
- Steele, J H. 1962. Environmental control of photosynthesis in the sea. *Limnology and Oceanography*, **7**(2), 137–150.
- Steele, J.H., & Henderson, E.W. 1981. A simple plankton model. *American Naturalist*, **117**(5), 676–691.
- Steele, John H, & Henderson, Eric W. 1992. The role of predation in plankton models. *Journal of Plankton Research*, **14**(1), 157–172.
- Stock, Charles A., Dunne, John P., & John, Jasmin. *Global-scale carbon and energy flows through the planktonic food web: an analysis with a coupled physical-biological model*.
- Stock, Charles a., Alexander, Michael a., Bond, Nicholas a., Brander, Keith M., Cheung, William W.L. L, Curchitser, Enrique N., Delworth, Thomas L., Dunne, John P., Griffies, Stephen M., Haltuch, Melissa a., Hare, Jonathan A., Hollowed, Anne B., Lehodey, Patrick, Levin, Simon A., Link, Jason S., Rose, Kenneth A., Rykaczewski, Ryan R., Sarmiento, Jorge L., Stouffer, Ronald J., Schwing, Franklin B., Vecchi, Gabriel A., & Werner, Francisco E. 2011. On the use of IPCC-class models to assess the impact of climate on Living Marine Resources. *Progress In Oceanography*, **88**(1-4), 1–27.
- Suzuki, Koji, Saito, Hiroaki, Isada, Tomonori, Hattori-Saito, Ai, Kiyosawa, Hiroshi, Nishioka, Jun, McKay, R. Michael. L., Kuwata, Akira, & Tsuda, Atsushi. 2009. Community structure and photosynthetic physiology of phytoplankton in the northwest subarctic Pacific during an in situ iron fertilization experiment (SEEDS-II). *Deep Sea Research Part II: Topical Studies in Oceanography*, **56**(26), 2733–2744.
- Takeda, Shigenobu, & Tsuda, Atsushi. 2005. An in situ iron-enrichment experiment in the western subarctic Pacific (SEEDS): Introduction and summary. *Progress In Oceanography*, **64**(2-4), 95–109.
- Thornton, D. 2002. Diatom aggregation in the sea : mechanisms and ecological implications. *European Journal of Phycology*, **37**(2), 149–161.
- Travers, M, Shin, Y J, Jennings, S, & Cury, P. 2007. Towards end-to-end models for investigating the effects of climate and fishing in marine ecosystems. *Progress in Oceanography*, **75**(4), 751–770.
- Uematsu, Mitsuo, Wells, Mark L., Tsuda, Atsushi, & Saito, Hiroaki. 2009. Introduction to Subarctic iron Enrichment for Ecosystem Dynamics Study II (SEEDS II). *Deep Sea Research Part II: Topical Studies in Oceanography*, **56**(26), 2731–2732.
- Umlauf, L, & Burchard, H. 2005. Second-order turbulence closure models for geophysical boundary layers. A review of recent work. *Continental shelf research*, **25**(7-8), 795–827.
- Van Cappellen, Philippe, Dixit, S, & van Beusekom, J. 2002. Biogenic silica dissolution in the oceans: Reconciling experimental and field-based dissolution rates. *Global biogeochemical cycles*, **16**(4), 1075.
- Walters, Carl, Christensen, Villy, & Pauly, Daniel. 1997. Structuring dynamic models of exploited ecosystems from trophic mass-balance assessments. *Review in Fish Biology and Fisheries*, **7**, 139–172.
- Ware, Daniel M, Thomson, Richard E, & Thompson, Richard E. 2005. Bottom-up ecosystem trophic dynamics determine fish production in the Northeast Pacific. *Science*, **308**(1280-1284), 1280–4.
- Werner, F E, Ito, S I, Megrey, B A, & Kishi, M J. 2007. Synthesis of the NEMURO model studies and future directions of marine ecosystem modeling. *ecological modelling*, **202**(1-2), 211–223.

- Whitney, F A, & Freeland, H J. 1999. Variability in upper-ocean water properties in the NE Pacific Ocean. *Deep Sea Research Part II: Topical Studies in Oceanography*, **46**(11-12), 2351–2370.
- Wong, C.S., Waser, N.A.D., Nojiri, Y., Johnson, W.K., Whitney, F.A., Page, J.S.C., & Zeng, J. 2002. Seasonal and interannual variability in the distribution of surface nutrients and dissolved inorganic carbon in the Northern North Pacific: Influence of El Nino. *Journal of Oceanography*, **58**(2), 227–243.
- Yoshie, N, Yamanaka, Y, Rose, K A, Eslinger, D L, Ware, D M, & Kishi, M J. 2007. Parameter sensitivity study of the NEMURO lower trophic level marine ecosystem model. *Ecological Modelling*, **202**(1-2), 26–37.
- Yuan, Jinchun, & Shiller, Alan M. 2001. The distribution of hydrogen peroxide in the southern and central Atlantic ocean. *Deep Sea Research Part II: Topical Studies in Oceanography*, **48**(13), 2947–2970.